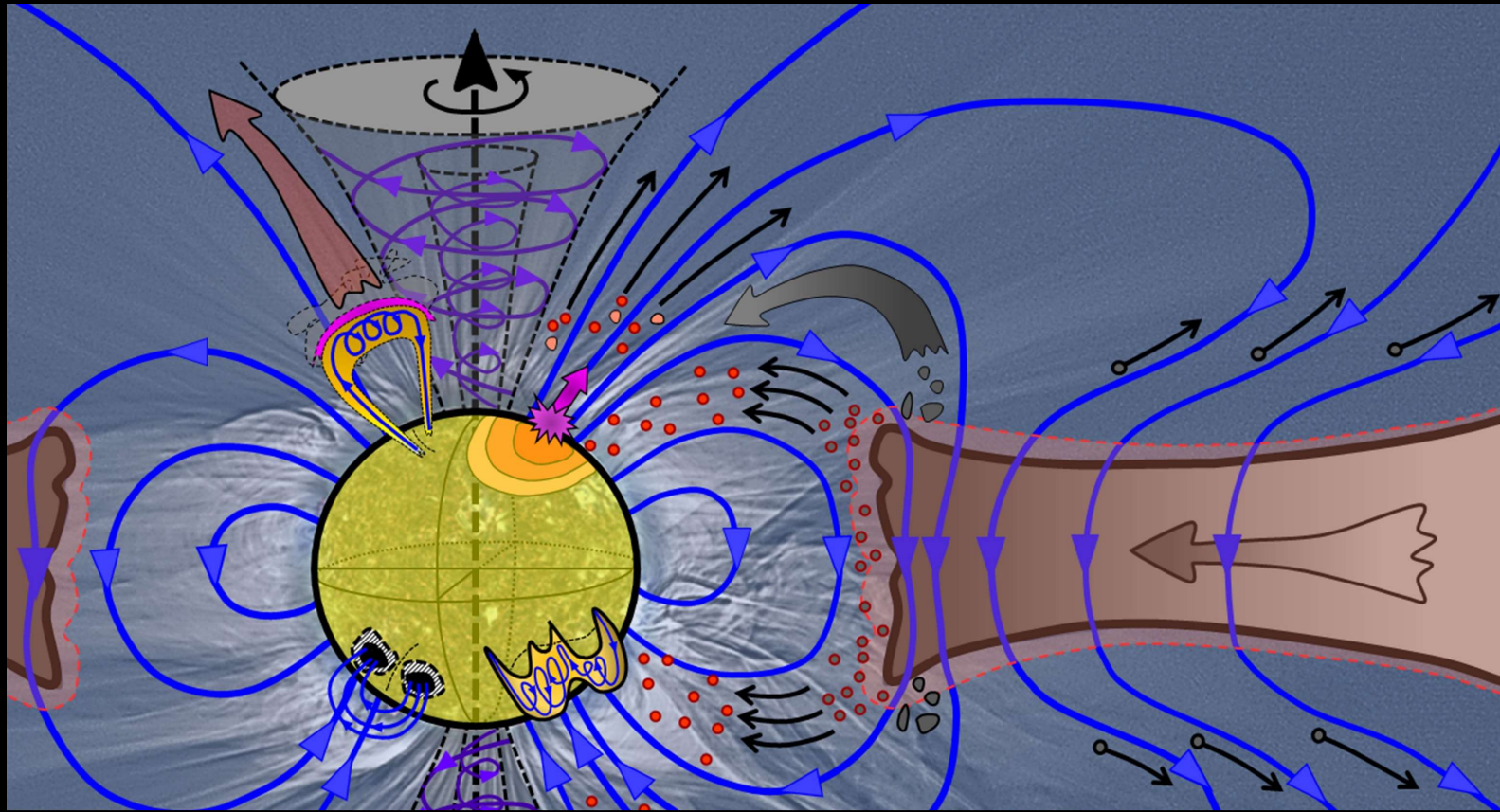


$$\frac{\partial \vec{B}}{\partial t} = \vec{\nabla} \times (\vec{v} \times \vec{B}) - \vec{\nabla} \times (\eta_{OD} \cdot \vec{\nabla} \times \vec{B}) + \vec{\nabla} \times \{ \eta_{AD} \cdot (\vec{\nabla} \times \vec{B}) \times \vec{B} \} - \vec{\nabla} \times [ \vec{\nabla} \times \{ \eta_{HD} \cdot (\vec{\nabla} \times \vec{B}) \times \vec{B} \} ]$$

U. v. Kusserow, Bremen

## MHD and the Formation of the Magnetic Solar System

A didactically oriented approach



$$\frac{\partial \vec{B}}{\partial t} = \vec{\nabla} \times (\vec{v} \times \vec{B}) - \vec{\nabla} \times (\eta_{OD} \cdot \vec{\nabla} \times \vec{B}) + \vec{\nabla} \times \{ \eta_{AD} \cdot (\vec{\nabla} \times \vec{B}) \times \vec{B} \} - \vec{\nabla} \times [ \vec{\nabla} \times \{ \eta_{HD} \cdot (\vec{\nabla} \times \vec{B}) \times \vec{B} \} ]$$

... something personal ...

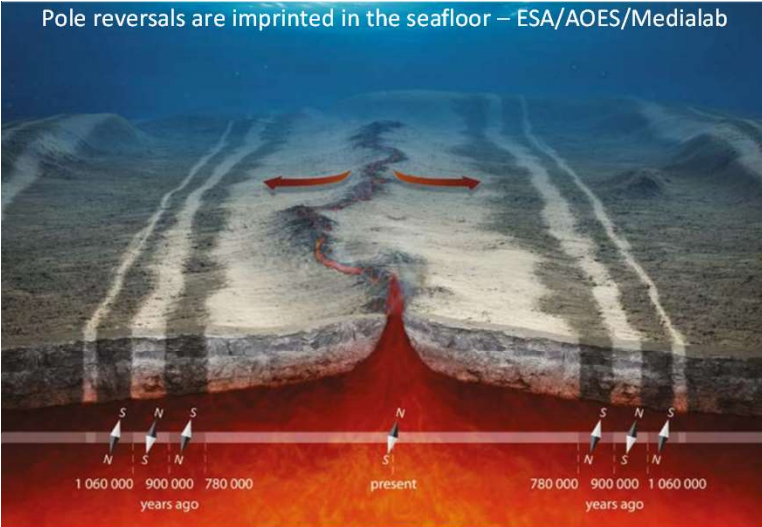
### Reversals of the Earth's Magnetic Field

Recent paleomagnetic and geochronologic data provide information on time and frequency of field reversals.

Allan Cox, Richard R. Doell, G. Brent Dalrymple

ment in techniques of determining the stability and reliability of rock magnetism for determining past geomagnetic field directions, and partly as a result of the vast increase in paleomagnetic data available. Although many of these paleomagnetic studies have focused on the problems of continental drift and polar wandering, interest in the reversal problem has also continued up to the present, and the observations of the early workers have been amply confirmed. The directions of remanent magnetization in many tens of thousands of rock samples, with ages in the range 0 to 30 million years, show a strikingly bimodal distribution; the directions are grouped about either the

#### Pole reversals are imprinted in the seafloor – ESA/AOES/Medialab



Astron. & Astrophys. 35, 69–78 (1974)

### Steady and Oscillatory $\alpha\omega$ -dynamics

W. Deinzer, H.-U. v. Kussrow and M. Stix  
Universitäts Sternwarte Göttingen

Received July 27, 1974

**Summary.** Using the model of Deinzer and Stix (1971) of an  $\alpha\omega$ -dynamo we investigate the problem whether the preferred magnetic field mode is steady or oscillatory for any particular strength and spatial distribution of the induction effects ( $\alpha$ -effect and non-uniform rotation). We find that a spatial separation of these two effects favours the steady modes, in contrast to an earlier assertion of Steenbeck and Krause (1969a). The steady

modes have dipolotype symmetry if the dynamo-number is positive, and quadrupolotype symmetry if the dynamo number is negative. The possible relevance of the steady dipole solutions to the dynamo operating in the Earth's interior is discussed.

**Key words:** dynamo —  $\alpha$ -effect — differential rotation — geomagnetism

#### 1. Introduction

It has been suggested by several authors (Parker, 1955; Steenbeck and Krause, 1969a; Deinzer and Stix, 1971; Roberts and Stix, 1972; Köhler, 1973) that the mean magnetic field of the Sun governing the 22-year cycle is an oscillatory solution of an " $\alpha\omega$ -dynamo": Non-uniform rotation creates toroidal magnetic flux from poloidal field components, and the " $\alpha$ -effect", an e.m.f.  $\alpha B$  parallel to the mean field existing in cyclonic convection, causes toroidal currents to flow and so to regenerate the poloidal field.

Are  $\alpha\omega$ -dynamics always oscillatory, or do steady solutions also exist? Or, more precisely, which type of solution is "dominant" (or "preferred") in a particular model in the sense that it is marginally stable for smaller values of the relevant magnetic Reynolds numbers? Parker (1971) has argued that steady solutions are preferred when the dynamo consists of a full sphere or a thick spherical shell such as the liquid core of the Earth; oscillatory modes dominate in a thin spherical shell dynamo such as the solar convection zone. Roberts (1972) computed solutions of a number of  $\alpha\omega$ -dynamics and found that oscillatory solutions were dominant even in dynamos occupying a full sphere; they could however be made steady by means of a (sufficiently strong) meridional circulation. Stix (1973) found that the dynamo model of Levy (1972a) has both steady and oscillatory solutions; which of these is preferred depends on the exact position of the rings of cyclones in Levy's model and on the sign of the "dynamo number".

$$P = R_1 R_2 = \frac{\alpha_0 R}{\eta} \frac{A \omega R^2}{\eta}$$

where  $\alpha_0$  is a characteristic value of  $\alpha$  in the northern hemisphere,  $A\omega$  is the total amount of differential rotation,

$R$  is the radius of the sphere and  $\eta$  is the (turbulent) magnetic diffusivity which in our models will be treated as a constant. In the most often investigated case only two magnetic Reynolds numbers,  $R_1$  and  $R_2$ , are relevant, and the frequencies and growth rates of the solutions solely depend on their product,  $P$ .

The models mentioned above show that in order to obtain oscillatory solutions with mean fields migrating from the poles toward the equator we must require that  $P < 0$ . With this sign of  $P$  Levy's model has preferred oscillatory solutions if the induction effects are confined to the outer third of the sphere. When  $P > 0$ , however, the model favours the steady mode irrespective of the positions of the induction effects (Stix, 1973). Thus, the situation is still not clear; we shall therefore investigate the question of oscillatory versus steady solutions further, using the model of Deinzer and Stix (1971); we shall refer to this article as "Paper I". This model has the advantage of having a more realistic latitude distribution of  $\alpha$  and  $\partial\omega/\partial r$  is still in the form of  $\delta$ -functions. But this form enables us to calculate solutions for a wide range of the characteristic parameters,  $r_1$  and  $r_2$  (the radial position of shear and  $\alpha$ -effect) and  $P$ , without a large expenditure of computing. We shall see in Section III how the  $(r_1, r_2)$  parameter space is divided into regions of steady and oscillatory solutions. We shall also see that, if steady solutions are possible, they are of dipole-type parity in the case  $P > 0$  and of quadrupole-type parity when  $P < 0$ .

If  $P > 0$ , steady dipolar solutions are plausible (Parker 1970; p. 399; see also the review of Roberts, 1971, p. 171). Consider a dipole field as shown in Fig. 1a. If the rate of rotation is larger in the outer parts of the

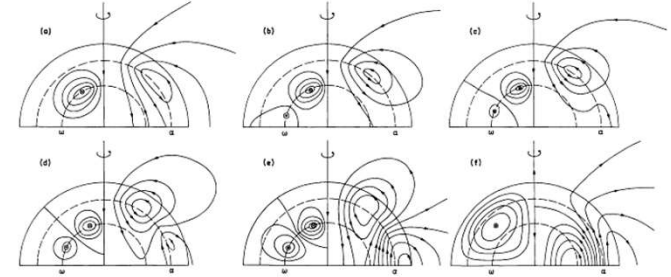


Fig. 7a-f. Meridian sections of dipolar magnetic fields, for the dynamo numbers  $P = 1389, 5400, 7198, 3000, 500, 0$ , with  $\alpha_0$  and  $A\omega$  both positive. The corresponding eigenvalues are marked with labels a-f in Fig. 3a. The right-hand sides show the lines of force of the poloidal field, and curves of constant toroidal field strength are drawn on the left-hand sides. All contours are drawn at equal spacing of the stream function  $A \cdot x \cdot \sin \theta$  on the right and the field strength  $B$  on the left. Encircled dots and crosses have the same meaning as in Fig. 1. The inner dashed circle indicates the shear surface, the outer indicates the  $\alpha$ -effect surface. Only the northern hemisphere is shown; the fields are antisymmetric with respect to the equatorial plane.

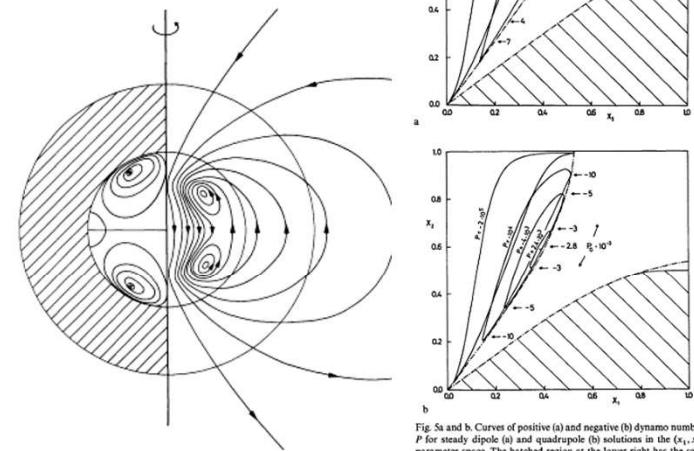
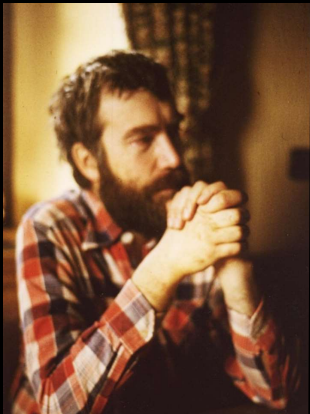


Fig. 10. The Earth as an  $\alpha\omega$ -dynamo, with  $x_1 = 0.9, x_2 = 0.6$ .  $P_{01} = 1558$ . On the left the mantle is hatched. See also the description of Fig. 7.

Fig. 5a and b. Curves of positive (a) and negative (b) dynamo numbers  $P$  for steady dipole (a) and quadrupole (b) solutions in the  $(x_1, x_2)$ -parameter space. The hatched region at the lower right has the same contours since the diagram is completely symmetric with respect to the line  $x_1 = x_2$ . In the regions between the two limiting curves oscillatory modes dominate; this is also the case within the small portion of Fig. 5b around  $x_2 \approx 0.5$  and  $0.75 \leq x_1 < 1$ . Some dynamo numbers,  $P_0$ , on the limiting curves are given.



Willi Deinzer



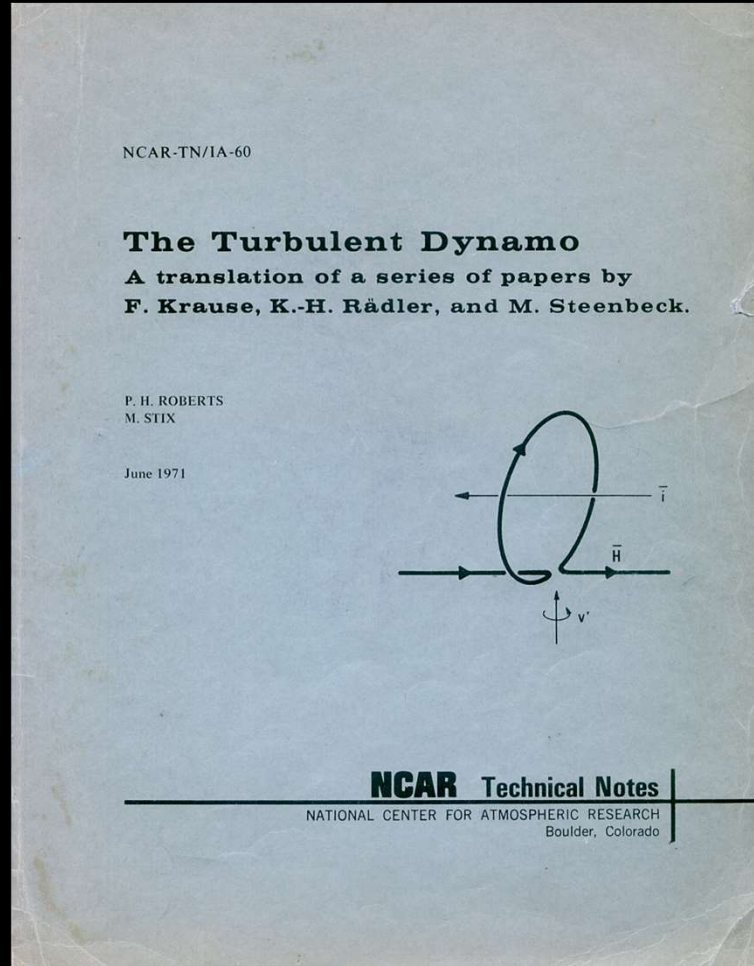
Michael Stix



Karl-Heinz Rädler  
(1935-2020)



Paul H. Roberts  
(1929-2022)



$$\begin{aligned} \Omega_{hknpr}^{(0)}(t') &\equiv \epsilon_{hij} \epsilon_{jkl} \epsilon_{lmn} \frac{\mu\sigma}{2t'} \int G(\xi, t') \epsilon_p \epsilon_r \mathbf{x} \\ &\times (2\pi)^{-3/2} \int \tilde{u}_{im}^{(0)}(\mathbf{h}) \exp(i\mathbf{h} \cdot \xi) d\mathbf{\xi} = \\ &= -\phi(t') \epsilon_{hkn} \delta_{pr} + \frac{2t'}{\mu\sigma} \psi(t') (4\epsilon_{hkn} \delta_{pr} - \epsilon_{hrn} \delta_{pk} - \epsilon_{hpn} \delta_{kr}), \end{aligned} \quad (170)$$

$$\begin{aligned} \Omega_{hnpqr}^{(0)}(t') &\equiv \epsilon_{hij} \epsilon_{jkl} \epsilon_{lmn} \left(\frac{\mu\sigma}{2t'}\right)^2 \int G(\xi, t') \epsilon_k \epsilon_p \epsilon_q \epsilon_r \mathbf{x} \\ &\times (2\pi)^{-3/2} \int \tilde{u}_{im}^{(0)}(\mathbf{h}) \exp(i\mathbf{h} \cdot \xi) d\mathbf{\xi} = \\ &= [\phi(t') - \frac{4t'}{\mu\sigma} \psi(t')] (\epsilon_{hnp} \delta_{qr} + \epsilon_{hnd} \delta_{pr} + \epsilon_{hnr} \delta_{pq}), \end{aligned} \quad (171)$$

$$\begin{aligned} \Omega_{hknpq}^{(1)}(t') &\equiv \epsilon_{hij} \epsilon_{jkl} \epsilon_{lmn} \frac{\mu\sigma}{2t'} \int G(\xi, t') \epsilon_p \mathbf{x} \\ &\times (2\pi)^{-3/2} \int \tilde{u}_{imq}^{(1)}(\mathbf{h}) \exp(i\mathbf{h} \cdot \xi) d\mathbf{\xi} = \\ &= \frac{1}{2} \phi(t') (\epsilon_{hnpq} \delta_{nk} + \epsilon_{npq} \delta_{hk}), \end{aligned} \quad (172)$$

$$\begin{aligned} \Omega_{hnpqr}^{(1)}(t') &\equiv \epsilon_{hij} \epsilon_{jkl} \epsilon_{lmn} \left(\frac{\mu\sigma}{2t'}\right)^2 \int G(\xi, t') \epsilon_k \epsilon_p \epsilon_q \mathbf{x} \\ &\times (2\pi)^{-3/2} \int \tilde{u}_{imr}^{(1)}(\mathbf{h}) \exp(i\mathbf{h} \cdot \xi) d\mathbf{\xi} = \\ &= [-\frac{1}{2} \phi(t') + \frac{2t'}{\mu\sigma} \psi(t')] (\epsilon_{nrq} \delta_{hp} + \epsilon_{nrp} \delta_{hq} + \epsilon_{hrq} \delta_{np} + \epsilon_{hrp} \delta_{nq}), \end{aligned} \quad (173)$$

$$\begin{aligned} \Omega_{hnpqr}^{(2)}(t') &\equiv \epsilon_{hij} \epsilon_{jkl} \epsilon_{lmn} \frac{\mu\sigma}{2t'} \int G(\xi, t') \epsilon_k \epsilon_r \mathbf{x} \\ &\times (2\pi)^{-3/2} \int \tilde{u}_{impq}^{(2)}(\mathbf{h}) \exp(i\mathbf{h} \cdot \xi) d\mathbf{\xi} = \\ &= \frac{t'}{5} \phi(t') (4\epsilon_{hpn} \delta_{qr} + \epsilon_{hqn} \delta_{pr} + \epsilon_{hrn} \delta_{pq}), \end{aligned} \quad (174)$$

P. H. Roberts, M. Stix, The Turbulent Dynamo, 1971

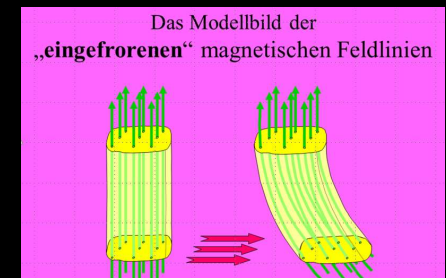


Hannes Alfvén (1908 - 1995)



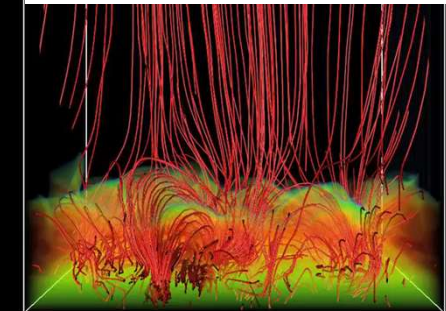
Hannes Alfvén Medaille

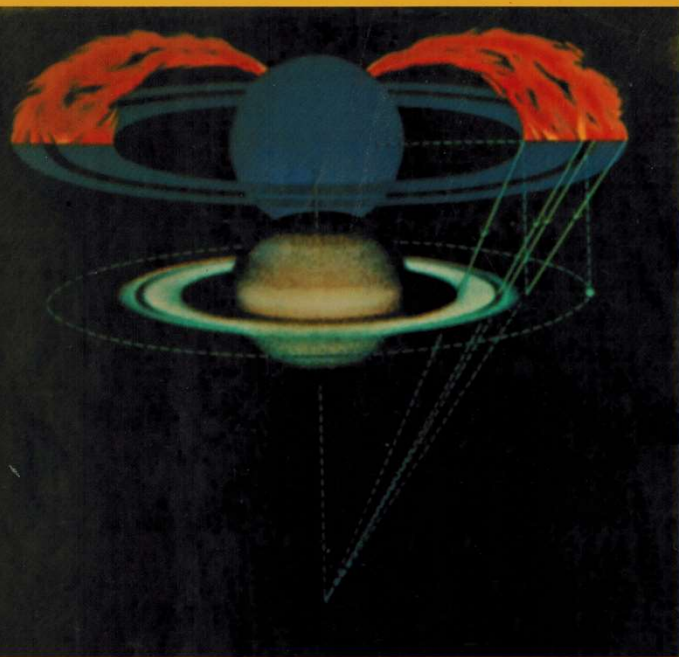
- 1937 Research into plasma physics, charged particle beams
- 1939 Theory of magnetic storms and auroras  
Theory of plasma dynamics in the Earth's magnetosphere  
Work on interplanetary, magnetospheric physics
- 1943 Development of the theorem of the freezing of magnetic field lines in electrically highly conductive matter
- 1970 Nobel Prize in Physics for fundamental achievements and discoveries in magnetohydrodynamics with fruitful applications in plasma physics
- 1976 Summary of his work on the influence of magnetic fields on the origin of our solar system
- 1987 Introduction of the term “nanoflare” to explain coronal heating



the low-frequency Ampère's law  
 $\mu_0 \mathbf{J} = \nabla \times \mathbf{B}$ ,  
Faraday's law  
 $\frac{\partial \mathbf{B}}{\partial t} = -\nabla \times \mathbf{E}$ ,  
and Ohm's law  
 $\mathbf{E} + \mathbf{v} \times \mathbf{B} = \eta \mathbf{J}$ .

Taking the curl of this equation and using Ampère's law and Faraday's law results in the induction equation,  
 $\frac{\partial \mathbf{B}}{\partial t} = \nabla \times (\mathbf{v} \times \mathbf{B}) + \frac{\eta}{\mu_0} \nabla^2 \mathbf{B}$ ,  
where  $\eta/\mu_0$  is the magnetic diffusivity





# Evolution of the Solar System

Hannes Alfvén  
Gustaf Arrhenius

HANNES ALFVEN AND GUSTAF ARRHENIUS

- 12.3 Accretion of an embryo
- 12.4 Mass balance of the jet stream
- 12.5 Energy balance in a jet stream
- 12.6 Accretion when the infall into the jet stream is constant
- 12.7 Discussion
- 12.8 Numerical values
- 12.9 Conclusions about the different types of accretion
- 12.10 Early temperature profile of accreted body
- 12.11 Conclusions about the temperature profile of planets
- 12.12 The accretional hot-spot front
- 12.13 Differentiation effect of the accretional heat front

## 13. Spin and Accretion

- 13.1 Grain impact and spin
- 13.2 Accretion from circular orbits by nongravitating embryo
- 13.3 Gravitational accretion
- 13.4 Giuli's theory of accretion
- 13.5 Statistical theory of accretion
- 13.6 Jet-stream accretion and planetary spins

## 14. Relations Between Comets and Meteoroids

- 14.1 Basic problems
- 14.2 Positive and negative diffusion; meteor streams as jet streams
- 14.3 Accretional mechanism in meteor streams
- 14.4 Observations of comet formation in a meteor stream
- 14.5 Long- and short-period comets
- 14.6 Inferences on the nature of comets from emission characteristics
- 14.7 Analogies between cometary and asteroidal streams
- 14.8 Comparison with the accretion of planets and satellites

## PART C PLASMA AND CONDENSATION

## 15. Plasma Physics and Heterogony

- 15.1 Summary of parts A and B and plan for parts C and D
- 15.2 Relation between experimental and theoretical plasma physics
- 15.3 The first and second approach to cosmic plasma physics
- 15.4 Strategy of analysis of heterogonic plasmas
- 15.5 Required properties of a model
- 15.6 Some existing theories

EVOLUTION OF THE SOLAR SYSTEM

## 16. Model of the Heterogonic Plasma

- 16.1 Magnetized central body
- 16.2 Angular momentum
- 16.3 The transfer of angular momentum
- 16.4 Support of the primordial cloud
- 16.5 The plasma as a transient state
- 16.6 Conclusions about the model
- 16.7 The heterogonic nebulae
- 16.8 Irradiation effects
- 16.9 The model and the heterogonic principle

## 17. Transfer of Angular Momentum and Condensation of Grains

- 17.1 Ferraro isorotation and partial corotation
- 17.2 Partial corotation of a plasma in magnetic and gravitational fields
- 17.3 A plasma in partial corotation
- 17.4 Discussion
- 17.5 Condensation of the plasma: the two-thirds law
- 17.6 Energy release during angular momentum transfer

## 18. Accretion of the Condensation Products

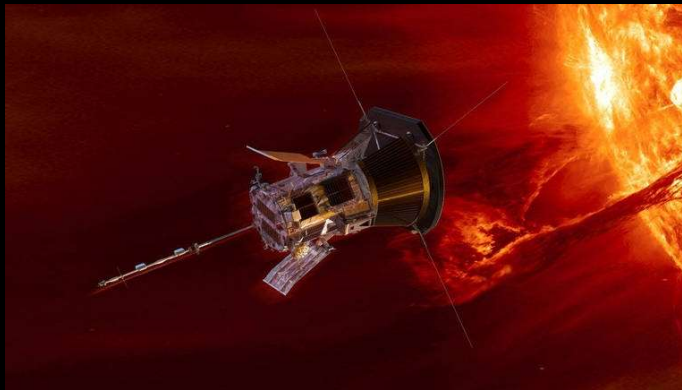
- 18.1 Survey
- 18.2 Evolution of orbits due to collisions
- 18.3 The Roche limit
- 18.4 Model of orbit development
- 18.5 Accretion inside  $r_{MH}$
- 18.6 Structure of the Saturnian rings
- 18.7 Accretion outside  $r_{MR}$
- 18.8 Formation of the asteroid belt
- 18.9 Conclusions about partial corotation
- 18.10 Satellite and planet formation
- 18.11 Accretion of volatile substances

## 19. Transplanetary Condensation

- 19.1 Interplanetary and transplanetary condensation
- 19.2 Limit between interplanetary and transplanetary space
- 19.3 Condensation of bodies in almost-parabolic orbits
- 19.4 Bodies with long-period orbits
- 19.5 Diffusion of almost-parabolic orbits: encounters with planets
- 19.6 Genetic relations of the comet-meteoroid complex
- 19.7 Conclusions about the meteoroid populations
- 19.8 Genealogy of the bodies in the solar system

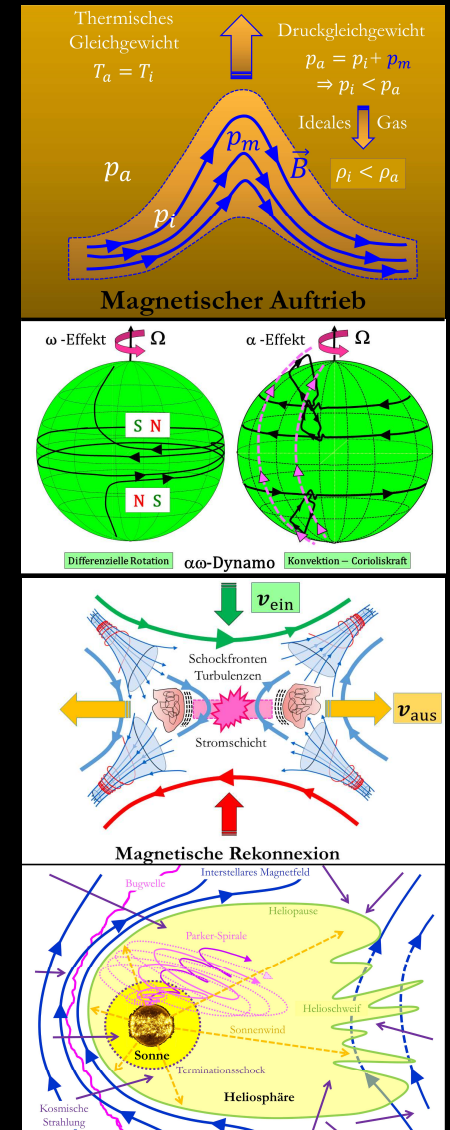


Eugene Newman Parker (1927 - 2022)



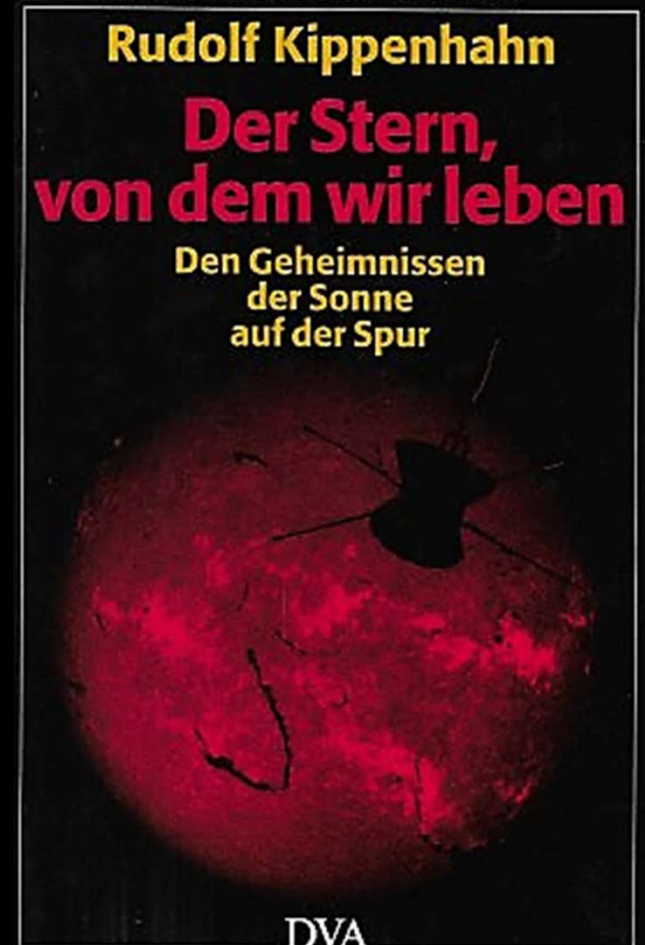
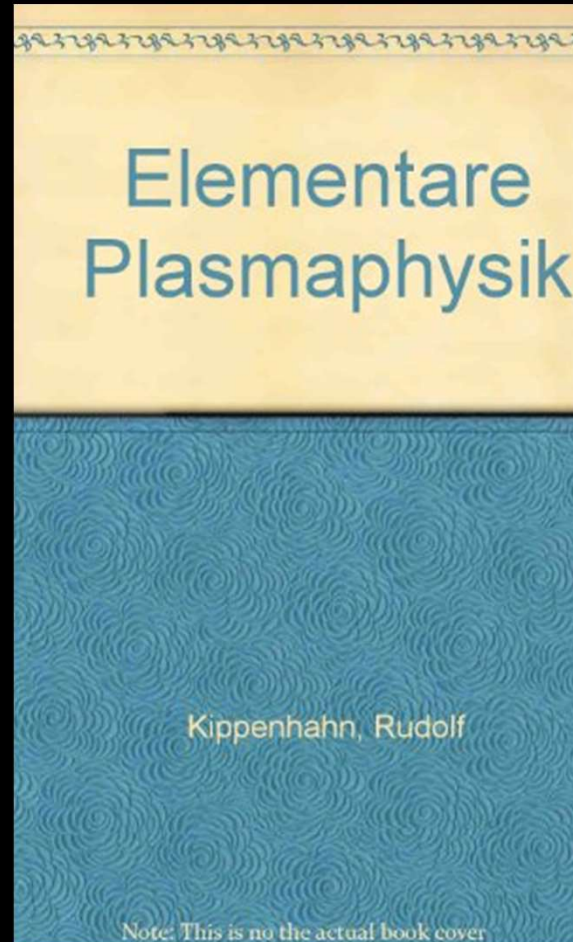
Parker Solar Probe (PSP) NASA/JHUAPL

- 1955 Discovery of **magnetic buoyancy** (“**Parker instability**”) as an upward force exerted on magnetic flux tubes subject to gravity in electrically conductive media
- 1955 Development of the idea that the influence of cyclonic movements (**alpha effect**) could be important for the function of a **dynamo cycle** to generate cosmic magnetic fields
- 1957/1958 Development of the Sweet-Parker model of **magnetic reconnection**
- 1958/1959 Development of a first magneto-hydrodynamic theory to describe the **solar wind model** design for the “**Parker spiral**”
- 1987 Introduction of the term “**nanoflare**” to explain **coronal heating**





Rudolf Kippenhahn (1926-2020)



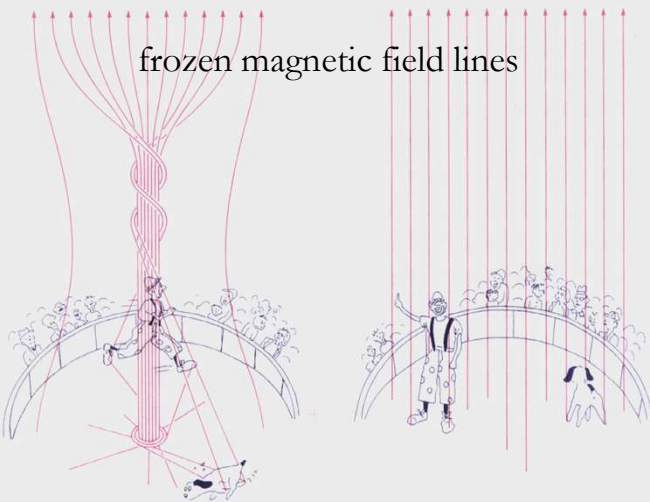


Evi Kippenhahn

# Mr. Tolkin and Mr. Meyer in the Plasmaland Circus

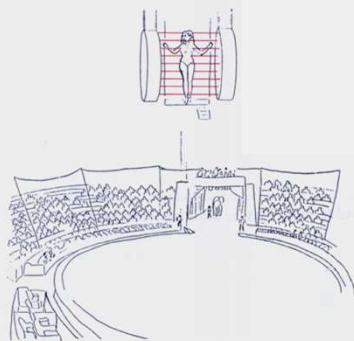


magnetic fields visible through glasses

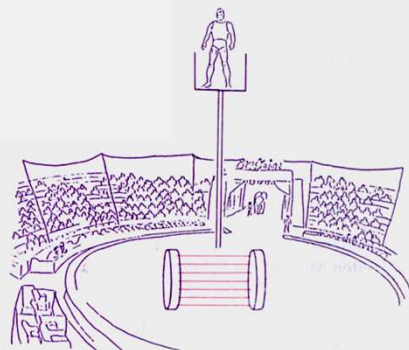


frozen magnetic field lines

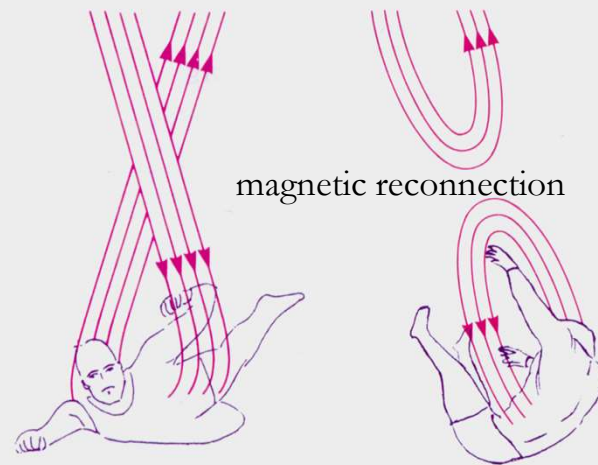
magnetic tension



magnetic pressure



magnetic Alfvén waves



magnetic reconnection

# Fundamentals of Didactic Analysis

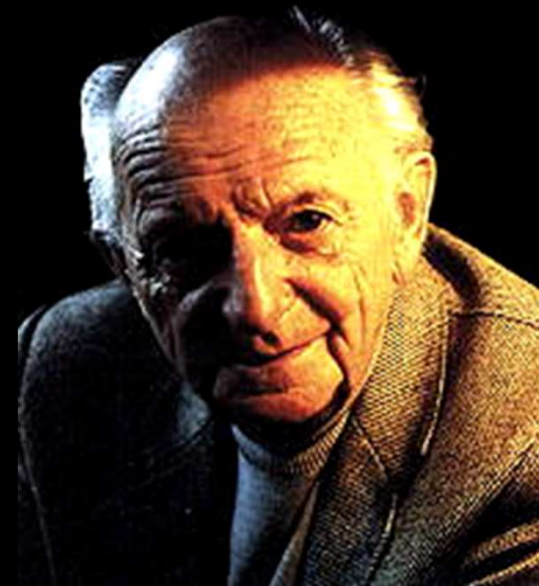
What do you do, why and how?

- Subject Didactics of Mathematics and Natural Sciences
- Scientific Cognitive Psychology
- Didactics of the Exact Natural Sciences
- Principle of Exemplary Learning
- Courage to leave Gaps



Wolfgang Klafki (1927 - 2016)  
German Educational Scientist

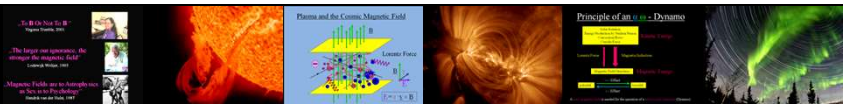
- Motivations
- Addressee References
- Future Significance
- Exemplarity
- Background Structures
- Historical References



Martin Wagenschein (1896 - 1988)  
German Physicist and Educator





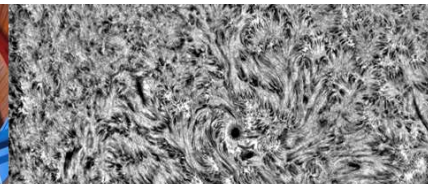
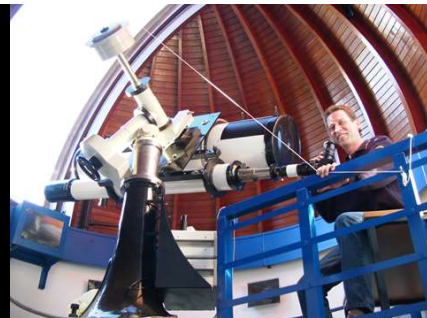
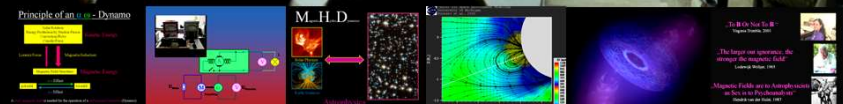


**K.-H. Rädler** ... for Popular Sciences ...  
Ulrich v. Kusserow | Oibers-Gesellschaft e.V. Bremen

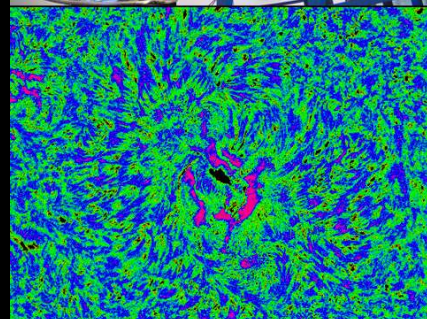


Public Outreach - Didactics - Science  
in the context of  
**Cosmic Magnetic Fields**

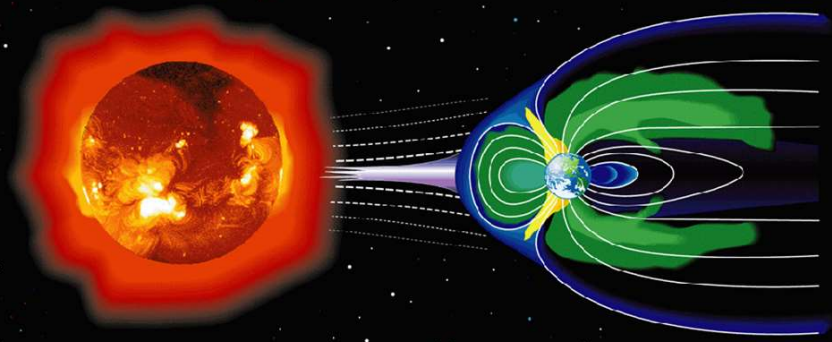
Monday, April 11, 2011, 13:30 h Helmholtz-Zentrum Dresden-Rossendorf



**Universität Bremen**  
THE MAGNETIC SUN  
Laboratory Experiment on Solar Physics for  
Advanced Students



Didactic Aspects of the Topic  
**Space Weather**



Lessons on Cosmic  
Magnetic Fields

Ulrich v. Kusserow  
Helmut Mikelskis

Professur Didaktik der  
Physik

Astrophysik Aktuell



Ulrich von Kusserow

# Magnetischer Kosmos

To B or not to B

SACHBUCH

 Springer Spektrum

Ulrich von Kusserow

# Chaos, Turbulenzen und kosmische Selbst- organisationsprozesse

EBOOK INSIDE

 Springer Spektrum

Ulrich von Kusserow · Eckart Marsch

# Magnetisches Sonnen- system



Solare Eruptionen,  
Sonnenwinde  
und Weltraumwetter

SACHBUCH

 Springer

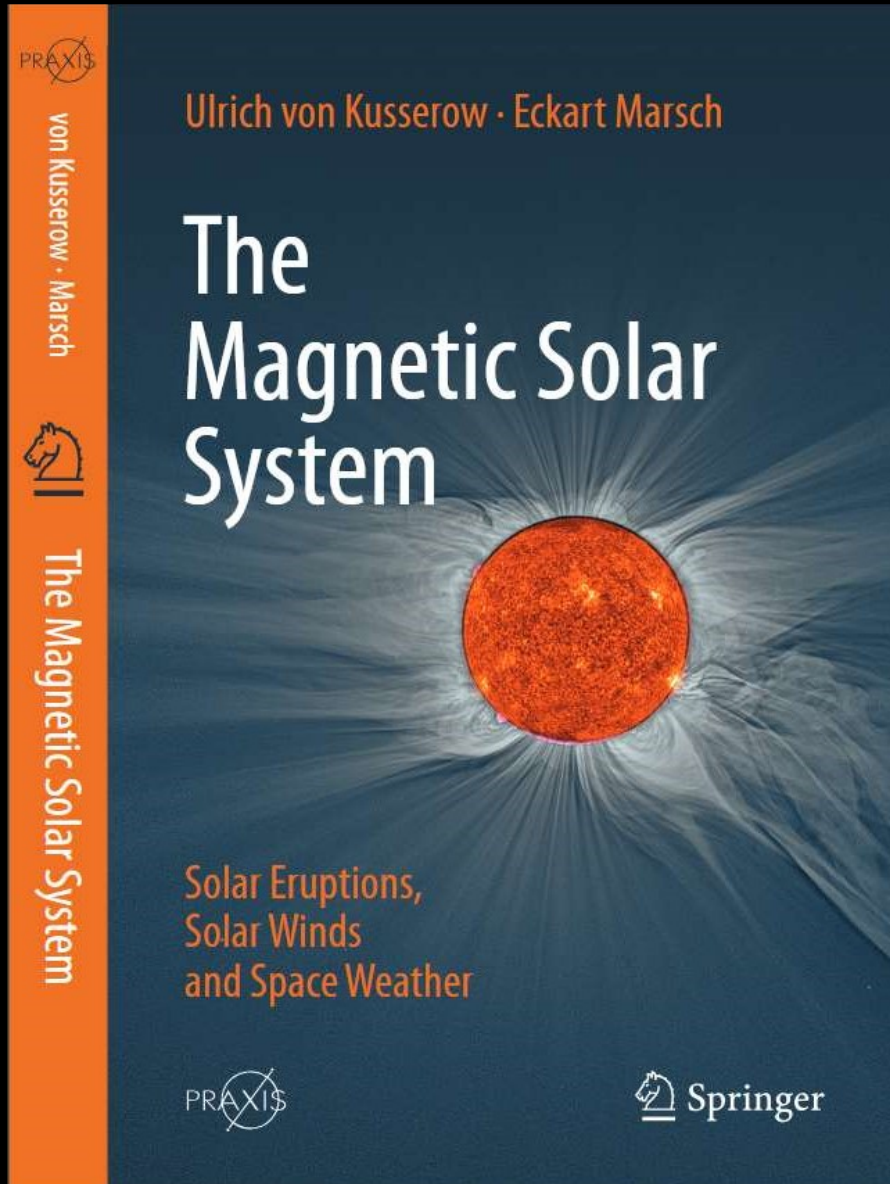


## Table of Contents

Prologue

1. The Solar System and the Heliosphere

2. Exploring the Sun and Heliosphere

3. The Active Magnetic Sun

4. The Solar Wind in Space

5. Parker Solar Probe and Solar Orbiter

6. Obstacles in the Solar Wind

7. Comets and their Tails

8. Magnetospheres, Ionospheres and Auroras

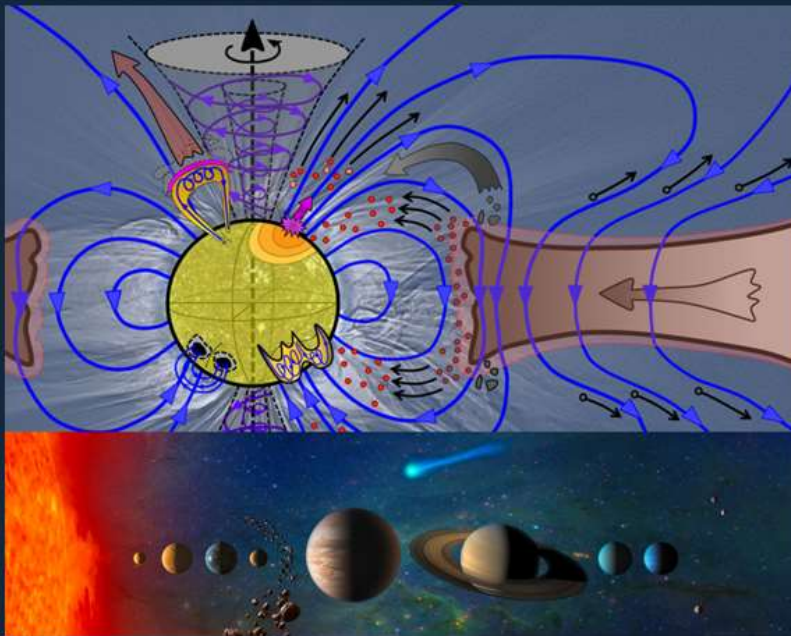
9. Exploring Space Weather

10. Epilogue

On the History of the Discovery of Solar and Heliospheric Processes

Ulrich von Kusserow

Zur **Entstehung** des  
Magnetischen Sonnensystems

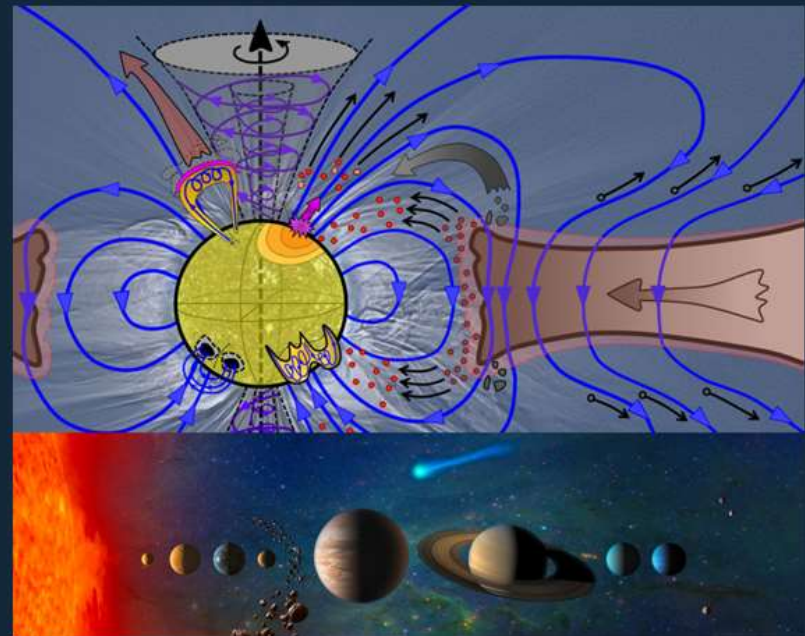


SACHBUCH

 Springer

Ulrich von Kusserow

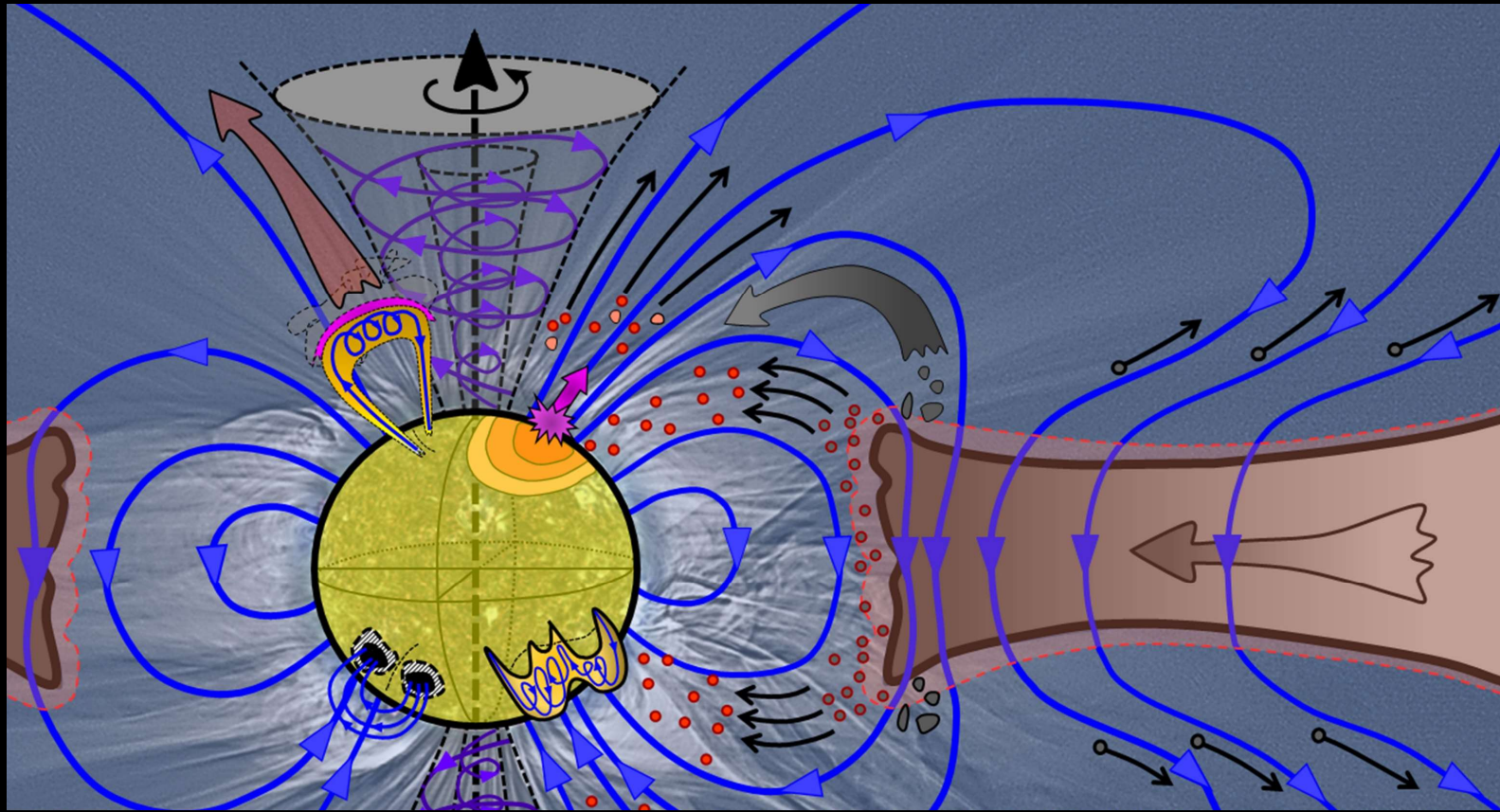
On the **Formation** of the  
Magnetic Solar System



PRAXIS

 Springer





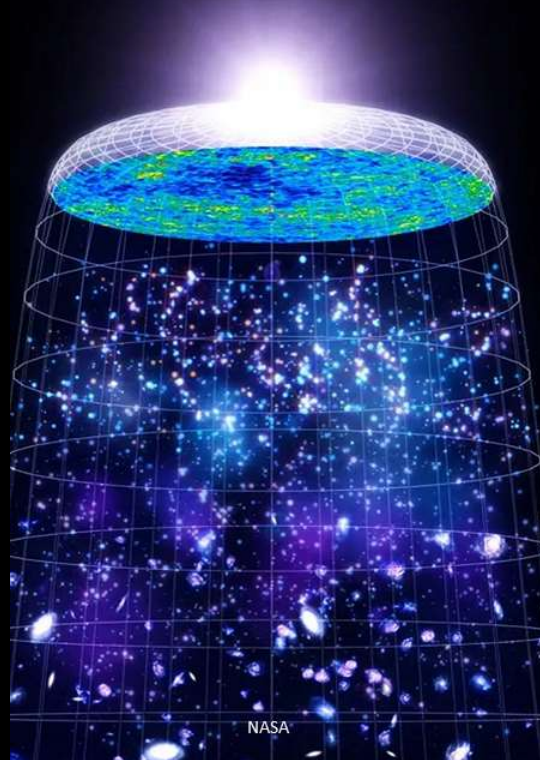
$$\frac{\partial \vec{B}}{\partial t} = \vec{\nabla} \times (\vec{v} \times \vec{B}) - \vec{\nabla} \times (\eta_{OD} \cdot \vec{\nabla} \times \vec{B}) + \vec{\nabla} \times \{ \eta_{AD} \cdot (\vec{\nabla} \times \vec{B}) \times \vec{B} \} - \vec{\nabla} \times [ \vec{\nabla} \times \{ \eta_{HD} \cdot (\vec{\nabla} \times \vec{B}) \times \vec{B} \} ]$$

Adressee References

# Adressee References

- Public Audience
- Amateur Astronomers
- Teachers
- Students
- Scientists

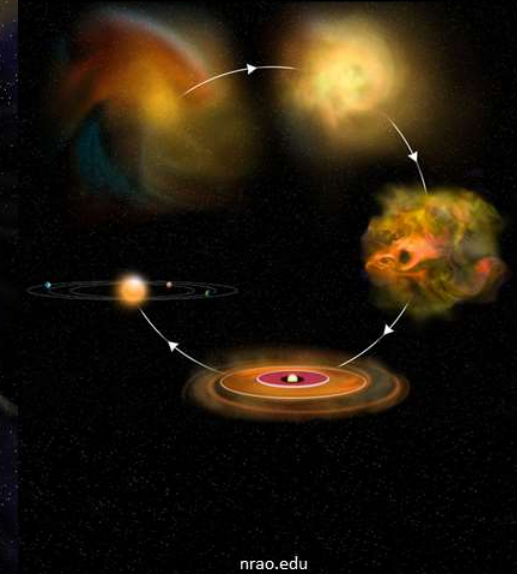
Formation of the Universe



Origin of Life

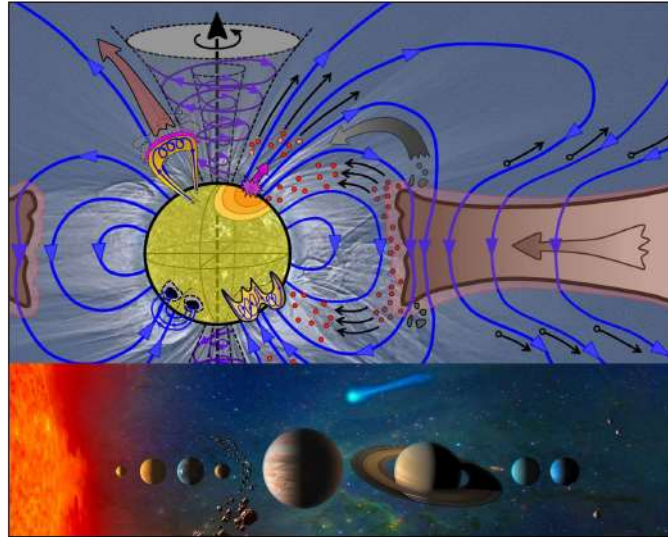


Formation of the Solar System



# Adressee References

- **Public Audience**
- Amateur Astronomers
- Teachers
- Students
- Scientists



U. v. Kusserow, M. Druckmüller, NASA

## Zur Entstehung des magnetischen Sonnensystems

Ulrich von Kusserow, Bremen

Seit der Antike haben Philosophen und Naturwissenschaftler, Astrophysiker und Planetenforscher eine Vielzahl unterschiedlicher Modellvorstellungen über die Entstehung unseres Sonnensystems entwickelt. Die Entdeckung und vergleichende Analyse extrasolarer Planetensysteme sonnenähnlicher Sterne, hochauflösende Abbildungen solcher extrem jungen Sternsysteme, die Auswertung umfangreichen Datenmaterials sowie gewonnene Erkenntnisse an-hand der Ergebnisse analytischer Modellrechnungen und Numerischer Simulationen mit Hilfe besonders leistungsfähiger Computer haben heute die Entwicklung relativ verlässlicher Theorien ermöglicht. Danach entstand die Protosonne durch den gravitativen Kollaps einer riesigen Molekül- und Staubwolke, bildeten sich die Planeten in der diesen sehr jungen Stern umkreisenden Akkretionsscheibe durch Agglomeration von zunehmend größer werdenden Materieverdichtungen aus. Außer der oft dominierenden Gravitation, den Turbulenzen, Instabilitäten sowie dem effektiven Drehimpulstransport in solchen rotierenden Systemen müssen dabei nachweislich insbesondere auch magnetische Prozesse eine zentrale Rolle gespielt haben.

In diesem reich bebilderten sowie durch Videosequenzen anschaulich gestalteten Vortrag werden die neuesten Ergebnisse zur Entstehung und Entwicklung extrasolarer junger protostellarer Systeme unter besonderer Berücksichtigung des Einflusses kosmischer Magnetfelder vorgestellt. Es wird erläutert, welche frühen Entwicklungsphasen das heutige Erscheinungsbild unseres so speziellen magnetischen Sonnensystems hervorgebracht haben könnten.

## Adressee References

- Public Audience
- **Amateur Astronomers**
- Teachers
- Students
- Scientists



LDN 1471: A Windblown Star Cavity - HST , NASA, ESA; Processing & License: Judy Schmidt

# Adressee References

- Public Audience
- **Amateur Astronomers**
- Teachers
- Students
- Scientists



## Adressee References

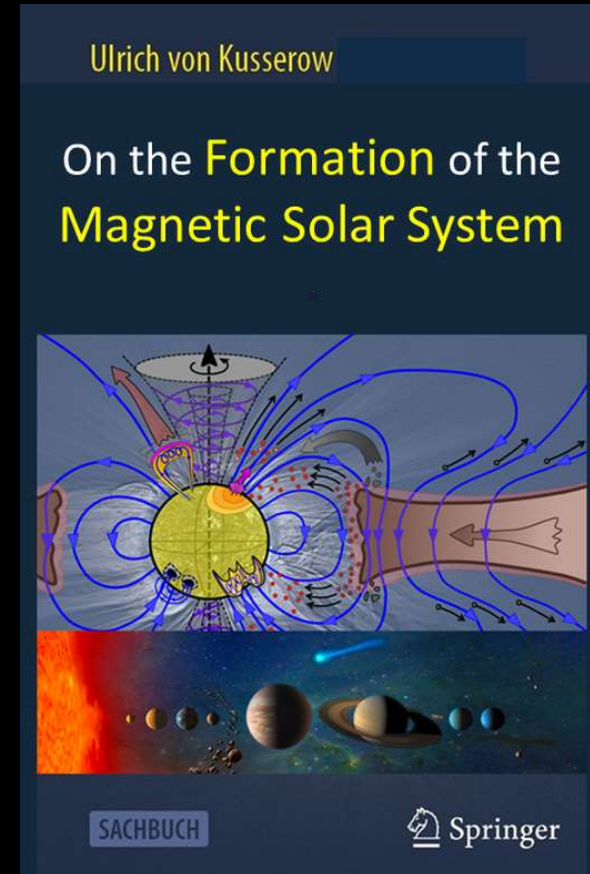
- Public Audience
- Amateur Astronomers
- **Teachers**
- Students
- Scientists





## Adressee References

- Public Audience
- Amateur Astronomers
- Teachers
- **Students**
- Scientists





## Adressee References

- Public Audience
- Amateur Astronomers
- Teachers
- Students
- **Scientists**



Participants "Protostars and Planets VII", 2023 Kyoto

# 19th MHD Days 2024

2–4 Dec 2024  
Leibniz Institute for Astrophysics Potsdam (AIP)

Mo. 02/12

14:00	<b>Opening</b> <i>Lecture Hall, Maria Margaretha Kirch Building, Leibniz Institute for Astrophysics Potsdam (AIP)</i>	<i>Oliver Gressel</i> 14:00 - 14:10
	<b>Interplays between dynamo and magneto-rotational instabilities</b> <i>Lecture Hall, Maria Margaretha Kirch Building, Leibniz Institute for Astrophysics Potsdam (AIP)</i>	<i>Axel Brandenburg</i> 14:10 - 14:50
15:00	<b>Sunspot simulations with potential field initial conditions</b> <i>Lecture Hall, Maria Margaretha Kirch Building, Leibniz Institute for Astrophysics Potsdam (AIP)</i>	<i>Markus Schmassmann</i> 14:50 - 15:10
	<b>Solar magnetic tornadoes ignite ambient shock waves: The surprising story of how torsional Alfvén waves can dissipate</b> <i>Oskar Steiner</i>	
	<b>Break</b> <i>Lecture Hall, Maria Margaretha Kirch Building, Leibniz Institute for Astrophysics Potsdam (AIP)</i>	15:30 - 16:00
16:00	<b>Harmonically forced and synchronized dynamos</b> <i>Lecture Hall, Maria Margaretha Kirch Building, Leibniz Institute for Astrophysics Potsdam (AIP)</i>	<i>Frank Stefani</i> 16:00 - 16:20
	<b>Orbit-Spin Coupling and Variations in the Length of the Hale Cycle</b> <i>Lecture Hall, Maria Margaretha Kirch Building, Leibniz Institute for Astrophysics Potsdam (AIP)</i>	<i>James Shirley</i> 16:20 - 16:40
	<b>Deep cyclic magnetic activity of the Sun by assimilating long-term observed photospheric magnetograms in a 3D dyna...</b> <i>Gopal Hazra</i>	
17:00	<b>Evaluating solar-like behavior in extra-long non-kinematic flux-transport solar dynamos</b> <i>Lecture Hall, Maria Margaretha Kirch Building, Leibniz Institute for Astrophysics Potsdam (AIP)</i>	<i>Fadil Inceoglu</i> 17:00 - 17:20

Di. 03/12

09:00	<b>Magnetic Fields and Cosmic Ray Electrons (CREs) in Halos of Star Forming Disk Galaxies</b> <i>Lecture Hall, Maria Margaretha Kirch Building, Leibniz Institute for Astrophysics Potsdam (AIP)</i>	<i>Ralf-Juergen Dettmar</i> 09:00 - 09:20
	<b>Zooming-in on radio relics: How density fluctuations explain the Mach number discrepancy, microgauss magnetic field...</b> <i>Joseph Whitnigham</i>	
	<b>Cosmic magnetic fields: A new window to the fundamental physics of the early Universe</b> <i>Lecture Hall, Maria Margaretha Kirch Building, Leibniz Institute for Astrophysics Potsdam (AIP)</i>	<i>Jennifer Schober</i> 09:40 - 10:00
10:00	<b>Early magnetic field growth in galaxy clusters; the crucial contribution from galaxy formation physics</b> <i>Lecture Hall, Maria Margaretha Kirch Building, Leibniz Institute for Astrophysics Potsdam (AIP)</i>	<i>Larissa Tevlin</i> 10:00 - 10:20
	<b>Turbulent plasma flow, its energies and structures: velocity vortices, magnetic field cocoons and plasmoids</b> <i>Lecture Hall, Maria Margaretha Kirch Building, Leibniz Institute for Astrophysics Potsdam (AIP)</i>	<i>Petr Jellinek</i> 10:20 - 10:40
	<b>Break</b> <i>Lecture Hall, Maria Margaretha Kirch Building, Leibniz Institute for Astrophysics Potsdam (AIP)</i>	10:40 - 11:00
11:00	<b>Taylor Instability Revisited</b> <i>Lecture Hall, Maria Margaretha Kirch Building, Leibniz Institute for Astrophysics Potsdam (AIP)</i>	<i>Valentin Skoutnev</i> 11:00 - 11:20
	<b>Stability of toroidal magnetic fields in radiative stellar interiors</b> <i>Lecture Hall, Maria Margaretha Kirch Building, Leibniz Institute for Astrophysics Potsdam (AIP)</i>	<i>Giovanni Licciardello</i> 11:20 - 11:40
	<b>Stability of toroidal magnetic fields in radiative stellar interiors: insights from direct numerical simulations and stellar e...</b> <i>Domenico G. Meduri</i>	
12:00	<b>MHD and the Formation of the Magnetic Solar System - A didactically oriented approach</b> <i>Lecture Hall, Maria Margaretha Kirch Building, Leibniz Institute for Astrophysics Potsdam (AIP)</i>	<i>Ulrich von Kusserow</i> 12:00 - 12:20
	<b>Group photo</b> <i>Lecture Hall, Maria Margaretha Kirch Building, Leibniz Institute for Astrophysics Potsdam (AIP)</i>	12:20 - 12:30

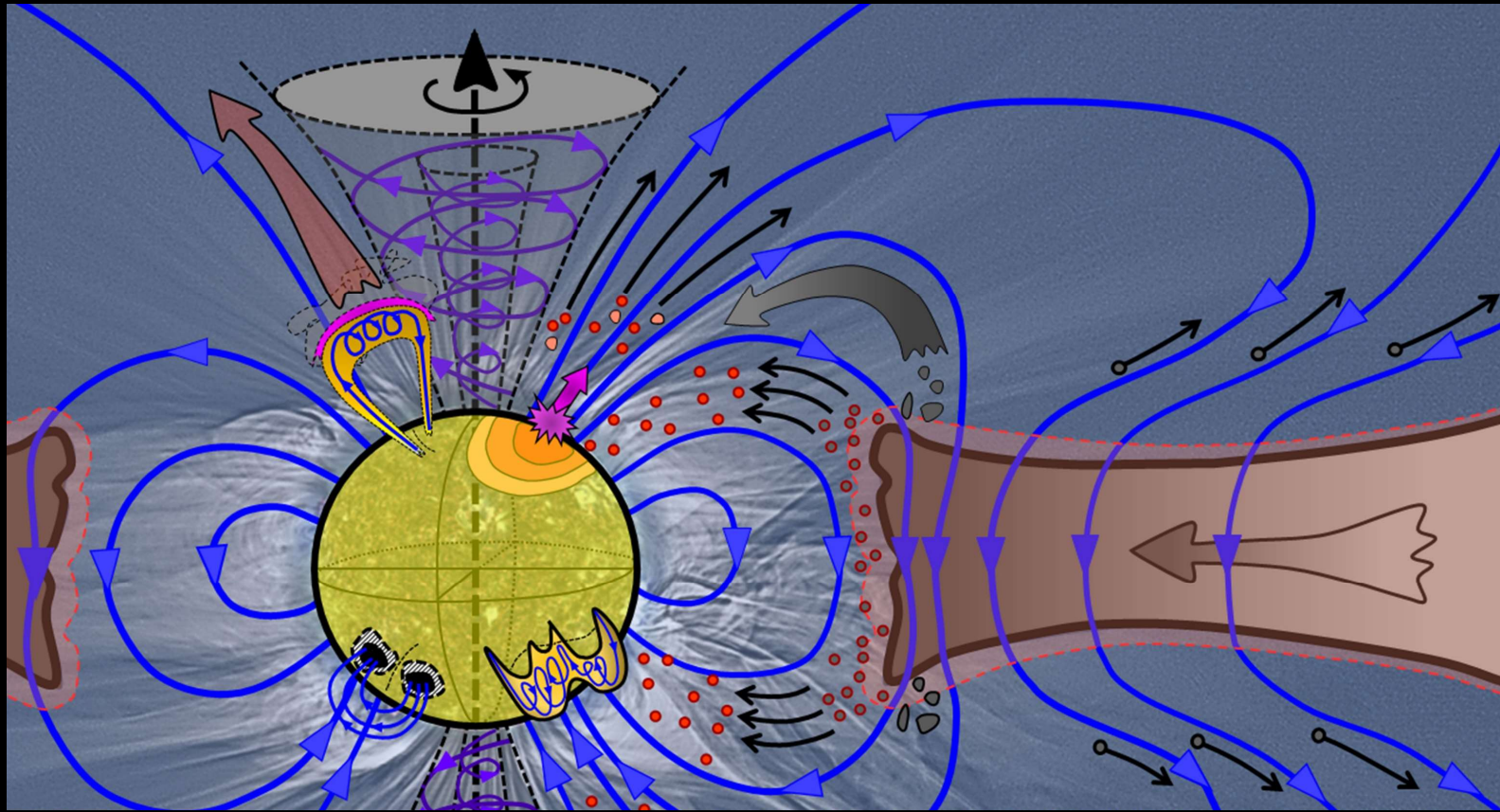
# 19th MHD Days 2024

2–4 Dec 2024  
Leibniz Institute for Astrophysics Potsdam (AIP)

Mi, 04/12

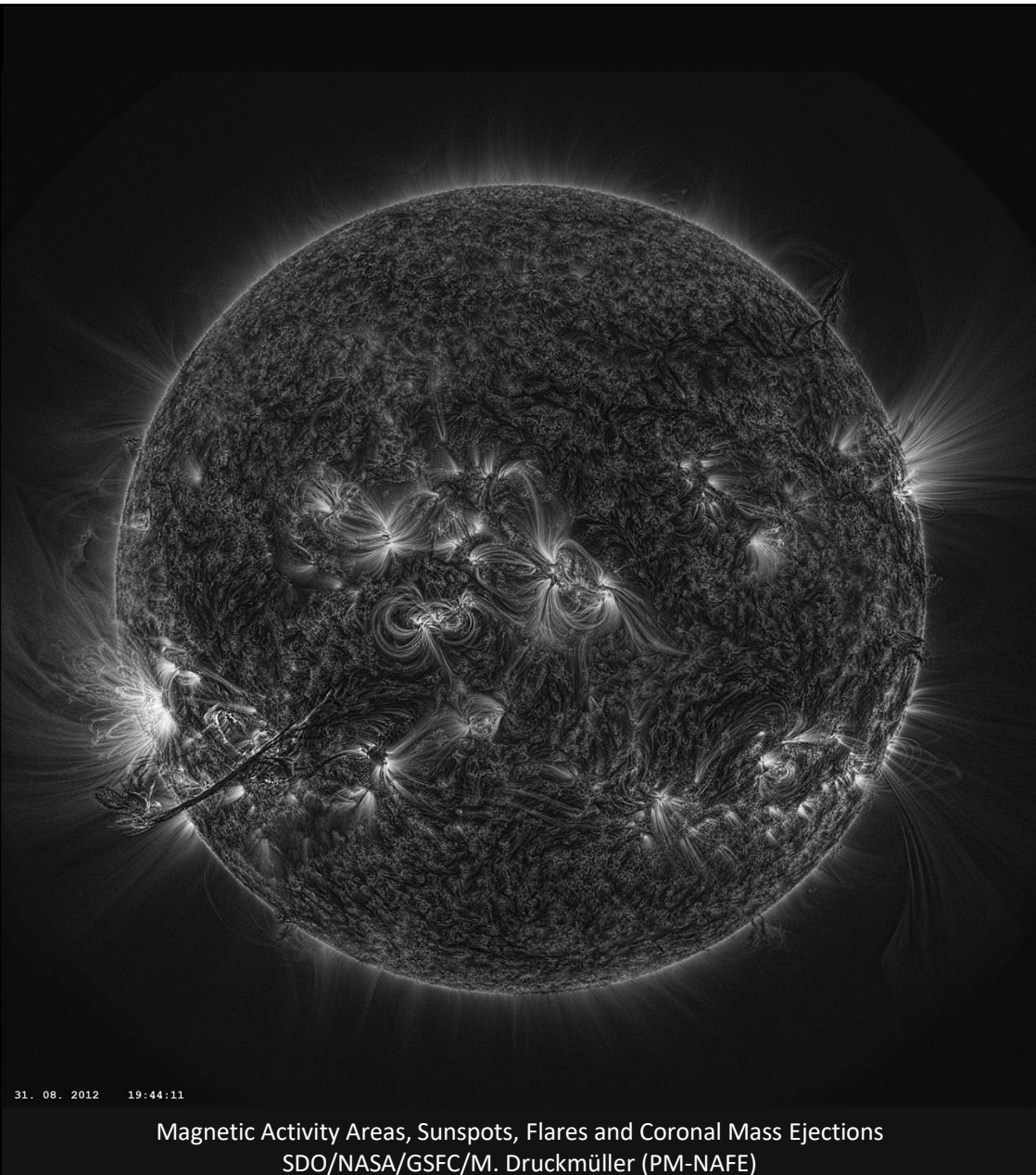
14:00	<b>Liquid metal MHD flows in the water-cooled lead lithium test blanket module for ITER</b> <i>Lecture Hall, Maria Margaretha Kirch Building, Leibniz Institute for Astrophysics Potsdam (AIP)</i>	<i>Leo Bühler</i> 14:00 - 14:20
	<b>Corner-mode instability of Rayleigh-Bénard convection in a vertical magnetic field</b> <i>Lecture Hall, Maria Margaretha Kirch Building, Leibniz Institute for Astrophysics Potsdam (AIP)</i>	<i>Thomas Boeck</i> 14:20 - 14:40
	<b>Convective instabilities in liquid metal duct flow in a fringing magnetic field</b> <i>Lecture Hall, Maria Margaretha Kirch Building, Leibniz Institute for Astrophysics Potsdam (AIP)</i>	<i>Chiara Mistrangelo</i> 14:40 - 15:00
15:00	<b>Two-dimensional Radiative MHD Rayleigh-Bénard Convection in Molten Salts</b> <i>Lecture Hall, Maria Margaretha Kirch Building, Leibniz Institute for Astrophysics Potsdam (AIP)</i>	<i>Panxin Li</i> 15:00 - 15:20
	<b>3D magneto-convective instabilities of liquid metal flow in a generic engineering-relevant model geometry</b> <i>Lecture Hall, Maria Margaretha Kirch Building, Leibniz Institute for Astrophysics Potsdam (AIP)</i>	<i>Biao Lyu</i> 15:20 - 15:40
	<b>Break</b> <i>Lecture Hall, Maria Margaretha Kirch Building, Leibniz Institute for Astrophysics Potsdam (AIP)</i>	15:40 - 16:00
16:00	<b>The Hall Effect in Neutron Stars</b> <i>Lecture Hall, Maria Margaretha Kirch Building, Leibniz Institute for Astrophysics Potsdam (AIP)</i>	<i>Rainer Hollerbach</i> 16:00 - 16:20
	<b>Dynamo action in a precessing cylinder.</b> <i>Lecture Hall, Maria Margaretha Kirch Building, Leibniz Institute for Astrophysics Potsdam (AIP)</i>	<i>Andre Giesecke</i> 16:20 - 16:40
	<b>Nonlinear flow transition in a precessing cylinder and its potential for hydromagnetic dynamo action at the DRESDYN f...</b> <i>Thomas Gundrum</i>	
17:00	<b>Characterizing dynamo coefficients in accretion disk turbulence</b> <i>Lecture Hall, Maria Margaretha Kirch Building, Leibniz Institute for Astrophysics Potsdam (AIP)</i>	<i>Oliver Gressel</i> 17:00 - 17:20
	<b>Global R-MHD simulations of Transition Disks</b> <i>Lecture Hall, Maria Margaretha Kirch Building, Leibniz Institute for Astrophysics Potsdam (AIP)</i>	<i>Eleftheria Sarafidou</i> 17:20 - 17:40

09:00	<b>Model reduction for MHD turbulence</b> <i>Lecture Hall, Maria Margaretha Kirch Building, Leibniz Institute for Astrophysics Potsdam (AIP)</i>	<i>Wolf-Christian Müller</i> 09:00 - 09:20
	<b>Exact Nonlinear Decomposition of Ideal-MHD Waves Using Eigenenergies</b> <i>Lecture Hall, Maria Margaretha Kirch Building, Leibniz Institute for Astrophysics Potsdam (AIP)</i>	<i>Abbas Raboonik</i> 09:20 - 09:40
	<b>As a matter of dynamical range – scale-dependent energy dynamics in magnetized turbulence and pushing simulation l...</b> <i>Philipp Grete</i>	
10:00	<b>Solving plasma problems using adaptive multiphysics coupling.</b> <i>Lecture Hall, Maria Margaretha Kirch Building, Leibniz Institute for Astrophysics Potsdam (AIP)</i>	<i>Simon Candelaresi</i> 10:00 - 10:20
	<b>Spatio-temporal correlation in three-dimensional incompressible MHD turbulence</b> <i>Lecture Hall, Maria Margaretha Kirch Building, Leibniz Institute for Astrophysics Potsdam (AIP)</i>	<i>Raquel Mausle</i> 10:20 - 10:40
	<b>Break</b> <i>Lecture Hall, Maria Margaretha Kirch Building, Leibniz Institute for Astrophysics Potsdam (AIP)</i>	10:40 - 11:00
11:00	<b>tbd.</b> <i>Lecture Hall, Maria Margaretha Kirch Building, Leibniz Institute for Astrophysics Potsdam (AIP)</i>	11:00 - 11:20
	<b>Capturing and modeling the launching of a jet around a forming massive star</b> <i>Lecture Hall, Maria Margaretha Kirch Building, Leibniz Institute for Astrophysics Potsdam (AIP)</i>	<i>André Oliva</i> 11:20 - 11:40
	<b>Non-ideal MHD processes in astrophysical jets</b> <i>Lecture Hall, Maria Margaretha Kirch Building, Leibniz Institute for Astrophysics Potsdam (AIP)</i>	<i>Giancarlo Mattia</i> 11:40 - 12:00
12:00	<b>Impact of magnetically-driven jets and radiative feedback on the formation of massive stars</b> <i>Lecture Hall, Maria Margaretha Kirch Building, Leibniz Institute for Astrophysics Potsdam (AIP)</i>	<i>Joshua Barquero Alvarado</i> 12:00 - 12:20
	<b>Closing</b> <i>Lecture Hall, Maria Margaretha Kirch Building, Leibniz Institute for Astrophysics Potsdam (AIP)</i>	<i>Rainer Arit</i> 12:20 - 12:30



$$\frac{\partial \vec{B}}{\partial t} = \vec{\nabla} \times (\vec{v} \times \vec{B}) - \vec{\nabla} \times (\eta_{OD} \cdot \vec{\nabla} \times \vec{B}) + \vec{\nabla} \times \{ \eta_{AD} \cdot (\vec{\nabla} \times \vec{B}) \times \vec{B} \} - \vec{\nabla} \times [ \vec{\nabla} \times \{ \eta_{HD} \cdot (\vec{\nabla} \times \vec{B}) \times \vec{B} \} ]$$

Motivations

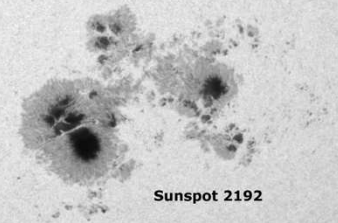


31. 08. 2012 19:44:11

Magnetic Activity Areas, Sunspots, Flares and Coronal Mass Ejections  
SDO/NASA/GSFC/M. Druckmüller (PM-NAFE)

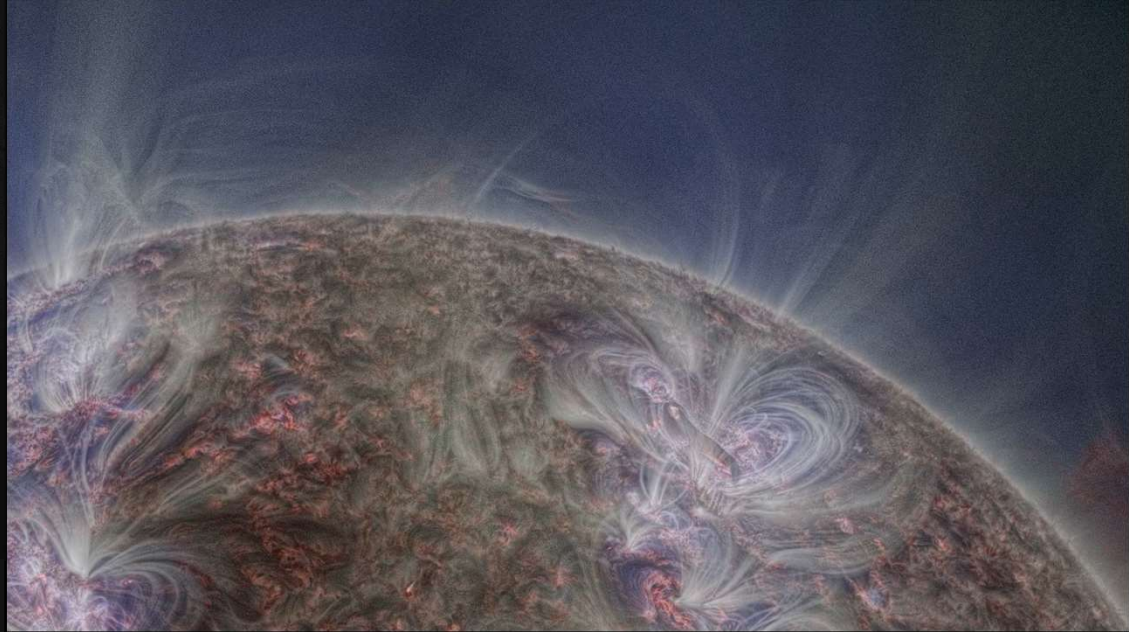
### X3.1 Flare, October 24, 2014

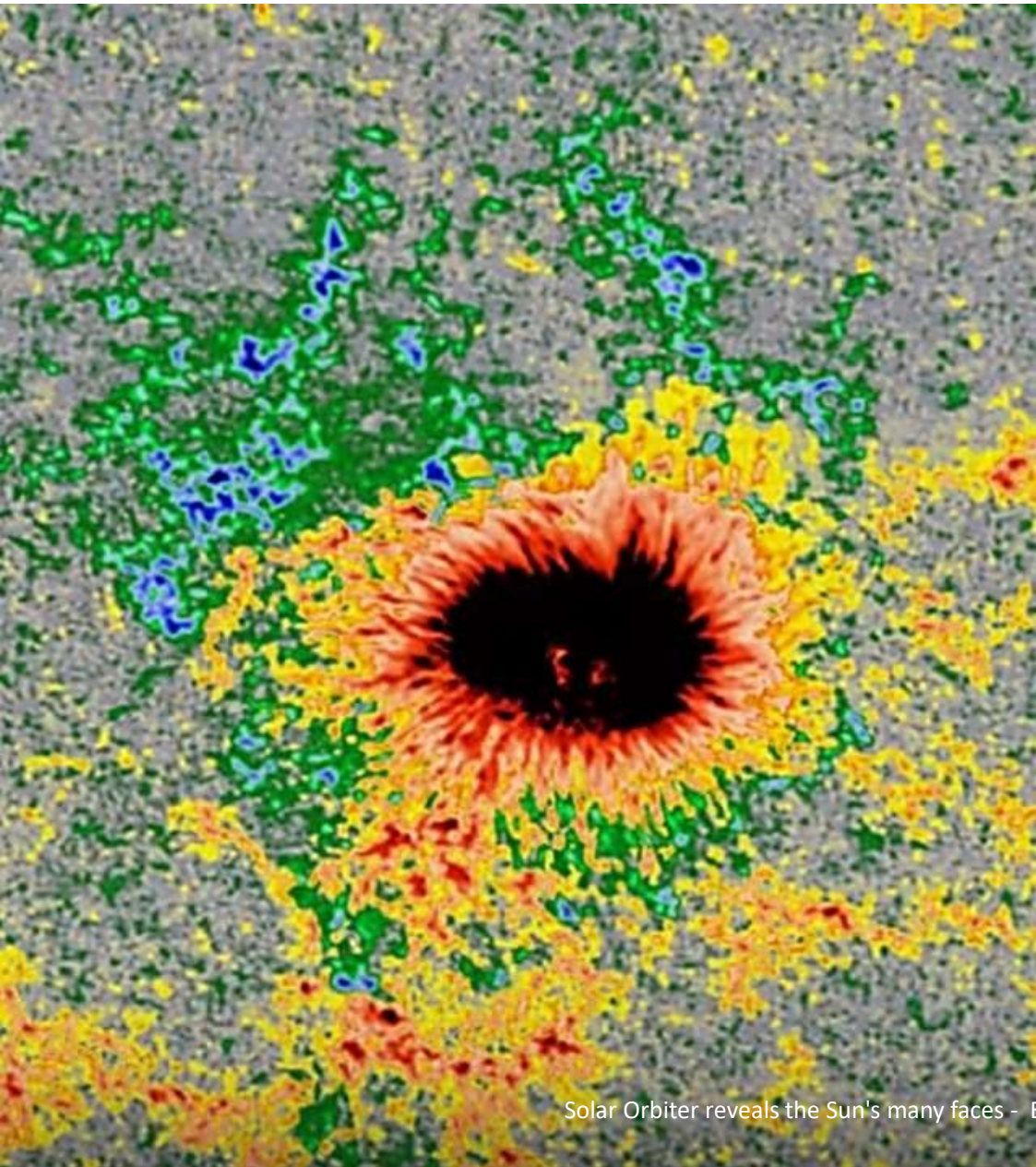
SDO AIA 304 A, 171 A, 211 A, PM-NAFE processing & HMI



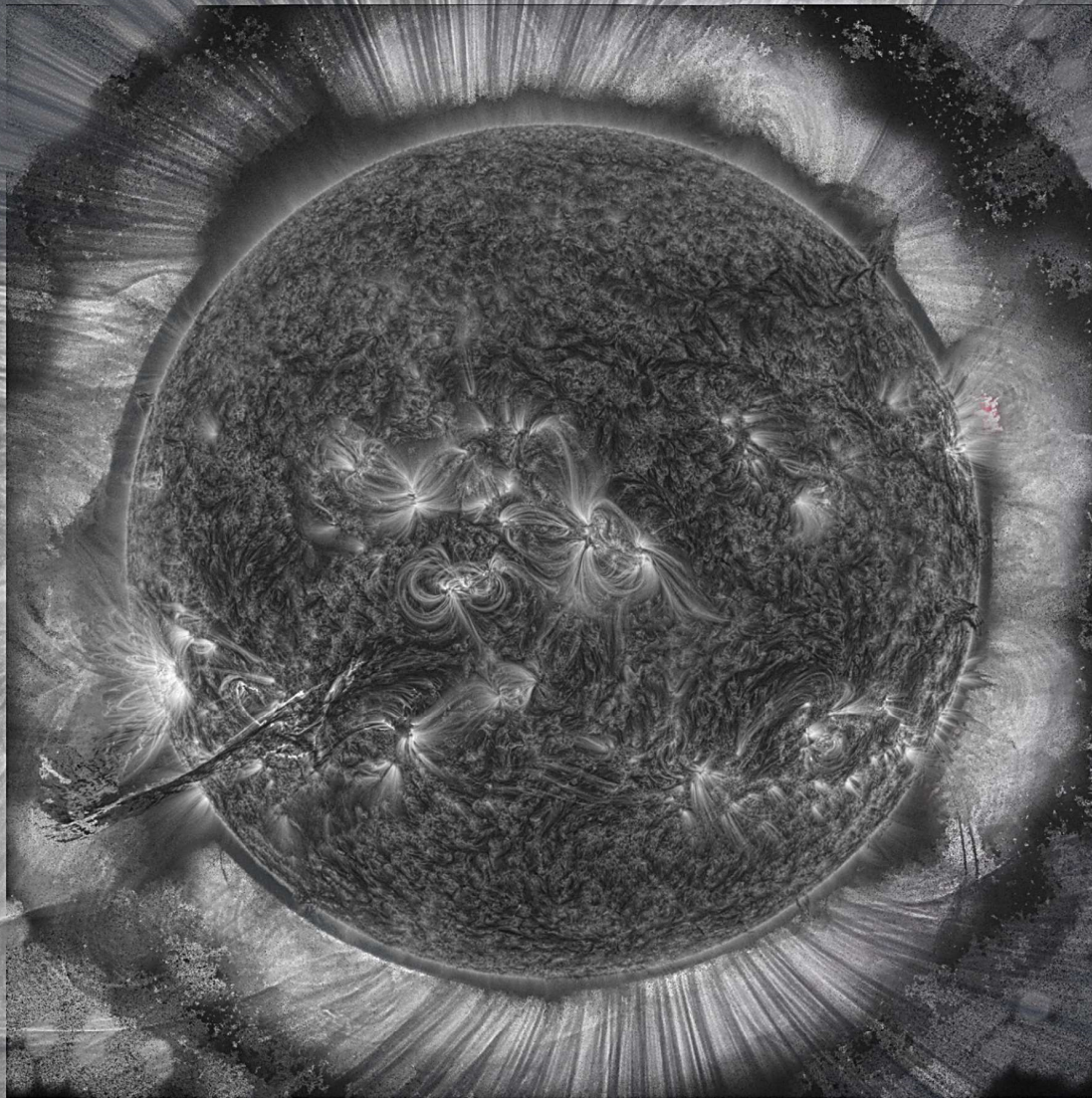
Sunspot 2192

© 2015 Miloslav Druckmüller

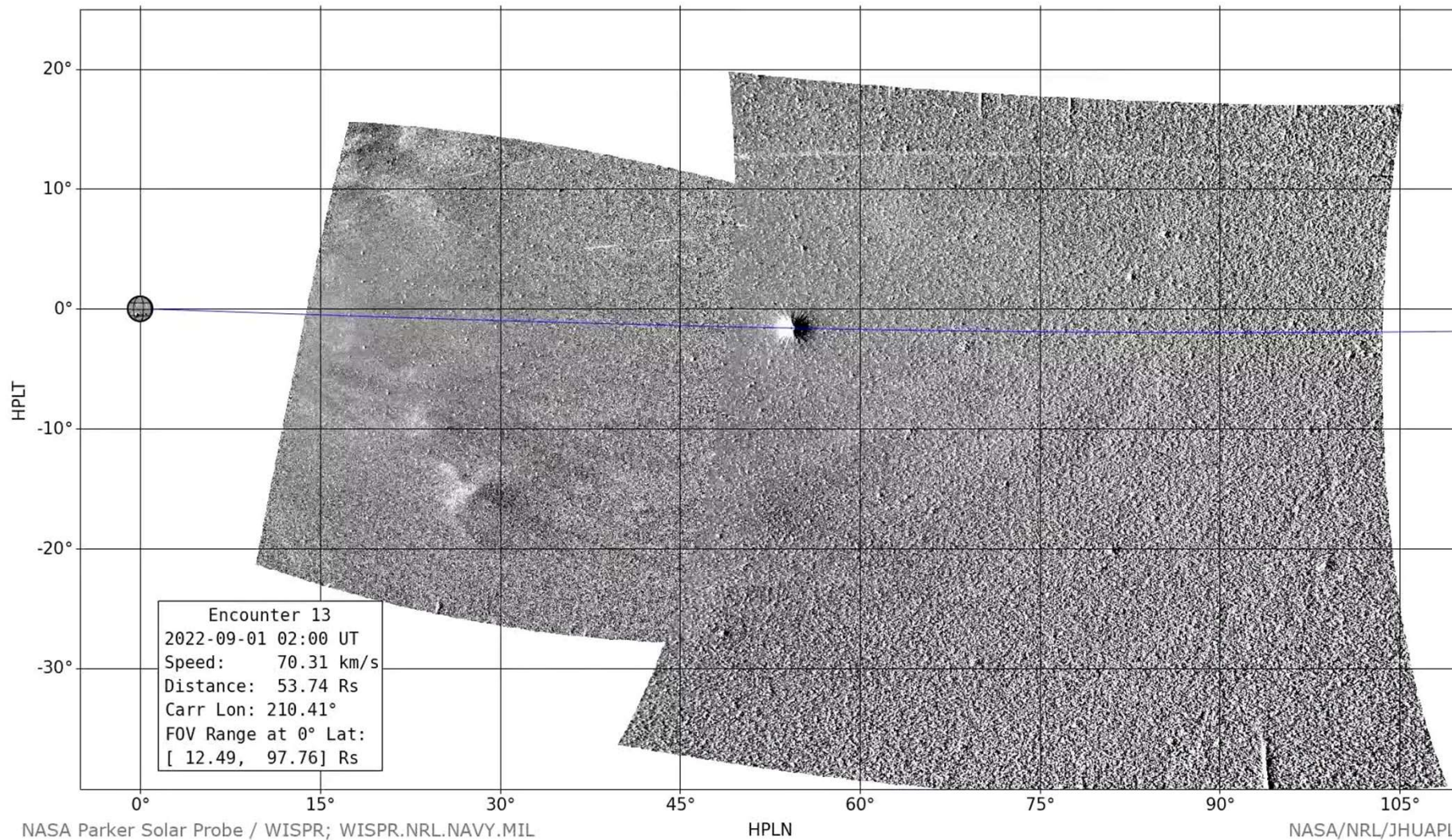




Solar Orbiter reveals the Sun's many faces - ESA & NASA/Solar Orbiter/PHI and EUI Teams



The Magnetic Sun, Corona and Solar Wind  
SDO/NASA/GSFC/M. Druckmüller (PM-NAFE)/U. v. Kusserow (Editing)



Conversion of measured signals into audio signals during a coronal mass ejection

NASA/Johns Hopkins APL/Naval Research Laboratory/Brendan Gallagher/Guillermo Stenborg/Emmanuel Masongsong/Lizet Casillas/Robert Alexander/David Malaspina

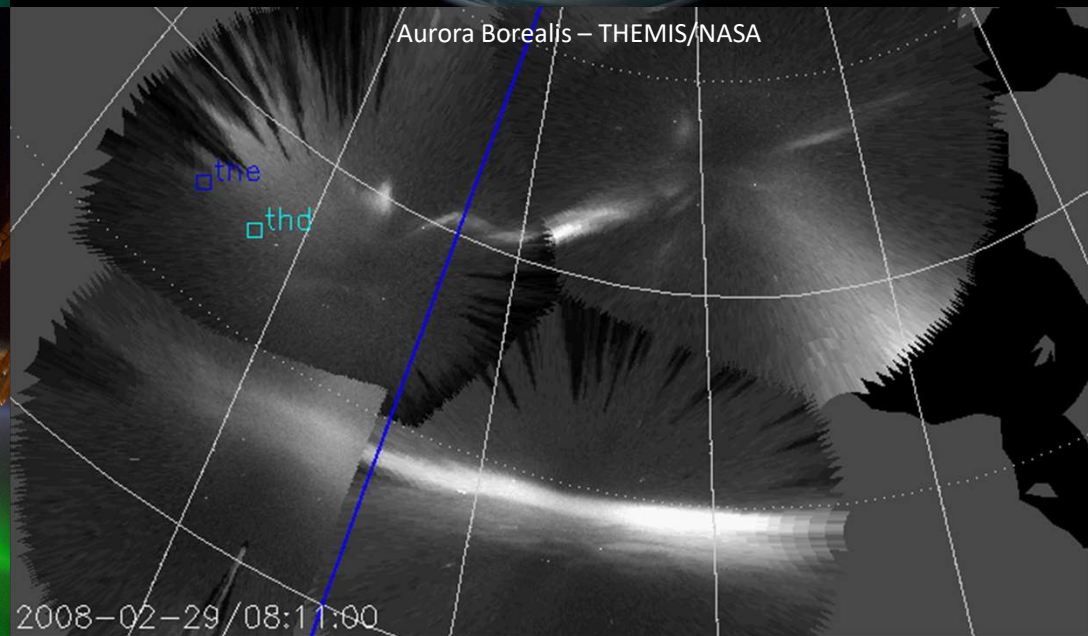


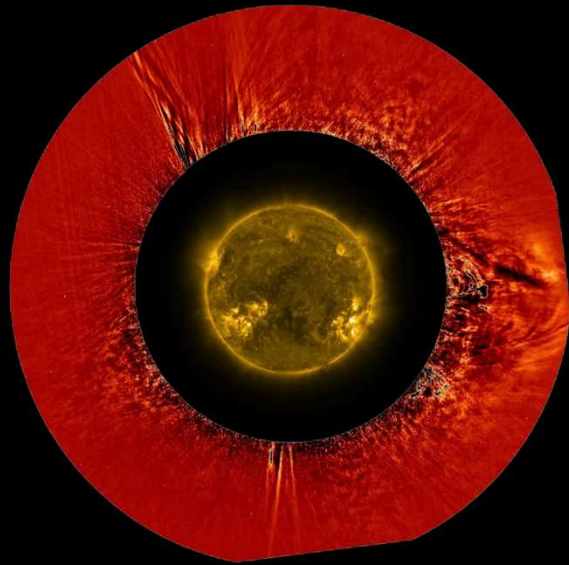


Aurora Borealis - Alexander Gerst, ESA

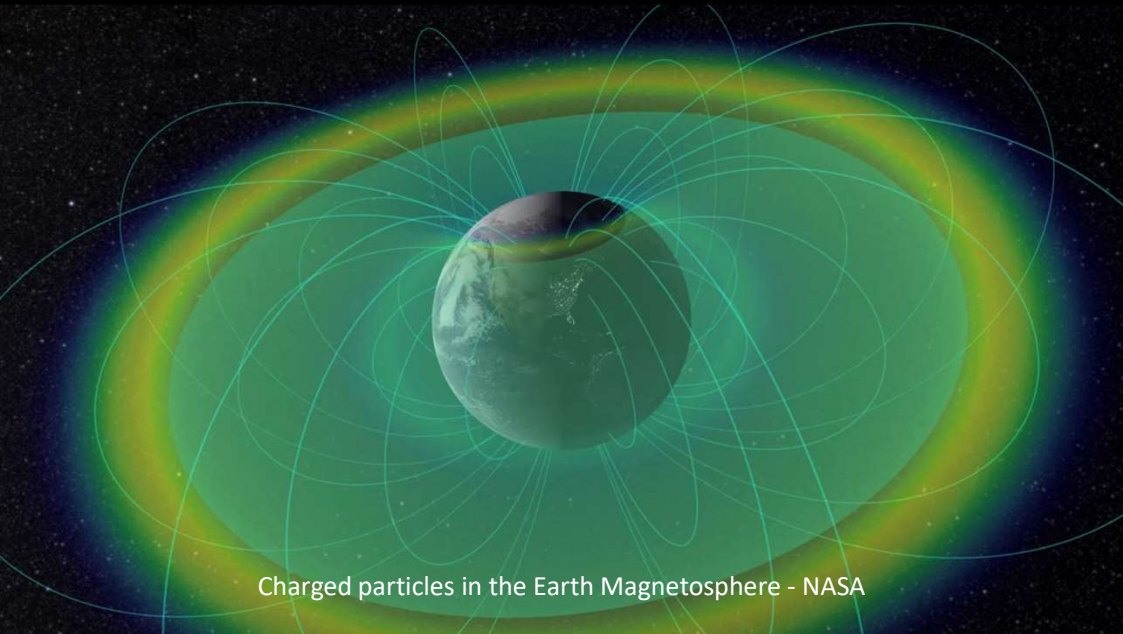


Aurora Borealis - THEMIS/NASA

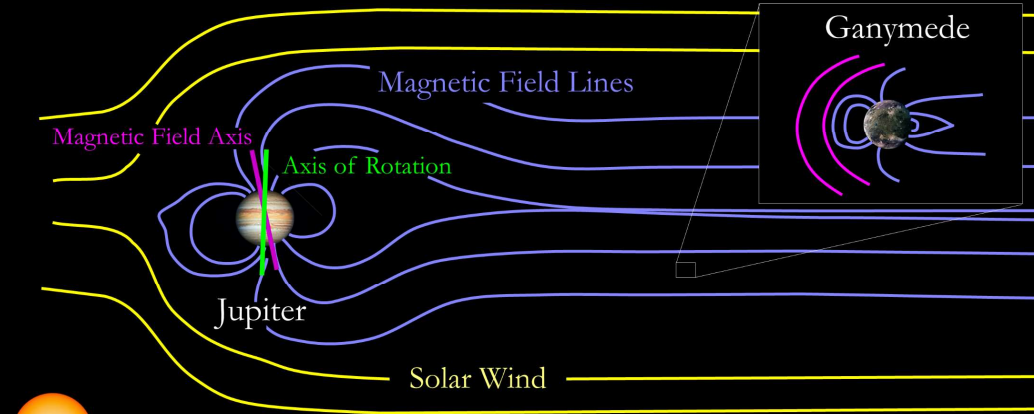




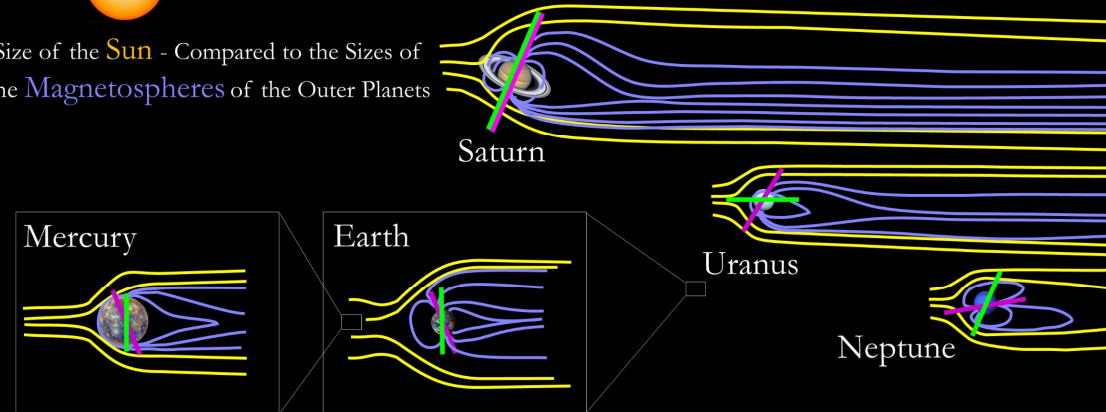
Solar Corona Turbulence - ESA & NASA/Solar Orbiter/Metis & EUI Teams and D. Telloni/INAF



Charged particles in the Earth Magnetosphere - NASA



Size of the Sun - Compared to the Sizes of the Magnetospheres of the Outer Planets



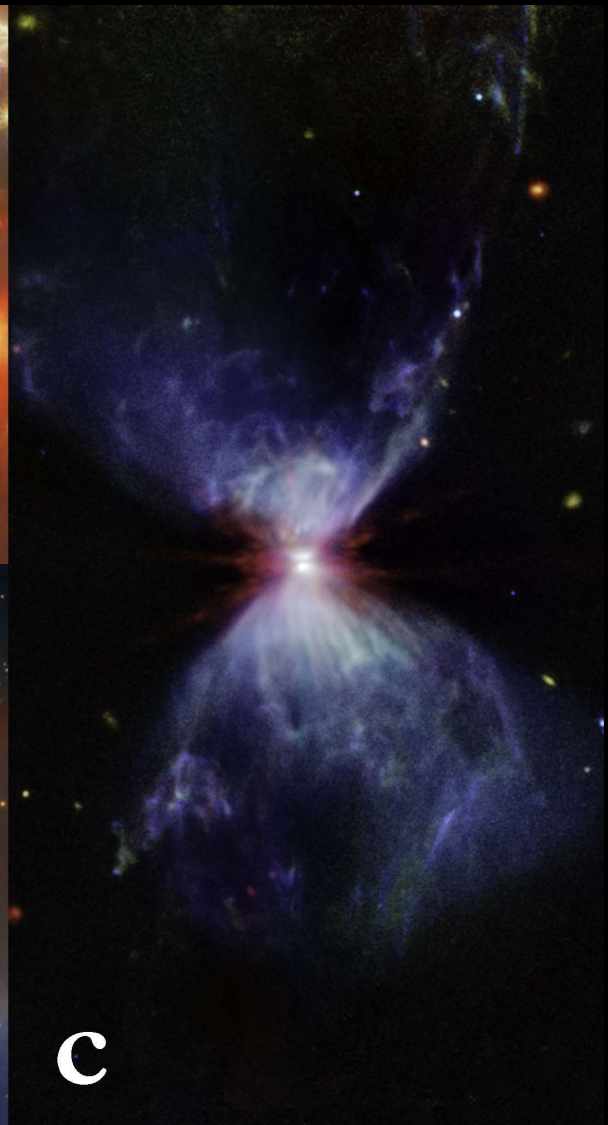
Magnetospheres of Planets and the Moon Ganymede in the Solar System - U. v. Kusserow/NASA



**a**

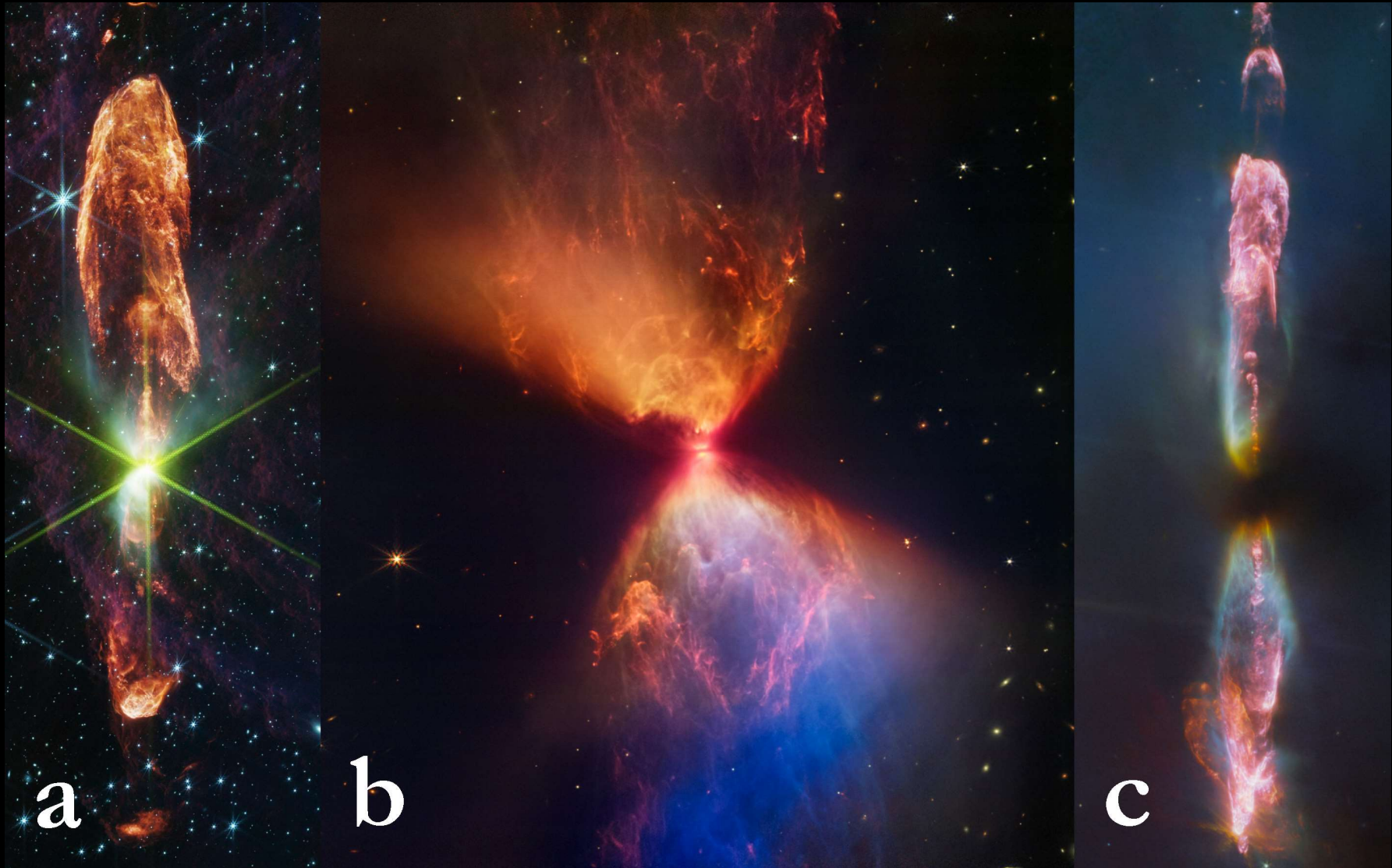


**b**

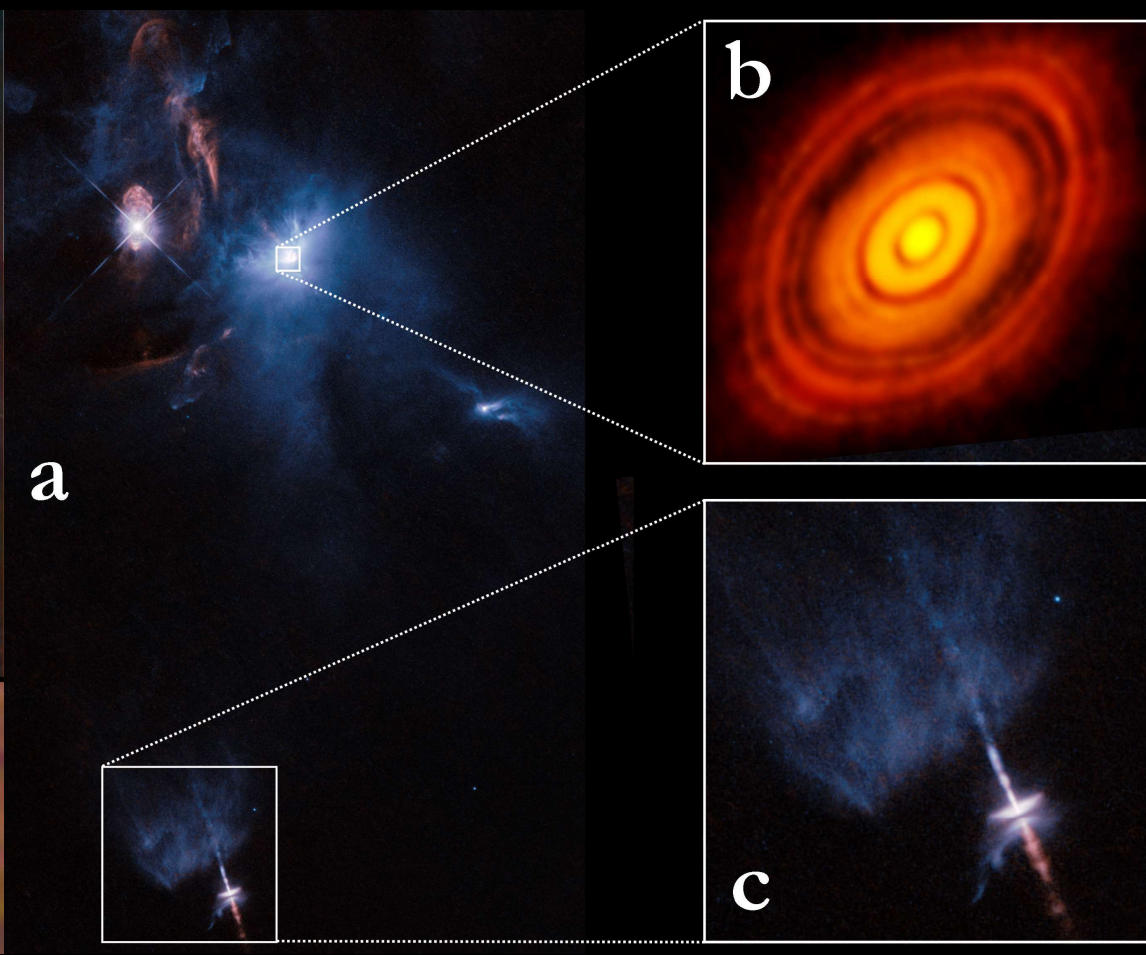
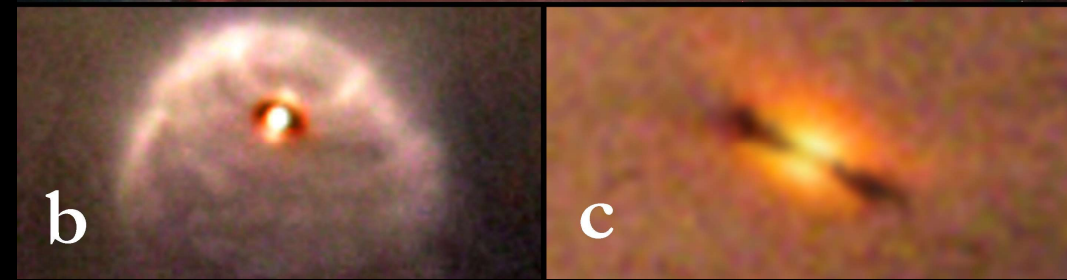
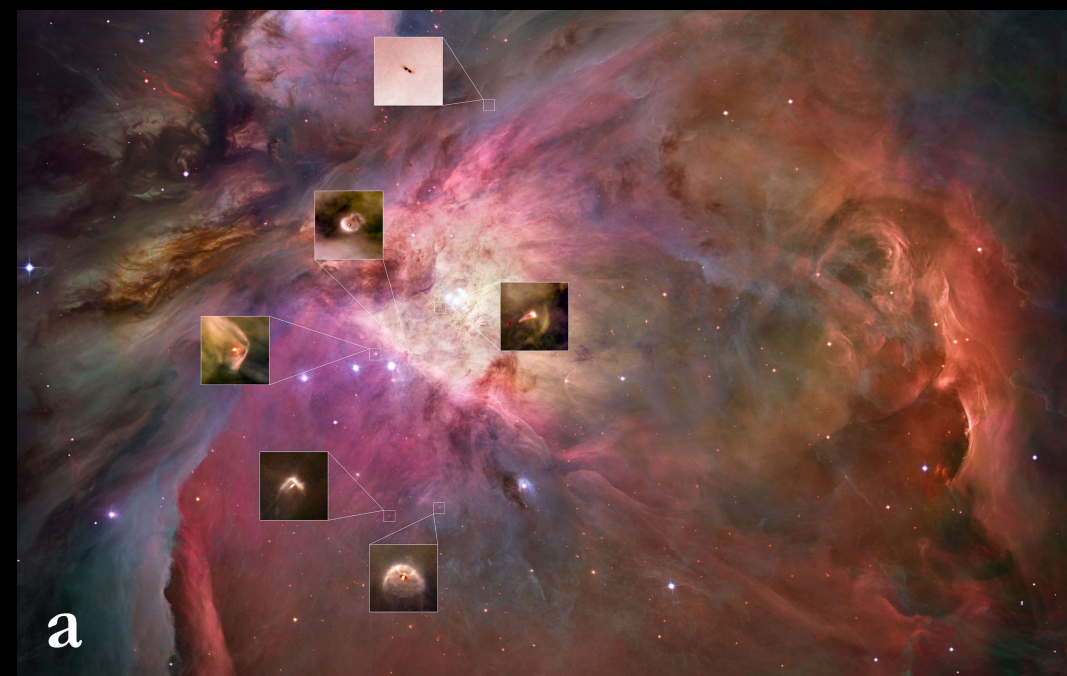


**c**

Infrared images of protostellar disk-jet structures taken with the James Webb Space Telescope. **a** Molecular clouds, **b** jets in the constellation Cygnus, **c** L 1527  
NASA/ESA/CSA/STScI/K. Pontoppidan (NASA-JPL) /J. Green (STScI) (2), NASA/ESA/CSA/STScI



Infrared images of the James Webb Space Telescope of stellar winds and Herbig-Haro objects of protostellar systems. a HH 46/47, b L 1527, c HH 2011  
NASA/ESA/CSA/STScI/J. DePasquale/A. M. Koekemoer, J. DePasquale/A. Pagan/A. M. Koekemoer, T. Ray (DIAS Dublin)



Proplyds in **a** the Orion Nebula, **b** Proplyd 473-245, **c** Proplyd 181-825  
 NASA, ESA, M. Robberto (Space Telescope Science Institute/ESA), the Hubble Space Telescope  
 Orion Treasury Project Team and L. Ricci (ESO)

Gas clouds and radiation bursts of jet-like bundled winds and accretion disks in the vicinity  
 of the young stars XZ Tauri, HL Tauri and V1213 Tauri in the constellation Taurus  
 ESA/Hubble und NASA, ALMA (ESO/NAOJ/NRAO), (Editing: U. v. Kusserow)

Radial Velocity 0  
Transit 0  
Imaging 0  
Microlensing 0

Year: 1991  
Exoplanets: 0

0 Timing Variations  
0 Orbital Brightness Modulation  
0 Astrometry  
0 Disk Kinematics

5,000 Exoplanets: Listen to the Sounds of Discovery (until March 21, 2022) - NASA/JPL-Caltech/M. Russo, A. Santaguida (SYSTEM Sounds)

# NASA EXOPLANET ARCHIVE

A SERVICE OF NASA EXOPLANET SCIENCE INSTITUTE

EXOPLANET EXPLORATION  
Planets Beyond Our Solar System



[Home](#) [About Us](#) [Data](#) [Tools](#) [Support](#) [Login](#)

**5,787**

Confirmed Planets  
11/06/2024



**570**

TESS Confirmed Planets  
11/04/2024



**7,341**

TESS Project Candidates  
11/02/2024



[View more Planet and Candidate statistics](#)



## Explore the Archive

## Transit Surveys

130,041,578 Light Curves



Launched in April 2018, TESS is surveying the sky for two years to find transiting exoplanets around the brightest stars near Earth.

[→](#)

[→](#)

[→](#)

[→](#)

[TESS](#)

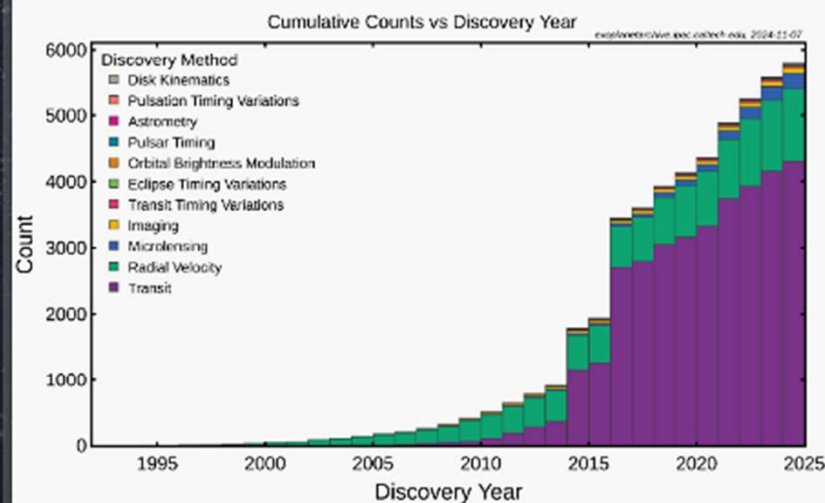
[Kepler](#)

[K2](#)

[KELT](#)

[UKIRT](#)

## Cumulative Exoplanet Discoveries by Year



[News](#) [→](#)

[1](#) [2](#) [3](#) [4](#)

[Plots](#) [→](#)

[1](#) [2](#) [3](#) [4](#)

HR 8799 b

HR 8799 c

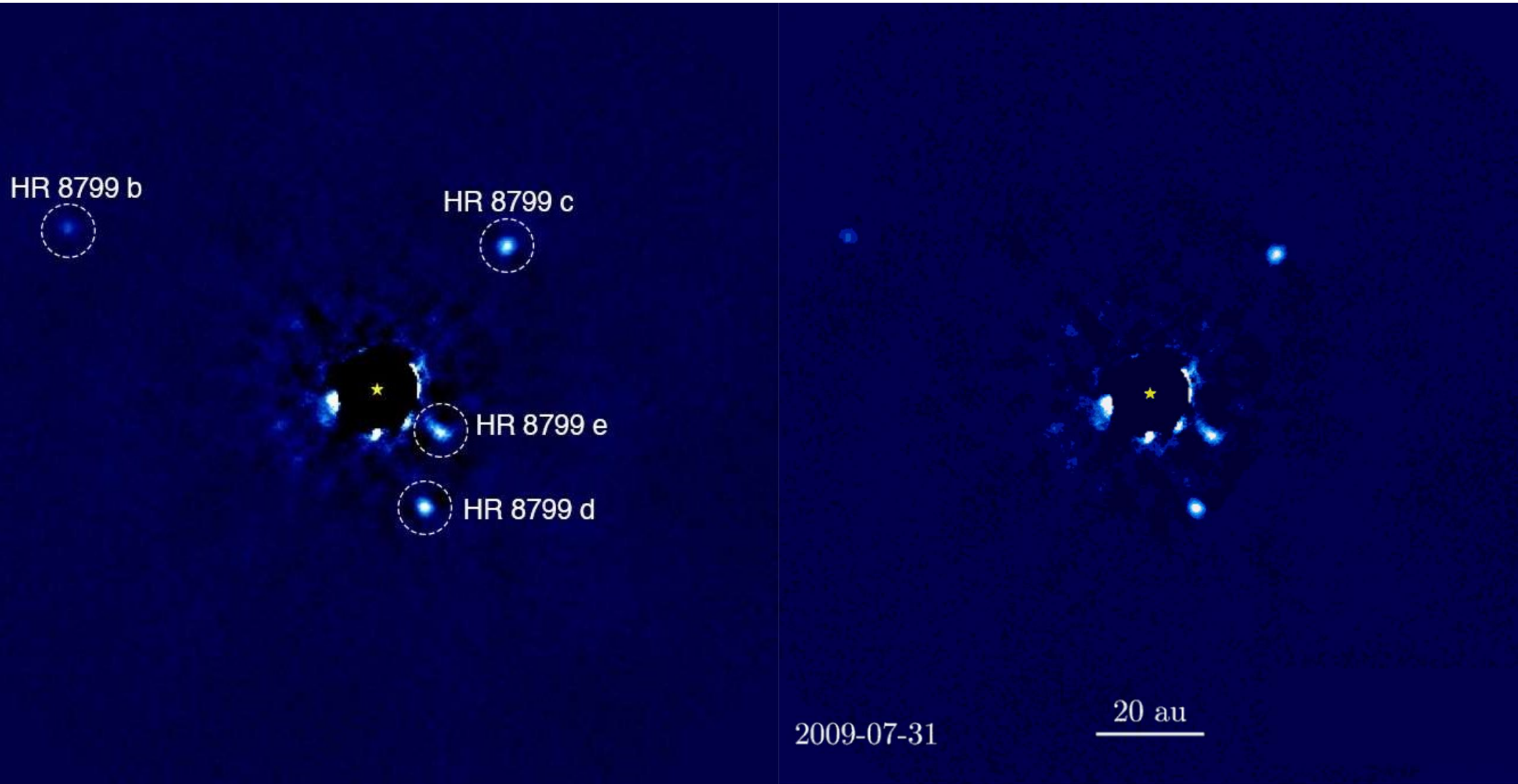
HR 8799 e

HR 8799 d

2009-07-31

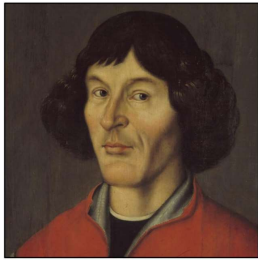
20 au

Orbit of the four exoplanets around the star HR 8799- Jason Wang et al.





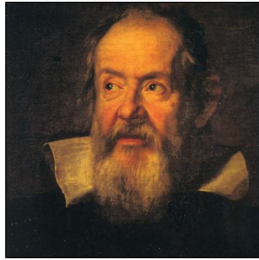




**Nikolaus Kopernikus**  
(1473-1543)



**Johann Daniel Titius**  
(1729-1796)



**Galileo Galilei**  
(1564-1641)



**William Gilbert**  
(1544-1603)



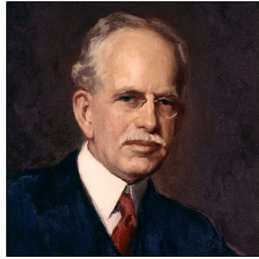
**Johannes Kepler**  
(1571-1630)



**Johann Elert Bode**  
(1747-1826)



**Wilhelm Herschel**  
(1738-1822)



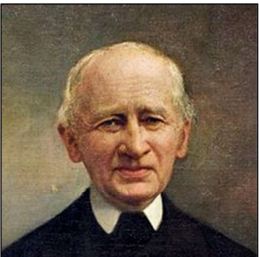
**George Ellery Hale**  
(1868-1938)



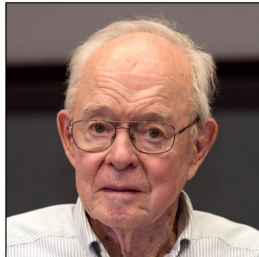
**Isaac Newton**  
(1643-1727)



**Giuseppe Piazzi**  
(1746-1826)



**Johann Gottfried Galle**  
(1746-1826)



**Eugen Newman Parker**  
(1927-2022)



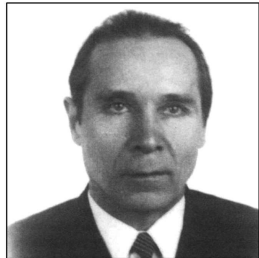
**Emanuel Swedenborg**  
(1688-1772)



**James H. Jeans**  
(1912-2007)



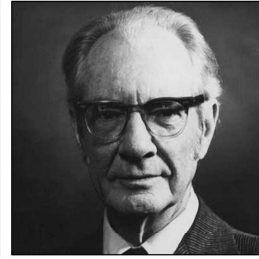
**Gerard Peter Kuiper**  
(1905-1973)



**Viktor S. Safronov**  
(1917-1999)



**Immanuel Kant**  
(1724-1804)



**Fred Lawrence Whipple**  
(1906-2004)



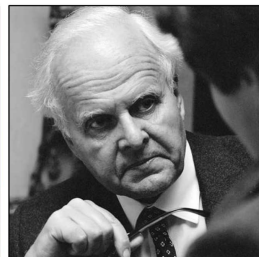
**Hannes O. G. Alfvén**  
(1908-1995)



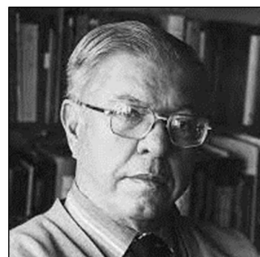
**Richard Larson**



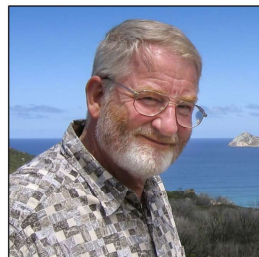
**Pierre-Simon Laplace**  
(1749-1827)



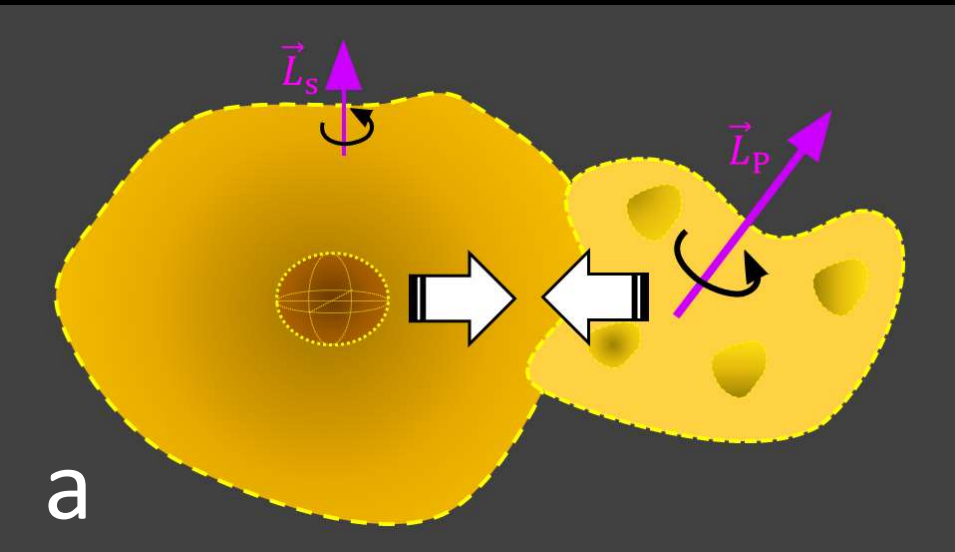
**Carl-Fr. v. Weizsäcker**  
(1912-2007)



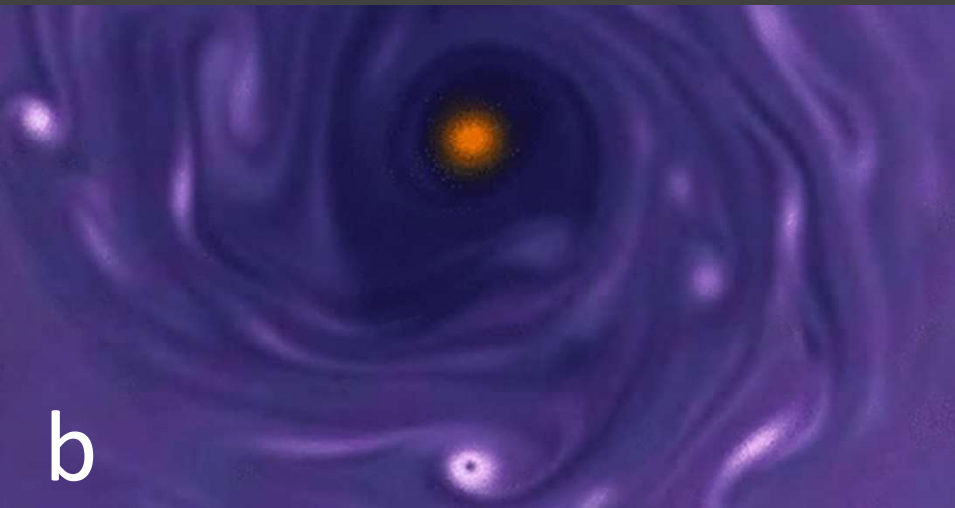
**Fred Hoyle**  
(1915-2001)



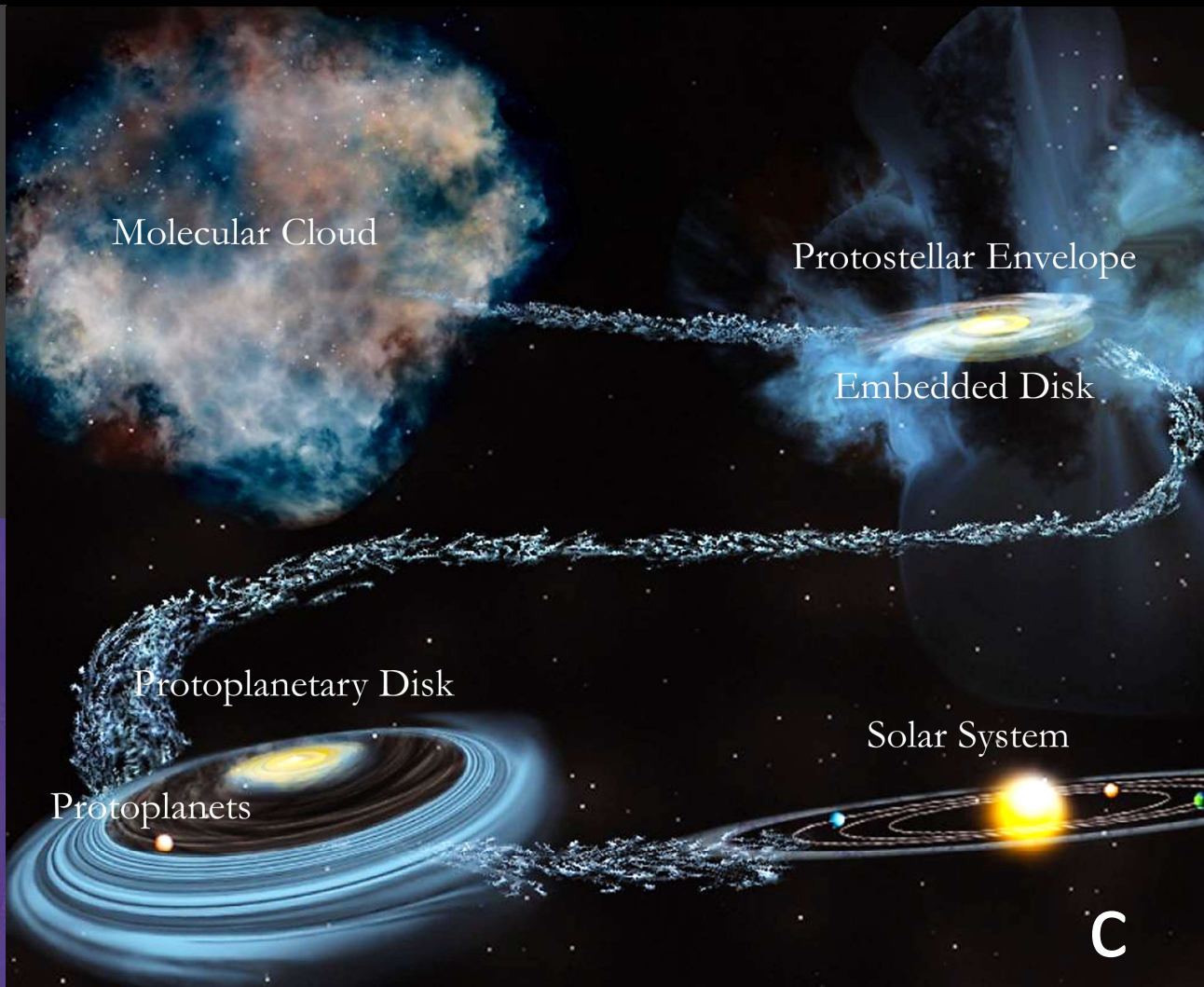
**Andrew J. R. Prentice**



a

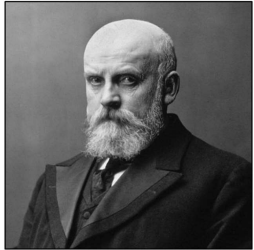


b



c

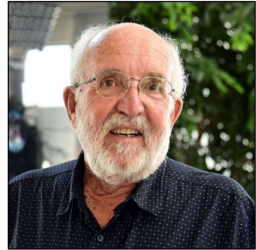
Simple models for the formation of the solar system through **a** collision processes, **b** turbulence and **c** within the framework of the modern nebular hypothesis  
U. v. Kusserow, J. S. Wettlaufer, B. Saxton/NSF/AUI/NRAO



**John Russell Hind**  
(1823-1895)



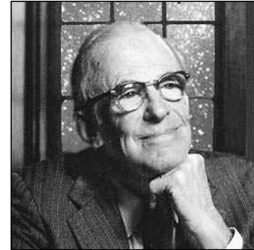
**Guillermo Haro**  
(1913-1988)



**Michel Mayor**



**Gibor Basri**



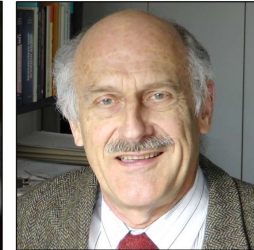
**Lyman Spitzer**  
(1914-1997)



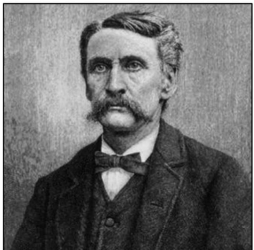
**Telemachos Mouschovias**



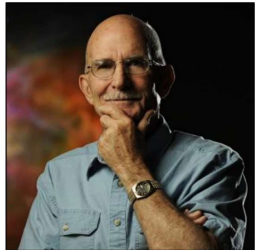
**John Hawley**  
(1958-2021)



**Hendrik Spruit**



**Sherburne W. Burnham**  
(1838-1921)



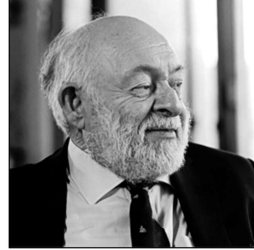
**Charles Robert O'Dell**



**Didier Queloz**



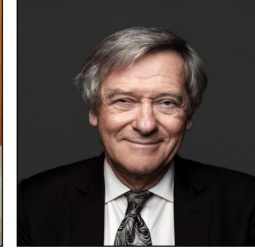
**Jean-François Donati**



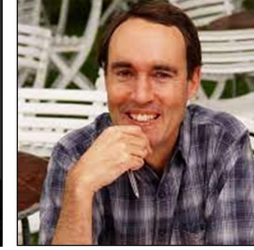
**Leon Mestel**  
(1927-2017)



**Nikolay Shakura**  
**Rashid Sunyaev**



**Roger Blandford**



**Matthew R. Bate**



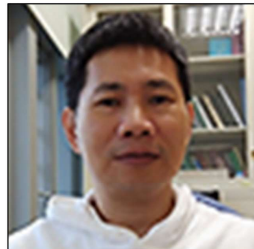
**George H. Herbig**  
(1920-2013)



**Mark J. McCaughrean**



**Gaël Chauvin**



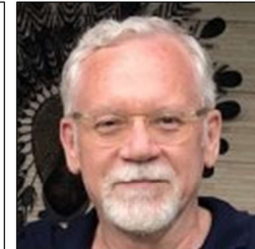
**Chin-Fei Lee**



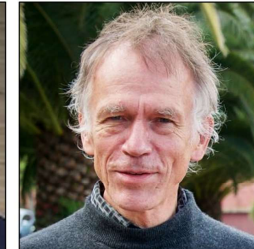
**Frank H.-S. Shu**  
(1943-2023)



**Steven Andrew Balbus**



**David G. Payne**



**Axel Brandenburg**

# Historical Discoveries related to the Formation of Extrasolar Star Systems and our Solar System also under Magnetic Influence

300 v. Chr.	Aristarch von Samos (310-230 v. Chr.)	Erstellung der Hypothese zum heliozentrischen Weltbild
1543	Nikolaus Kopernikus (1473-1543)	Nachweis des Umlaufes der Planeten um die Sonne, der Umdrehung der Erde um die eigene Achse
1600	William Gilbert (1544-1603)	In seinem Buch „De Magnete“ beschreibt er die Erde als einen großen Magnet, worauf er aufgrund der breitenabhängigen Inklination von Magnetnadel schloss
1609, 1610	Galileo Galilei (1564-1642)	Teleskopische Entdeckung der Umläufe von Monden des Jupiters sowie der Venusphasen
1609-1619	Johannes Kepler (1571-1630)	Formulierung seiner drei Gesetze zum Umlauf der Planeten auf elliptischen Bahnen um die Sonne
1630	René Descartes (1596-1650)	Modell über den Ursprung des Sonnensystems
1684	Isaac Newton (1643-1727)	Beweis der Gültigkeit der drei Keplerschen Gesetze
1687	Isaac Newton (1643-1727)	Veröffentlichung der Grundlagen der klassischen Mechanik und des universellen Gravitationsgesetzes
um 1704		Erstmalige Verwendung des Begriffs „Sonnensystem“
1734	Emanuel Swedenborg (1688-1772)	Entwicklung einer ersten Nebelhypothese zur Entstehung des Sonnensystems
1749	George-Louis Leclerc (1707-1788)	Idee zur Entstehung des Sonnensystems durch Zusammenstoß der Sonne mit Kometen
1755	Immanuel Kant (1724-1804)	Aussagen über die Vielfalt der Sterne in der Milchstraße, die von Planetensystemen umgeben sind
1766	Johann Daniel Titius (1729-1796)	Aufstellung einer empirisch ermittelten Beziehung über den Abstand der Planeten von der Sonne
1772	Johann Elert Bode (1747-1826)	Veröffentlichung der Titius-Bode-Regel zum Abstand der Planeten von der Sonne
1796	Pierre-Simon Laplace (1749-1827)	Entwicklung der Nebularhypothese zur Entstehung des Sonnensystems, wonach Planeten durch Zentrifugalkräfte, Abkühlungs- und Verdichtungsprozesse in konzentrischen, die Sonne umgebenden Gasringen entstehen
1781	Friedrich Wilhelm Herschel (1738-1822)	Entdeckung des Uranus
1846	Johann Gottfried Galle (1812-1910) Heinrich Louis d'Arrest (1822-1875)	Entdeckung des Neptun
1852	John Russell Hind (1823-1895)	Entdeckung des jungen, von der Masse her sonnenähnlichen variablen Sterns T Tauri im Sternbild des Stiers

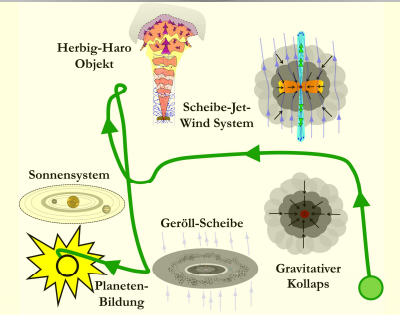
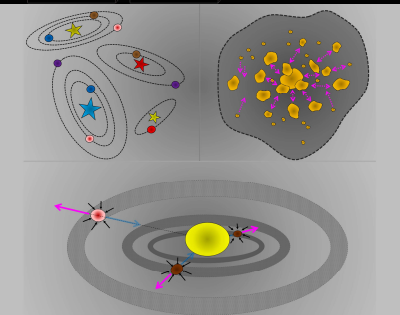
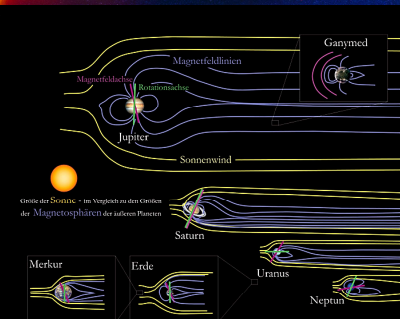
1951,1952 1956,1966	Harold C. Urey (1893-1981)	Entwicklung eines kosmochemischen Gas-Staub Entstehungsmodells für das Sonnensystem, bei dem auch die Ionisation, die Beschleunigung geladener Gaspartikel und ein dadurch vermittelter Drehimpulstransport eine zentrale Rolle spielen könnte
1951,1962 1981	Louis Jacot (1906-?)	Vielzahl von Ideen zur Sonnensystem-Entstehung: Verwirbelungen in Wirbeln, Planetenbildung durch Materieauswurf aus der Sonne, spiralförmige Planetenorbits, Mondentstehung aus äquatorialen Ausbuchtungen der Planeten, Erklärbarkeit der Unterschiede zwischen inneren und äußeren Planeten durch Wirbelverhalten
1955,1960	Fred Hoyle (1915-2001)	Entwicklung der Idee zur Sonnensystem-Entstehung, dass ein magnetisches Drehmoment zwischen der Protosonne und der sie umgebenden Scheibe eine magnetische Kopplung und den Transport von Drehimpuls bewirkt haben könnte
1955	Bernard F. Burke (1928-2018) Kenneth Linn Franklin (1923-2007)	Entdeckung vom Jupiter ausgehender Ausbrüche dekametrischer, polarisierter Radiowellen, die auf die Existenz eines starken jovianischen Magnetfeldes schließen lassen, in dem hochenergetische Elektronen beschleunigt werden
1956	Leon Mestel (1927-2017) Lyman Spitzer (1914-1997)	Anhand der Polarisation stellarer Strahlung, die beim Auftreffen auf interstellaren Staub verschleiert wird, schließen sie auf die Gegenwart magnetischer Felder
1957	Hannes O. G. Alfvén (1908-1995)	Bestimmung der minimalen „kritischen“ Masse, von der ab kalte, elektrisch perfekt elektrisch leitende, magnetisierte interstellare Wolken aufgrund ausreichender Eigengravitation kollabieren können
1959	Eugene N. Parker (1927-2022)	Gewinnung tiefer Erkenntnisse über den Einfluss magnetischer Felder auf die Fragmentation von Molekülwolken, über die Bedeutung ambipolarer Diffusion auf die Entkopplung von Magnetfeldern und Materie für den Kollaps von Molekülwolken
1960-1978	William H. McCrea (1904-1999)	Berücksichtigung nichtlinearer MHD-Terme in der magnetischen Induktionsgleichung für nur teilweise ionisiertes Plasma
1962	Evry Schatzman (1920-2010)	Entwicklung der Vorstellung von der Existenz eines Interplanetaren Magnetfeldes, das mit dem Sonnenwind getragen wird
		Einführung des Begriffs „Solar Wind“
		Entwicklung der „Flocken/Protoplanet“-Hypothese, nach der sich die Sonne und die Proto planeten in einer galaktischen Wolke entwickelten, in der flockenartige Turbulenzen durch Agglomeration für die Ausbildung einer jungen Protosonne, Rotationsinstabilitäten für ein Auseinanderbrechen in kleinere Proto planeten und die zentral gelegene größere junge Sonne sorgten.
		Entdeckung der Bedeutung magnetischer Felder für die Abbremsung von Sternen

		Akkretionsscheiben durch einsetzende magnetische Rekonnexion
2000	Alan Boss	Nachweis möglicher Fragmentation rotierender Wolken aufgrund magnetischer Spannungen bei ambipolarer Materiediffusion in Simulationsrechnungen
2000	Arieh Königl Ralf E. Pudritz	Erklärung der Jet-Kollimation durch den „hoop-stress“ („Reifenstress“) in helikalen Magnetfeldern
2002	Francesca Bacciotti u. a.	Entdeckung der Rotation protostellarer Jets (kontroverse Diskussion)
2003	Richard B. Larson	Grundlegende Arbeit über die Physik der Sternentstehung
2003	Christian Fendt	Erste numerische Abschätzungen zu magnetischen protoplanetaren Ausflüssen aus zirkumplanetaren Akkretionsscheiben
2004	Richard M. Crutcher	Beobachtung von Wolkenkernen mit darin parallelen magnetischen Feldern der Flussdichte 1 Milligauss, woraus er schloss, dass Turbulenzen zu schwach für die Verformung von Magnetfeldern sein könnten
2006	Derek Ward-Thomson	Nachweis für die Einflussnahme sowohl von Turbulenzen als auch Magnetfeldern auf die Ausbildung und Entwicklung prästellarer Wolkenkerne
2008	Antonio Chrysostomou u. a.	Aufstellen der Hypothese, dass Jet Rotation schon in frühen Evolutionsphasen vorhanden sein könnte, und dass dadurch überschüssiger Drehimpuls weggetragen wird, wodurch der Protostern an Masse gewinnen kann
2013	Martina M. Romanova u.a.	Erste dreidimensionale MHD-Simulation angeregter Wellen in Akkretionsscheiben durch bipolare stellare Magnetosphären, wodurch sich Spiralstrukturen ausbilden
2014	Deniss Stepanovs Christian Fendt Somayeh Sheikhezami	Erste MHD-Modellierung episodischen Ausstoßes von Materiejets, die durch oszillierende Scheibendynamo-Prozesse ausgelöst werden
2021	Lotfi Ben-Jaffel u. a.	Erste Entdeckung der Signatur eines Magnetfeldes eines Exoplaneten

Die Farbkodierung der Schrift kennzeichnet historische Ereignisse im Zusammenhang

- mit der Entdeckung des Aufbaus und der Entstehung des Sonnensystems
- mit der Entdeckung von Magnetfeldern im Sonnensystem
- mit der Entwicklung der Scheiben-Jet-Strukturen protostellarer Systeme

[https://ulrich-von-kusserow.de/images/Beitraege/Buecher/Entstehung\\_Magnetisches\\_Sonnensystem/Historische\\_Entdeckungen\\_Extrasolare\\_Sternsysteme\\_Magnetische\\_Entstehungsprozesse.pdf](https://ulrich-von-kusserow.de/images/Beitraege/Buecher/Entstehung_Magnetisches_Sonnensystem/Historische_Entdeckungen_Extrasolare_Sternsysteme_Magnetische_Entstehungsprozesse.pdf)



## On the Formation of the Magnetic Solar System Phases of Development History

- Structure and dynamics of the heliocentric Solar System  
Kopernikus, Galilei, Kepler, Newton, Titius & Bode, Herschel, Le Verrier & Galle
- Discovery of magnetic fields in the Solar System  
Gilbert, Hale, Babcock, Pioneer 10
- Early Models of the Formation of the Solar System  
Descartes, Swedenborg, Leclerce, Kant, Laplace, ...
- Early observations and theories on the development of star systems  
Hind, Burnham, Herbig & Haro, Kleinman & Low, Hertzsprung & Russell, Jeans, Hayashi
- Advanced computer-aided analytical modeling
- Theories on influence of magnetic fields on the development of star systems  
Parker, Mestel, Spitzer, Blandford, Pudritz, Shu, Balbus & Hawley, Wetherill
- Age of discoveries with the HST, VLT, VLA ...
- Era of sophisticated numerical simulations
- Age of discoveries with ALMA, SOFIA, ...
- Age of Discovery with the JWST, ELT, SKA, ngVLA, ...

from  
1543

from  
1600

from  
1630

from  
1852

from  
1955

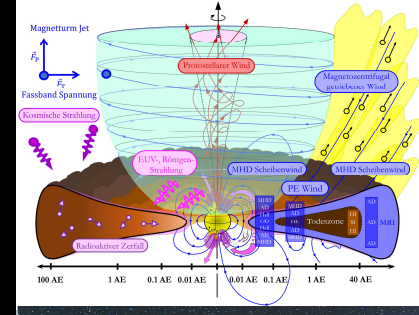
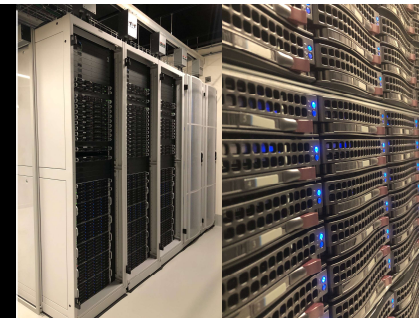
from  
1959

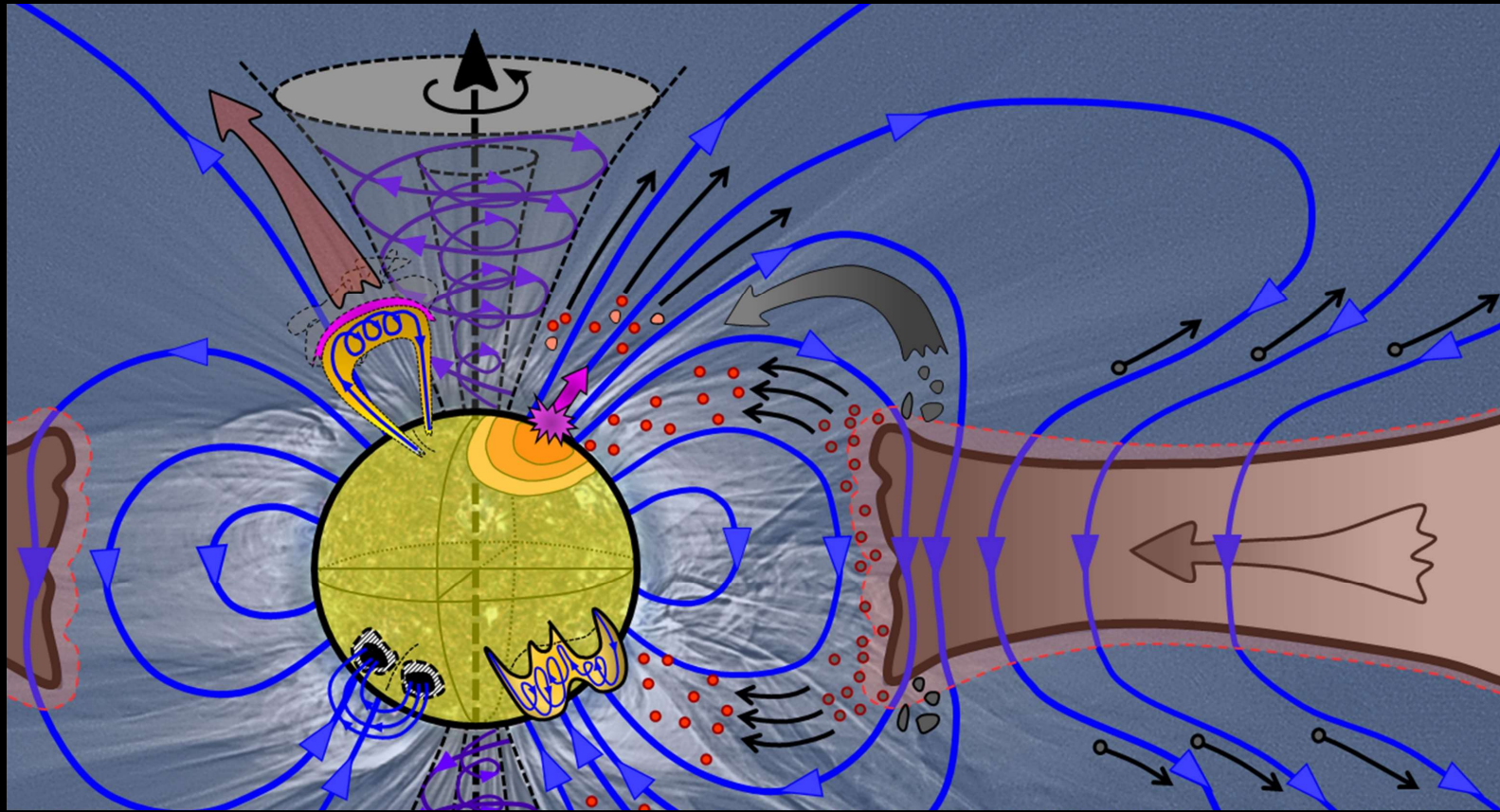
from  
1990

from  
1990

from  
2004

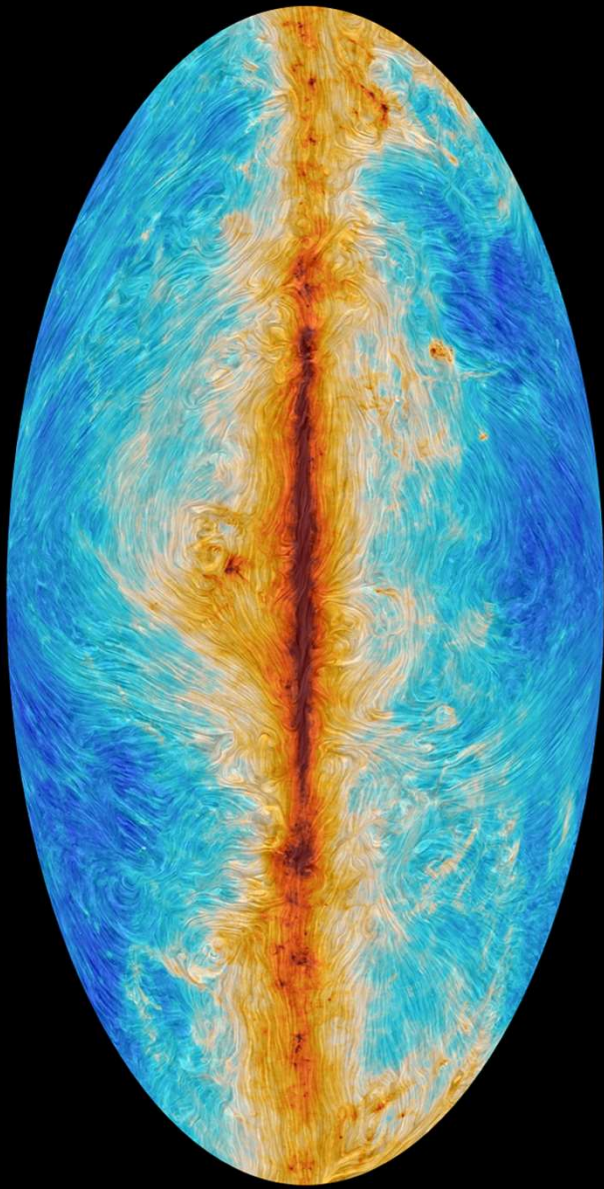
from  
2022





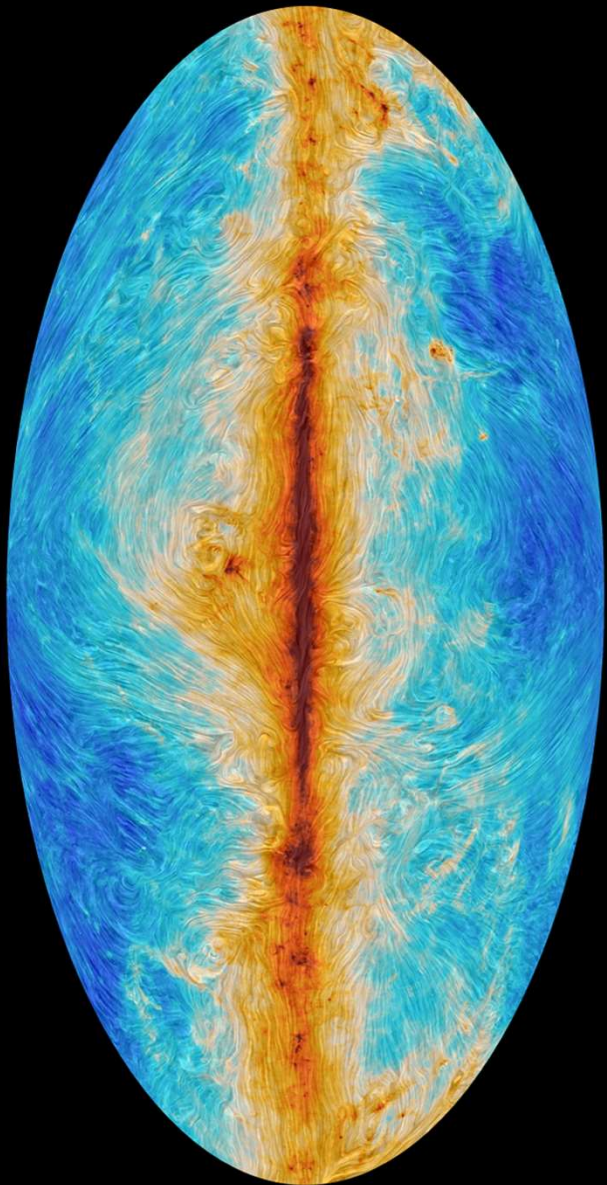
$$\frac{\partial \vec{B}}{\partial t} = \vec{\nabla} \times (\vec{v} \times \vec{B}) - \vec{\nabla} \times (\eta_{OD} \cdot \vec{\nabla} \times \vec{B}) + \vec{\nabla} \times \{ \eta_{AD} \cdot (\vec{\nabla} \times \vec{B}) \times \vec{B} \} - \vec{\nabla} \times [ \vec{\nabla} \times \{ \eta_{HD} \cdot (\vec{\nabla} \times \vec{B}) \times \vec{B} \} ]$$

Background Structures

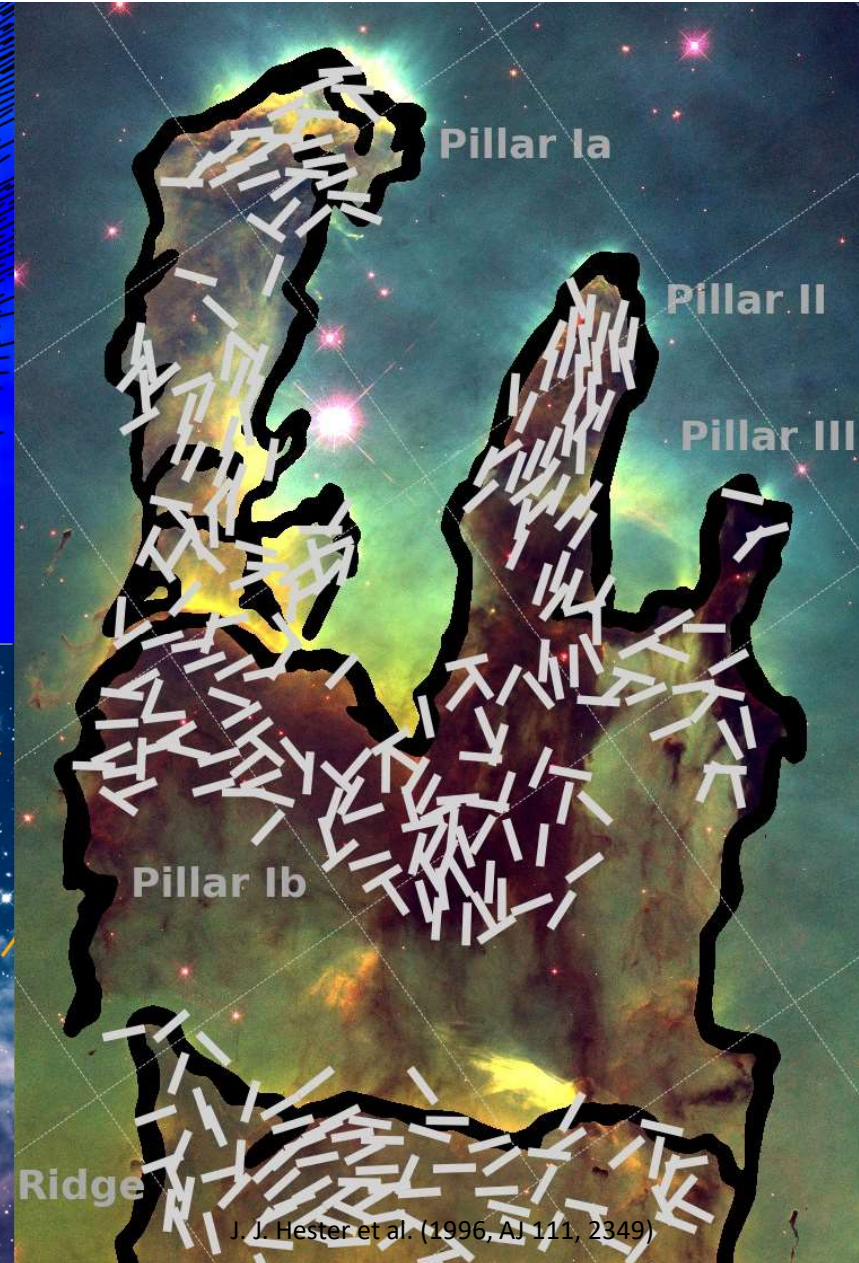
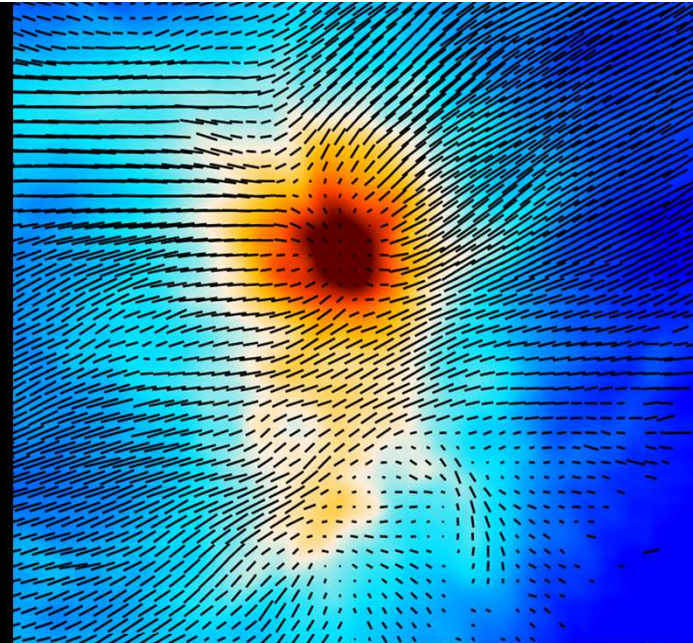


Magnetic fields are likely to direct the gas into orbit around the black hole in the centre of the Milky Way  
NASA / SOFIA; NASA / HST

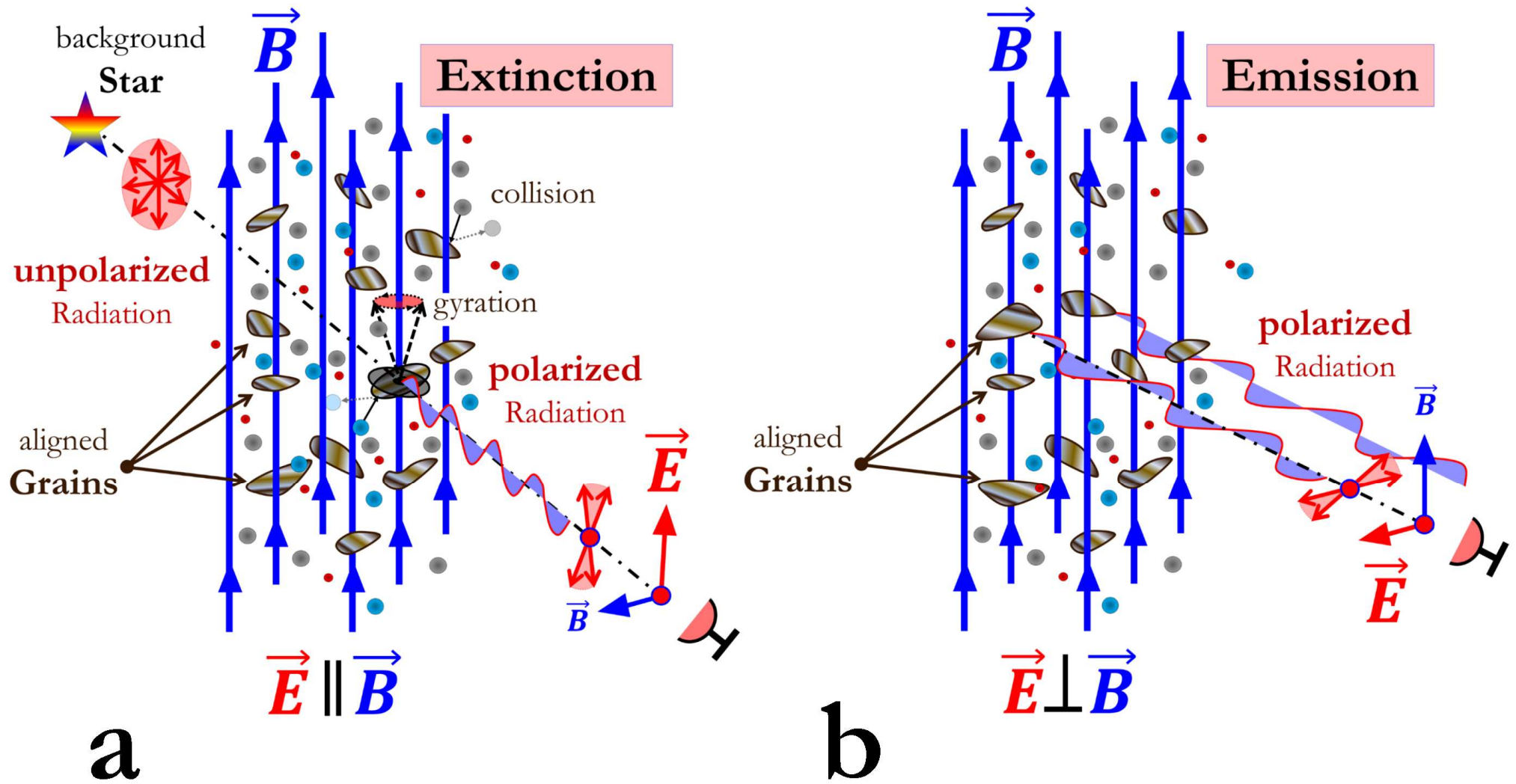




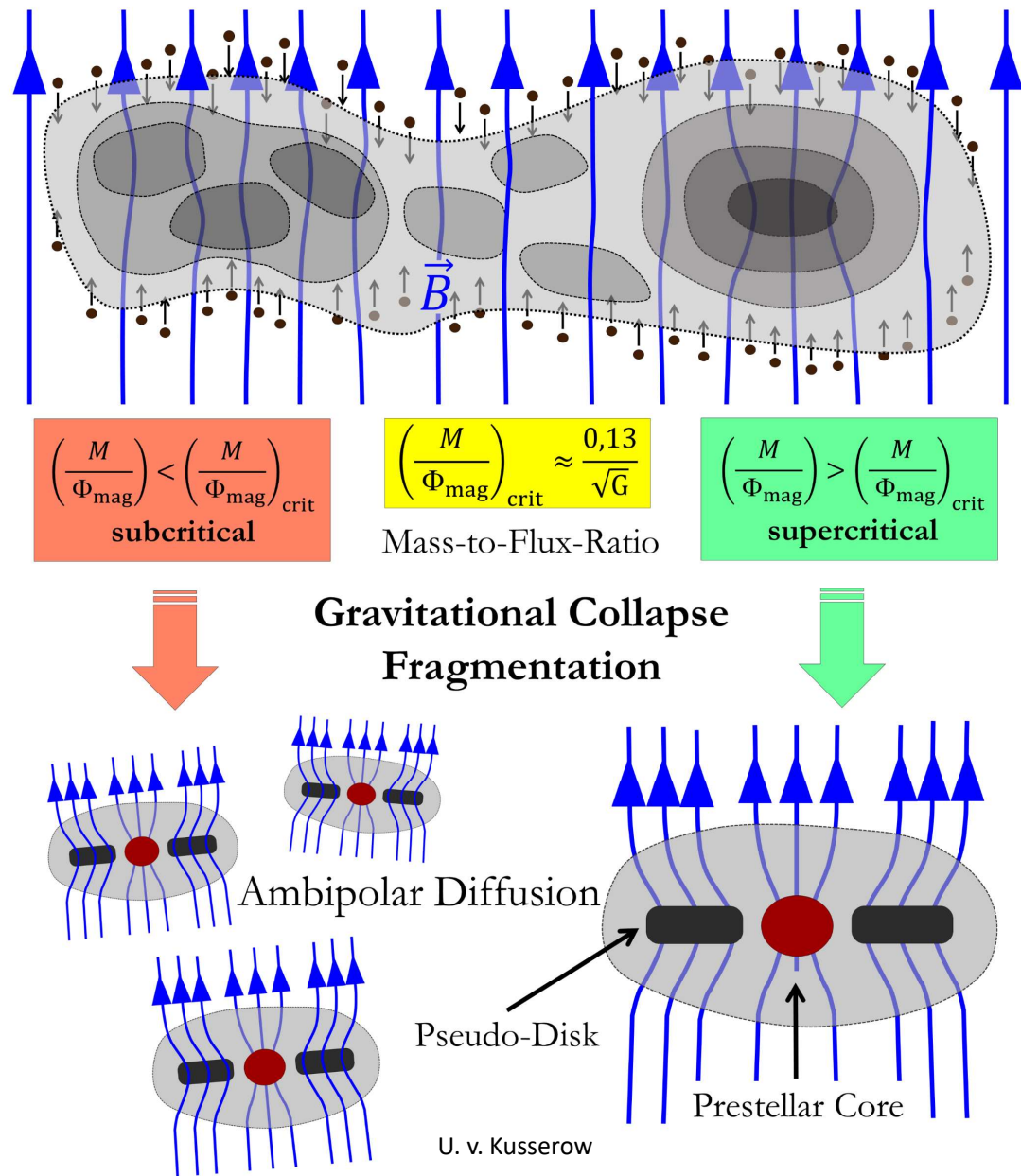
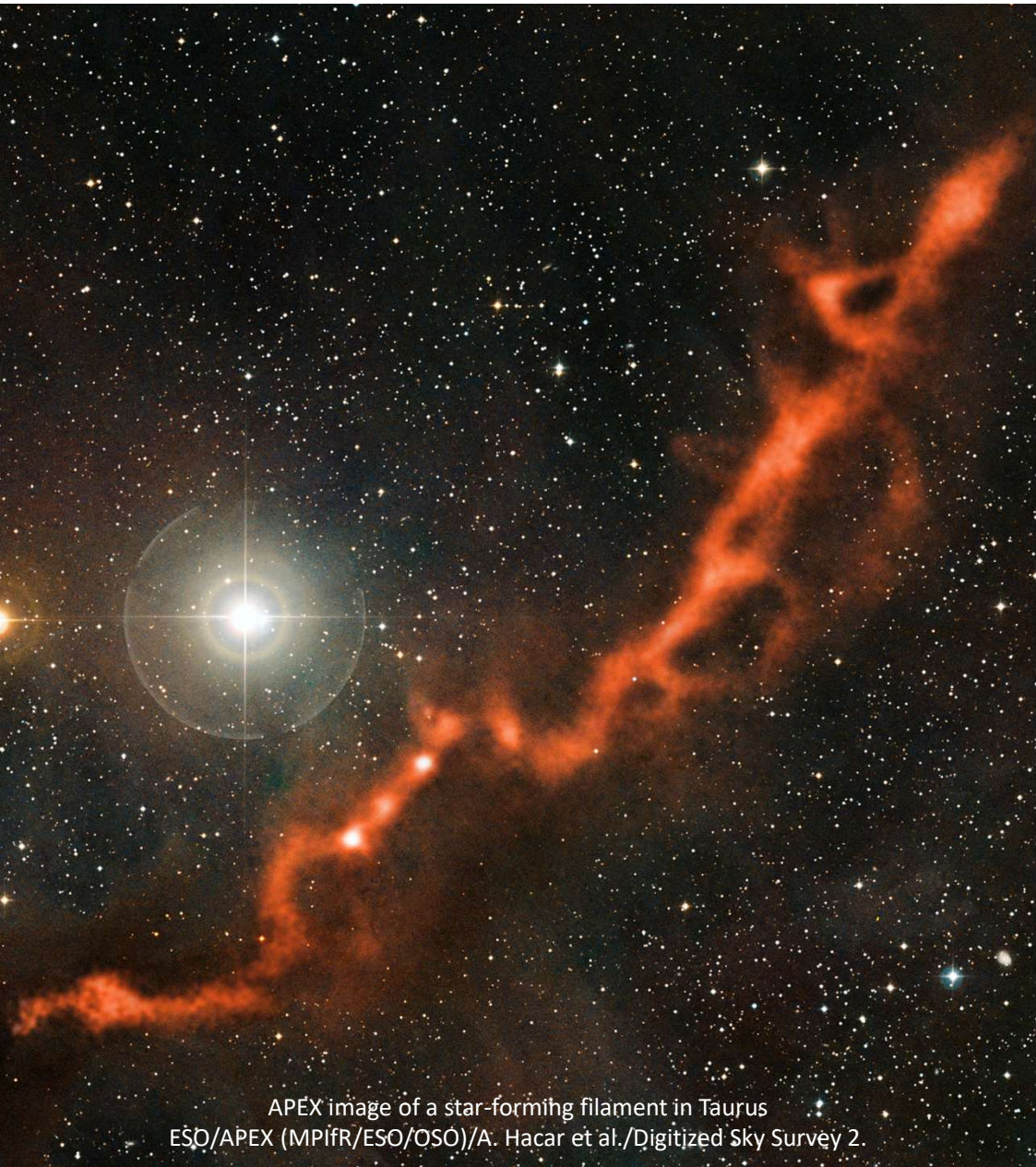
ESA and the Planck Collaboration, HAWC+/SOFIA/D. T. Chuss et al., J. Wang et al.

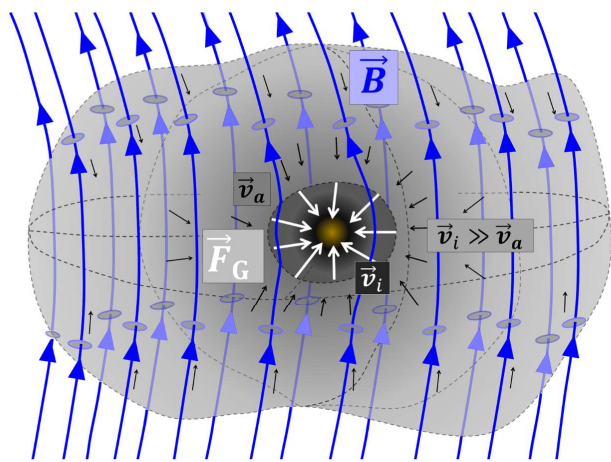


J. J. Hester et al. (1996, AJ 111, 2349)

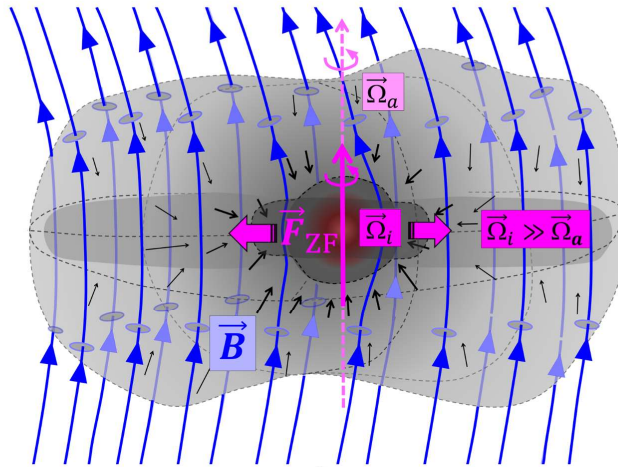


Determination of the orientation of interstellar magnetic fields based on the orientation of dust grains using the polarization of the radiation emitted by a star behind them (a) or by asymmetric dust particles themselves (b). - U. v. Kusserow (after A. Lazarian)

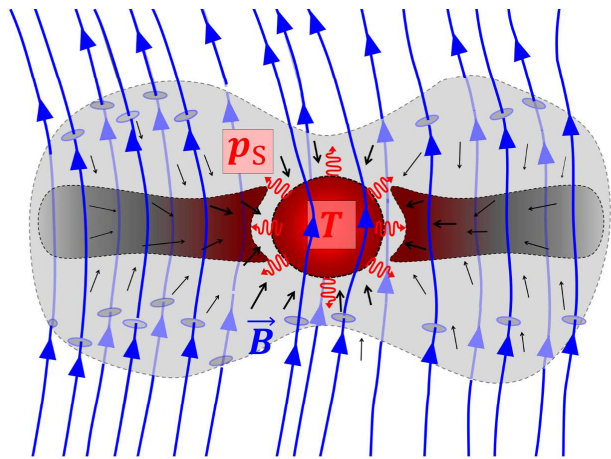




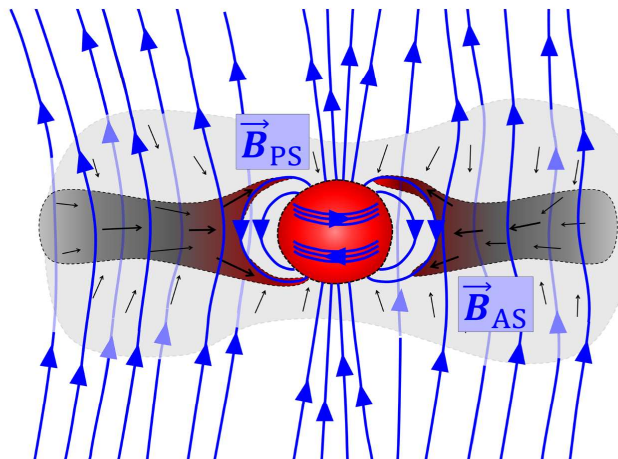
**a**



**b**

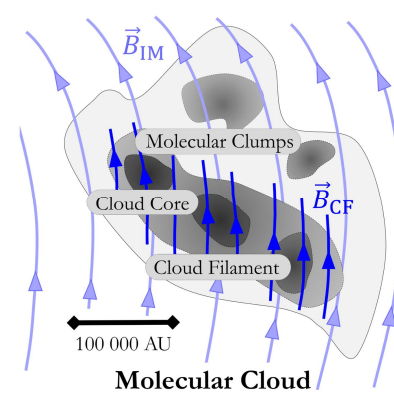


**c**

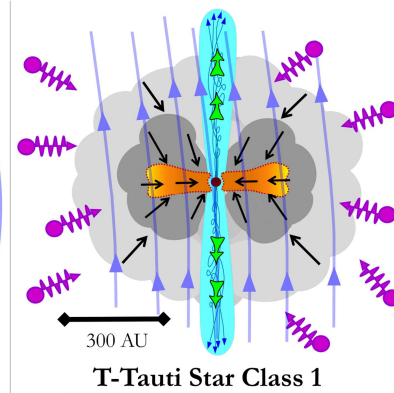


**d**

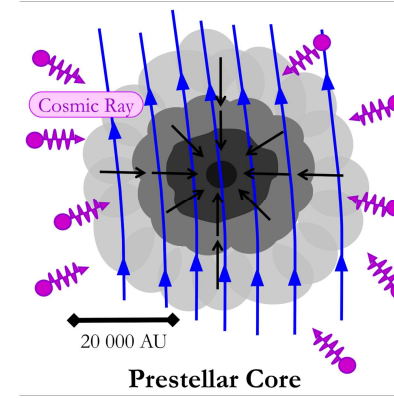
Evolution of Prestellar Cores and Protostars, Pseudodisks and Accretion Disks in a Magnetized Molecular Cloud  
U. v. Kusserow



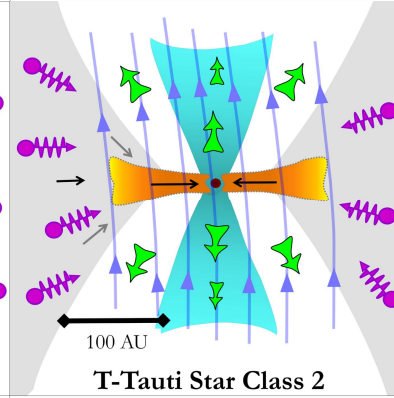
**Molecular Cloud**



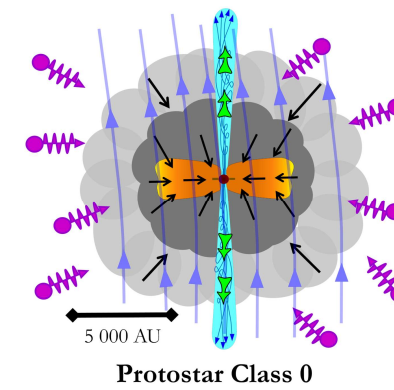
**T-Tauri Star Class 1**



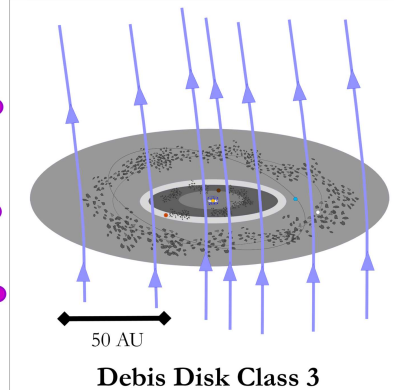
**Prestellar Core**



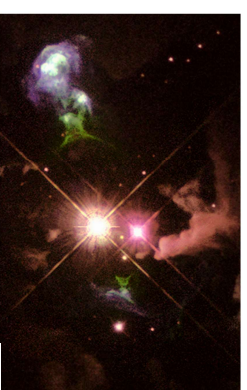
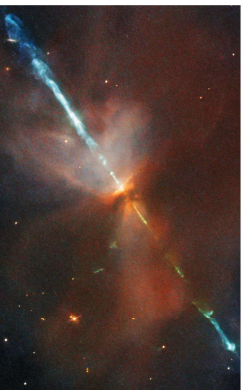
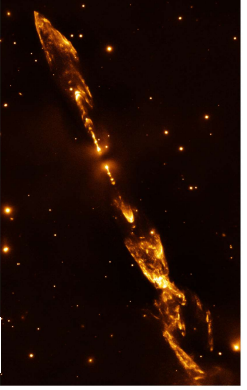
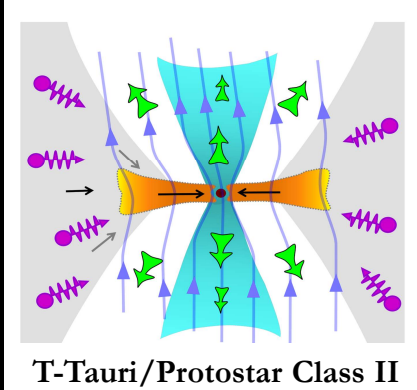
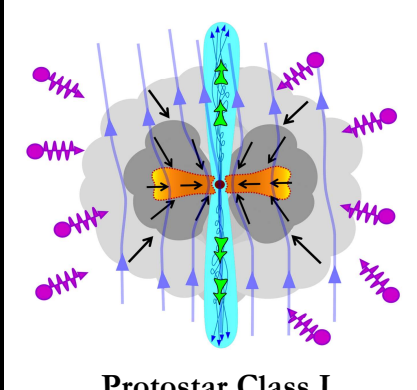
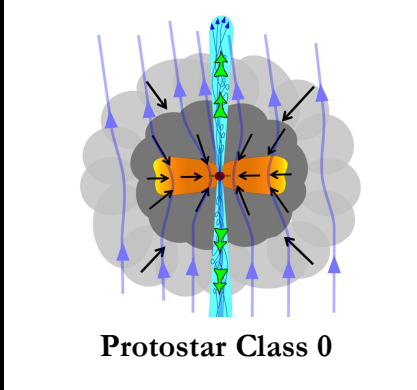
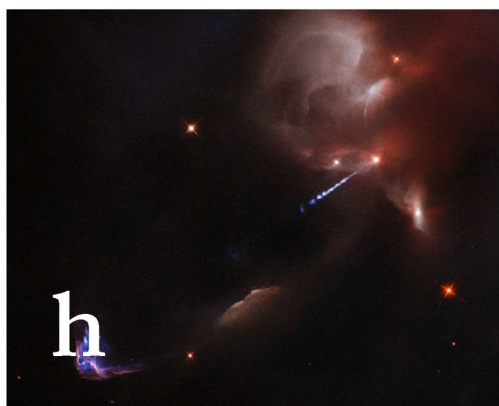
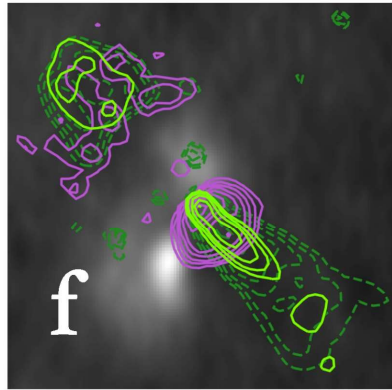
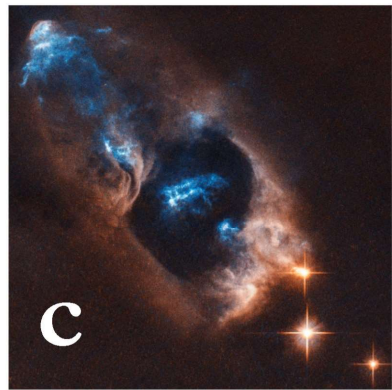
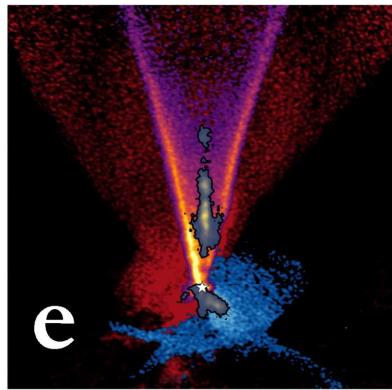
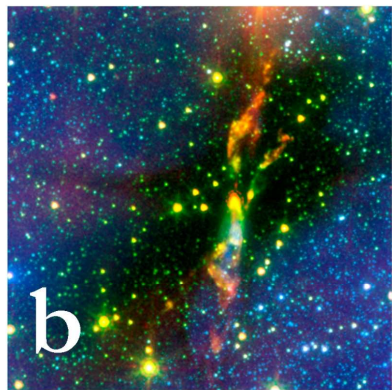
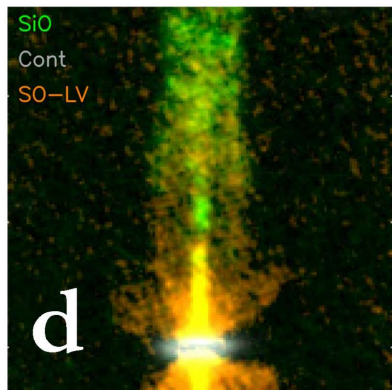
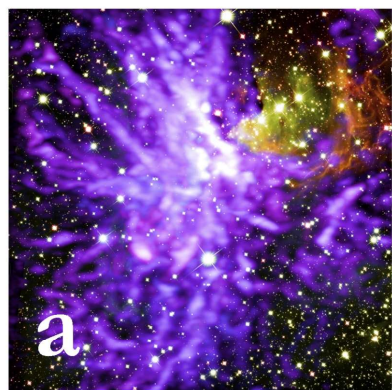
**T-Tauri Star Class 2**

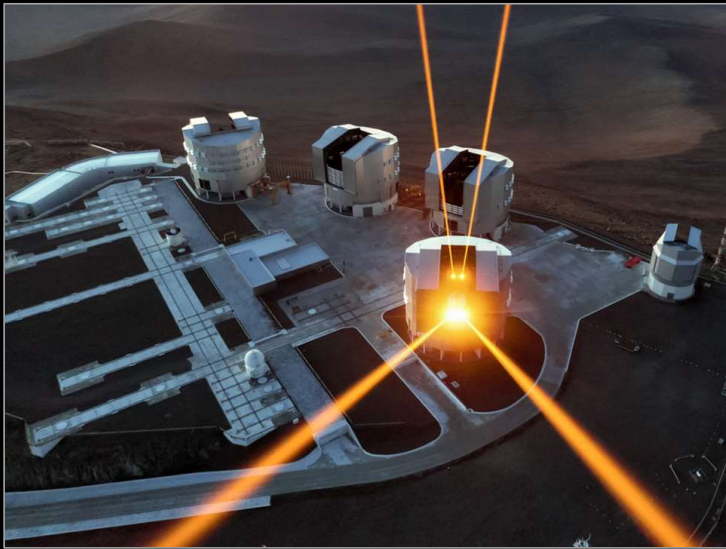


**Protostar Class 0**



**Debris Disk Class 3**





Very Large Telescope (VLT) ESO



Stratospheric Observatory for Infrared Astronomy (SOFIA)



Hubble Space Telescope (HST) NASA



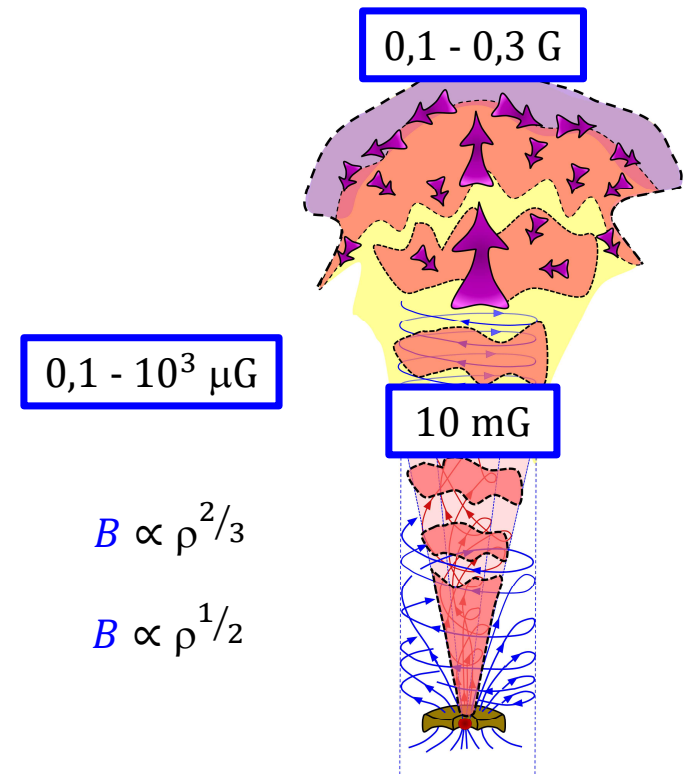
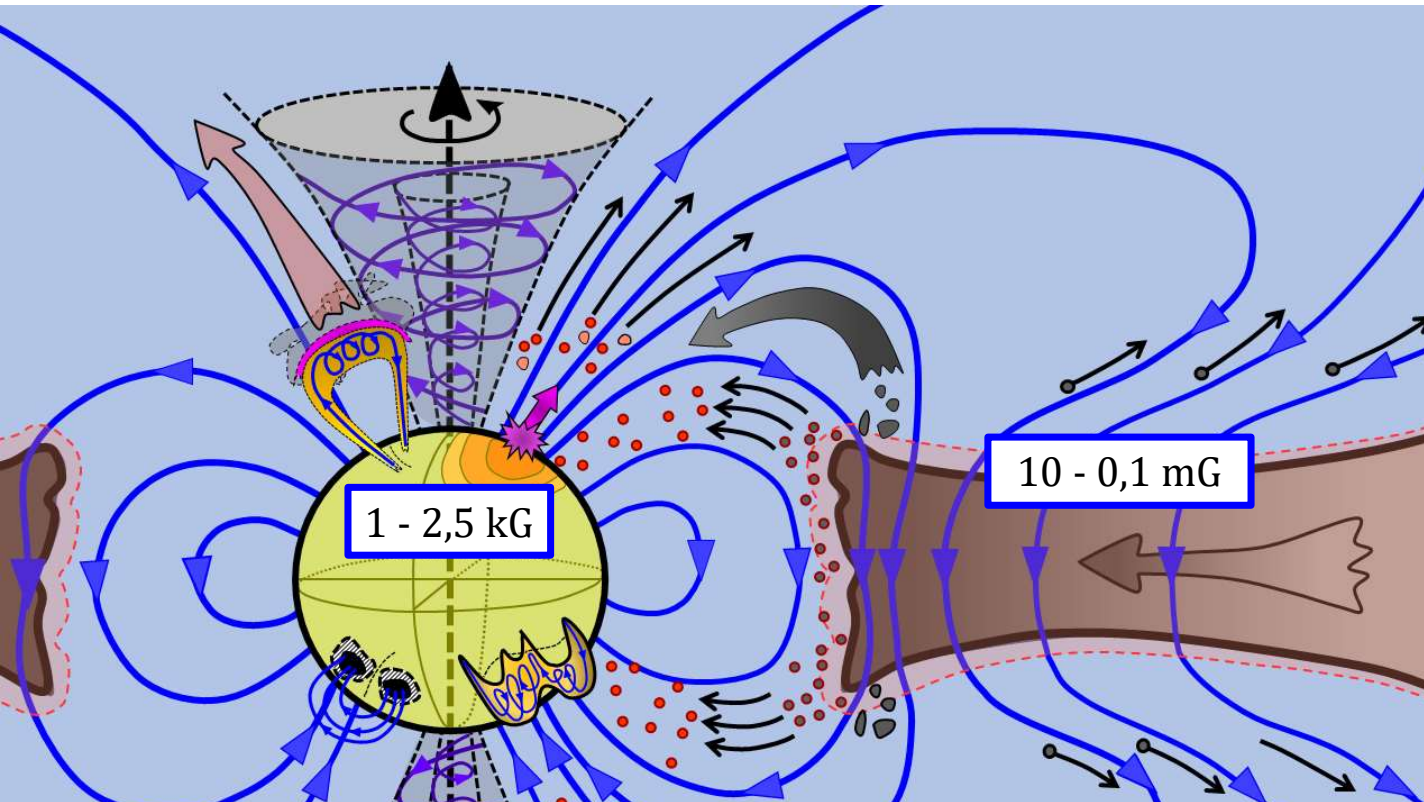
European Large Telescope (ELT) ESO



Atacama Large Millimeter/submillimeter Array (ALMA) ESO



James Webb Space Telescope (JWST) NASA



## Determination of the Magnetic Flux Density $\vec{B}$

(strength, orientation, direction)

Component in the line of sight to the observer ( $B_{LOS}$ )

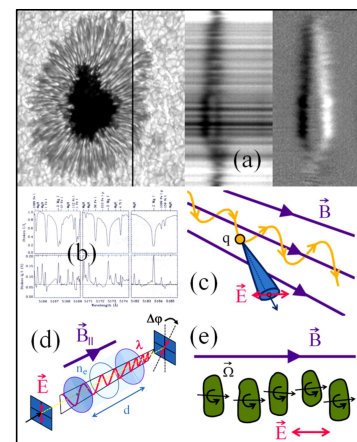
Component in the plane of the sky ( $B_{POS}$ )

Galactic magnetic field models

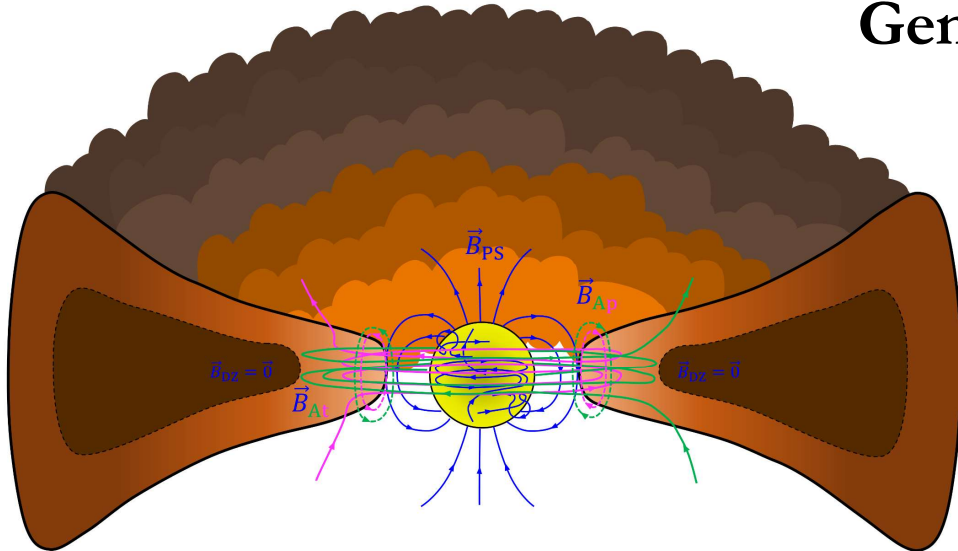
- Zeeman effect splitting
- Stokes parameter
- Synchrotron radiation
- Faraday rotation
- Polarization of dust emission
- Polarization of starlight (dust quenching)

- Hanle effect
- Ion-to-neutral linewidth ratio
- Atomic alignment Ratio of perpendicular to parallel velocity fluctuations

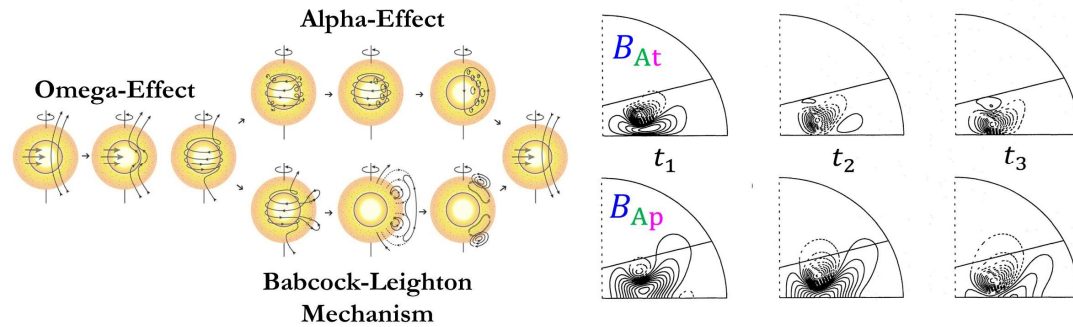
U. v. Kusserow



# Generation and Transport of Magnetic Fields



- Generation of galactic magnetic fields by the **Bierman battery effect (1)**
- Existence of **magnetic seed fields** in molecular clouds
- **Dynamo processes (2)** in **prestellar cores** and **protostars (2)**
- **Accretion disk dynamo** processes (2)
- Magnetic field transport in **accretion disks** and **protostellar wind systems (3)**
- Dynamo processes in **protoplanets**
- Dynamo processes in **protomoons**



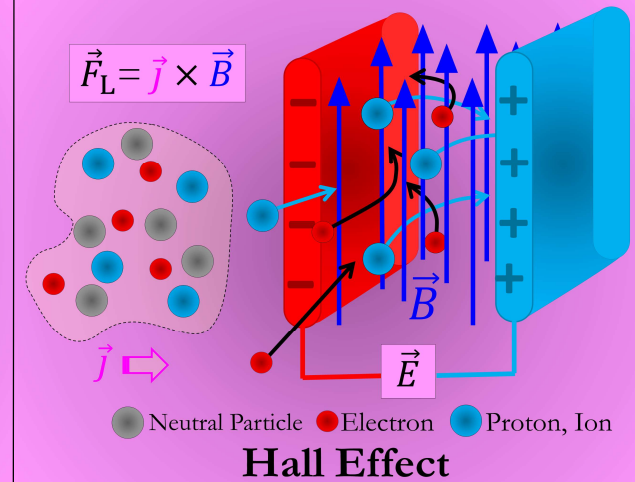
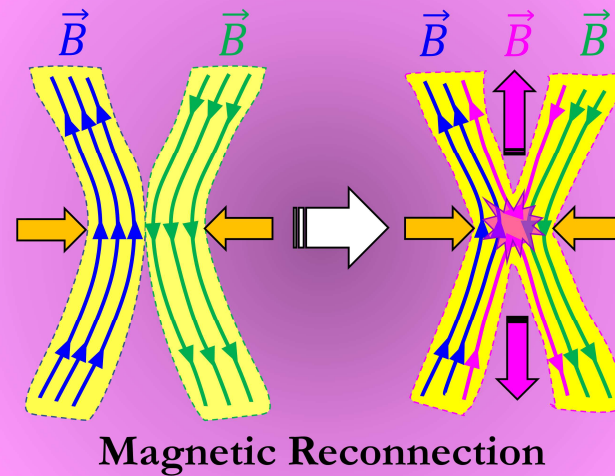
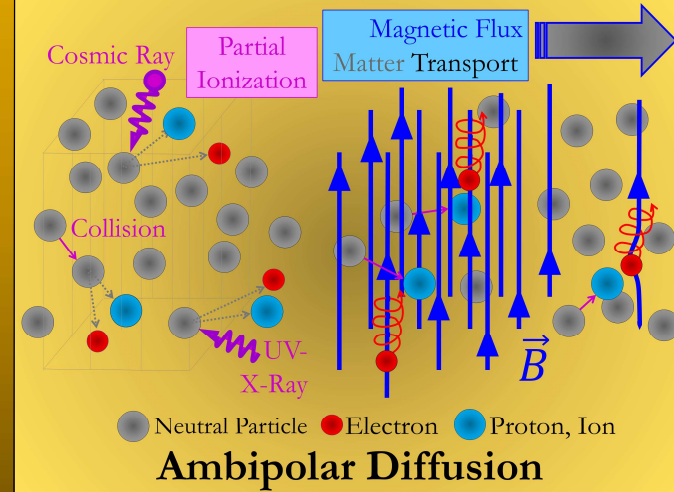
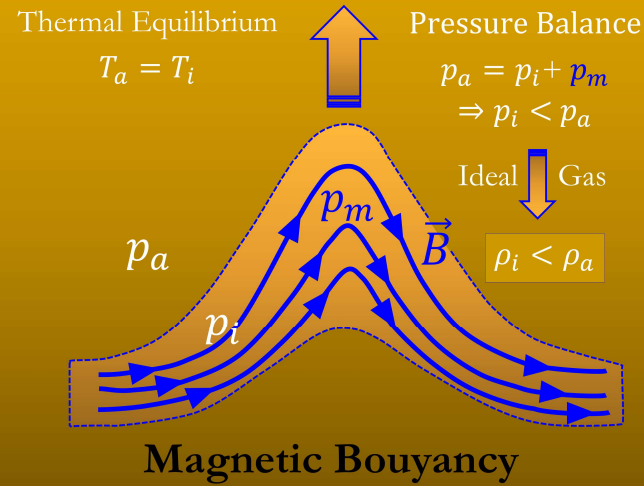
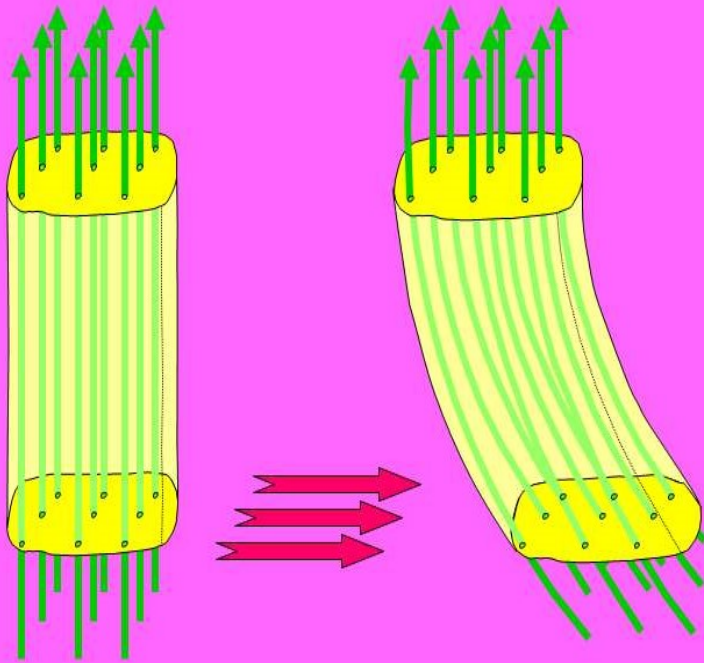
$$(1) \quad \frac{\partial \vec{B}}{\partial t} = \frac{m_H}{2e} \cdot \frac{\vec{\nabla} p \times \vec{\nabla} \rho}{\rho^2}$$

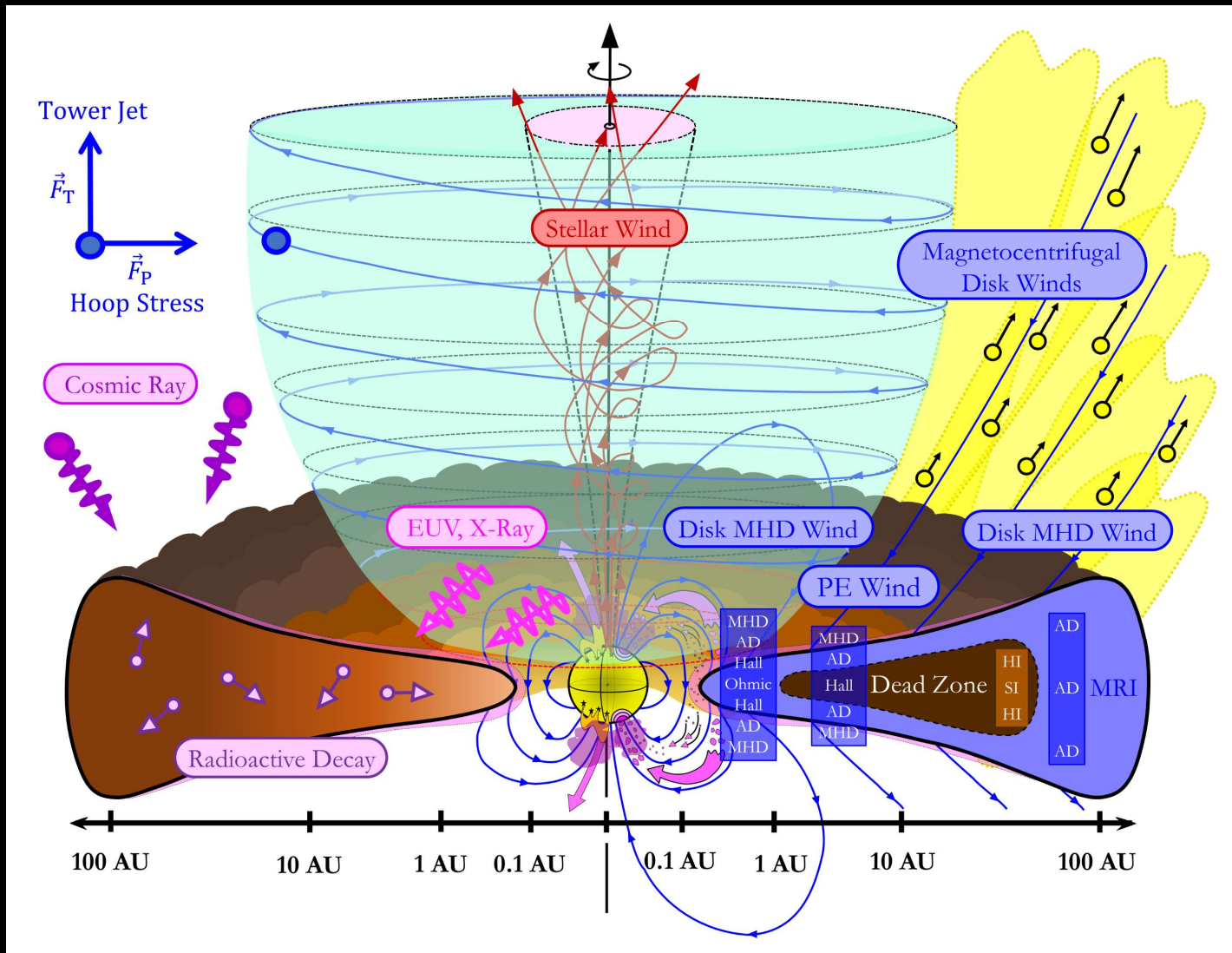
$$(2) \quad \frac{\partial \vec{B}}{\partial t} = \underbrace{\vec{\nabla} \times (\vec{v} \times \vec{B})}_{\omega \text{ - Effect}} + \underbrace{\vec{\nabla} \times (\alpha \cdot \vec{B})}_{\alpha \text{ - Effect}} + \underbrace{\eta \cdot \vec{\nabla}^2 \vec{B}}_{\text{Diffusion-Term}}$$

$$(3) \quad \frac{\partial \vec{B}}{\partial t} = \vec{\nabla} \times \left[ \vec{v} \times \vec{B} - \eta_{OR} \vec{\nabla} \times \vec{B} - \eta_{HE} (\vec{\nabla} \times \vec{B}) \times \vec{B} - \eta_{AD} \left( (\vec{\nabla} \times \vec{B}) \times \vec{B} \right) \times \vec{B} \right]$$



# Model image of "Frozen" in Magnetic Field Lines

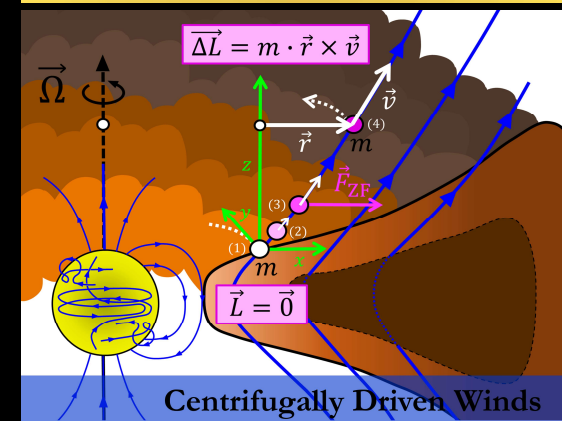
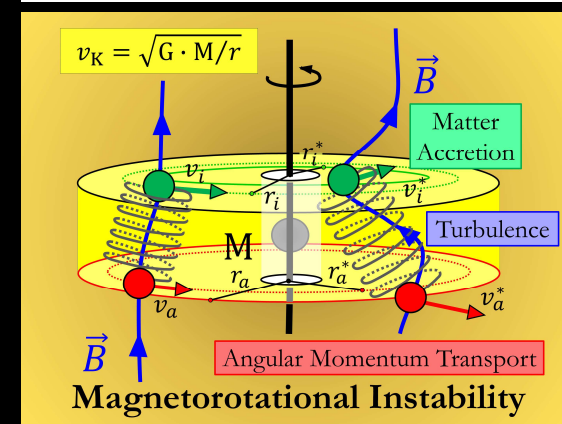
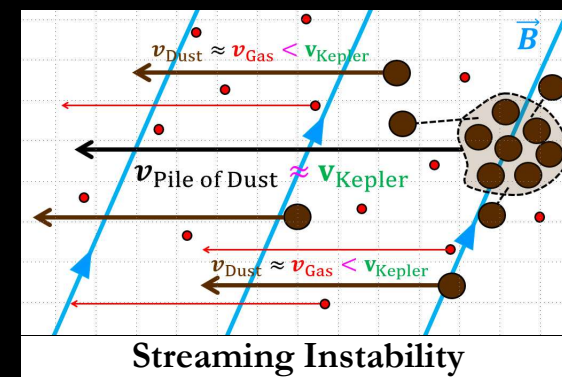


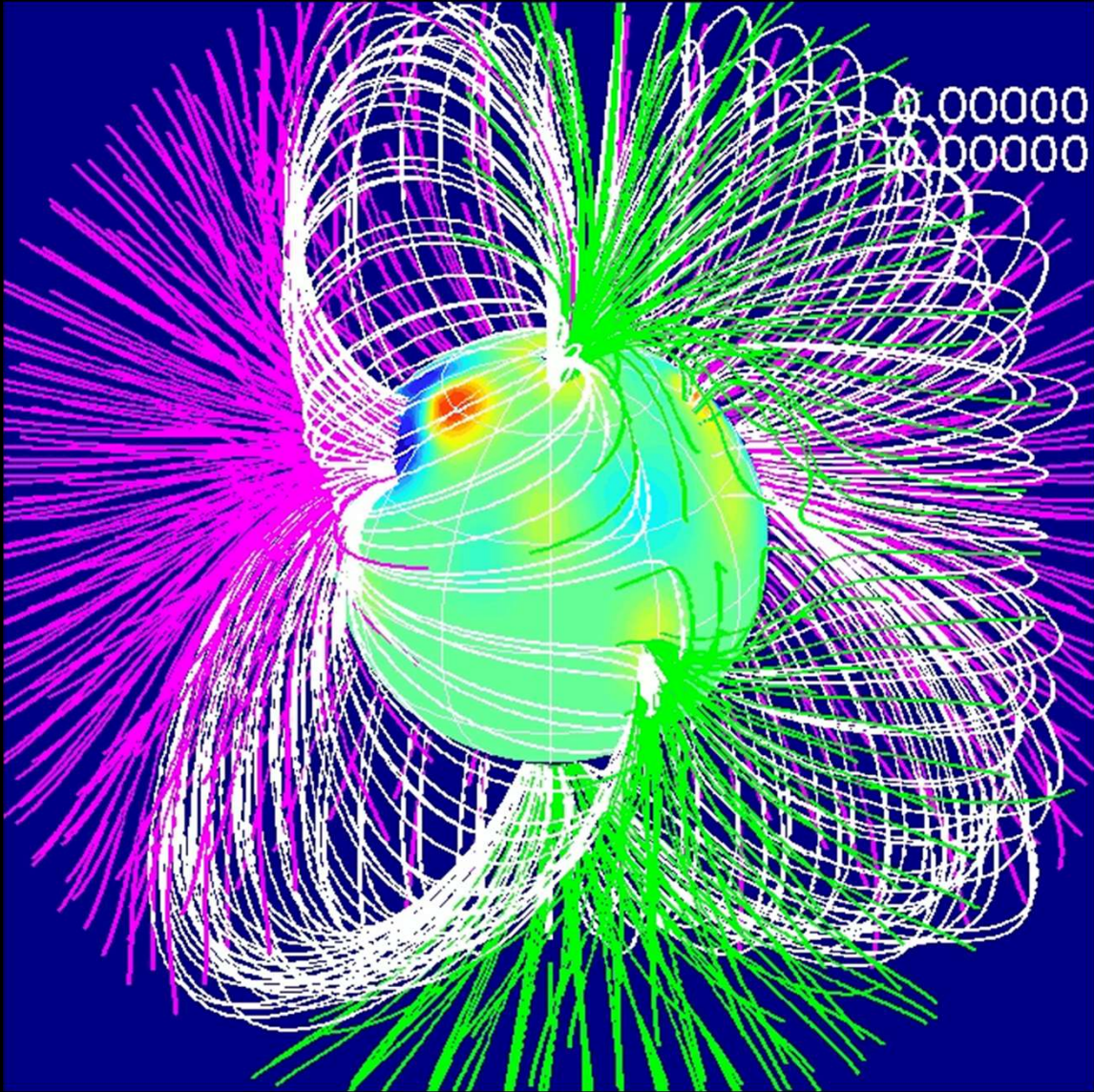
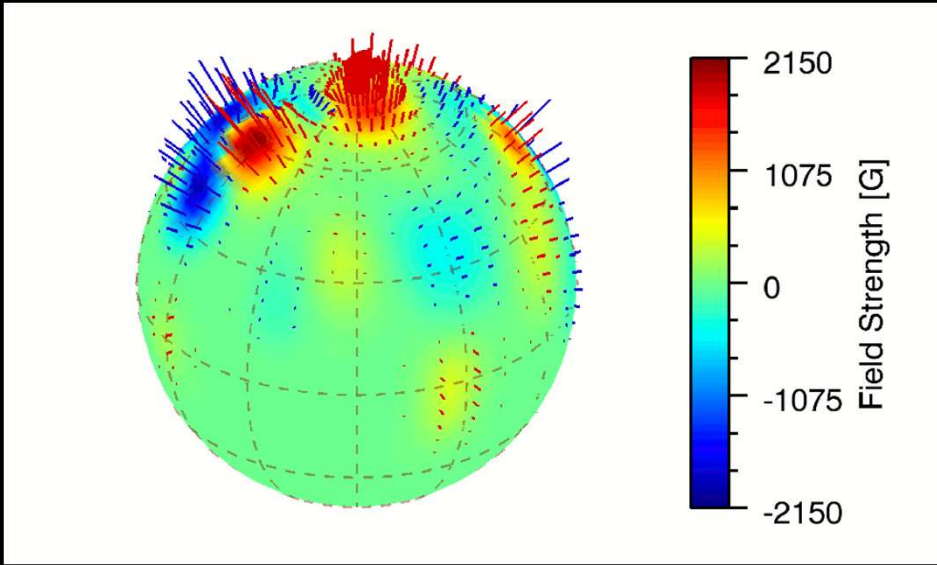
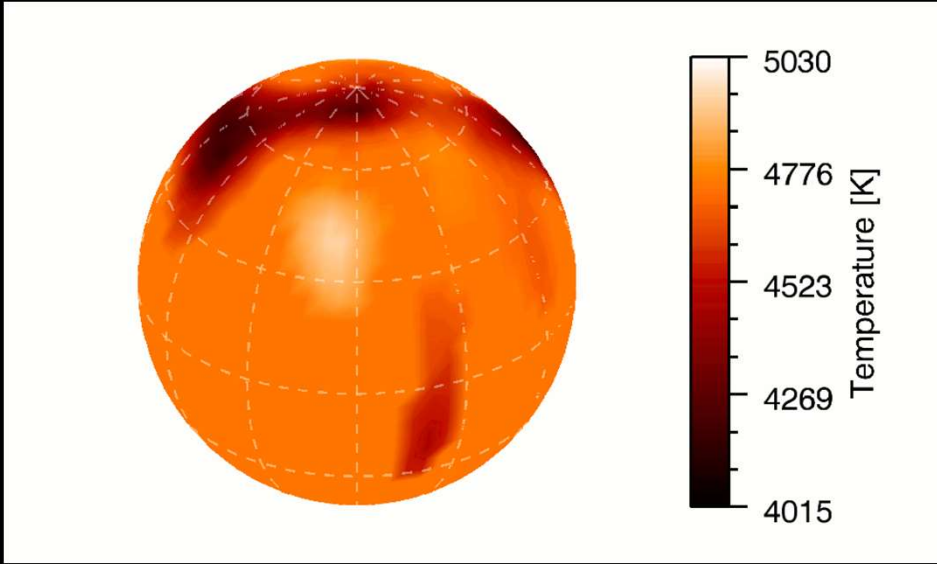


$$\frac{\partial \vec{B}}{\partial t} = \vec{\nabla} \times (\vec{v} \times \vec{B}) - \vec{\nabla} \times (\eta_{OD} \cdot \vec{\nabla} \times \vec{B}) + \vec{\nabla} \times \{ \eta_{AD} \cdot (\vec{\nabla} \times \vec{B}) \times \vec{B} \} - \vec{\nabla} \times [ \vec{\nabla} \times \{ \eta_{HD} \cdot (\vec{\nabla} \times \vec{B}) \times \vec{B} \} ]$$

# Angular Momentum Transport Processes in Star Formation

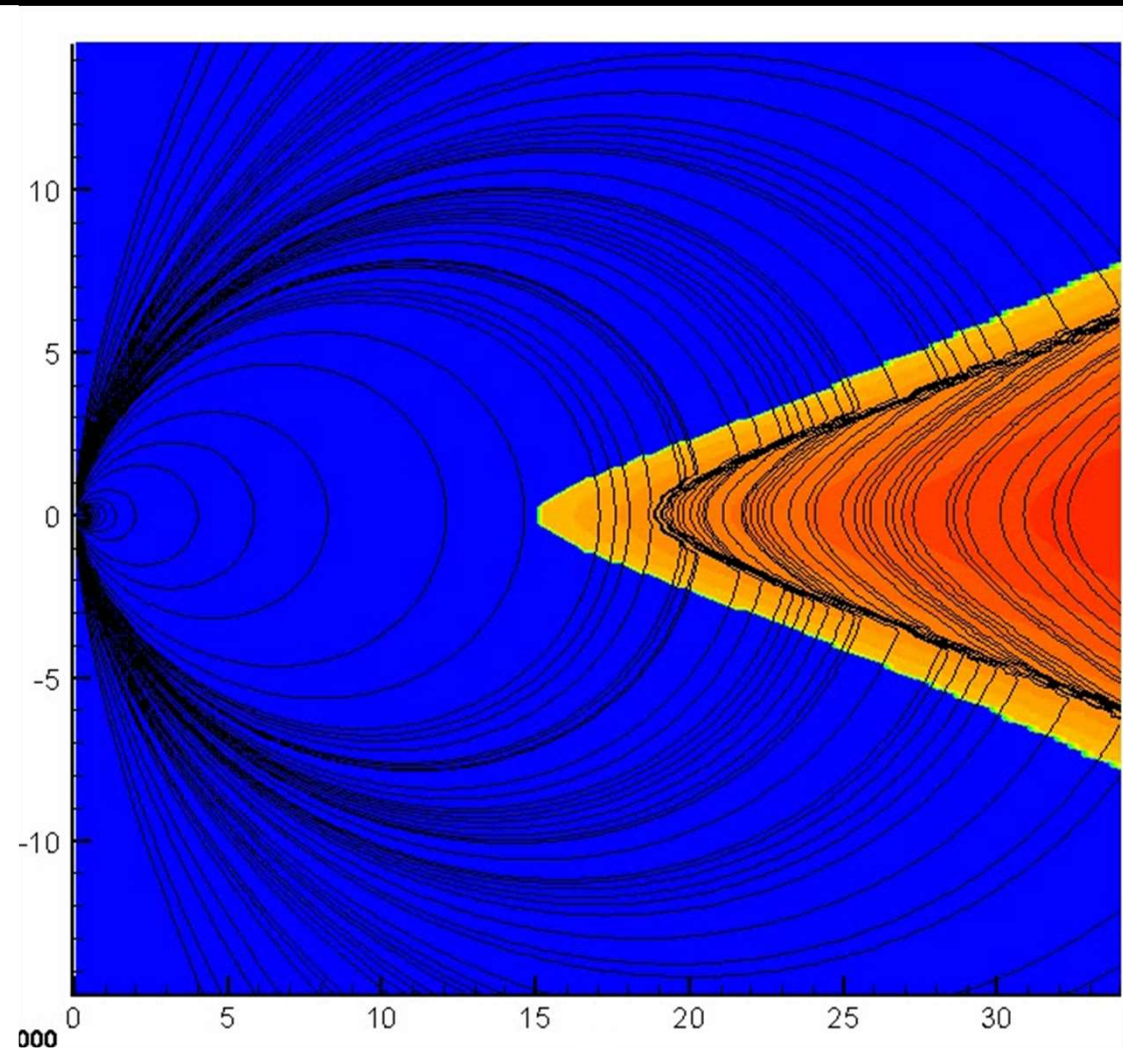
- Angular momentum exchange due to the **passage** of **star formation regions** through the galactic spiral arms
- Angular momentum exchange between by **collisions** of **molecular and dust clouds**
- Angular momentum exchange between **prestellar cores/pseudodisks** and the **surrounding clouds**, rotating with different speeds
- Removal of angular momentum by magnetohydrodynamic **Alfvén-waves** after the generation of magnetic fields
- Angular momentum exchange between gas and dust particles (**streaming instability**)
- Angular momentum transport due to friction processes, hydrodynamic instabilities and the **magnetorotational instability (MRI)** in accretion disks
- Removal of angular momentum in **magnetized protostellar and disk winds**
- Migration processes due to angular momentum exchange between **gas particles, pebbles, planetesimals** and **protoplanets** and the **accretion disk**
- Angular momentum transfer through **contact** between the **accretion disk** and the **molecular clouds bordering** it
- Angular momentum input through **streamers flowing into the protoplanetary disk** from outside
- Effective angular momentum removal from the magnetosphere of the young pre-main sequence star by continuous **magnetized stellar wind** and **coronal mass ejections**
- Angular momentum transport in **young multiple star systems**



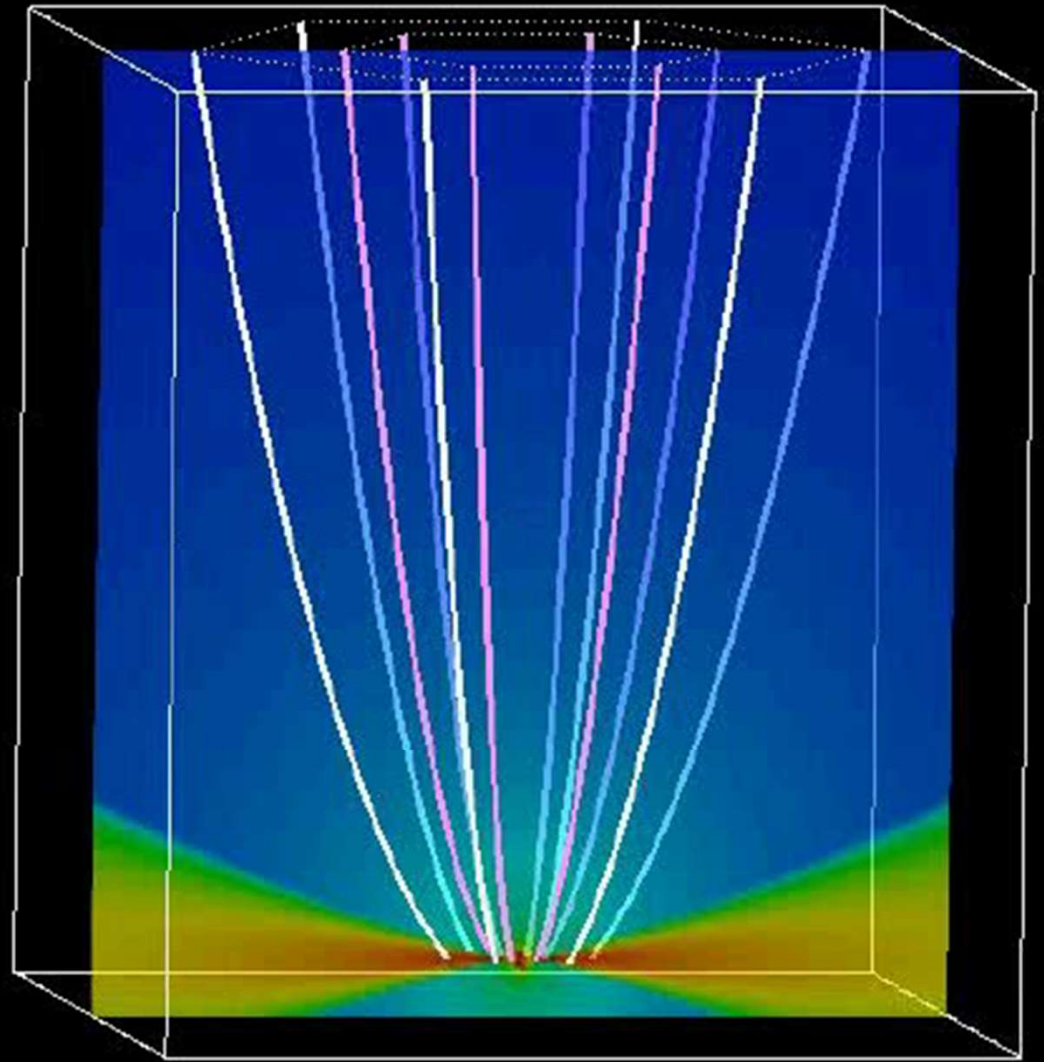


Zeeman-Doppler-Imaging study of II Pegasi - PEPSI/K. G. Strassmeier et al.

Stellar environment II Pegasi with a magnetic-field extrapolation out to 2.2 stellar radii

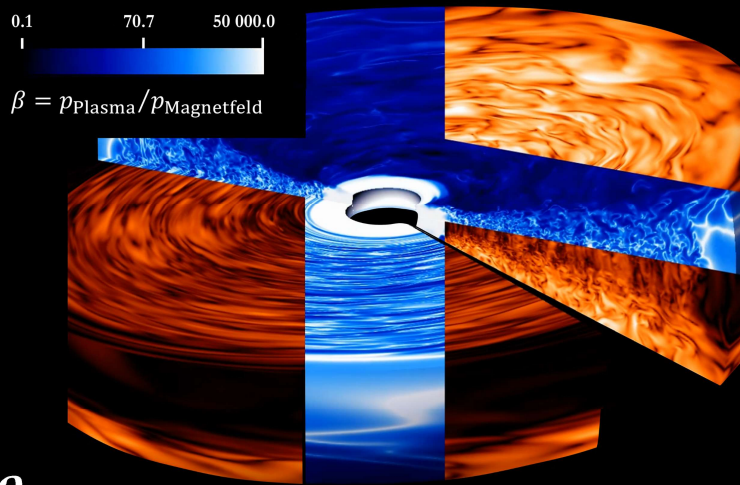


Inflow of matter from the accretion disk via the magnetosphere to the protostar - C. Fendt MPIA Heidelberg

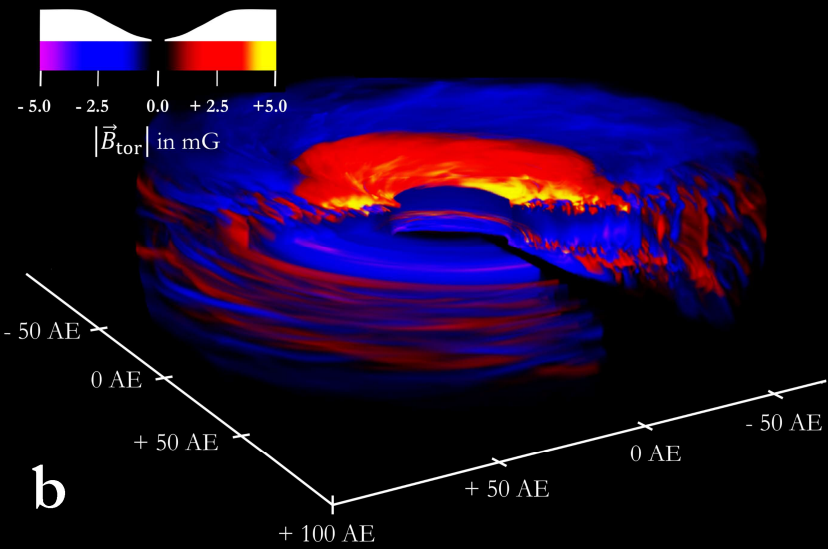


Toroidal winding of magnetic fields in 'Tower Jets' - Gakai

# Turbulence and Accretion in 3D Global MHD Simulations of Stratified Protoplanetary Disk

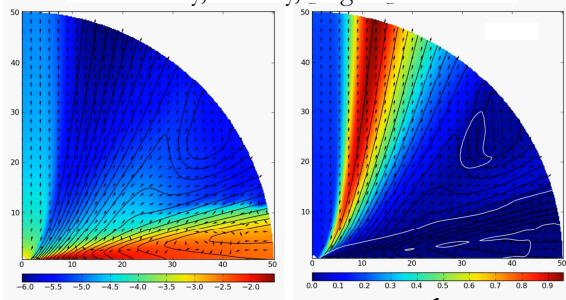


**a**



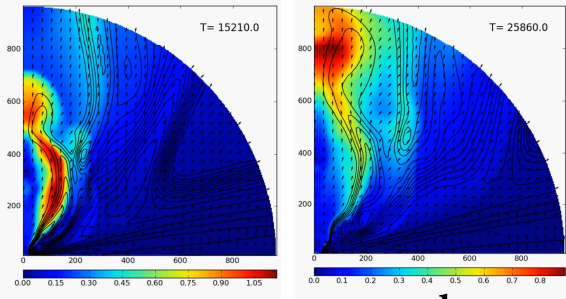
**b**

Accretion, disk-jet simulation  
density, velocity, magnetic field



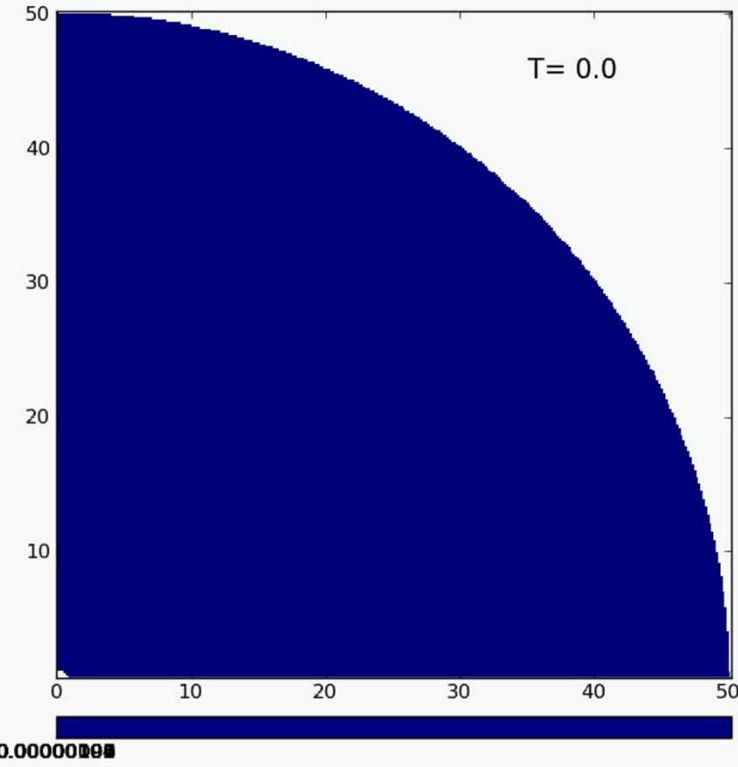
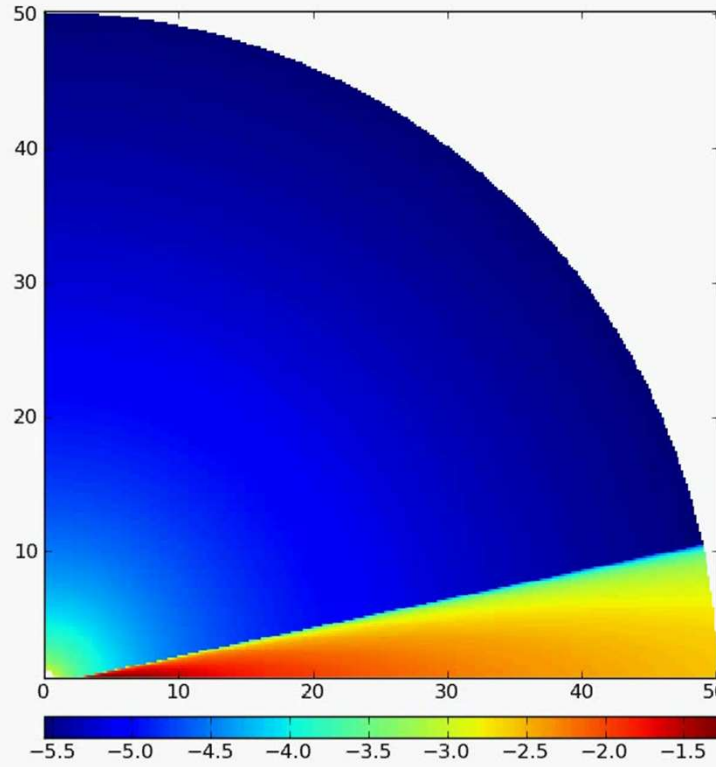
a

b



c

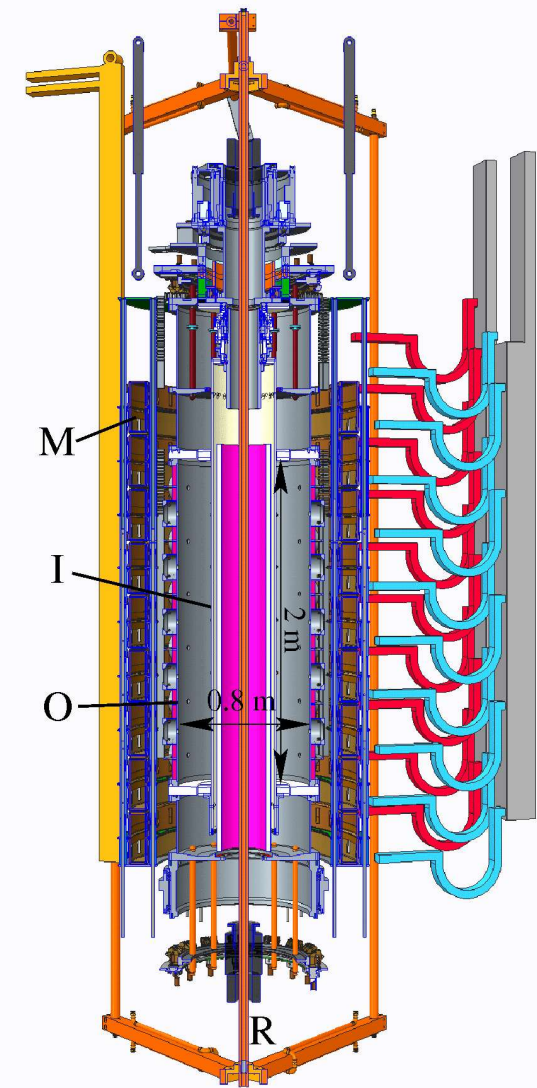
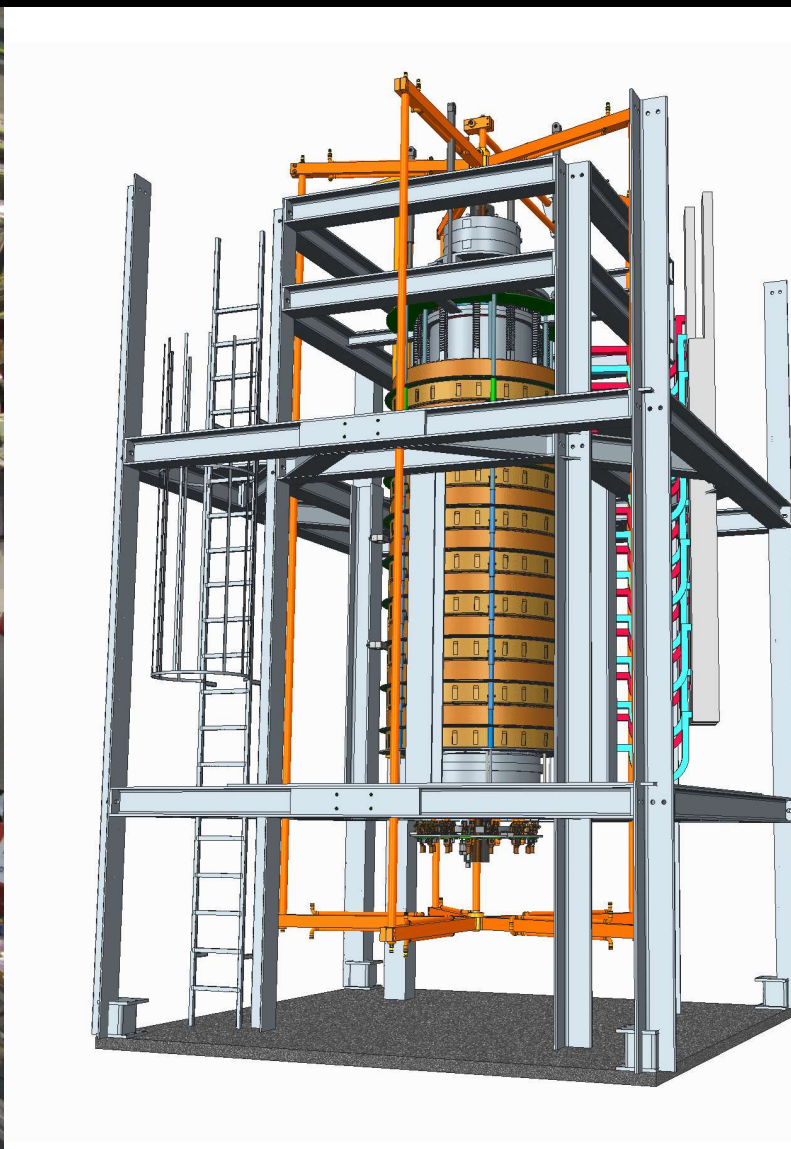
d



Results of MHD simulations of accretion ejection including magnetic field generation by a disk dynamo - C. Fendt et al.



Setup of the PROMISE Experiment - F. Stefani et al. (FZDR)



Design of the future MRI/TI experiment - F. Stefani et al. (FZDR)



## Liquid metal experiments on the helical magnetorotational instability

*F. Stefani<sup>1</sup>, G. Gerbeth<sup>1</sup>, Th. Gundrum<sup>1</sup>,  
J. Szklarski<sup>2</sup>, G. Rüdiger<sup>3</sup>, R. Hollerbach<sup>4</sup>*

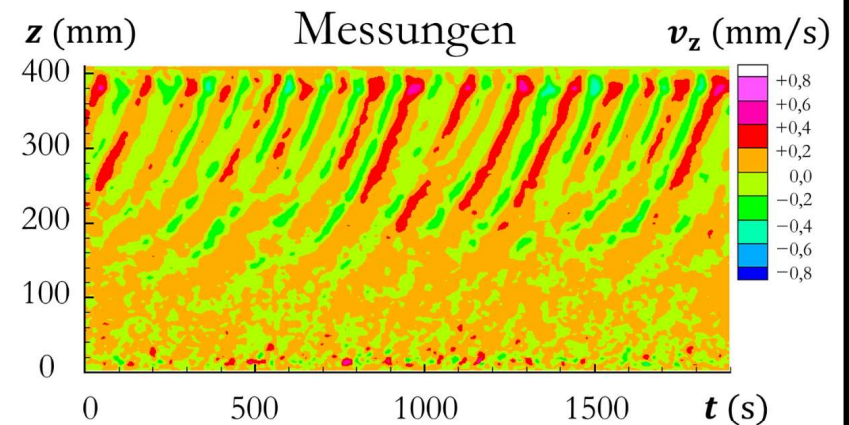
<sup>1</sup> *Forschungszentrum Dresden-Rossendorf, P.O. Box 510119, D-01314 Dresden,  
Germany*

<sup>2</sup> *Institute of Fundamental Technological Research, 21, Świętokrzyska, 00-049 Warsaw,  
Poland*

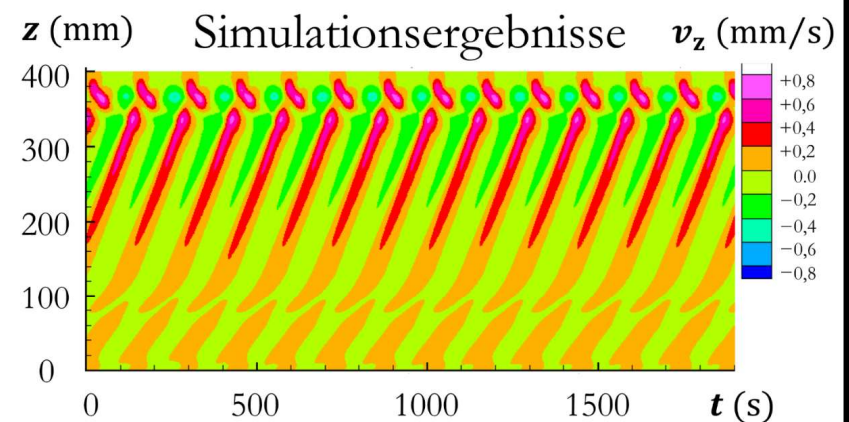
<sup>3</sup> *Astrophysikalisches Institut Potsdam, An der Sternwarte 16, D-14482 Potsdam,  
Germany*

<sup>4</sup> *Department of Applied Mathematics, University of Leeds, Leeds, LS2 9JT, UK*

The magnetorotational instability (MRI) plays an essential role in the formation of stars and black holes. By destabilizing hydrodynamically stable Keplerian flows, the MRI triggers turbulence and enables outward transport of angular momentum in accretion discs. We present the results of a liquid metal Taylor-Couette experiment under the influence of helical magnetic fields that show typical features of MRI at Reynolds numbers of the order 1000 and Hartmann numbers of the order 10. Particular focus is laid on an improved experiment in which split end caps are used to minimize the Ekman pumping.



**b**



**c**

## Experimental Confirmation of the Standard Magnetorotational Instability Mechanism with a Spring-Mass Analogue

Derek M.H. Hung,<sup>1,2</sup> Eric G. Blackman,<sup>3,4,\*</sup> Kyle J. Caspary,<sup>2</sup> Erik P. Gilson,<sup>2</sup> and Hantao Ji<sup>1,2,†</sup>

<sup>1</sup>*Department of Astrophysical Sciences, Princeton University, Princeton, New Jersey 08544, USA*

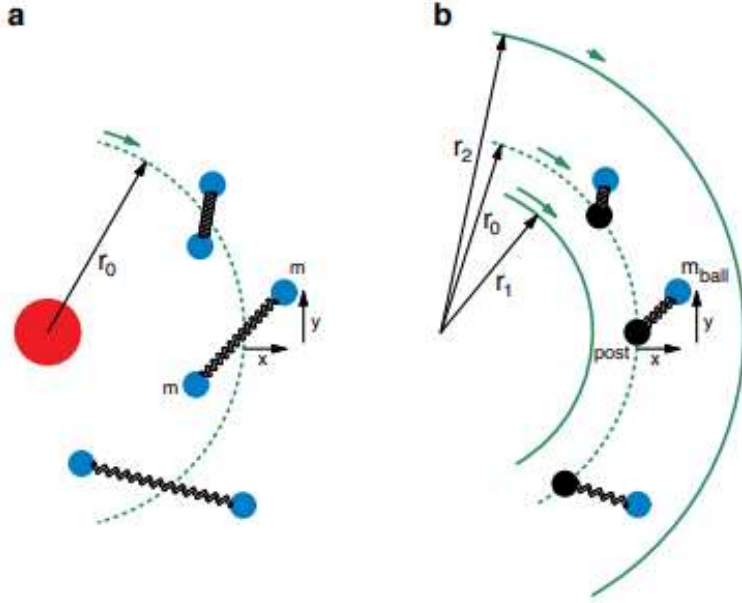
<sup>2</sup>*Princeton Plasma Physics Laboratory, Princeton, New Jersey 08543, USA*

<sup>3</sup>*Department of Physics and Astronomy, University of Rochester, Rochester, NY 14627, USA*

<sup>4</sup>*Laboratory for Laser Energetics, University of Rochester, Rochester NY, 14623, USA*

(Dated: December 13, 2018)

The Magnetorotational Instability (MRI) has long been considered a plausibly ubiquitous mechanism to destabilize otherwise stable Keplerian flows to support radially outward transport of angular momentum. Such an efficient transport process would allow fast accretion in astrophysical objects such as stars and black holes to release copious kinetic energy that powers many of the most luminous sources in the universe. But the standard MRI under a purely vertical magnetic field has heretofore never been directly measured despite numerous efforts over more than a decade. Here we report an unambiguous laboratory demonstration of the spring-mass analogue to the standard MRI by comparing motion of a spring-tethered ball within different rotating flows. The experiment corroborates the theory: efficient outward angular momentum transport manifests only for cases with a weak spring in quasi-Keplerian flow. Our experimental method accomplishes this in a new way, thereby connecting solid and fluid mechanics to plasma astrophysics.



Analogue of standard MRI in a purely vertical magnetic field

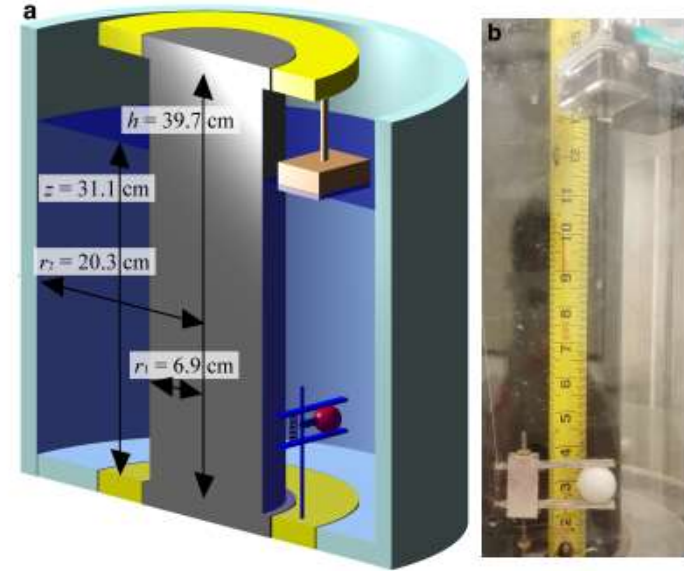


FIG. 4. Experimental apparatus and diagnostics. **a** Schematic of the modified Taylor-Couette device [48], with the inner and outer cylinder radii of  $r_1 = 6.9$  cm and  $r_2 = 20.3$  cm respectively, and the height of  $h = 39.7$  cm. The device was filled with water to a depth of 31.1 cm and the top was open to allow access. A GoPro HERO4 camera was partially submerged to minimize optical distortion. The camera was supported by an attachment and co-rotated with the ring (yellow) at  $\Omega_3$ . A 1-inch-diameter neutrally buoyant test mass (red) was tethered by an unstretched spring to a vertical post and held by a spring-loaded jaw-clamp. At  $t = 0$  a release line (not shown) was pulled from above allowing the vertical spring to relax, releasing the mass. **b** Photograph of the test mass and release mechanism. The camera is visible at the top of the image.

## Laser experiment for the study of accretion dynamics of Young Stellar Objects: design and scaling

G. Revet,<sup>1,2</sup> B. Khair,<sup>3</sup> J. Béard,<sup>4</sup> R. Bonito,<sup>5</sup> S. Orlando,<sup>5</sup> M. V. Starodubtsev,<sup>2</sup> A. Ciardi,<sup>6</sup> and J. Fuchs<sup>1,2,7</sup>

<sup>1</sup>LULI - CNRS, École Polytechnique, CEA: Université Paris-Saclay; UPMC  
Univ Paris 06: Sorbonne Universités - F-91128 Palaiseau cedex, France

<sup>2</sup>Institute of Applied Physics, 46 Ulyanov Street, 603950 Nizhny Novgorod, Russia

<sup>3</sup>Flash Center for Computational Science, Department of Astronomy  
& Astrophysics, The University of Chicago, IL, United States

<sup>4</sup>LNCMI, UPR 3228, CNRS-UGA-UPS-INSA, 31400 Toulouse, France

<sup>5</sup>INAF (Istituto Nazionale di Astrofisica) - Osservatorio Astronomico di Palermo, Palermo, Italy

<sup>6</sup>LERMA, Observatoire de Paris, PSL Research University, CNRS,  
Sorbonne University, UPMC Univ. Paris 06, F-75005, Paris, France

<sup>7</sup>ELI-NP, "Horia Hulubei" National Institute for Physics and Nuclear Engineering,  
30 Reactorului Street, RO-077125, Bucharest-Magurele, Romania

A new experimental set-up designed to investigate the accretion dynamics in newly born stars is presented. It takes advantage of a magnetically collimated stream produced by coupling a laser-generated expanding plasma to a  $2 \times 10^5$  G (20 T) externally applied magnetic field. The stream is used as the accretion column and is launched onto an obstacle target that mimics the stellar surface. This setup has been used to investigate in details the accretion dynamics, as reported in Ref. [1]. Here, the characteristics of the stream are detailed and a link between the experimental plasma expansion and a 1D adiabatic expansion model is presented. Dimensionless numbers are also calculated in order to characterize the experimental flow and its closeness to the ideal MHD regime. We build a bridge between our experimental plasma dynamics and the one taking place in the Classical T Tauri Stars (CTTSs), and we find that our set-up is representative of a high plasma  $\beta$  CTTS accretion case.

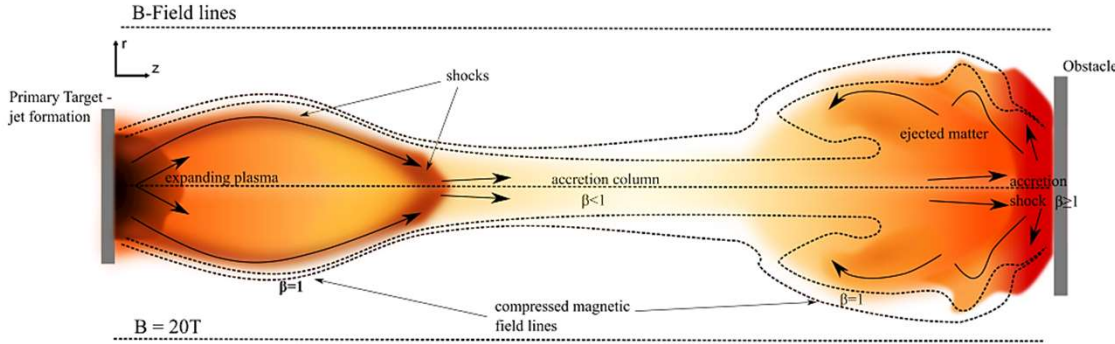


FIG. 1. Schematic of the accretion experiment performed using a magnetically collimated supersonic flow generated by a laser. The plasma generation and expansion takes place at the primary target location (left side of the image). The jet formed via the interaction with the  $2 \times 10^5$  G (20 T) magnetic field is launched onto a secondary, obstacle target, where the laboratory accretion takes place. As a spatial scale indication, note that the cavity tip is located at  $\sim 0.6$  cm from the primary target surface, for a magnetic field of  $2 \times 10^5$  G (20 T) and a laser intensity as the one use at the ELFIE laser facility (see main text). The colors used in the schematic are meant to give indication of the higher density zones (darker) vs. the lower density zones (lighter), the shading of colors used is in no sense quantitative. Ref. [1] displays results of that accretion setup for a distance between the primary and the obstacle target of about 1.2 cm.

	Laboratory	CTTS
B-Field [T]	20	$50.10^{-4}$
Material	$C_2H_3Cl$ (PVC)	H
Atomic number	10.4	1.28
	Stream	Stream
Spatial transversal scale [cm]	0.1	$0.5 \times 10^{10}$
Charge state	2.5	1
Electron Density [ $cm^{-3}$ ]	$1 \times 10^{18}$	$1 \times 10^{11}$
Ion density [ $cm^{-3}$ ]	$1.9 \times 10^{17}$	$1 \times 10^{11}$
Density [ $g\ cm^{-3}$ ]	$3 \times 10^{-6}$	$2 \times 10^{-13}$
Te [eV]	10	0.22
Ti [eV]	10	0.22
Flow velocity [ $km\ s^{-1}$ ]	100 – 1000	500
Sound speed [ $km\ s^{-1}$ ]	31	7.4
Alfven speed [ $km\ s^{-1}$ ]	325	304
Electron mean free path [cm]	$2.7 \times 10^{-5}$	0.7
Electron collision time [ns]	$2 \times 10^{-4}$	35
Ion mean free path [cm]	$1.4 \times 10^{-6}$	1
Ion collision time [ns]	$1.4 \times 10^{-3}$	$2.4 \times 10^3$
Magnetic diffusion time [ns]	45	$4 \times 10^{21}$
Electron Larmor radius [cm]	$3.8 \times 10^{-5}$	$2 \times 10^{-2}$
Electron gyrofrequency [ $s^{-1}$ ]	$1.4 \times 10^8$	$1.2 \times 10^8$
Ion Larmor radius [cm]	$1 \times 10^{-3}$	1
Ion gyrofrequency [ $s^{-1}$ ]	$6 \times 10^4$	$5.2 \times 10^4$
Electron magnetization	0.7	30
Ion magnetization	$1.4 \times 10^{-3}$	0.9
Mach number	24	67
Alfven Mach number	2.3	1.6
Reynolds	$5 \times 10^6$	$6 \times 10^{11}$
Magnetic Reynolds	68	$4 \times 10^{10}$
Peclet	$7 \times 10^2$	$6 \times 10^9$
$\beta_{ther}$	$1 \times 10^{-2}$	$7 \times 10^{-4}$
$\beta_{dyn}$	10	5
Euler number	2.9	1.6
Alfven number	$2.5 \times 10^{-3}$	$2.1 \times 10^{-3}$

Parameters of the laboratory accretion stream, with respect to those of the accretion stream in CTTSs, for the incoming stream

# Laboratory formation of a scaled protostellar jet by coaligned poloidal magnetic field

B. ALBERTAZZI, A. CIARDI, M. NAKATSUTSUMI, T. VINCI, J. BÉARD, R. BONITO, J. BILLETTE, M. BORGHESI, Z. BURKLEY, [...] AND J. FUCHS +19 authors

SCIENCE · 17 Oct 2014 · Vol 346, Issue 6207 · pp. 325-328 · DOI: 10.1126/science.1259694

## Stellar outflows replicated in miniature

Astronomers observe tight bright jets beaming from the poles of many celestial objects. But what focuses them so well? Albertazzi *et al.* recreated a scaled-down plasma jet in a laboratory setting to match the behavior of those in young stellar objects. The experiments show that the jets are collimated by a poloidal magnetic field aligned with the same axis. A conelike shock also emerges, as the expanding plasma is abruptly confined by the magnetic field.

### Abstract:

Although narrow bipolar jets of matter have been observed to emerge from a wide variety of astrophysical systems, the question of their formation and morphology, **past their launching by magneto-centrifugal forces**, is still open. Our scaled laboratory experiments, representative of outflows from young stellar objects (YSOs), reveal that stable collimation of the entire flow into a narrow jet can result from the presence of a large-scale poloidal magnetic field that is consistent with **observations**. The observed plasma flow focuses and creates an interior cavity, giving rise, close to the source, to a standing conical shock from which the jet emerges. Together with astrophysical full-scale simulations, we conclude that this can also explain recently discovered X-ray emission features observed from low-density regions at the base of protostellar jets, such as the well-studied jet HH 154.

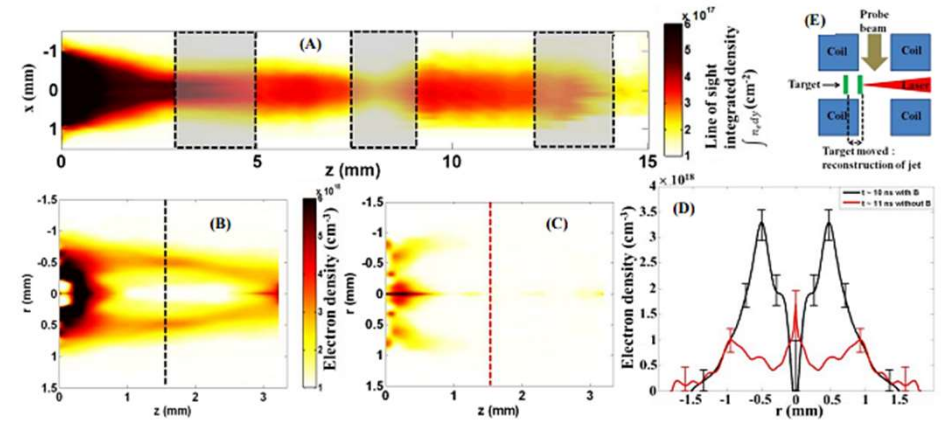
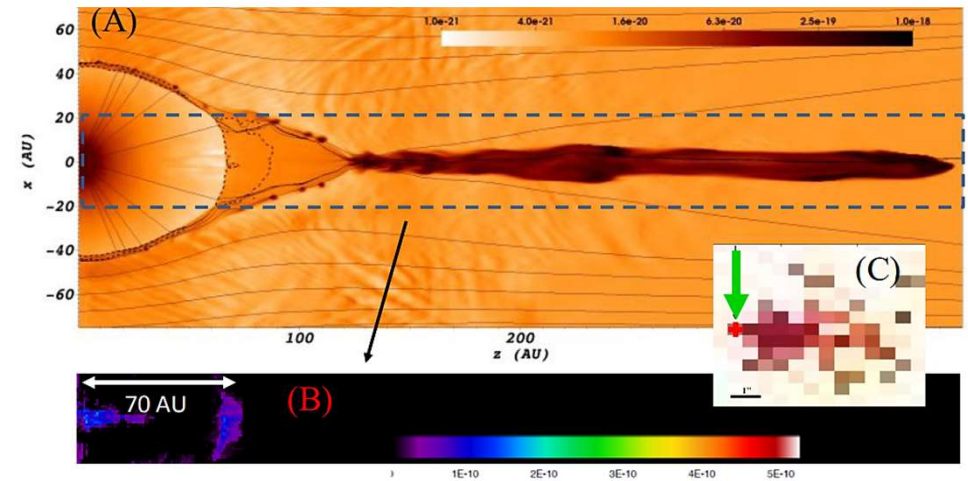
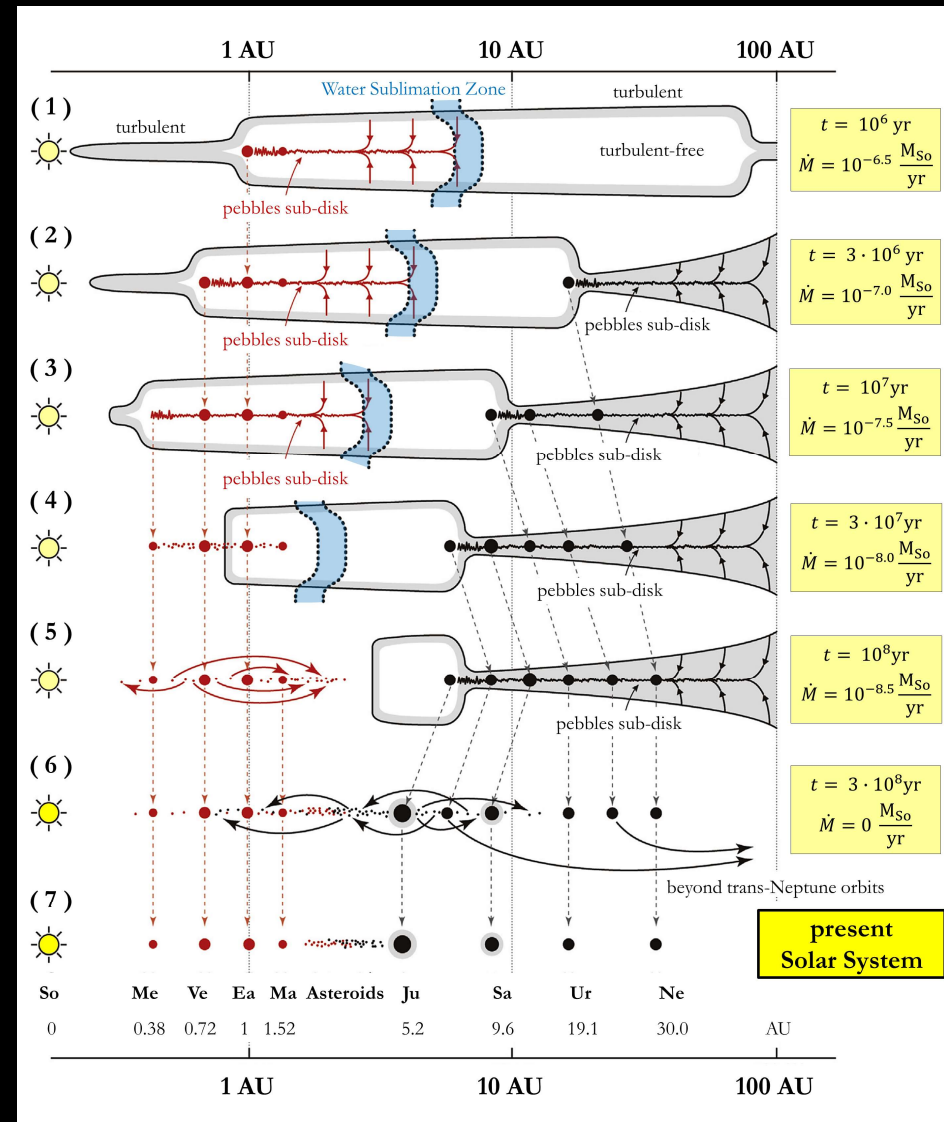
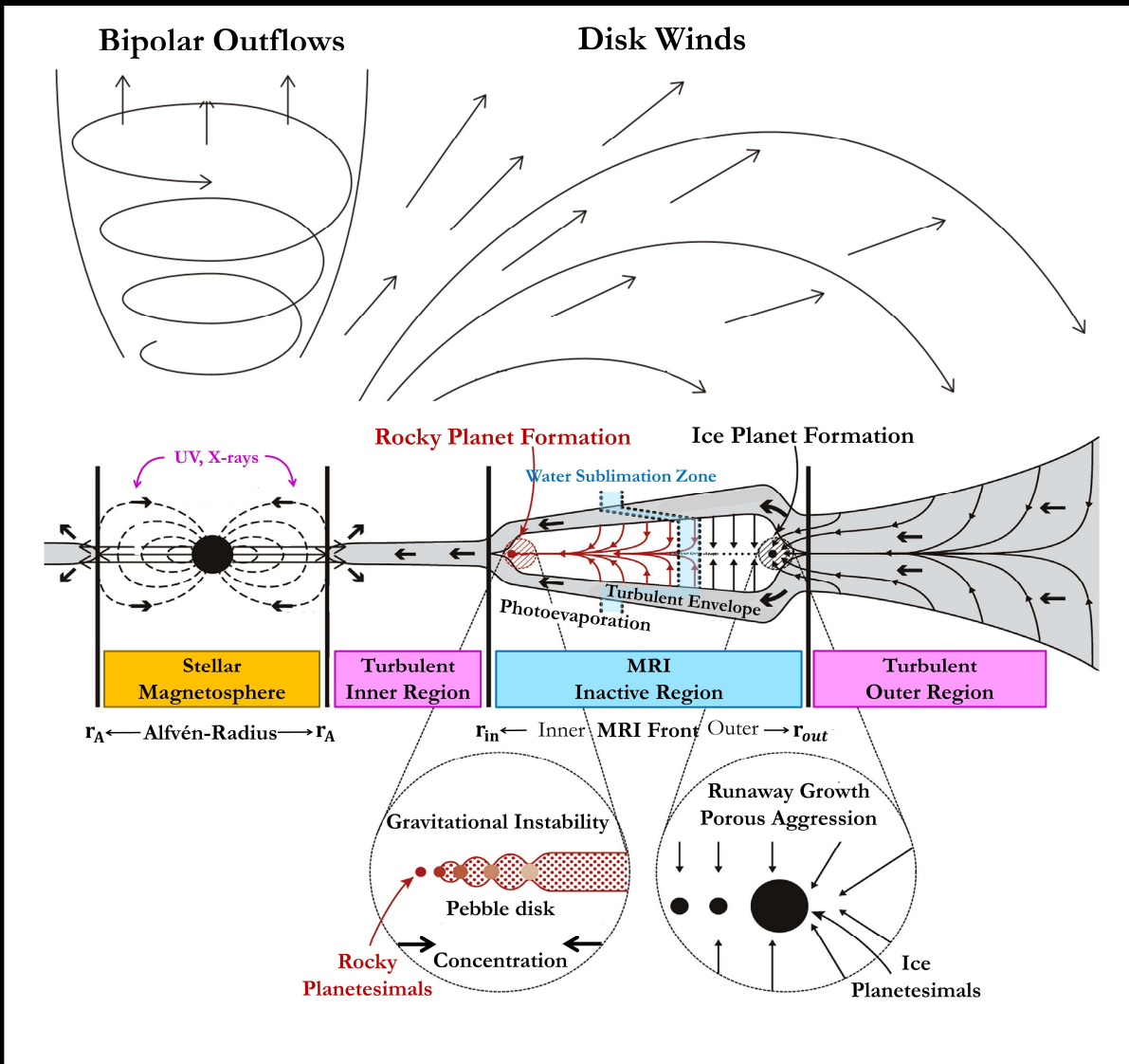


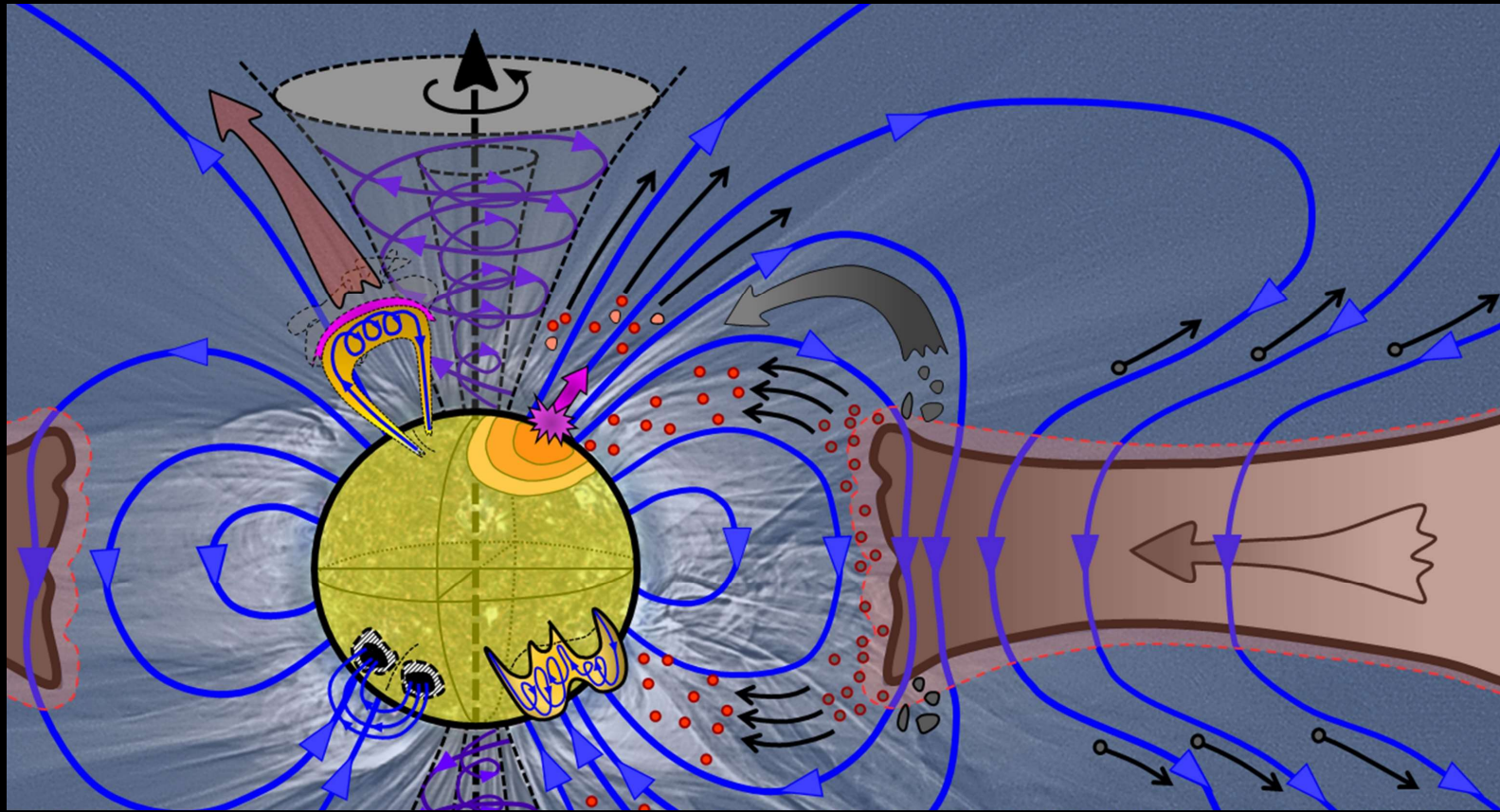
**Fig. 1. Laboratory demonstration of jet formation by axial magnetic field.** (A) Plasma integrated density measured 20 ns after the laser irradiation (coming from the right) of a CH target (left) immersed in the z-oriented 0.2 MG magnetic field. Four spatially patched images are used (see E). Shaded areas are linear interpolation in between observed sections of the jet. (B-C) Abel inverted density maps in the case with (B) and without (C) magnetic field, and (D) lineouts (along the dashed lines shown in B and C), show the cavity region, and plasma convergence on axis, induced by the magnetic field. The error bars on (D) represent the difference in the plasma density retrieved from the upper and lower measured phase maps (see Methods).



3D simulation of jet formation and collimation in a young star system embedded in a 5 mG axial magnetic field

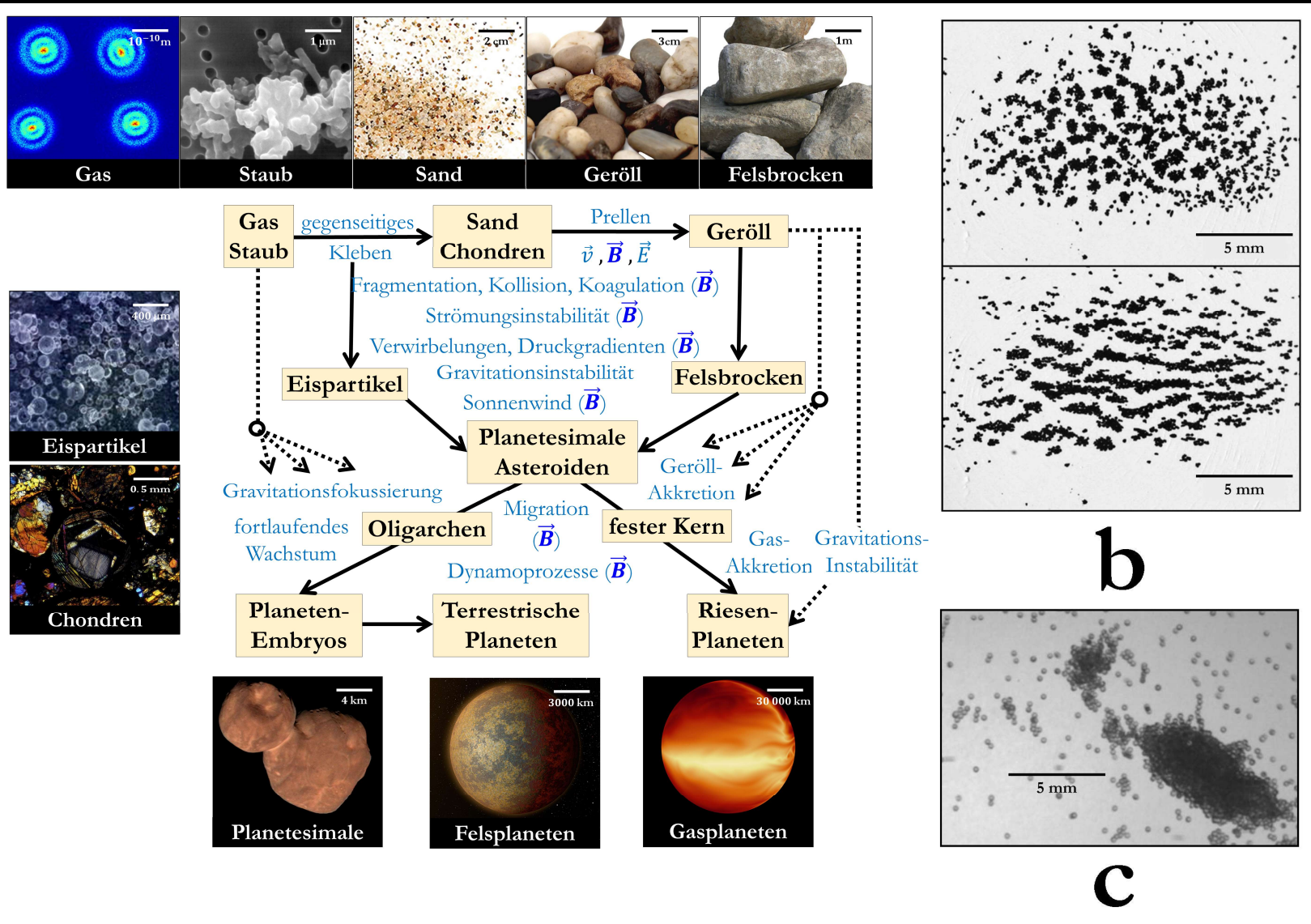


Tandem model of planet formation of solar system-like planetary systems - Y. Imaeda, T. Ebisuzaki



$$\frac{\partial \vec{B}}{\partial t} = \vec{\nabla} \times (\vec{v} \times \vec{B}) - \vec{\nabla} \times (\eta_{OD} \cdot \vec{\nabla} \times \vec{B}) + \vec{\nabla} \times \{ \eta_{AD} \cdot (\vec{\nabla} \times \vec{B}) \times \vec{B} \} - \vec{\nabla} \times [ \vec{\nabla} \times \{ \eta_{HD} \cdot (\vec{\nabla} \times \vec{B}) \times \vec{B} \} ]$$

Exemplarity



Formation of planetesimals and planets from dust and gas with possible influences of magnetic fields

U. v. Kusserow, A. S. Stodolna et al., E. K. Jessberger et al., J. Kashuba, NASA/JHUAPL/Southwest Research Institute/R. Tkachenko

*Cosmic Magnetic Fields:  
From Planets, to Stars and Galaxies  
Proceedings IAU Symposium No. 259, 2008  
K.G. Strassmeier, A.G. Kosovichev & J.E. Beckman, eds.*

© 2009 International Astronomical Union  
doi:10.1017/S1743921309030592

## The role of magnetic fields for planetary formation

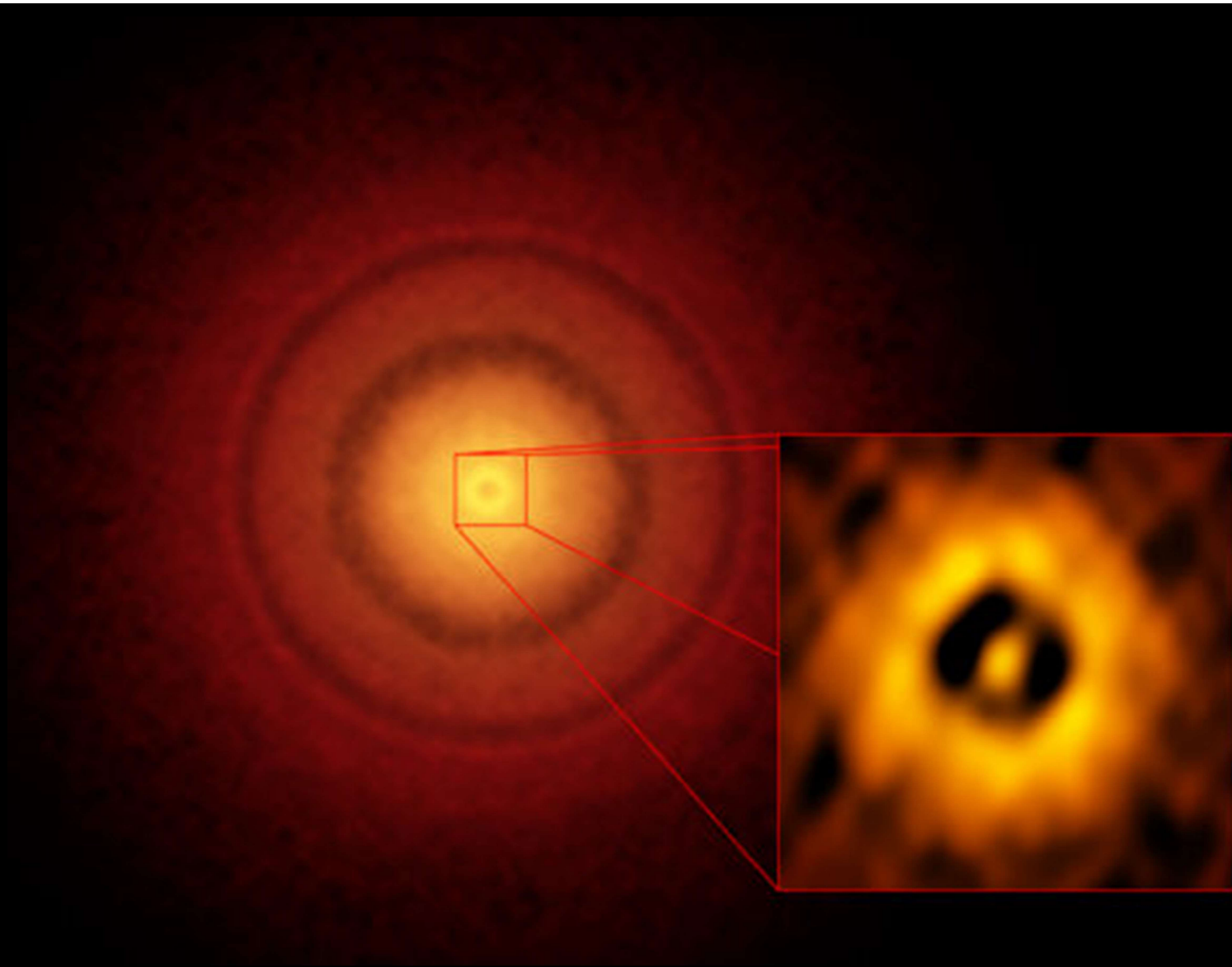
Anders Johansen

Leiden Observatory, Leiden University, P.O. Box 9513, 2300 RA Leiden, The Netherlands  
email: [ajohan@strw.leidenuniv.nl](mailto:ajohan@strw.leidenuniv.nl)

**Abstract.** The role of magnetic fields for the formation of planets is reviewed. Protoplanetary disc turbulence driven by the magnetorotational instability has a huge influence on the early stages of planet formation. Small dust grains are transported both vertically and radially in the disc by turbulent diffusion, counteracting sedimentation to the mid-plane and transporting crystalline material from the hot inner disc to the outer parts. The conclusion from recent efforts to measure the turbulent diffusion coefficient of magnetorotational turbulence is that turbulent diffusion of small particles is much stronger than naively thought. Larger particles – pebbles, rocks and boulders – get trapped in long-lived high pressure regions that arise spontaneously at large scales in the turbulent flow. These gas high pressures, in geostrophic balance with a sub-Keplerian/super-Keplerian zonal flow envelope, are excited by radial fluctuations in the Maxwell stress. The coherence time of the Maxwell stress is only a few orbits, where as the correlation time of the pressure bumps is comparable to the turbulent mixing time-scale, many tens or orbits on scales much greater than one scale height. The particle overdensities contract under the combined gravity of all the particles and condense into gravitationally bound clusters of rocks and boulders. These planetesimals have masses comparable to the dwarf planet Ceres. I conclude with thoughts on future priorities in the field of planet formation in turbulent discs.

**Keywords.** Diffusion – instabilities – MHD – planetary systems: protoplanetary disks – solar system: formation – turbulence





Sun-like Star TW Hydrae - S. Andrews (Harvard-Smithsonian CfA), ALMA (ESO/NAOJ/NRAO) |

## Three-dimensional Global Simulations of Type-II Planet-disk Interaction with a Magnetized Disk Wind: I. Magnetic Flux Concentration and Gap Properties

YUHIKO AOYAMA<sup>1,2</sup> AND XUE-NING BAI<sup>1,3</sup>

<sup>1</sup>*Institute for Advanced Study, Tsinghua University, Beijing 100084, China*

<sup>2</sup>*Kavli Institute for Astronomy and Astrophysics, Peking University, Beijing 100084, China*

<sup>3</sup>*Department of Astronomy, Tsinghua University, Beijing 100084, China*

### ABSTRACT

Giant planets embedded in protoplanetary disks (PPDs) can create annulus density gaps around their orbits in the type-II regime, potentially responsible for the ubiquity of annular substructures observed in PPDs. Despite of substantial amount of works studying type-II planet migration and gap properties, they are almost exclusively conducted under the viscous accretion disk framework. However, recent studies have established magnetized disk winds as the primary driving disk accretion and evolution, which can co-exist with turbulence from the magneto-rotational instability (MRI) in the outer PPDs. We conduct a series of 3D global non-ideal magneto-hydrodynamic (MHD) simulations of type-II planet-disk interaction applicable to the outer PPDs. Our simulations properly resolve the MRI turbulence and accommodate the MHD disk wind. We found that the planet triggers the poloidal magnetic flux concentration around its orbit. The concentrated magnetic flux strongly enhances angular momentum removal in the gap, which is along the inclined poloidal field through a strong outflow emanating from the disk surface outward of the planet gap. The resulting planet-induced gap shape is more similar to an inviscid disk, while being much deeper, which can be understood from a simple inhomogeneous wind torque prescription. The corotation region is characterized by a fast trans-sonic accretion flow that is asymmetric in azimuth about the planet and lacking the horseshoe turns, and the meridional flow is weakened. The torque acting on the planet generally drives inward migration, though the migration rate can be affected by the presence of neighboring gaps through stochastic, planet-free magnetic flux concentration.

*Keywords:* Extrasolar gaseous giant planets, Magnetohydrodynamical simulations, Protoplanetary disks, Planet formation

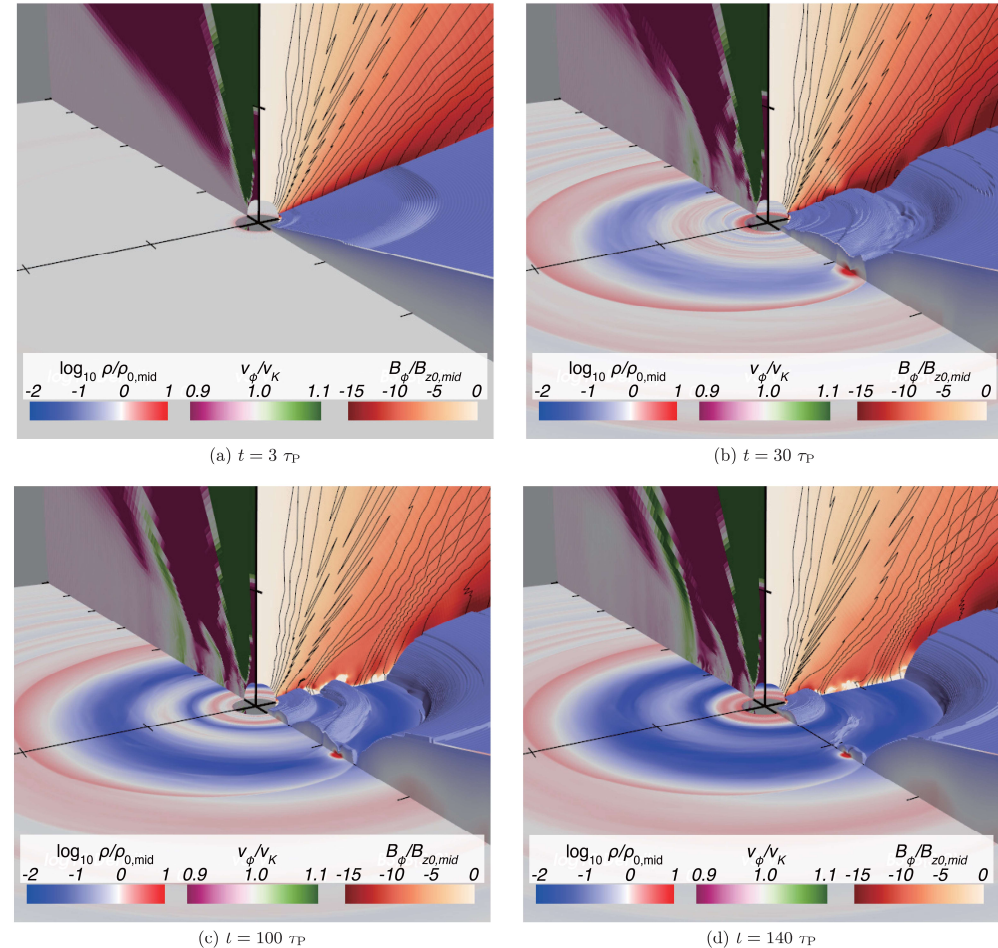


**Figure 1.** Snapshots of simulation results at  $t = 3, 30, 100,$  and  $140 \tau_P$  in the fiducial run Mt1Am3. In each panel, the bottom slice shows the midplane density, the left and right vertical walls show  $\phi$ -averaged  $v_\phi/v_K$  and  $B_\phi/B_{z,0}$ , respectively, and the blue iso-surface marks a constant density of  $\rho = \rho_{0,\text{mid}} e^{-2H}$ , where  $\rho_{0,\text{mid}} = \rho_0 R^{-q\rho}$ . The black lines on the right wall show the contours of equi-spaced azimuthally-averaged poloidal magnetic fluxes. Along the three axes ( $x = R \sin \phi$ ,  $y = R \cos \phi$ ,  $z$ ), the black ticks have a uniform spacing of 5 in code units.

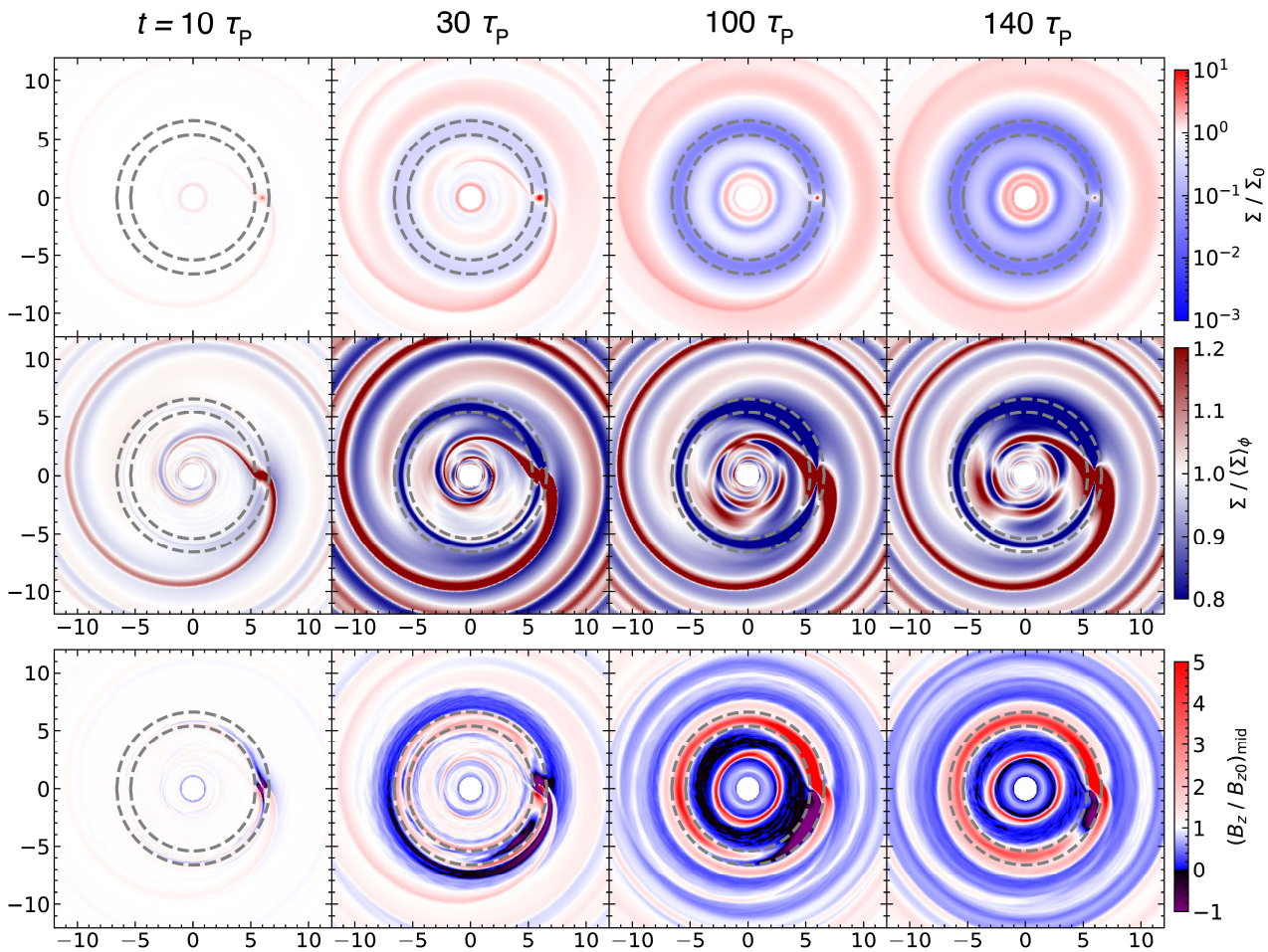


**Figure 2.**  $R$ - $\phi$  plots of surface density (top) and vertical magnetic field averaged within  $|z| < H$  (bottom) normalized by the initial values and surface density normalized by the average at the orbit (middle), at  $t = 10, 30, 100,$  and  $140 \tau_p$  from left to right. The time average is taken over  $10 \tau_p$  before the quoted values. The grey dashed circles correspond to  $R = R_P \pm r_H$ .

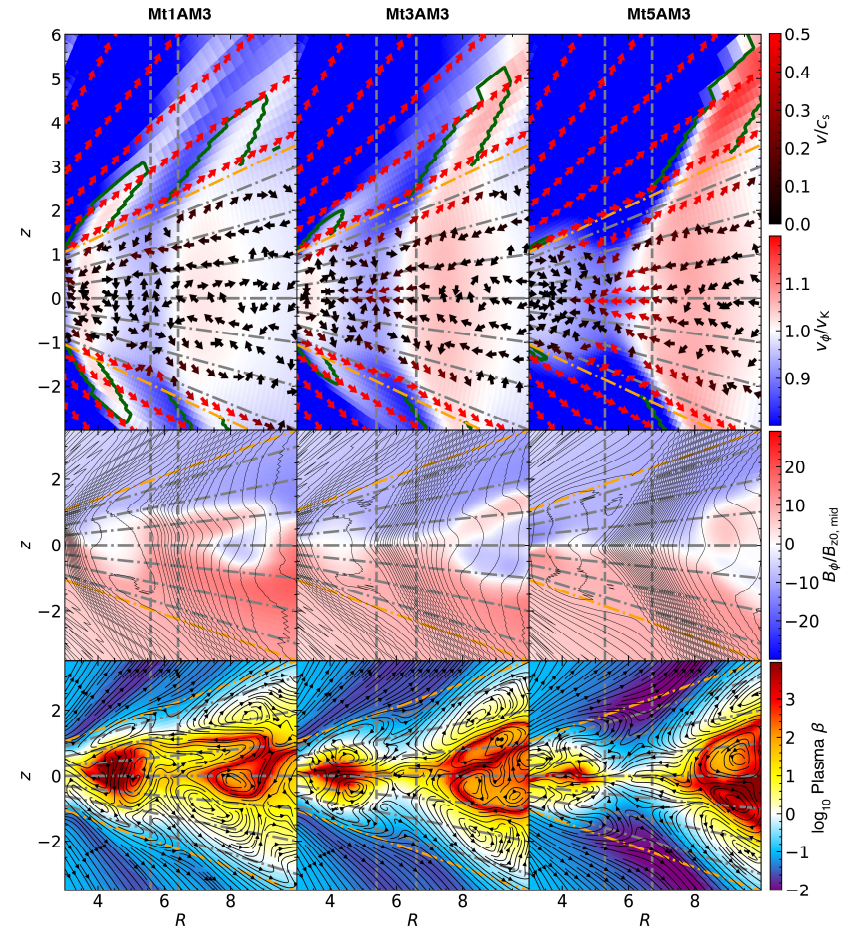
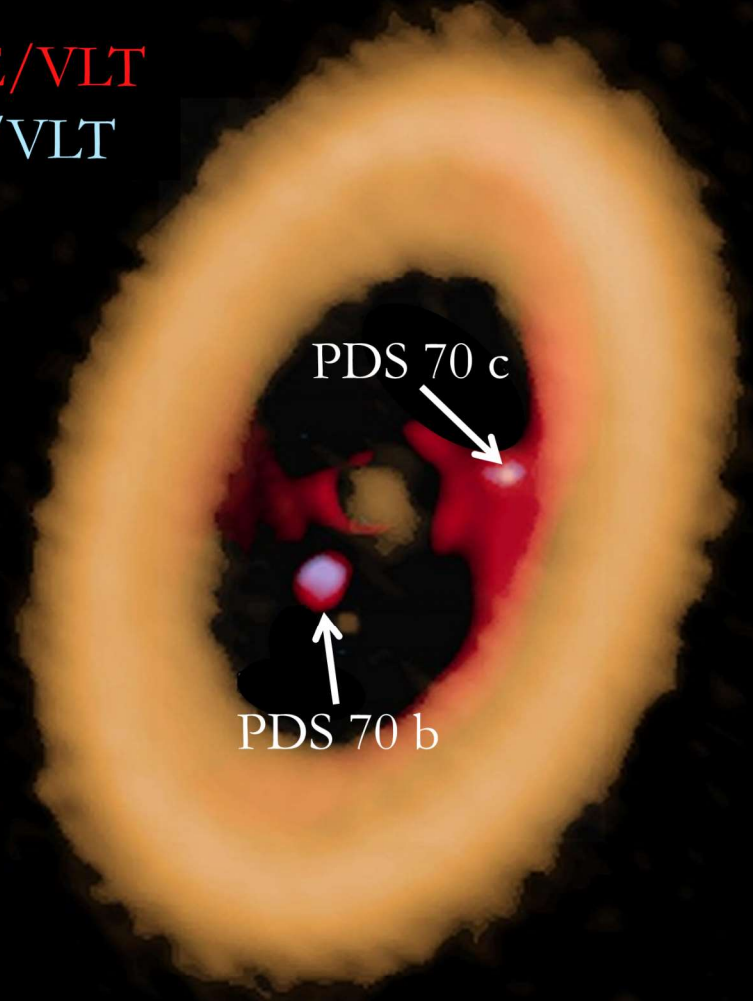
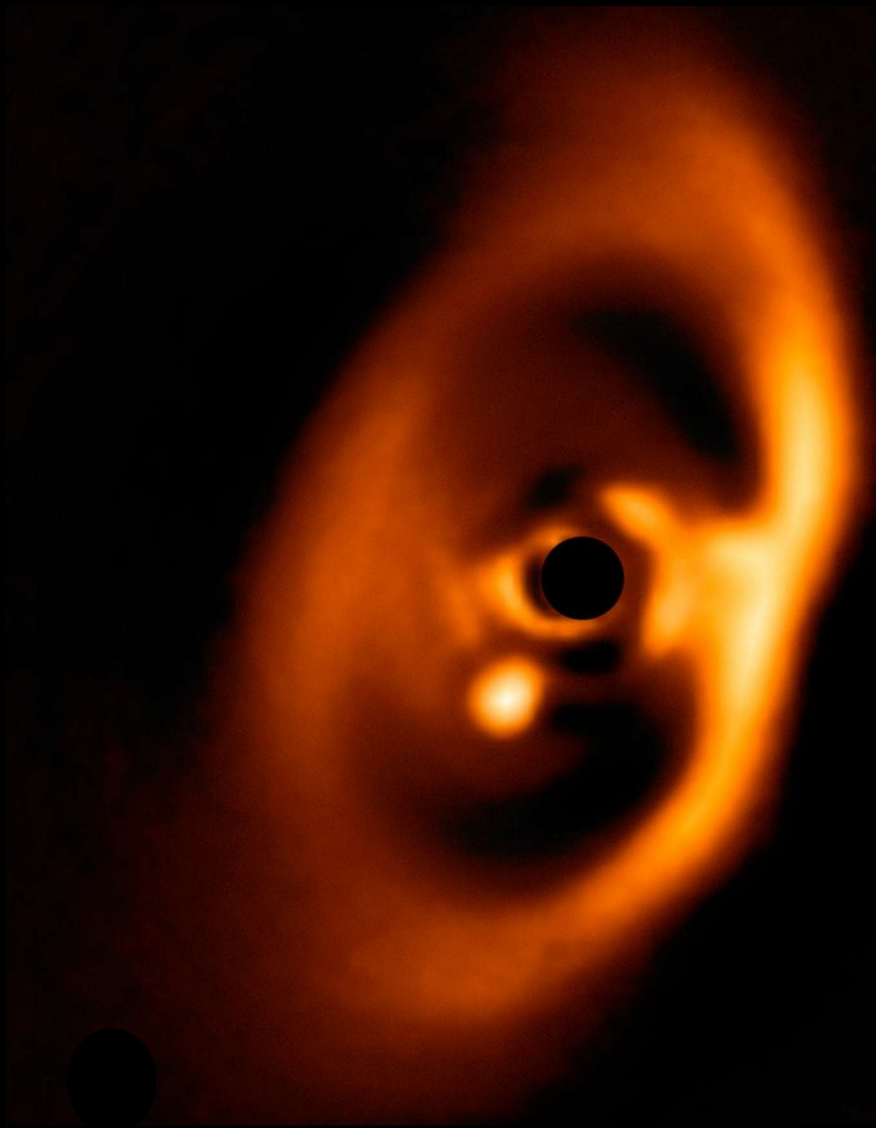


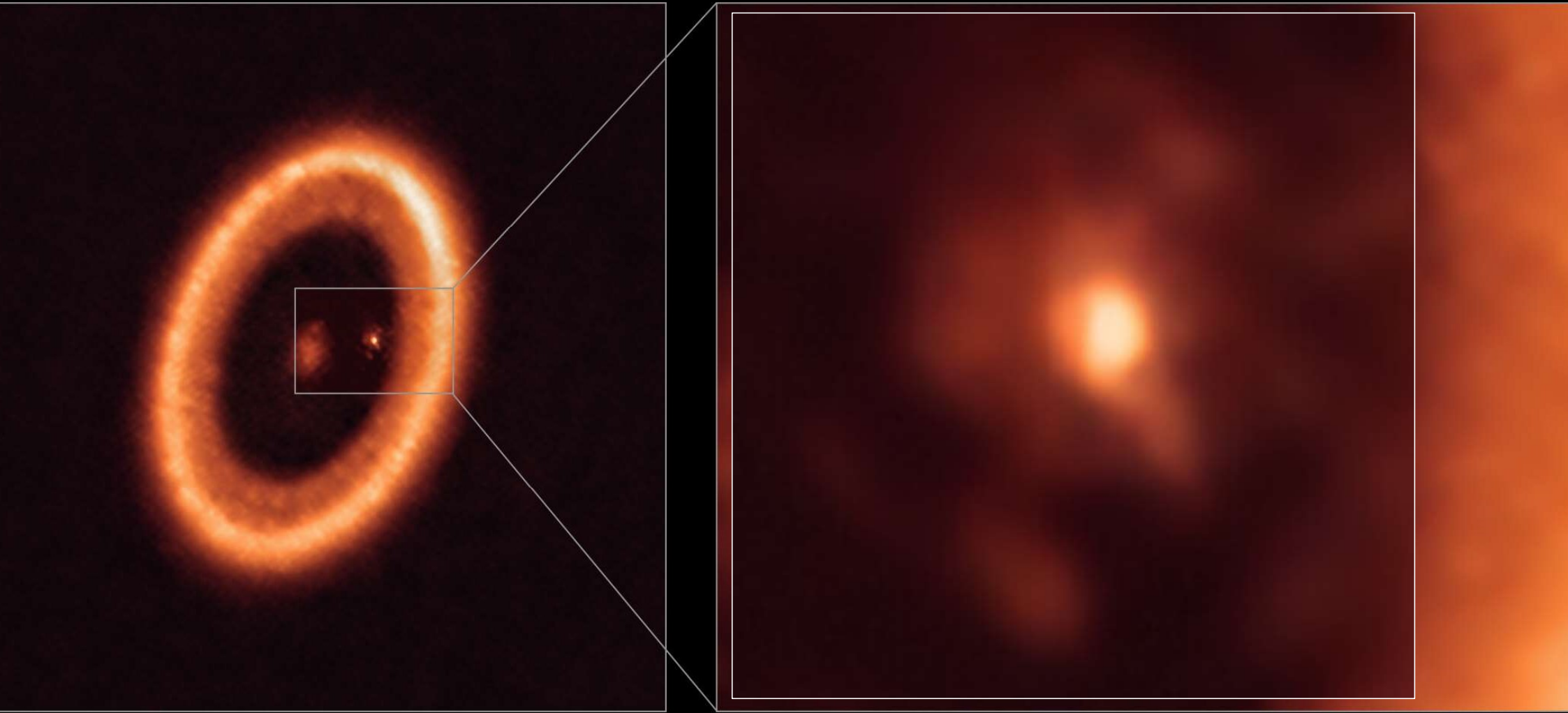
**Figure 11.** The  $R$ - $z$  slices of the disk in Mt1Am3, Mt3Am3, and Mt5Am3 from left to right, respectively. Top: poloidal velocity (arrow) and disk-rotation velocity (background color). Middle: isocontour of the poloidal magnetic flux function  $\Phi_B$  and toroidal magnetic field (background color). Bottom: momentum streamline (black lines) and plasma  $\beta$  (background color). All quantities are averaged in  $0 < \phi < 2\pi$  and  $130 < t/\tau_p < 140$ . The vertical and horizontal grey dashed lines show  $R = R_P \pm r_H$  and  $z/H = -3, -2, -1, 0, 1, 2, 3$  from bottom to top, respectively. The orange dash-dotted and green lines correspond to the disk surface ( $z/H = 3.5$ ) and Alfvén surface where the poloidal velocity equals to the poloidal Alfvén velocity. Note that  $v_K$  is based on cylindrical coordinates, and  $B_{z0, \text{mid}}$  is the initial vertical field in the midplane.

ALMA  
SHERE/VLT  
MUSE/VLT

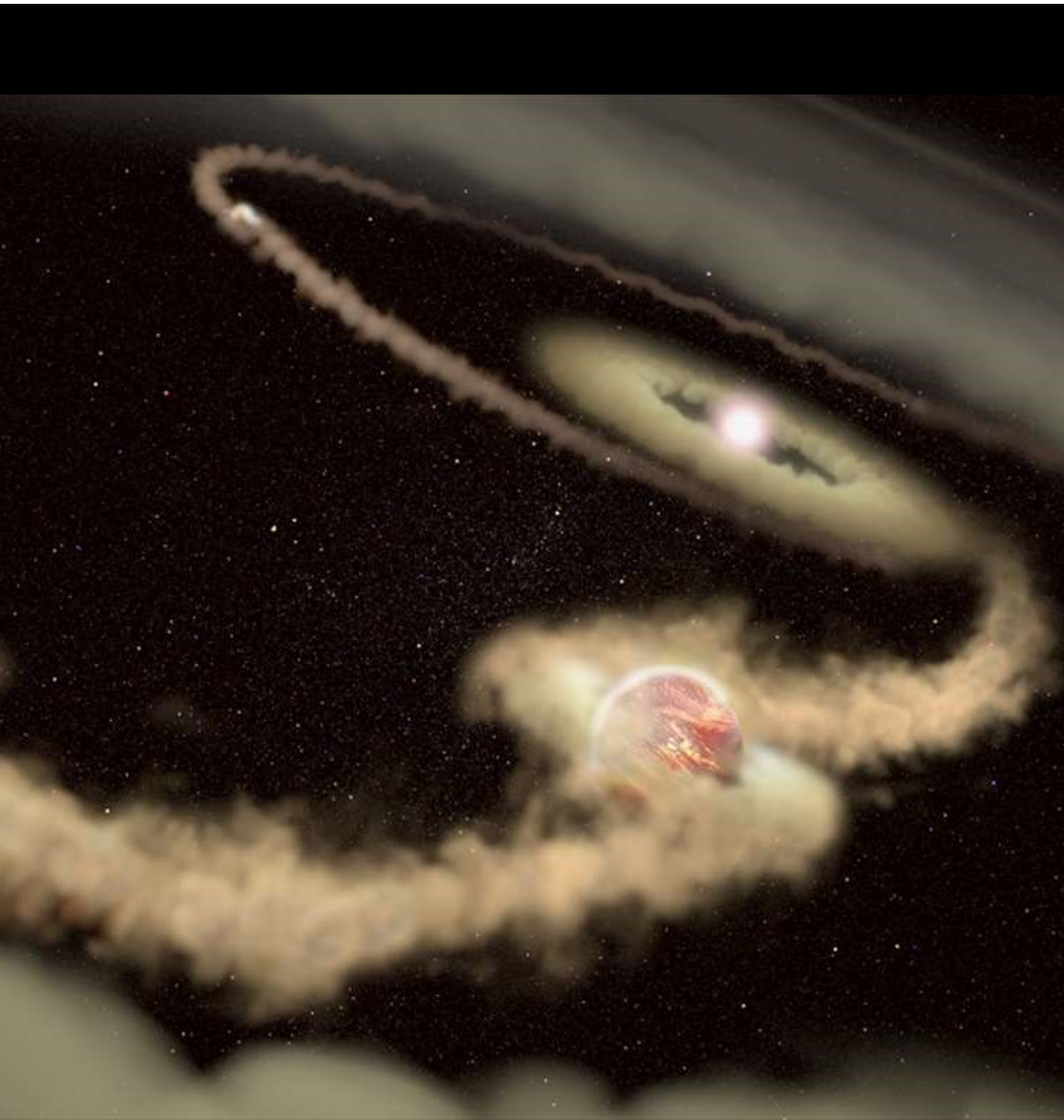


Protoplanetary disk of PDS 70 with the planet PDS 70b - VLT/ SPHERE ESO/A. Müller et al.

ALMA and VLT datas in a composite image of PDS 70 - ALMA (ESO/NOAJ/NRAO) A. Isella; ESO



Close-up view showing PDS 70b and PDS 70c with its “circumplanetary disk” - ALMA (ESO/NAOJ/NRAO)/Benisty et al.



Artist's illustration of exoplanets PDS 70 b and c - J. Olmsted (STScI)

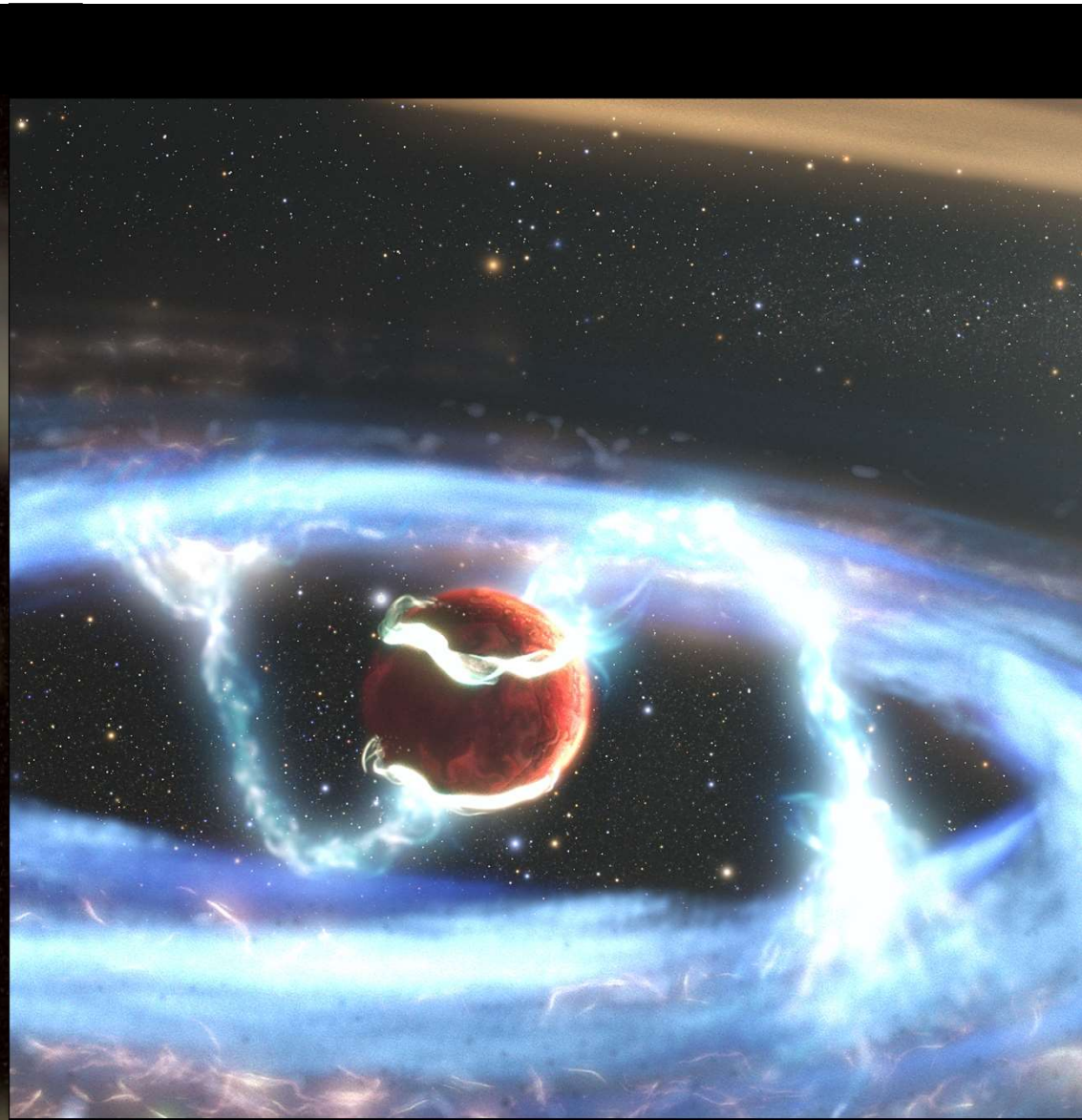


Illustration of the forming exoplanet PDS 70b collecting material from a circumplanetary disk  
McDonald Observatory–University of Texas, Y. Zhou (UT Austin)

## Effective dust growth in laminar circumplanetary discs with magnetic wind-driven accretion

Yuhito Shibaie<sup>1</sup>\* and Shoji Mori<sup>2</sup>

<sup>1</sup>Physikalisches Institut & NCCR Planets, Universität Bern, CH-3012 Bern, Switzerland  
<sup>2</sup>Astronomical Institute, Tohoku University, 6-3 Aramaki, Aoba-ku, Sendai 980-8578, Japan

Accepted 2022 November 16. Received 2022 November 10; in original form 2022 April 20

### ABSTRACT

It has been considered that large satellites around gas planets form *in situ* circumplanetary discs (CPDs). However, dust particles supplied into CPDs drift toward the central planets before they grow into satellitesimals, building blocks of the satellites. We investigate the dust growth in laminar CPDs with magnetic wind-driven accretion. In such laminar discs, dust particles can settle on to the mid-plane and grow large by mutual collision more efficient than in classical turbulent CPDs. First, we carry out 3D local MHD simulations of a CPD including all the non-ideal MHD effects (Ohmic resistivity, Hall effect, and ambipolar diffusion). We investigate if the disc accretion can be governed by magnetic wind-driven accretion and how laminar the disc can be, in a situation where the magnetic disc wind can be launched from the disc. Secondly, we model 1D steady CPDs consistent with the results of the MHD simulations and calculate the steady radial distributions of the dust profiles in the modelled discs, taking account of the collisional growth, radial drift, fragmentation, and vertical stirring by the Kelvin–Helmholtz instability. We show that satellitesimals can form in such CPDs if the dust-to-gas mass ratio of the inflow to the discs is larger than 0.02, which is 50 times smaller than the critical value in turbulent CPDs. This condition can be satisfied when enough amount of dust piles up at the gas pressure bump created by the planets. This result shows that satellitesimals would form in laminar CPDs with magnetic wind-driven accretion.

**Key words:** accretion, accretion discs – MHD – planets and satellites: formation.

### 1 INTRODUCTION

It is generally accepted that the large satellites around Jupiter and Saturn formed from small solid materials inside their circumplanetary discs (CPDs), byproducts of the gas accretion of the gas planets, like planets form in protoplanetary discs (PPDs). There are mainly two *in situ* formation scenarios for the major satellites: the satellite–accretion scenario (e.g. Mosqueira & Estrada 2003; Canup & Ward 2006) and the pebble-accretion scenario (Shibaie et al. 2019; Ronnet & Johansen 2020). The former needs a lot of satellitesimals (km sized or larger), building blocks of the satellites, but the satellitesimals formation is not easy. Dust particles supplied to the disc quickly grow to pebbles (cm–m sized) by their mutual collision, but they then fall into the central planets due to the headwind receiving from the gas rotating with sub-Keplerian speed. Shibaie et al. (2017) found that the *in situ* formation of satellitesimals is difficult unless the dust-to-gas mass ratio of the inflow on to the CPDs is larger than unity, which is not realistic (Homma et al. 2020; Szulágyi, Binkert & Surville 2022). On the other hand, Drazkowska & Szulágyi (2018) and Batygin & Morbidelli (2020) argued that if the discs have strong radial outflows on the mid-planes, the particles can pile up at the points where the inward drift and the outward advection are balanced and satellitesimals form by the streaming instability from the gathered particles. In this work, we propose another solution to avoid the drift barrier to the satellitesimal formation.

\*E-mail: yuhito.shibaie@unibe.ch

Previous works modelled their CPDs as the classical  $\alpha$  disc models (Shakura & Sunyaev 1973), where their dynamics and evolution are governed by single parameter  $\alpha$ , the strength of the turbulence of the discs, in the literature of the satellite formation (e.g. Shibaie et al. 2017). However, the  $\alpha$  parameter can be distinguished into two different kinds of parameters based on the physical properties: the efficiency of the angular momentum transport,  $\alpha_{\text{acc}}$ , and the diffusion strength of dust particles,  $\alpha_{\text{diff}}$ . The former determines the evolution of the gas accretion disc and the latter excites the motion of dust (and gas) particles (Yoodin & Lithwick 2007). If  $\alpha_{\text{acc}}$  is high, the gas surface density is low and thereby the drift time-scale of pebble can be long. On the other hand, if  $\alpha_{\text{diff}}$  is low, the collision rate remains high as the particles settle on the mid-plane, provided the collision speed is not determined by the diffusion, and thus particles grow quickly. Drazkowska & Duillemond (2018) found that this is effective for the planetesimal formation in PPDs. In this paper, we investigate if it also works in the satellitesimal formation.

In the case of PPDs, the two values of  $\alpha$  can be different when the disc is governed by the layered accretion or the magnetic wind-driven accretion. It has been considered that the most effective accretion mechanism of PPDs is the magneto-rotational instability (MRI) (Balbus & Hawley 1991, 1998). However, Gammie (1996) found that one of the non-ideal magnetohydrodynamic (MHD) effects, Ohmic resistivity prevents the MRI around the mid-plane, which is called ‘dead-zone’, while it is active only at the surface of the disc. In that case, the disc becomes a layered structure and the gas flows inward only at the upper layer. Okuzaki & Hirose (2011) carried out 3D ohmic-resistive MHD simulations and showed that the layered accretion occurs and  $\alpha_{\text{acc}} \sim 5\text{--}30 \alpha_{\text{diff}}$  in the inner regions of

PPDs. On the other hand, Bai (2015) calculated 3D MHD simulations including all three non-ideal MHD effects (Ohmic resistivity, Hall effect, and ambipolar diffusion) and found that the MRI is dead not only on the mid-plane but also at the whole height of the discs.<sup>1</sup> Therefore, PPDs would be laminar rather than turbulent. In that case, the angular momentum is transported at the surface of the disc where the large-scale magnetic field lines are bent. This accretion mechanism is called magnetic wind-driven accretion, because gas escapes from the disc along with the magnetic field lines, which is called ‘disc wind’ (see also Section 2.2 for detailed explanations). Bai (2015) argued that  $\alpha_{\text{acc}} \geq 10 \alpha_{\text{diff}}$  by a simple estimate from the outcome value of the rms vertical velocity fluctuation of the simulation results.

Most of the numerical simulations of CPDs calculated in previous works are not MHD but hydrodynamics (HD). Machida, Inutsuka & Matsumoto (2006) and Gressel et al. (2013) carried out global 3D MHD simulations of CPDs, though the former was ideal, and the latter included only Ohmic resistivity. They found that jet structures can form around the centre of the CPDs like the star formation process. In the simulation by Gressel et al. (2013), MRI is active at the surface layers of the CPDs but is dead inside the discs. It has also been considered that MRI is dead in most of the regions of CPDs other than the surfaces because of the short typical length scale of the discs (Fuji et al. 2014; Keith & Wardle 2014; Turner, Lee & Sano 2014; Fuji et al. 2017). These works calculated the Elsasser number and the plasma beta of CPDs in 1D disc models. In this work, we carry out 3D local non-ideal MHD simulations of CPDs to investigate if the discs are laminar and the magnetic wind-driven accretion dominates the disc accretion. This is the first work that carries out 3D MHD simulations of CPDs with all the non-ideal MHD effects, but the simulations are performed not in global but in local shearing boxes.

In Section 2, we perform 3D local non-ideal MHD simulations of a CPD. We consider situations where the magnetic disc wind can be launched from the disc and investigate if the disc state can be governed by the magnetic wind-driven accretion and  $\alpha_{\text{acc}}$  is much larger than  $\alpha_{\text{diff}}$ . In Section 3, we calculate the evolution of dust particles in 1D CPDs modelled to be consistent with the results of the MHD simulations and investigate the condition for the satellitesimal formation. In Section 4, we estimate the region where the disc wind is launched against the vertical gas inflow ignored in the MHD simulations. We then discuss the results of MHD simulations comparing with those of the previous works. We also discuss the feasibility of the obtained condition for the satellitesimal formation; it can be reached even when the gas gap is open. We also perform the parameter studies of the satellitesimal formation. We finally conclude this work in Section 5.

### 2 NON-IDEAL MHD SIMULATIONS OF CPDS

#### 2.1 Setups

We perform non-ideal MHD simulations of a CPD with an open source MHD code *Athena*<sup>3</sup> (Stone et al. 2008). The simulations are

<sup>1</sup>Bai & Stone (2015) also found that the MRI is dead at the whole height of PPDs by MHD simulations including Ohmic resistivity and ambipolar diffusion.

<sup>2</sup>The word ‘disc wind’ is used for general mass-loss from PPDs, and it launches not only from magnetic wind-driven accretion discs but also from MRI turbulent discs (Suzuki et al. 2016).

<sup>3</sup>https://github.com/athena-code/athena

### Effective dust growth in laminar CPDs 5445

performed in local 3D stratified shearing boxes, reproducing four different locations in a CPD,  $r = 3, 10, 30$ , and  $100 R_J$ , where  $r$  is the distance from the central planet, and  $R_J$  is the Jupiter radius.

Here we put two simplifications in the CPD simulations. First, we do not set the vertical gas inflow to CPDs as the boundary condition. The inflowing boundary condition in such shearing box simulations has not been investigated well so far. In addition, the inflowing boundary condition can easily break the simulation. Such disc-wind simulations taking into account the inflow effects is a future challenge. Nevertheless, we discuss if the disc has enough potential to launch the wind even with the inflow by using the simulation results, in Section 4.1. Second, we do not consider any horizontal gas flow either, because shearing box simulations do not have the concept of inward/outward directions.

The simulation boxes are orbiting the central planet with Kepler angular velocity  $\Omega_K = \sqrt{GM_p/r^3}$ , where  $G$  is the gravitational constant and  $M_p = 1 M_J$  (one Jupiter mass) is the mass of the central planet. The simulations are carried out with Cartesian coordinates  $(x, y, z)$  for the radial, azimuthal, and vertical dimensions. Previous MHD simulations in the inner regions of PPDs showed that the final properties do not depend on the horizontal box sizes and resolutions (Bai & Stone 2013), and we have confirmed that it is also true in our cases. Thus, we use simulation boxes with the vertical and horizontal box sizes of  $16 H_p$  and  $0.5 H_p$  and the resolutions of 25 and 8 cells per  $H_p$ , respectively, where  $H_p$  is the gas scale height of the CPDs. The gas scale height is  $H_p = c_s/\Omega_K$ , where  $c_s$  is the sound speed, and  $c_s = \sqrt{k_B T/m_p}$ , where  $k_B$ ,  $T$ , and  $m_p = 3.9 \times 10^{-26}$  g are the Boltzmann constant, disc temperature, and mean molecular mass, respectively.

We set the gas temperature profile of the CPD as  $T = 160(r/10R_J)^{-3/4}$  K, which is consistent with the ice mass fractions of the Galilean satellites (e.g. Kuskov & Kronrod 2005), and assume the gas is isothermal in each simulation box. Although the assumed temperature is lower than that of turbulent discs, we note that the heating can occur at high altitude in magnetic wind-driven accretion discs, and the mid-plane temperature can be lower (Mori, Bai & Okuzaki 2019). As the initial conditions, we set the gas surface density as  $\Sigma_g = 1000(r/10R_J)^{-3/2}$  g cm<sup>-2</sup> (see Section 4.2 for the reason why we choose this profile) and the density distribution in hydrostatic equilibrium. We fix the dust-to-gas ratio of 0.1  $\mu\text{m}$ -sized dust particles as  $f_{\text{dg}} = 1 \times 10^{-9}$ .

We also set the initial magnetic field as  $\mathbf{B}_0 = (0, 0, B_0)$ , where  $B_0$  is characterized by a parameter  $\beta_0 = 8\pi\rho_p\omega_c^2/B_0^2$ , which is assumed as  $\beta_0 = 10^3$  in this work. Depending on the direction of  $B_0$ , the Hall effect amplifies or damps the magnetic field. We here take  $B_0$  to be aligned with the disc rotation vector, in which the magnetic field is amplified by the Hall effect.

We give the magnetic diffusivities of the non-ideal MHD effects with calculating the balance between the ionization and recombination, basically following Mori et al. (2019). The magnetic diffusivities depend on the number densities of charged particles (electrons, ions, and charged dust particles). The ionization sources are cosmic rays, stellar X-rays, and radiocollisions. The cosmic ray ionization rate is described in Sano et al. (2000) which is based on Umebayashi & Nakano (1981). The ionization rate of the X-ray follows the fitting formula consistent with Igea & Glassgold (1999) and Bai & Goodman (2009), but we neglect components that directly reach the disc surface. We set the X-ray temperature to be 51 keV and the X-ray luminosity to be  $2 \times 10^{39}$  erg s<sup>-1</sup>. Also, the location of the CPD is assumed to be 5.2 au from the protostar. The latter is the median value of the luminosity of the Solar-mass stars in the Orion Nebula Cluster (Gammie et al.

5446 *Y. Shibaie and S. Mori*

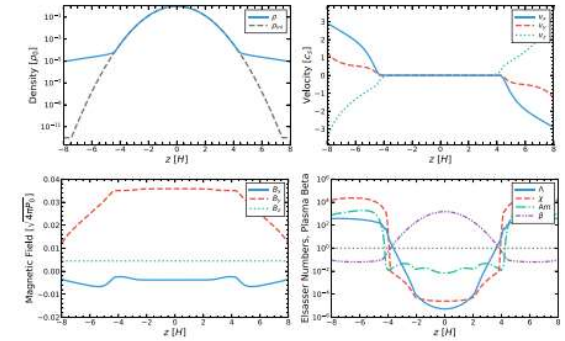


**Figure 1.** Vertical profiles of the temporal and horizontal average for a representative run at  $r = 10 R_J$ . Upper left: gas density at the final state ( $\rho$ , solid) and initial state ( $\rho_0$ , dashed), normalized by the initially set density on the mid-plane,  $\rho_0$ . Upper right: three components of the gas velocity ( $v_x$ ,  $v_y$ ,  $v_z$ ). Lower left: three components of the magnetic field. Lower right: Elsasser numbers for Ohmic resistivity ( $\beta$ ), Hall effect ( $\beta_A$ ), ambipolar diffusion ( $\beta_{Am}$ ), and plasma beta ( $\beta$ ).

2000). The radiocollide ionization rate is set as a constant value of  $7.6 \times 10^{-19}$  s<sup>-1</sup> (Umebayashi & Nakano 2008). We consider the recombination in gas phase and on dust particles. We limit the total diffusivities to  $300 c_s H_p$  to avoid the calculation time step to be too short.

We also consider the ionization by far-ultraviolet radiation (FUV) above its penetration depth. The stellar FUV rays are scattered around the wall of the gaps and partially enter the CPDs, which is reduced to 4 per cent of the stellar luminosity (Turner et al. 2012). We assume the stellar FUV luminosity as  $2 \times 10^{33}$  erg s<sup>-1</sup>, and so the FUV flux reaches to the CPDs is equivalent to the luminosity of  $8 \times 10^{29}$  erg s<sup>-1</sup>. The stellar FUV luminosity is set as a higher value than that of the current sun because it should have been higher in the past (e.g. Yang & Krumholz 2012). The penetration depth is then about 0.03 cm<sup>-1</sup>, following the ionization modes in Perez-Becker & Chiang (2011). We obtain the ionization fraction of  $3 \times 10^{-5}$  in the FUV layer with a similar treatment used in Bai & Stone (2013).

### 2.2 Results

#### 2.2.1 Magnetic disc wind of CPDs

The obtained results of the four simulations at the different places are qualitatively similar, so we focus on the simulation results at  $r = 10 R_J$ . Fig. 1 represents the vertical profiles of the density, velocity, and magnetic fields of the simulation result. These are the temporal and horizontal average over the last 10 orbits of the total 50 orbits. However, after the vertical profiles reach these states shown in the figure, the profiles are almost steady and have only small variation. These vertical profiles are like those of PPDs with wind-driven accretion (e.g. Bai & Stone 2013).

The upper two panels of Fig. 1 show that the magnetic disc wind is launched from the surfaces of the CPD ( $|z| = 4 H_p$ ). At  $|z| > 4 H_p$ , the density profile deviates from the equilibrium profile given as the initial profile (upper left panel) and the gas flows out vertically (upper right). This is explained by the behaviour of the magnetic field (lower left). The gas is pushed up to the surfaces of the CPD by the toroidal magnetic field amplified at  $|z| < 4 H_p$ . The gas then gains angular momentum via the poloidal field threading the disc around its surfaces, thereby flowing away as the disc wind. The disc wind is launched continuously in this situation.

The magnetic field profile can be explained by the Elsasser numbers of the diffusivities (lower right). The Elsasser number of a diffusivity  $\eta$  is defined as

$$\Lambda = \frac{v^2}{\Omega \eta} \quad (1)$$

where  $v$  is the Alfvén speed. When the Elsasser number is less than unity, the non-ideal MHD effects are stronger than the magnetic induction due to the shear flow. Around the mid-plane, the Ohmic diffusion is the dominant MHD process. Perturbations of magnetic field are quickly diffused, and so the magnetic field is constant. In addition, ambipolar diffusion dominates over the magnetic induction within  $4 H_p$ . For these reasons, the MRI turbulence is fully suppressed below  $4 H_p$ , and therefore the CPD is laminar. Nevertheless, the Hall effect at  $z = 2\text{--}4 H_p$  amplifies the magnetic field with the shear flow (i.e. Hall-shear instability; Kunz 2008). The amplified toroidal field diffuses into the CPD, so that the magnetic field is still strong even in the disc.

#### 2.2.2 Magnetic wind-driven accretion

The disc wind flowing out from the surfaces of CPDs takes the disc angular momentum from the gas around the surfaces. The gas

**GLOBAL HYDROMAGNETIC SIMULATIONS OF A PLANET EMBEDDED IN A DEAD ZONE:  
 GAP OPENING, GAS ACCRETION, AND FORMATION OF A PROTOPLANETARY JET**

O. GRESSEL<sup>1,2</sup>, R. P. NELSON<sup>2</sup>, N. J. TURNER<sup>3</sup>, AND U. ZIEGLER<sup>4</sup>

<sup>1</sup> NORDITA, KTH Royal Institute of Technology and Stockholm University, Roslagstullsbacken 23, SE-106 91 Stockholm, Sweden; oliver.gressel@nordita.org

<sup>2</sup> Astronomy Unit, Queen Mary University of London, Mile End Road, London E1 4NS, UK; r.p.nelson@qmul.ac.uk

<sup>3</sup> Jet Propulsion Laboratory, California Institute of Technology, Pasadena, CA 91109, USA; neal.j.turner@jpl.nasa.gov

<sup>4</sup> Leibniz-Institut für Astrophysik Potsdam (AIP), An der Sternwarte 16, D-14482, Potsdam, Germany; uziegler@aip.de

Received 2013 July 5; accepted 2013 October 17; published 2013 November 25

**ABSTRACT**

We present global hydrodynamic (HD) and magnetohydrodynamic (MHD) simulations with mesh refinement of accreting planets embedded in protoplanetary disks (PPDs). The magnetized disk includes Ohmic resistivity that depends on the overlying mass column, leading to turbulent surface layers and a dead zone near the midplane. The main results are: (1) the accretion flow in the Hill sphere is intrinsically three-dimensional for HD and MHD models. Net inflow toward the planet is dominated by high-latitude flows. A circumplanetary disk (CPD) forms. Its midplane flows outward in a pattern whose details differ between models. (2) The opening of a gap magnetically couples and ignites the dead zone near the planet, leading to stochastic accretion, a quasi-turbulent flow in the Hill sphere, and a CPD whose structure displays high levels of variability. (3) Advection of magnetized gas onto the rotating CPD generates helical jets that launch magnetocentrifugally driven outflows. During one specific epoch, a highly collimated, one-sided jet is observed. (4) The CPD's surface density is  $\sim 30 \text{ g cm}^{-2}$ , small enough for significant ionization and turbulence to develop. (5) The accretion rate onto the planet in the MHD simulation reaches a steady value  $8 \times 10^{-3} M_J \text{ yr}^{-1}$  and is similar in the viscous HD runs. Our results suggest that gas accretion onto a forming giant planet within a magnetized PPD with a dead zone allows rapid growth from Saturnian to Jovian masses. As well as being relevant for giant planet formation, these results have important implications for the formation of regular satellites around gas giant planets.

**Key words:** magnetohydrodynamics (MHD) – methods: numerical – planets and satellites: formation – protoplanetary disks

*Online-only material:* color figures

**1. INTRODUCTION**

Gas giant planets are widely believed to form via core nucleated accretion, a scenario that begins with the formation of a solid rock and ice core in a protoplanetary disk (PPD) by the agglomeration of smaller bodies (planetesimals) and which concludes with the accretion of a gaseous envelope from the surrounding nebula (Mizuno 1980). Although it has been suggested that giant planets may form through the direct gravitational fragmentation of a massive PPD during its early evolution (Boss 1998), circumstantial evidence for core accretion having operated in the solar system is provided by the inferred existence of significant cores in Saturn, Uranus, (e.g., Saumon & Guillot 2004) and Neptune. It can further be argued that the substantial numbers of relatively low-mass super-Earth and Neptune-like extrasolar planets being discovered (e.g., Lissauer et al. 2011) indicate that core accretion is a common mode of planetary formation outside of the solar system.

Detailed one-dimensional (1D) models of gas giant planet formation indicate that envelope accretion occurs in two distinct stages: (1) a quasi-static contraction phase during which the envelope mass grows slowly over timescales  $\geq 1 \text{ Myr}$  (Pollack et al. 1996) and (2) a runaway growth phase during which the envelope accretes dynamically onto the planet. This latter phase normally arises once the envelope exceeds the core mass, corresponding to a total planet mass  $\geq 35 M_J$ . Prior to runaway gas accretion, the protoplanet remains embedded in the nebula and the bloated envelope is envisaged to connect smoothly onto the surrounding disk. During the runaway phase, however, the

planet contracts down to a size  $\approx 3$  Jupiter radii and gas accretion is expected to occur through a circumplanetary disk (CPD) if forms by the flow of gas into the planet Hill sphere (Papaloizou & Nelson 2005). We note that the 1D envelope calculations indicate that planets with Saturn-like masses ( $\sim 0.2\text{--}0.6 M_J$ ) are likely to experience maximal gas accretion (Pollack et al. 1996), as the flow onto the planet is relatively unimpeded the compressional heating of the envelope for these mass. Although these 1D quasi-static calculations cannot determine the details of the hydrodynamic (HD) flow, so some doubt remains about the actual accretion rate, it is noteworthy that extrasolar planets with masses similar to Saturn are common even though existing calculations suggest that once a planet enters the runaway gas-accretion phase it should grow rapidly beyond this mass if it is in the presence of a significant gas reservoir. One motivation for performing the calculations presented in this paper is to address this issue and to examine whether or not a possible bottleneck exists that can prevent the formation of planets in this mass range.

The formation of a gas giant planet through gas accretion is the action of tidal torques lead to the formation of an annular gap around the vicinity of the planet (Lin & Papaloizou 1993; Bryden et al. 1999; Kley 1999; Lubow et al. 1999). This material also heralds the transition of the planet's migration from type I (Ward 1997) during the embedded phase to type II where the gap has formed (Lin & Papaloizou 1986; Nelson et al. 2000). Material then feeds onto the planet through the gap at the viscous

<sup>3</sup> Out of 720 confirmed extrasolar planets listed on [exoplanets.org](http://exoplanets.org), approximately 170 have masses in the range  $0.2\text{--}1 M_J$ .

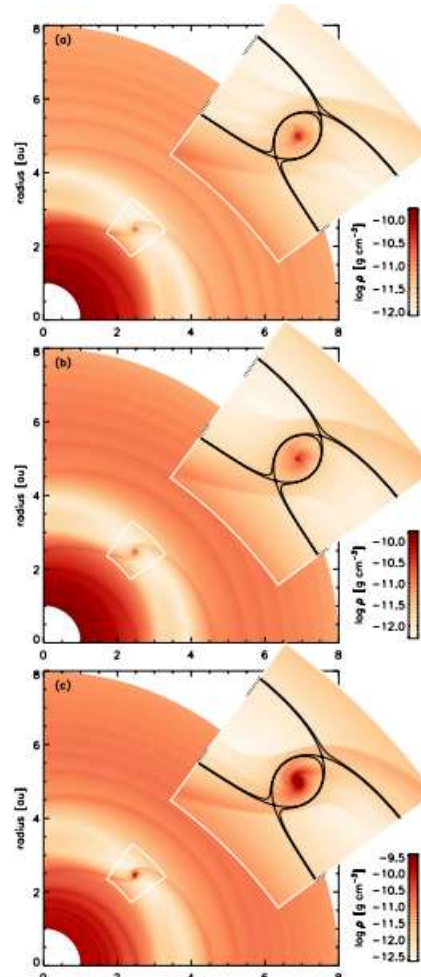


**Figure 1.** Midplane slices of  $\log(\rho)$ . From top to bottom: (a) MHD run, (b) HD run with cooling, (c) isothermal HD run. Black contours indicate the potential surfaces passing through the Lagrange points L1 and L2. (A color version of this figure is available in the online journal.)

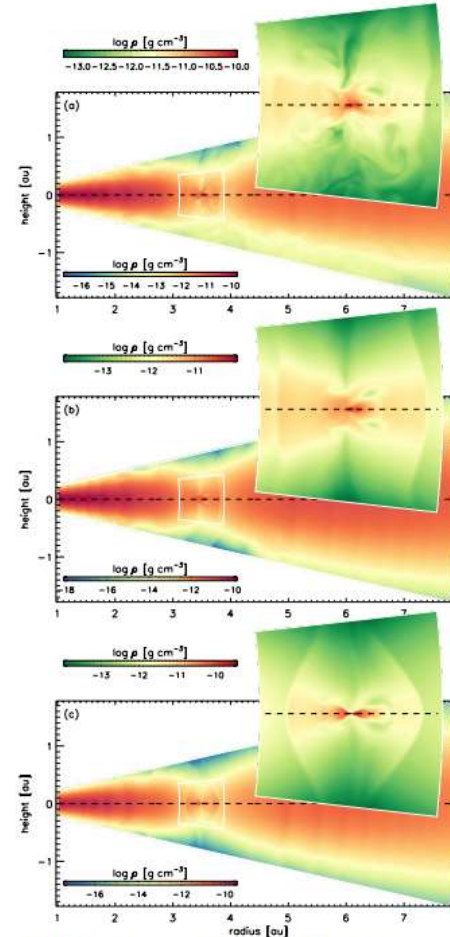


**Figure 2.** Meridional plane showing  $\log(\rho)$  at the planet location (note the separate color bars for the insets). From top to bottom: (a) MHD run, (b) HD run with cooling, (c) isothermal HD run. Black contours indicate the potential surfaces passing through the Lagrange points L1 and L2. (A color version of this figure is available in the online journal.)

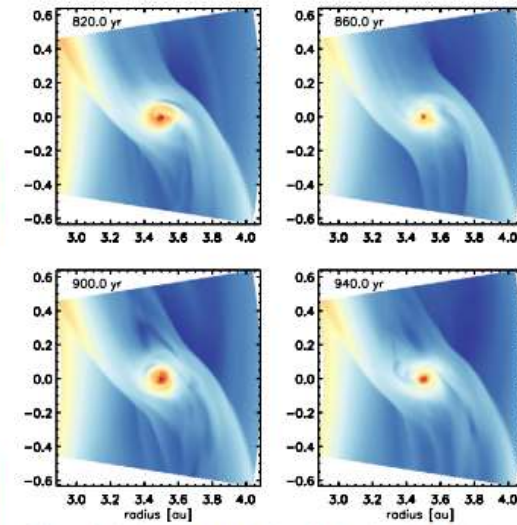


**Figure 12.** Similar to Figure 11, but for midplane slices of the gas density. (A color version of this figure is available in the online journal.)

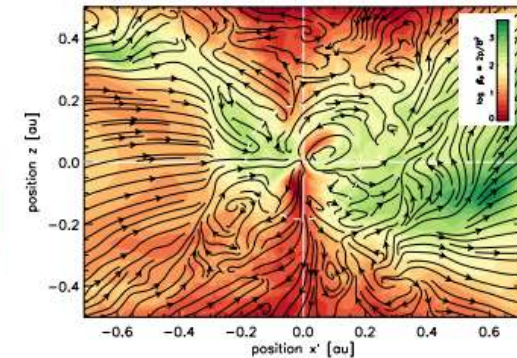


**Figure 13.** Radial-vertical slice of the logarithm of the plasma parameter,  $\beta_p \equiv 2\rho/B^2$ , and projected magnetic field lines. Averages are taken over eight planet orbits at the time corresponding to the last panel in Figure 11. (A color version of this figure is available in the online journal.)



## Magnetically driven outflows from Jovian circum-planetary accretion disks

Ch. Fendt\*

Institut für Physik, Universität Potsdam, Am Neuen Palais 10, 14469 Potsdam, Germany  
Astrophysikalisches Institut Potsdam, An der Sternwarte 16, 14482 Potsdam, Germany

Received 1 August 2003 / Accepted 6 October 2003

**Abstract.** We discuss the possibility to launch an outflow from the close vicinity of a protoplanetary core considering a model scenario where the protoplanet surrounded by a *circum-planetary* accretion disk is located in a *circum-stellar* disk. For the *circum-planetary* disk accretion rate we assume  $\dot{M}_{cp} = 6 \times 10^{-3} M_J \text{ yr}^{-1}$  implying peak disk temperatures of about 2000 K. The estimated disk ionization degree and Reynolds number allow for a sufficient coupling between the disk matter and the magnetic field. We find that the surface magnetic field strength of the protoplanet is probably not more than 10 G, indicating that the *global* planetary magnetosphere is dominated by the *circum-planetary* disk magnetic field of  $\leq 50$  G. The existence of a gap between *circum-planetary* disk and planet seems to be unlikely. The estimated field strength and mass flow rates allow for asymptotic outflow velocities of  $\geq 60 \text{ km s}^{-1}$ . The overall outflow geometry will be governed by the orbital radius, resembling a hollow tube or cone perpendicular to the disk. The length of the outflow built up during one orbital period is about 100 AU, depending on the outflow velocity. Outflows from *circum-planetary* disks may be visible in shock excited emission lines along a tube of diameter of the orbital radius and thickness of about 100 protoplanetary radii. We derive particle densities of  $3000 \text{ cm}^{-3}$  in this layer. Energetically, protoplanetary outflows cannot survive the interaction with a *protostellar* outflow. Due to the efficient angular momentum removal by the outflow, we expect the protoplanetary outflow to influence the early planet angular momentum evolution. If this is true, planets which have produced an outflow in earlier times will rotate slower at later times. The mass evolution of the planet is, however, hardly affected as the outflow mass loss rate will be small compared to the mass accumulated by the protoplanetary core.

**Key words.** ISM: jets and outflows – stars: planetary systems: formation – stars: planetary systems: protoplanetary disks

### 1. Introduction

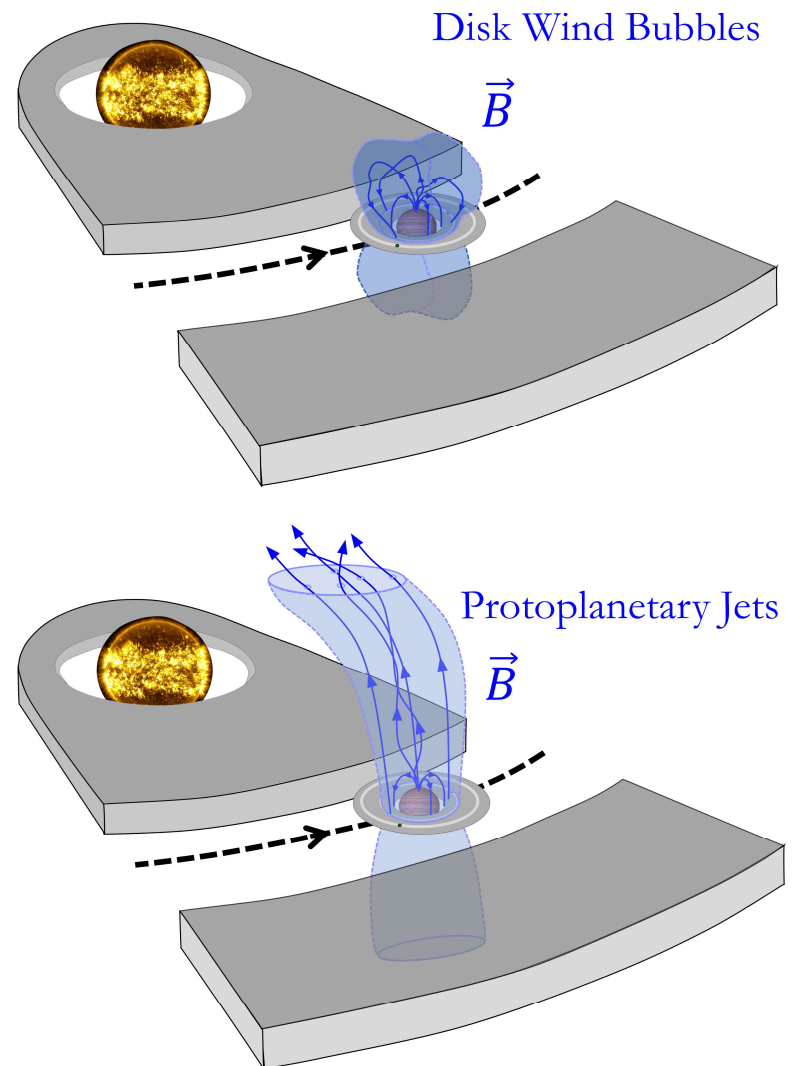
With the discovery of *extrasolar planets* during the last decade the scientific interest in planet formation has been increased substantially. In particular, with the help of the computational power existing today, it has become possible to perform numerical simulations of a *circumstellar* accretion disk containing and building up an orbiting *protoplanetary core* (e.g. Kley 1999; Bryden et al. 1999; Lubow et al. 1999; Kley et al. 2001; D’Angelo et al. 2002; Tanigawa & Watanabe 2002; D’Angelo et al. 2003a,b; Bate et al. 2003). Although differing in certain aspects (spatial resolution of the region close to the protoplanet, number of dimensions treated) these simulations have provided us with the same general results. In particular, the simulations show how tidal interaction between the protoplanet and the disk material opens up a *gap* in the *circum-stellar* accretion disk along the orbit of the planetary core. Mass accretion in the *circum-stellar* disk, however, continues across the gap. The *circum-stellar* disk material entering the Roche lobe of the protoplanet becomes captured and finally accreted by the protoplanetary core. The simulations also demonstrate how the

accretion stream initially affected by strong shocks waves eventually builds up a *circum-planetary* sub-disk in almost Keplerian rotation close to the planet.

On the other hand, in the context of *astrophysical jets* it is well established that outflow formation is causally connected to the presence of an *accretion disk* and strong *magnetic fields* (see Blandford & Payne 1982; Pudritz & Norman 1986; Camenzind 1990; Shu et al. 1994). This statement holds for a wide range in outflow energy and spatial scale – for young stellar objects, microquasars and active galactic nuclei. Observations as well as theoretical models strongly suggest that *astrophysical sources* of outflows are (highly) magnetized. The magnetic field is responsible for acceleration and collimation and for lifting the matter from the disk into the outflow.

In the scenario of planet formation within a *circum-stellar* accretion disk, the presence of a magnetic field can be expected as well. A central *protostellar* dipolar magnetic field of 1000 G surface field strength may provide only about 20  $\mu\text{G}$  at 5 AU distance. This (weak) field, however, may act as a seed field for dynamo action taking place in the *circum-stellar* accretion disk, in the *protoplanetary core*, or in the *circum-planetary* disk. Most of the present-day Solar system planets carry a substantial

\* e-mail: cfendt@aip.de

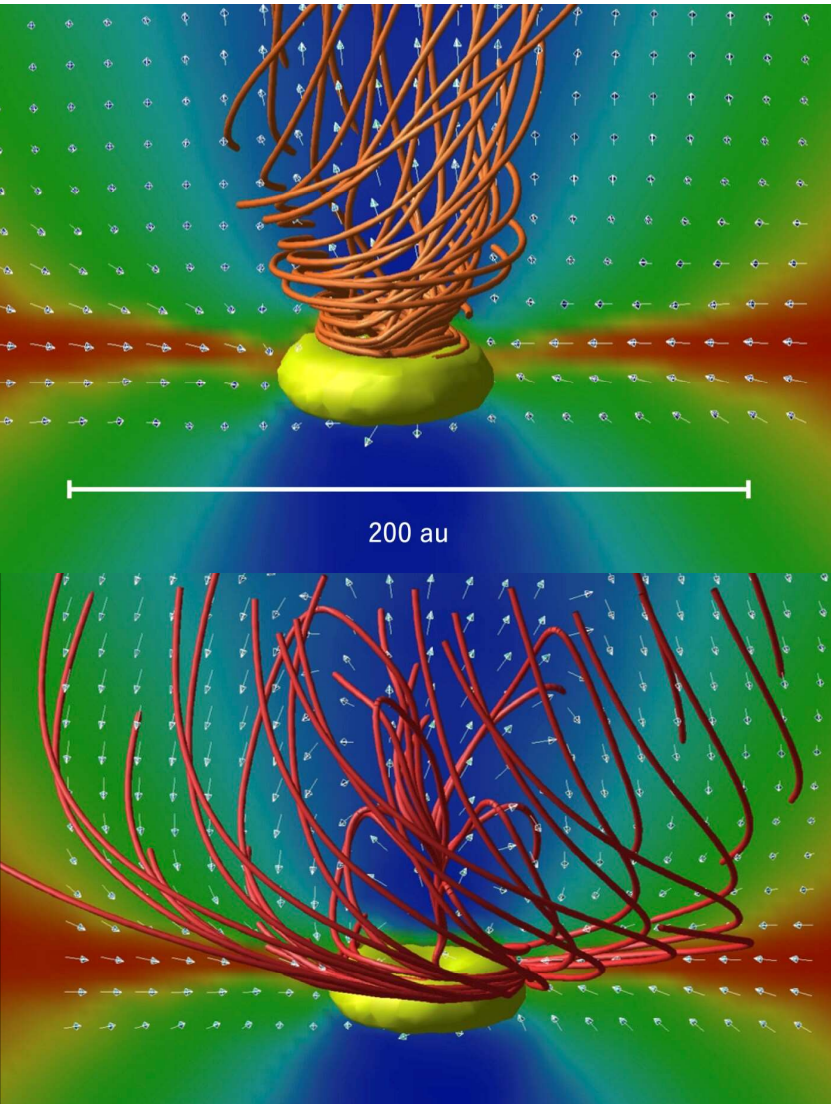
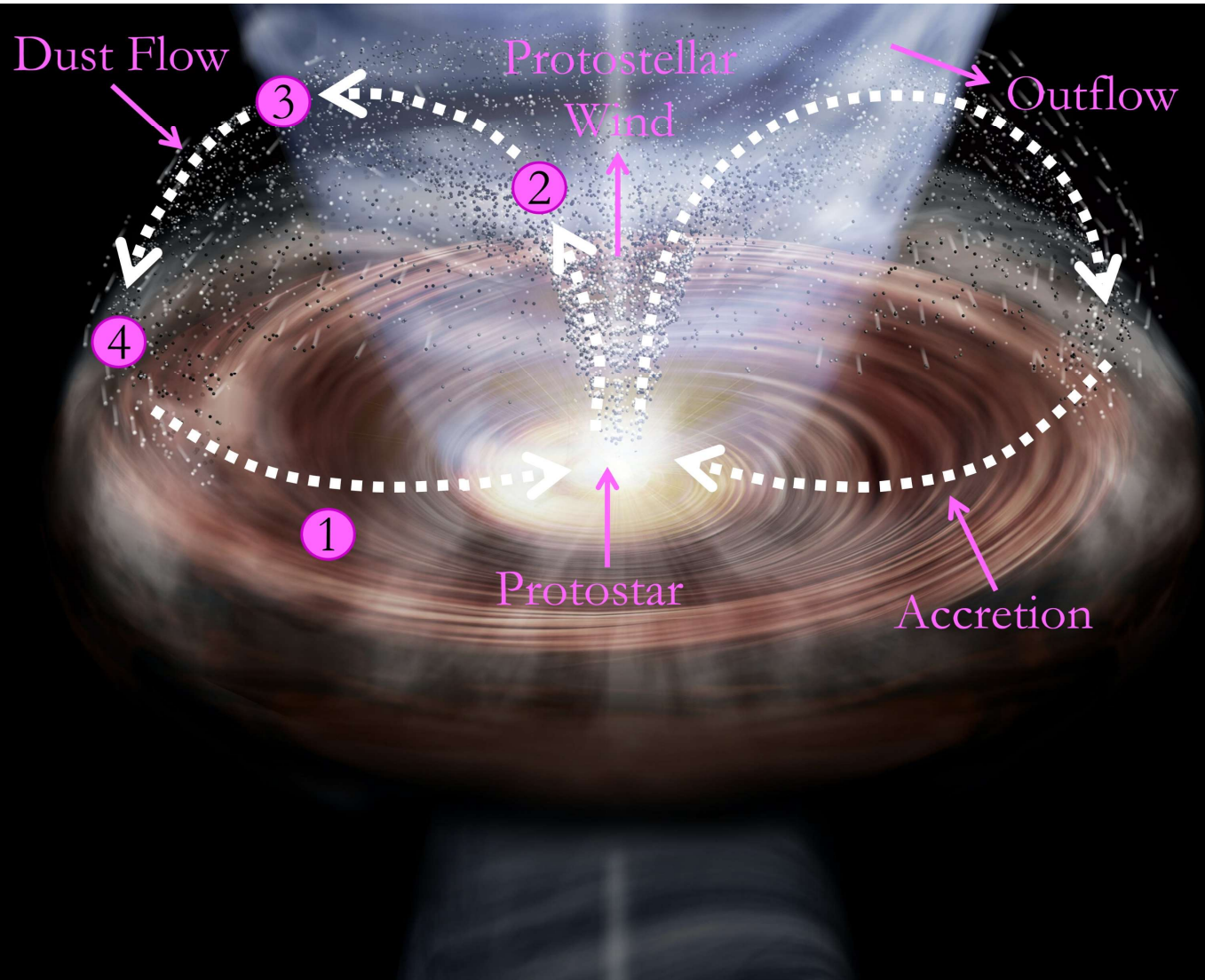


Magnetized protoplanetary disk winds - U. v. Kusserow/C. Fendt (2023)

# Entstehung des magnetischen Sonnensystems Formation of the magnetic Solar System

## Zirkumplanetare Scheiben, Jets - Circumplanetary Disks, Jets

- C. Fendt (2003) Magnetically driven outflows from Jovian circum-planetary accretion disks
- Z. Fu, S. Huang, C. Yu (2024) Boundary Layers of Circumplanetary Disks around Spinning Planets II. Global Modes with Azimuthal Magnetic Fields
- Y. I. Fujii et al. (2017) Orbital Evolution of Moons in Weakly Accreting Circumplanetary Disks
- O. Gressel, R. P. Nelson, N. J. Turner (2013) Global hydromagnetic simulations of a planet embedded in a dead zone: Gap opening, gas accretion, and formation of a protoplanetary jet
- L. Krapp et al. (2024) A thermodynamic criterion for the formation of Circumplanetary Disks
- J. Li et al. (2024) Challenge of direct imaging of exoplanets within structures: disentangling real signal from point source from background light
- N. Maeda et al. (2024) Delivery of Dust Particles from Protoplanetary Disks onto Circumplanetary Disks of Giant Planets
- N. Oberg et al. (2022) Circumplanetary disk ices - I. Ice formation vs. viscous evolution and grain drift
- A. Schneeberger, O. Mousis (2024) Impact of Jupiter's heating and self-shadowing on the Jovian circumplanetary disk structure
- Y. Shibaike, S. Mori (2022) Effective dust growth in laminar circumplanetary discs with magnetic wind-driven accretion
- Y. Shibaike, C. Mordasini (2024) Constraints on PDS 70 b and c from the dust continuum emission of the circumplanetary discs considering in situ dust evolution
- A. G. Taylor, F. C. Adams (2024) Formation and Structure of Circumplanetary Disks and Envelopes during the Late Stages of Giant Planet Formation
- A. G. Taylor, F. C. Adams (2024) Radiative Signatures of Circumplanetary Disks and Envelopes During the Late Stages of Giant Planet Formation
- W. R. Ward, R. M. Canup (2010) Circumplanetary Disk Formation
- Z. Zhu (2015) Accreting Circumplanetary Disks: Observational Signatures



"Ash rain" drifting outwards above the accretion disk near the protostar, driven by matter ejection in protostellar winds

Y. Tsukamoto/Kagoshima University, M. N. Machida, S. Inutsuka (Editing: U. v. Kusserow)

Results of simulation calculations: electrically charged particles are preferentially transported poleward due to their binding to the magnetic fields in collimated protostellar jet streams (above), neutral particles drift more strongly outwards because of centrifugal forces (below)

## Streams and Bubbles: Tidal Shaping of Planetary Outflows

MORGAN MACLEOD <sup>1</sup>, ANTONIJA OKLOPČIĆ <sup>2</sup>, FABIENNE NAIL <sup>2</sup> AND DION LINSSEN <sup>2</sup>

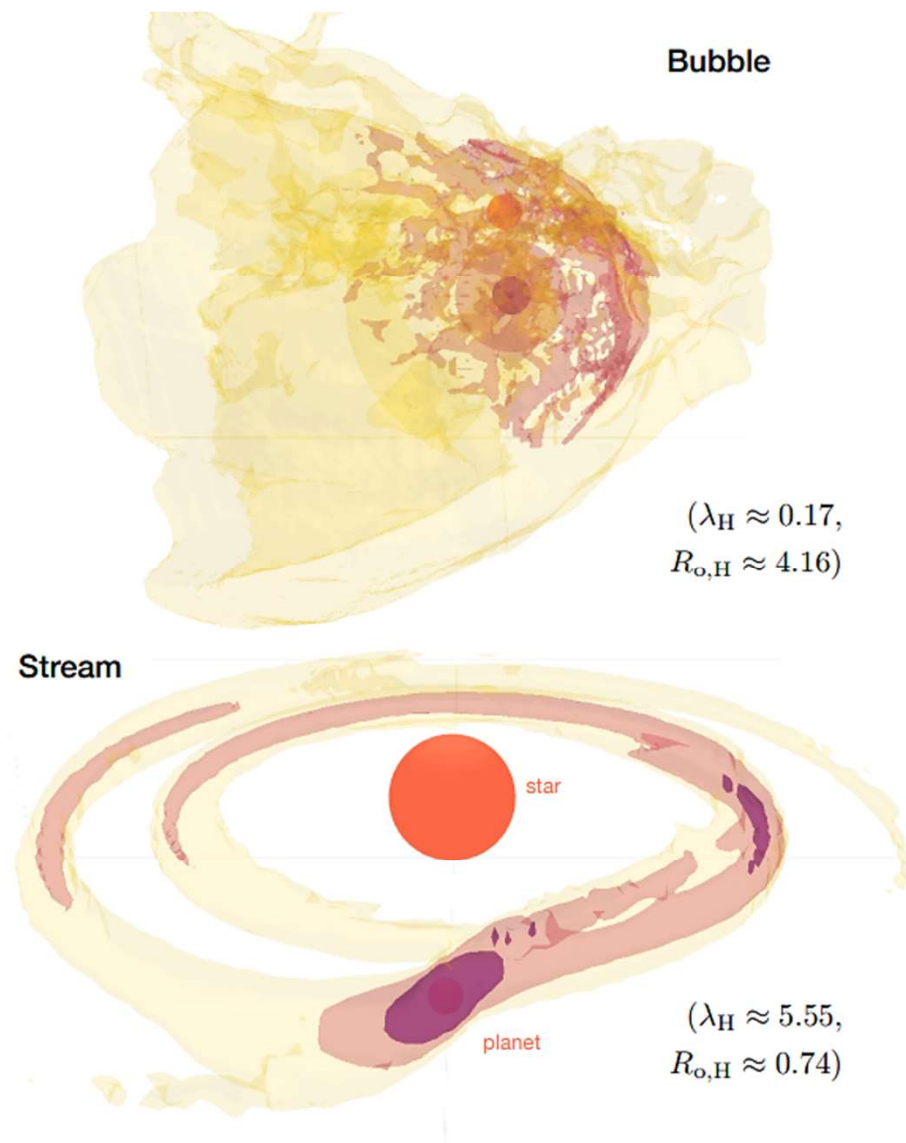
<sup>1</sup>*Institute for Theory & Computation, Center for Astrophysics, Harvard & Smithsonian, Cambridge, MA, 02138, USA*

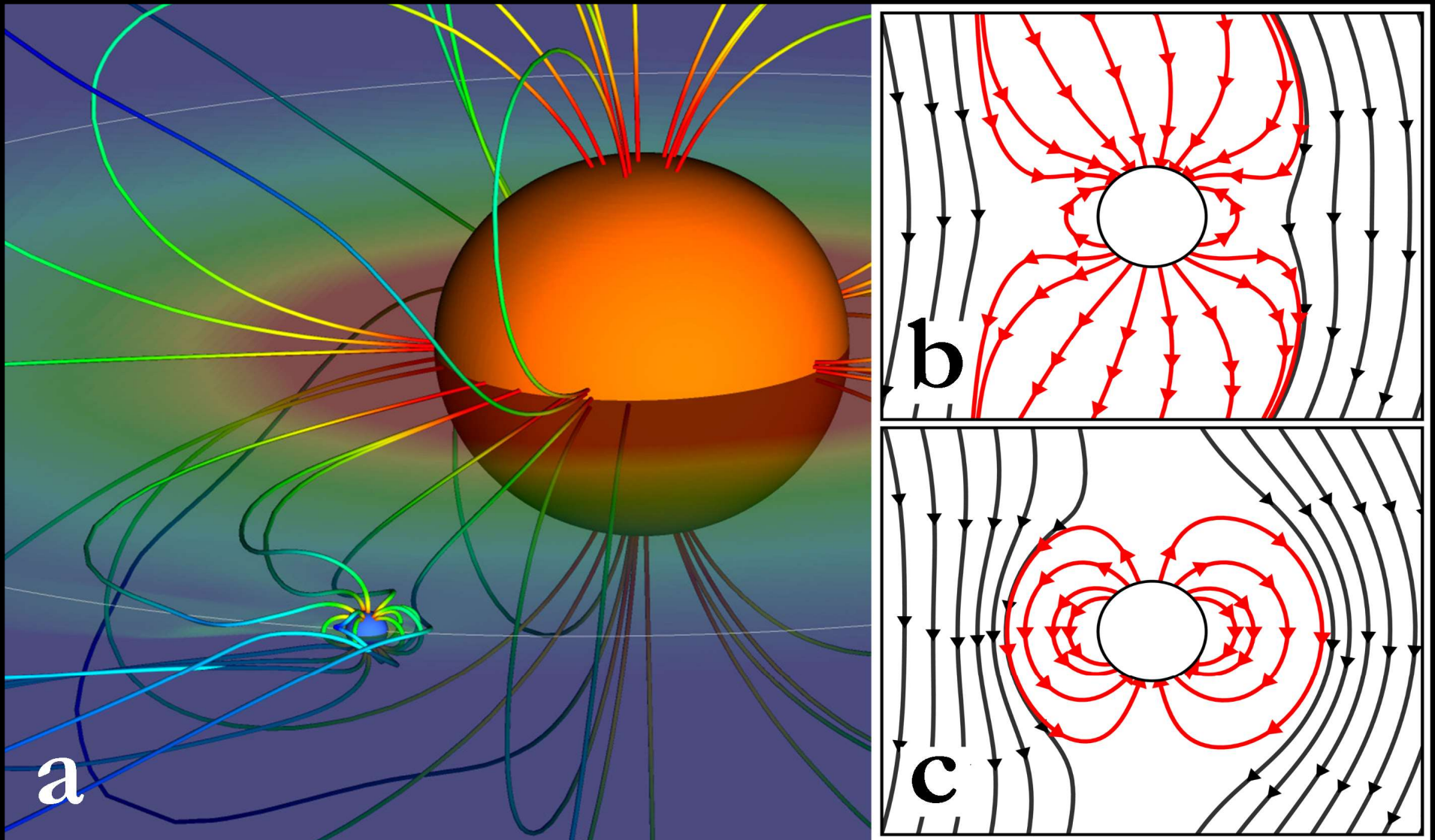
<sup>2</sup>*Anton Pannekoek Institute for Astronomy, University of Amsterdam, Science Park 904, NL-1098 XH Amsterdam, The Netherlands*

### ABSTRACT

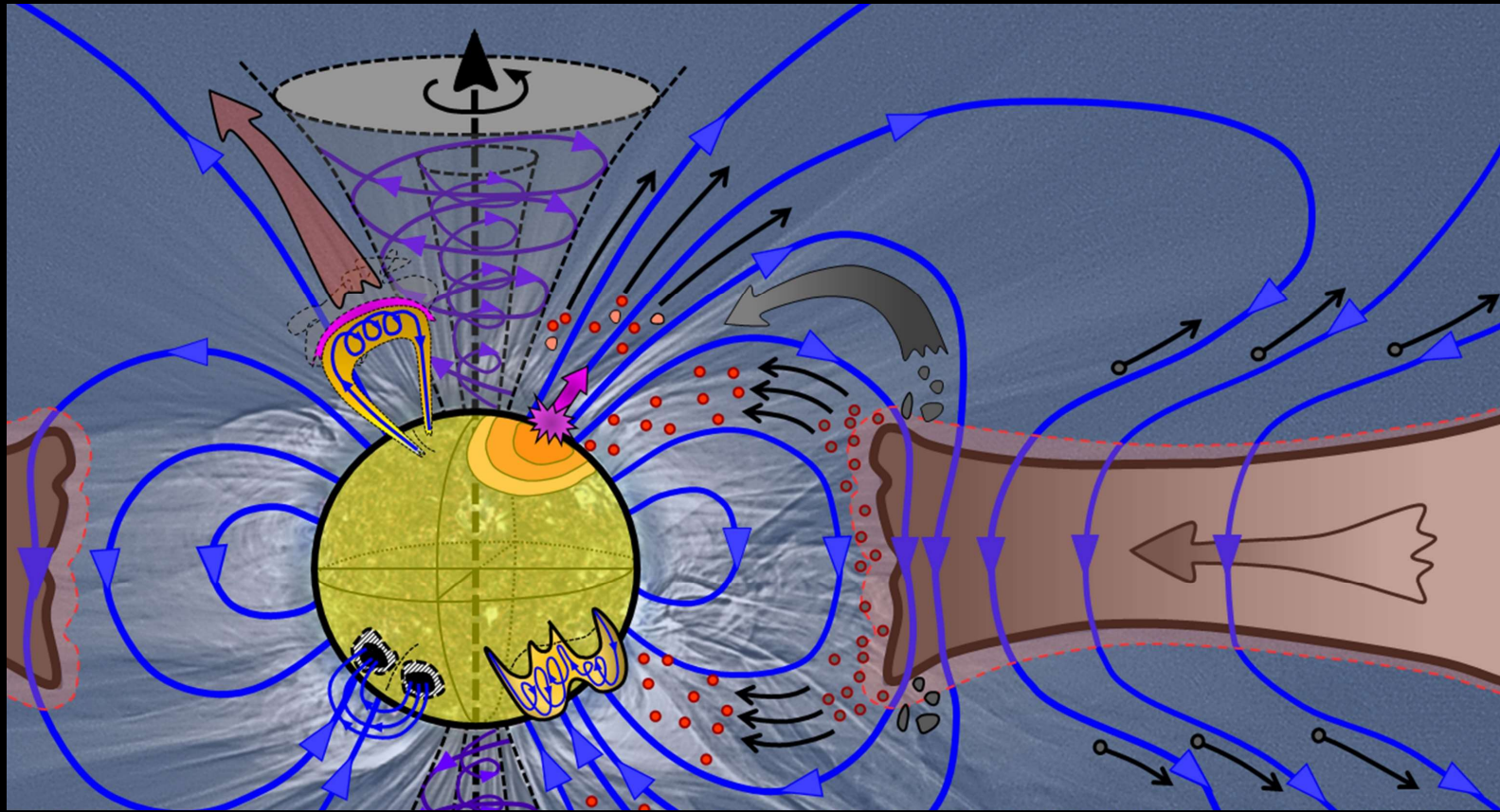
Planets lose mass to atmospheric outflows, and this mass loss is thought to be central in shaping the bimodal population of gaseous giant and rocky terrestrial exoplanets in close orbits. We model the escape of planetary atmospheres in three dimensional gas dynamic simulations in order to study their emergent morphology. Planetary outflows show a range of shapes from fast, isotropic outflows bounded by bow shocks to slower motion confined to thin streams. We show that a crucial factor is the role of the tidal gravity and orbiting reference frame in which planets lose mass. Flows can be characterized by the dimensionless Rossby number evaluated at the scale of the Hill sphere. Flows with a low Rossby number are significantly deviated and shaped by the stellar gravity, while those with a high Rossby number are comparatively unaffected. Rossby number alone is sufficient to predict outflow morphology as well as kinematic gradients across transit. The known exoplanet population should span a range of outflow Rossby numbers and thus shapes. We can use this information to constrain outflow physics and to inform observing strategies.

*Keywords:* Exoplanet atmospheric dynamics, Tidal interaction, Transits



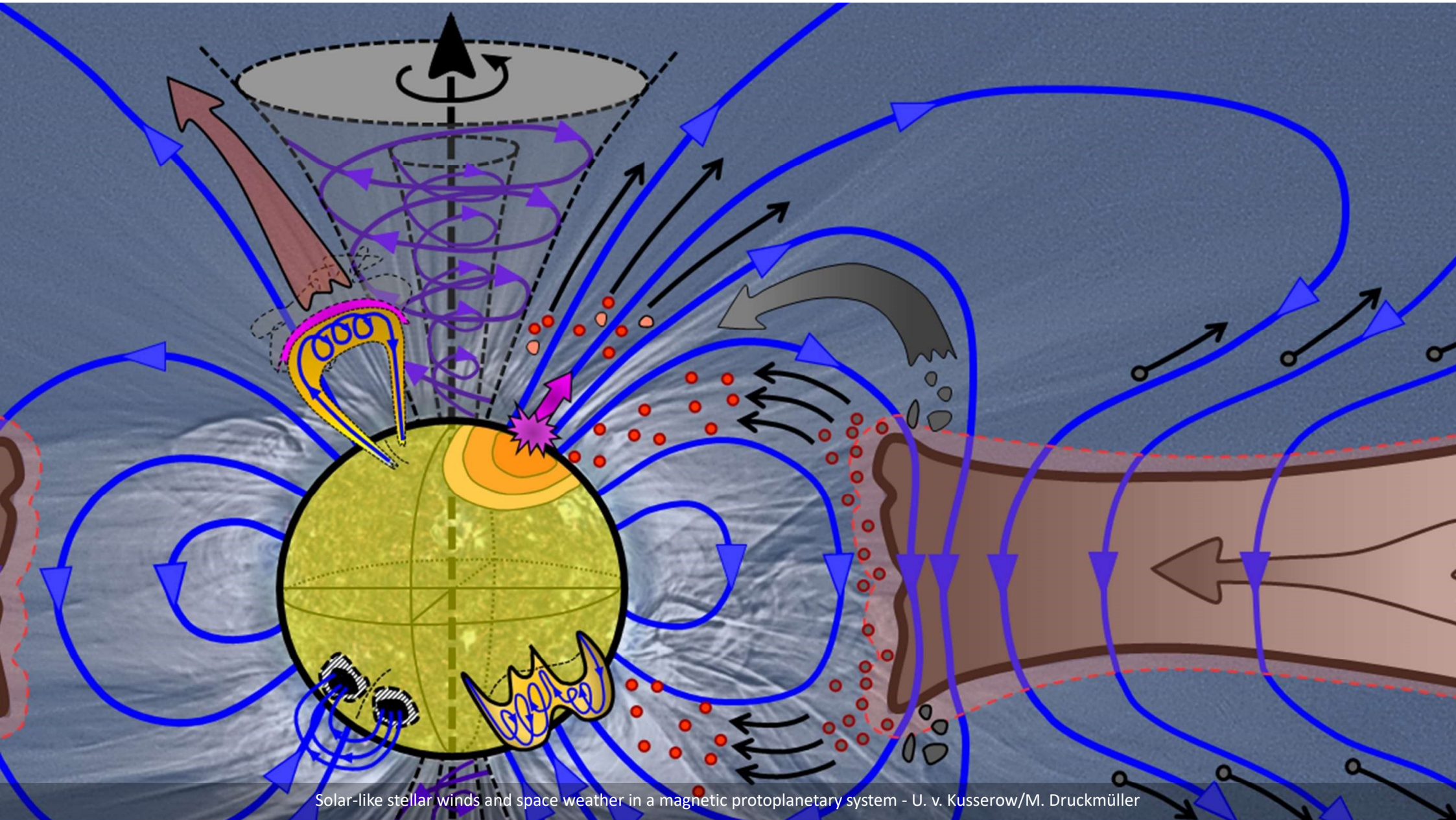


Interaction of stellar and planetary magnetic fields (a). Based on the results of computer simulations, different magnetic field topologies arise in the vicinity of the planets depending on the relative orientation of stellar and planetary fields to each other (b and c) - A. Strugarek, compilation: U. v. Kusserow

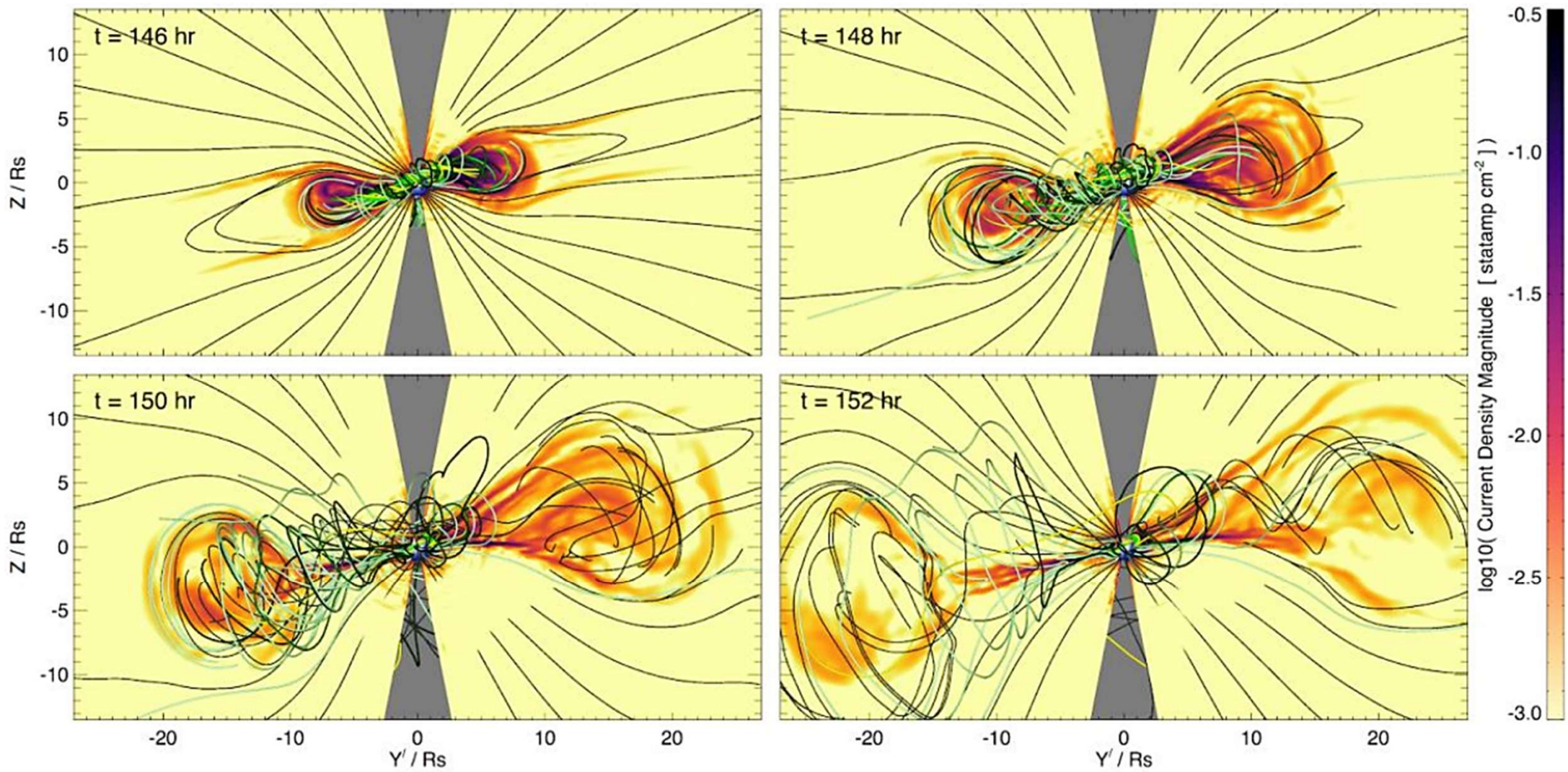


$$\frac{\partial \vec{B}}{\partial t} = \vec{\nabla} \times (\vec{v} \times \vec{B}) - \vec{\nabla} \times (\eta_{OD} \cdot \vec{\nabla} \times \vec{B}) + \vec{\nabla} \times \{ \eta_{AD} \cdot (\vec{\nabla} \times \vec{B}) \times \vec{B} \} - \vec{\nabla} \times [ \vec{\nabla} \times \{ \eta_{HD} \cdot (\vec{\nabla} \times \vec{B}) \times \vec{B} \} ]$$

Future Significance



Solar-like stellar winds and space weather in a magnetic protoplanetary system - U. v. Kusserow/M. Druckmüller



3D simulation of a massive (Carrington scale) stellar coronal eruption initiated from a magnetogram - B. J. Lynch et al. (2019)



## THE ROLE OF TURBULENT MAGNETIC RECONNECTION IN THE FORMATION OF ROTATIONALLY SUPPORTED PROTOSTELLAR DISKS

R. SANTOS-LIMA<sup>1</sup>, E. M. DE GOUVEIA DAL PINO<sup>1</sup>, AND A. LAZARIAN<sup>2</sup>

<sup>1</sup> Instituto de Astronomia, Geofísica e Ciências Atmosféricas, Universidade de São Paulo, R. do Matão, 1226, São Paulo, SP 05508-090, Brazil

<sup>2</sup> Department of Astronomy, University of Wisconsin, Madison, WI 53706, USA

Received 2011 September 13; accepted 2011 December 8; published 2012 February 10

### ABSTRACT

The formation of protostellar disks out of molecular cloud cores is still not fully understood. Under ideal MHD conditions, the removal of angular momentum from the disk progenitor by the typically embedded magnetic field may prevent the formation of a rotationally supported disk during the main protostellar accretion phase of low-mass stars. This has been known as the magnetic braking problem and the most investigated mechanism to alleviate this problem and help remove the excess of magnetic flux during the star formation process, the so-called ambipolar diffusion (AD), has been shown to be not sufficient to weaken the magnetic braking at least at this stage of the disk formation. In this work, motivated by recent progress in the understanding of magnetic reconnection in turbulent environments, we appeal to the diffusion of magnetic field mediated by magnetic reconnection as an alternative mechanism for removing magnetic flux. We investigate numerically this mechanism during the later phases of the protostellar disk formation and show its high efficiency. By means of fully three-dimensional MHD simulations, we show that the diffusivity arising from turbulent magnetic reconnection is able to transport magnetic flux to the outskirts of the disk progenitor at timescales compatible with the collapse, allowing the formation of a rotationally supported disk around the protostar of dimensions  $\sim 100$  AU, with a nearly Keplerian profile in the early accretion phase. Since MHD turbulence is expected to be present in protostellar disks, this is a natural mechanism for removing magnetic flux excess and allowing the formation of these disks. This mechanism dismisses the necessity of postulating a hypothetical increase of the ohmic resistivity as discussed in the literature. Together with our earlier work which showed that magnetic flux removal from molecular cloud cores is very efficient, this work calls for reconsidering the relative role of AD in the processes of star and planet formation.

**Key words:** accretion, accretion disks – diffusion – ISM: magnetic fields – magnetohydrodynamics (MHD) – stars: formation – turbulence

DRAFT VERSION MAY 25, 2024

Preprint typeset using L<sup>A</sup>T<sub>E</sub>X style emulateapj v. 01/23/15

## APPLICATIONS OF FAST MAGNETIC RECONNECTION MODELS TO THE ATMOSPHERES OF THE SUN AND PROTOPLANETARY DISKS

FULVIA PUCCI<sup>1</sup>, K. ALKENDRA P. SINGH<sup>2,3</sup>, UMA GORTI<sup>4,5</sup>, MARCO VELLI<sup>6</sup>, NEAL J. TURNER<sup>1</sup>, DISHA VARSHNEY<sup>2</sup>, MARIA ELENA INNOCENTI<sup>7</sup>

<sup>1</sup> Jet Propulsion Laboratory, California Institute of Technology, 4800 Oak Grove Drive, Pasadena, California 91109, USA

<sup>2</sup> Plasma Astrophysics Research Laboratory, Department of Physics, Institute of Science, BHU, Varanasi 221005, India

<sup>3</sup> Astronomical Observatory, Graduate School of Science, Kyoto University, Yamashina, Kyoto 607-8471, Japan

<sup>4</sup> Department of Earth, Planetary, and Space Sciences, UCLA, 595 Charles Young Drive East, Los Angeles, California 90095, USA

<sup>5</sup> NASA Ames Research Center, MS 245-1, PO Box 1, Moffett Field, California 94035, USA

<sup>6</sup> SETI Institute, 339 Bernardo Ave Suite 200, Mountain View, California 94043, USA and

<sup>7</sup> Institut für Theoretische Physik, Ruhr-Universität Bochum, Bochum, Germany

Draft version May 25, 2024


### ABSTRACT

Partially-ionized plasmas consist of charged and neutral particles whose mutual collisions modify magnetic reconnection compared with the fully-ionized case. The collisions alter the rate and locations of the magnetic dissipation heating and the distribution of energies among the particles accelerated into the non-thermal tail. We examine the collisional regimes for the onset of fast reconnection in two environments: the partially-ionized layers of the solar atmosphere and the protoplanetary disks that are the birthplaces for planets around young stars. In both these environments, magnetic nulls readily develop into resistive current sheets in the regime where the charged and neutral particles are fully coupled by collisions, but the current sheets quickly break down under the ideal tearing instability. The current sheets collapse repeatedly, forming magnetic islands at successively smaller scales, till they enter a collisionally-decoupled regime where the magnetic energy is rapidly turned into heat and charged-particle kinetic energy. Small-scale, decoupled fast reconnection in the solar atmosphere may lead to preferential heating and energization of ions and electrons that escape into the corona. In protoplanetary disks such reconnection causes localized heating in the atmospheric layers that produce much of the infrared atomic and molecular line emission observed with the Spitzer and James Webb Space Telescopes.

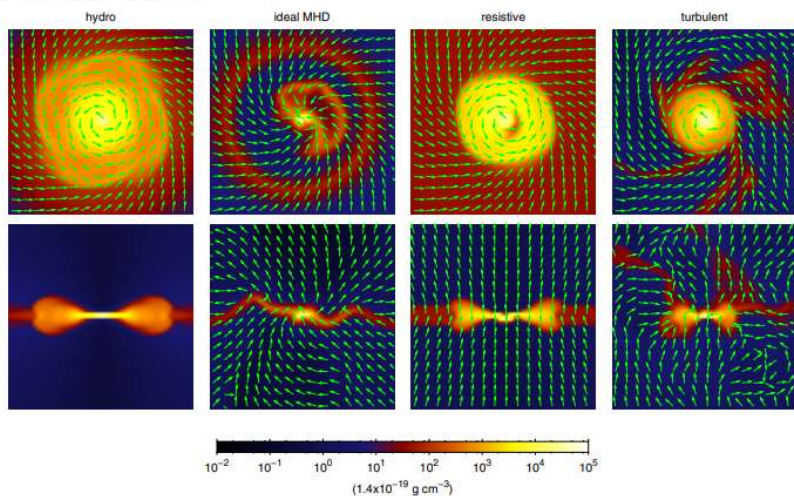


**Figure 2.** Face-on (top) and edge-on (bottom) density maps of the central slices of the collapsing disk models listed in Table 1 at a time  $t = 9 \times 10^{11}$  s ( $\approx 0.03$  Myr). The arrows in the top panels represent the velocity field direction, and those in the bottom panels represent the magnetic field direction. From left to right columns: (1) the pure hydrodynamic rotating system, (2) the ideal MHD model, (3) the MHD model with an anomalous resistivity  $10^3$  times larger than the ohmic resistivity, i.e.,  $\eta = 1.2 \times 10^{20}$  cm<sup>2</sup> s<sup>-1</sup>, and (4) the turbulent MHD model with turbulence injected from  $t = 0$  until  $t = 0.015$  Myr. All the MHD models have an initial vertical magnetic field distribution with intensity  $B_z = 35$   $\mu$ G. Each image has a side of 1000 AU.

## YSO Jets Magnetocentrally Driven by Reconnecting Atmospheric Avalanche Accretion Streams Above Inner Circumstellar Disks

YISHENG TU <sup>1</sup>, ZHI-YUN LI,<sup>1</sup> ZHAOHUAN ZHU,<sup>2</sup> XIAO HU,<sup>1,3</sup> AND CHUN-YEN HSU<sup>1</sup>

<sup>1</sup>*Astronomy Department, University of Virginia, Charlottesville, VA 22904, USA*

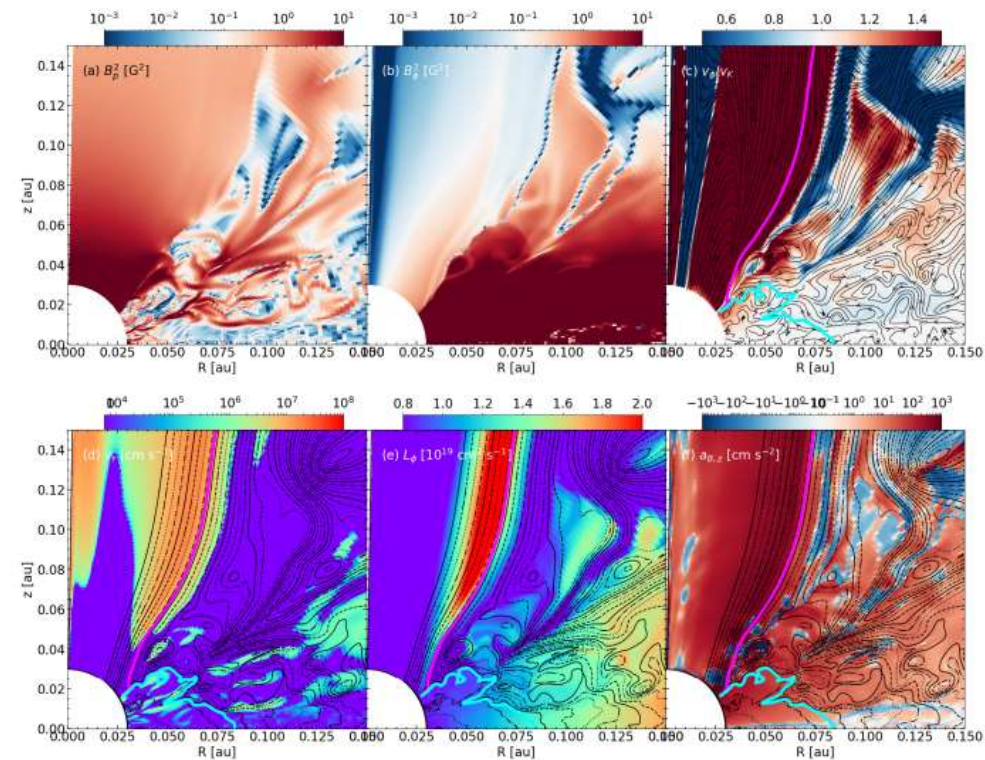
<sup>2</sup>*Department of Physics and Astronomy, University of Nevada, Las Vegas, NV, 89154-4002, USA*

<sup>3</sup>*Department of Astronomy, University of Florida, Gainesville, FL 32608, USA*

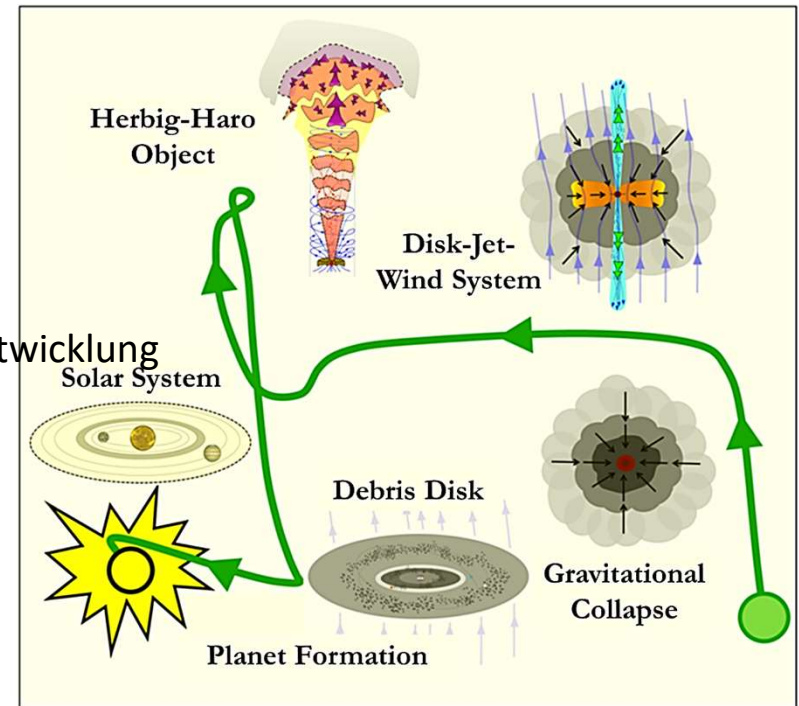
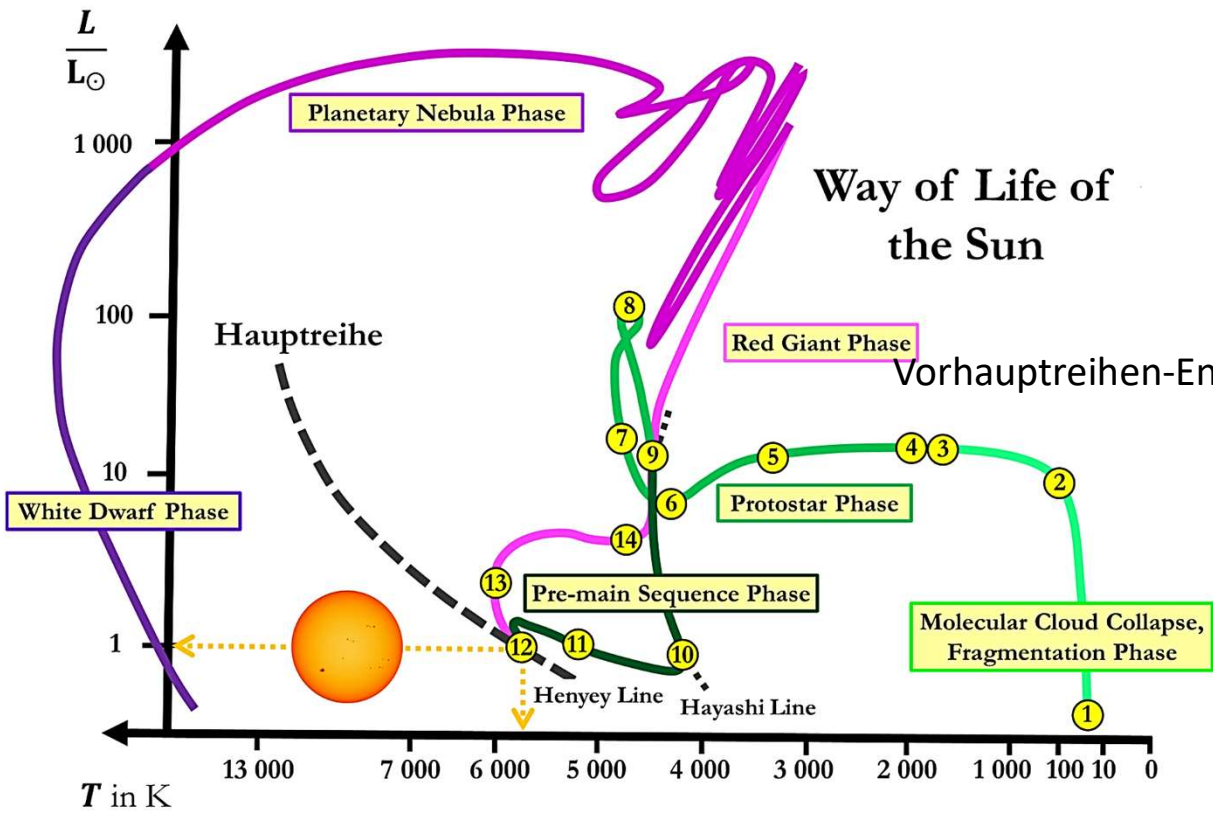
### ABSTRACT

Fast, collimated jets are ubiquitous features of young stellar objects (YSOs). They are generally thought to be powered by disk accretion, but the details are debated. Through 2D (axisymmetric) MHD simulations, we find that a fast ( $> 100$  km/s) collimated bipolar jet is continuously driven along the north and south poles of the circumstellar disk that is initially magnetized by a large-scale open poloidal field and contains a thermally ionized inner magnetically active zone surrounded by a dead zone. The fast jet is primarily driven magneto-centrifugally by the release of the gravitational binding energy of the so-called “avalanche accretion streams” near the boundary of an evacuated poloidal field-dominated polar region and a thick disk atmosphere raised by a toroidal magnetic field. Specifically, the fast outflow is driven along the upper (open) branch of the highly pinched poloidal field lines threading the (strongly magnetically braked) accretion streams where the density is relatively low so that the lightly loaded material can be accelerated magneto-centrifugally along the open field line to a high speed. The highly pinched poloidal magnetic fields threading the avalanche accretion streams tend to reconnect, enabling mass to accrete to the center without dragging along the poloidal magnetic flux with it. The reconnection provides a potential heating source for producing chondrules and calcium- and aluminum-rich inclusions (CAIs).

*Keywords:* Accretion (14) — Jets (870) — Circumstellar disks (235) — Young stellar objects (1834)



# Way of Life of the Sun



Pre-main Sequence Evolution

### Molecular Cloud Collapse, Fragmentation Phase

- ① Compression and Fragmentation of the Gas Cloud, Formation of Bok Globules
- ② Termination of Isothermal collapse, Formation Quasi-hydrostatic Core, Adiabatic Increase in Central Temperature
- ③ Dissociation of Hydrogen Molecules, Core Collapse, Formation of Protostar, Onset of Ionization

### Developments in the Protostar Phase

- ④ Protostellar Disk Formation, Onset of Deuterium Burning
- ⑤ Dynamo Generated Magnetic Fields, Sunspots, Prominences, Flares, Solar Wind
- ⑥ Obstruction of Matter Accretion by Solar Wind
- ⑦ Akkretionshülle zunehmend durchsichtiger
- ⑧ Transition from Dust to Gas Photosphere

### Developments in the Pre-main Sequence Phase

- ⑨ Crossing the Birthline, Hydrostatic Contraction of the almost Fully Convective Star along the Hayashi Line
- ⑩ Beginning of Central Radiative Transport, Development along Heney Line
- ⑪ Beginning of Hydrogen Nuclear Fusion
- ⑫ Reaching the Main Sequence



## Origin and Evolution of Magnetic Field in PMS Stars: Influence of Rotation and Structural Changes

Constance Emeriau-Viard and Allan Sacha Brun

Laboratoire AIM Paris-Saclay CEA/DSM—CNRS—Université Paris Diderot, IRFU/DAP CEA Paris-Saclay,  
 F-91191 Gif-sur-Yvette Cedex, France; [constance.emeriau@cea.fr](mailto:constance.emeriau@cea.fr), [sacha.brun@cea.fr](mailto:sacha.brun@cea.fr)

Received 2017 March 27; revised 2017 June 19; accepted 2017 June 20; published 2017 August 24

### Abstract

During stellar evolution, especially in the pre-main-sequence phase, stellar structure and rotation evolve significantly, causing major changes in the dynamics and global flows of the star. We wish to assess the consequences of these changes on stellar dynamo, internal magnetic field topology, and activity level. To do so, we have performed a series of 3D HD and MHD simulations with the ASH code. We choose five different models characterized by the radius of their radiative zone following an evolutionary track computed by a 1D stellar evolution code. These models characterized stellar evolution from 1 to 50 Myr. By introducing a seed magnetic field in the fully convective model and spreading its evolved state through all four remaining cases, we observe systematic variations in the dynamical properties and magnetic field amplitude and topology of the models. The five MHD simulations develop a strong dynamo field that can reach an equipartition state between the kinetic and magnetic energies and even superequipartition levels in the faster-rotating cases. We find that the magnetic field amplitude increases as it evolves toward the zero-age main sequence. Moreover, the magnetic field topology becomes more complex, with a decreasing axisymmetric component and a nonaxisymmetric one becoming predominant. The dipolar components decrease as the rotation rate and the size of the radiative core increase. The magnetic fields possess a mixed poloidal-toroidal topology with no obvious dominant component. Moreover, the relaxation of the vestige dynamo magnetic field within the radiative core is found to satisfy MHD stability criteria. Hence, it does not experience a global reconfiguration but slowly relaxes by retaining its mixed stable poloidal-toroidal topology.

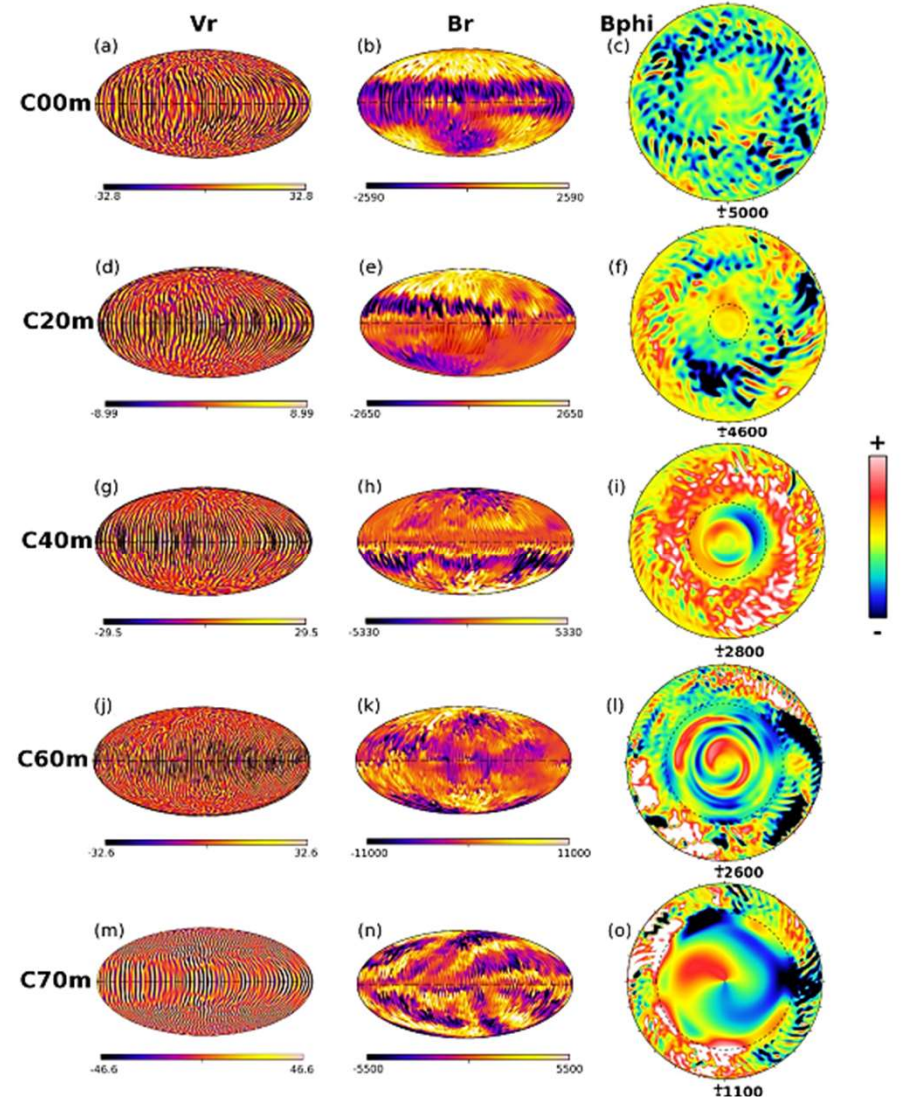
**Key words:** convection – dynamo – magnetohydrodynamics (MHD) – stars: interiors – stars: magnetic field

### 1. Stellar Evolution and Magnetism

Stellar rotation is known to significantly change over the course of stellar evolution (Gallet & Bouvier 2013). Once the star is formed, i.e., at the end of the protostellar phase, it enters the pre-main-sequence (PMS) phase. This stage is characterized by a strong contraction of the star under the action of gravitation and the absence of long-term thermonuclear reactions. When H burning occurs at the center of the star and stellar contraction stops, the young star arrives on the main sequence (MS), where it will spend the majority of its lifetime. The very beginning of this stage, when the H burning starts, is called the zero-age main sequence (ZAMS). This stage also corresponds to a rapid overall increase of the rotation of the star.

At the very beginning of the PMS phase, stellar rotation remains constant since the star is in a disk-locking phase until about 3–10 Myr, when it decouples from the vanishing disk. Then as the star contracts under the influence of gravitation, stellar rotation increases as a consequence of angular momentum conservation until it reaches the ZAMS. Later, on the MS, stellar rotation decreases as contraction stops and magnetic winds start braking the star. This is not the only drastic evolution that young stars experience during this phase of stellar evolution, as their luminosity also varies by a large factor. The internal structure is too strongly impacted as the star evolves along the PMS phase. Indeed, starting from a fully convective state, their radiative zone grows continuously, due to the ignition of thermonuclear reactions in their deep core, such as occupying most of their interior upon their arrival on the ZAMS. These major changes impact the star's properties, especially their internal rotation and magnetic field.

Stellar rotation rate, internal rotation, and magnetic field are strongly linked through complex physical processes. At the very beginning of stellar evolution, stars are meant to rotate quite fast since they contract and accrete angular momentum from the disk. However, observations led, for instance, by Bouvier et al. (1986, 2014) show that they only rotate at 1/10 of their breakup velocity. Hence, some physical processes prevent stars from spinning up at the very beginning of their PMS evolution. Magnetic field is a likely candidate to explain this phenomenon, as it controls the interaction between the star and its disk. Even after the disk-locking phase, magnetic field has a strong link with rotation through wind-braking and core-envelope coupling. Magnetic field can also possibly modify the transport of angular momentum in stellar interiors through Maxwell stresses. For instance, it has been invoked to explain the flat rotation profile in the radiative interior of the Sun, along with other processes such as internal waves (Charbonnel & Talon 2005; Eggenberger et al. 2005). It is quite clear that a feedback loop between rotation and magnetic field must exist. On one hand, the rotation impacts the magnetic field through dynamo processes, and especially through the shearing of magnetic field lines by the differential rotation of the convective envelope (e.g., the  $\Omega$ -effect). On the other hand, magnetic field topology and amplitude impact braking by the wind. Evidence of such an influence was studied, for instance, by Pizzolato et al. (2003), Wright et al. (2011), Gondoin (2012), Reiners et al. (2014), Matt et al. (2015), and Blackman & Owen (2016). These analyses showed a correlation between coronal X-ray emission and stellar rotation in late-type MS stars, revealing the existence of two regimes. In the first one, at Rossby numbers greater than 0.1–0.3, the X-ray emission is



Left and middle columns : shell slices at the surface of radial velocity and radial magnetic field for the five MHD simulations. Right column: equatorial slice of  $B_{\phi}$  for each model.

# The High-resolution Accretion Disks of Embedded protoStars (HADES) simulations. I. Impact of Protostellar Magnetic Fields on the Accretion Modes

Brandt A. L. Gaches<sup>1</sup>\*, Jonathan C. Tan<sup>1,2</sup>, Anna L. Rosen<sup>3,4</sup>, and Rolf Kuiper<sup>5</sup>

<sup>1</sup> Department of Space, Earth and Environment, Chalmers University of Technology, Gothenburg SE-412 96, Sweden

<sup>2</sup> Department of Astronomy, University of Virginia, 530 McCormick Road, Charlottesville, VA 22904, USA

<sup>3</sup> Department of Astronomy, San Diego State University, San Diego, CA 92182, USA

<sup>4</sup> Computational Science Research Center, San Diego State University, San Diego, CA 92182, USA

<sup>5</sup> Faculty of Physics, University of Duisburg-Essen, Lotharstraße 1, 47057, Duisburg, Germany

Accepted XXX. Received YYY; in original form ZZZ

## ABSTRACT

How embedded, actively accreting low-mass protostars accrete their mass is still greatly debated. Observations are now piecing together the puzzle of embedded protostellar accretion, in particular with new facilities in the near-infrared. However, high-resolution theoretical models are still lacking, with a stark paucity of detailed simulations of these early phases. Here we present high-resolution non-ideal magneto-hydrodynamic simulations of a Solar mass protostar accreting at rates exceeding  $10^{-6} M_{\odot} \text{ yr}^{-1}$ . We show the results of the accretion flow for four different protostellar magnetic fields, 10 G, 500 G, 1 kG, and 2 kG, combined with a disk magnetic field. For weaker (10 G and 500 G) protostar magnetic fields, accretion occurs via a turbulent boundary layer mode, with disk material impacting across the protostellar surface. In the 500 G model, the presence of a magnetically dominated outflow focuses the accretion towards the equator, slightly enhancing and ordering the accretion. For kG magnetic fields, the disk becomes truncated due to the protostellar dipole and exhibits magnetospheric accretion, with the 2 kG model having accretion bursts induced by the interchange instability. We present bolometric light curves for the models and find that they reproduce observations of Class I protostars from YSOVAR, with high bursts followed by an exponential decay possibly being a signature of instability-driven accretion. Finally, we present the filling fractions of accretion and find that 90% of the mass is accreted in a surface area fraction of 10-20%. These simulations will be extended in future work for a broader parameter space, with their high resolution and high temporal spacing able to explore a wide range of interesting protostellar physics.

**Key words.** Stars: protostars – Accretion, accretion disks – Methods: numerical

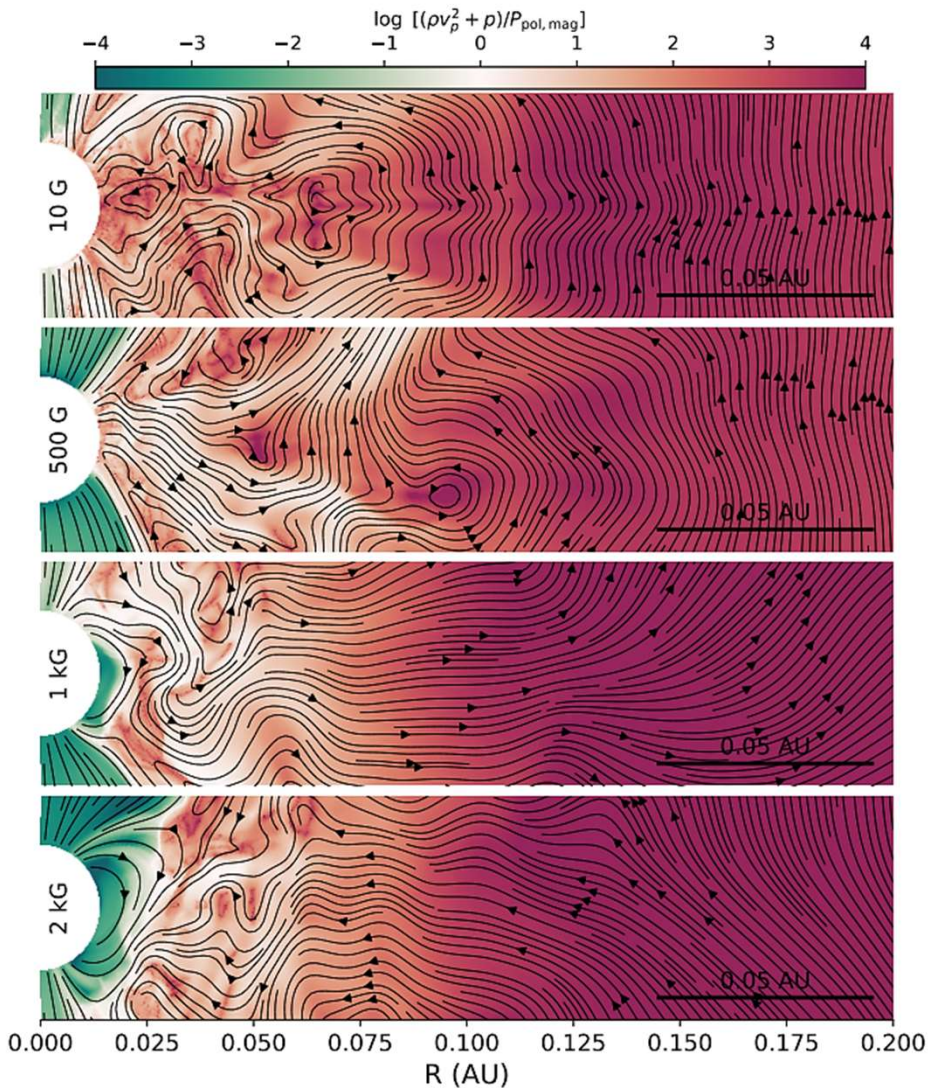
## 1. Introduction

Protostars are the bloated embryos of main-sequence stars that are actively accreting material from their natal environments. In the earlier phases of evolution, low-mass protostars are still deeply embedded within their natal cores and surrounded by relatively massive disks, resulting in substantial accretion rates,  $\dot{m}_{\star} \geq 10^{-7} M_{\odot} \text{ yr}^{-1}$ . Direct knowledge of how protostars accrete their mass typically comes from observations at more evolved stages, such as T-Tauri stars, when the central protostar is exposed, the disks have been largely depleted and the accretion rates drop below  $\dot{m}_{\star} \leq 10^{-8} M_{\odot} \text{ yr}^{-1}$ . Since these objects are exposed, it becomes significantly more feasible to observe emission from the accretion zones, primarily in the form of X-rays (Feigelson & Montmerle 1999; Feigelson et al. 2007), ultraviolet emission (Manara et al. 2023) and hydrogen recombination emission (Fischer et al. 2023). There are indirect methods to estimate the accretion rate, such as determining the properties of protostellar outflows and inferring the accretion rate via theoretical models (e.g. Avison et al. 2021). Modern observational facilities, such as the Very Large Telescope Interferometer (VLTI) with the GRAVITY instrument, are now probing the accretion of more embedded systems, tracing evolutionary times

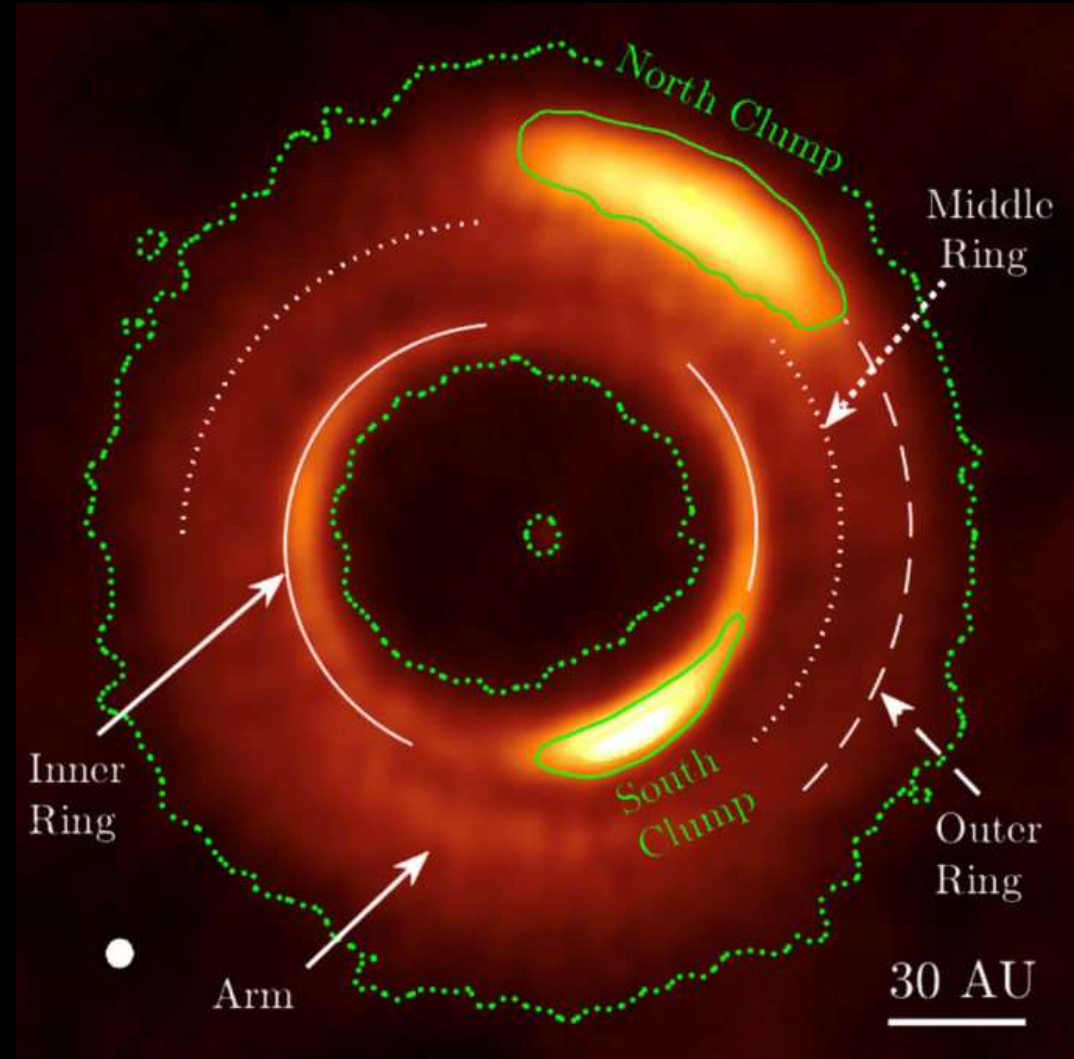
when most of the protostar’s mass has already been accumulated (e.g., Gravity Collaboration et al. 2023b,a). During the main accretion phases of protostar formation, the protostar’s natal core and disk obscure the accretion zone, complicating efforts to directly probe the inner accretion disks and follow how the material is delivered onto the protostar.

Multi-physics star formation simulations can capture the earliest phases of star formation from the large scales (sub-parsec for core-scale simulations and 1-10s of parsec for molecular cloud simulations) (e.g. Dale et al. 2012; Rosen et al. 2016; Offner & Chaban 2017; Seifried et al. 2017; Cunningham et al. 2018; Wurster et al. 2019; Rosen & Krumholz 2020; Grudić et al. 2021; Rosen 2022; Suin et al. 2024), but must use sub-grid prescriptions to model the protostar as an unmagnetized sink particle which accretes mass from an assumed accretion region (Offner et al. 2009; Bleuler & Teyssier 2014). These simulations are broadly able to reproduce the accretion rates from analytic accretion models (i.e. Shu 1977; Bonnell et al. 2001; McKee & Tan 2003). However, these parsec-scale simulations cannot resolve the accretion flow directly onto the protostar due to resolution constraints: resolving from molecular cloud scales to the protostellar surface requires spanning 7-8 orders of magnitude across length scales. The combined theoretical and observational challenges mean the underlying physical processes of protostel-

\* E-mail: brandt.gaches@chalmers.se



†† The ratio of the poloidal ram pressure plus thermal pressure to the poloidal magnetic pressure within the inner 0.2 AU of the disk



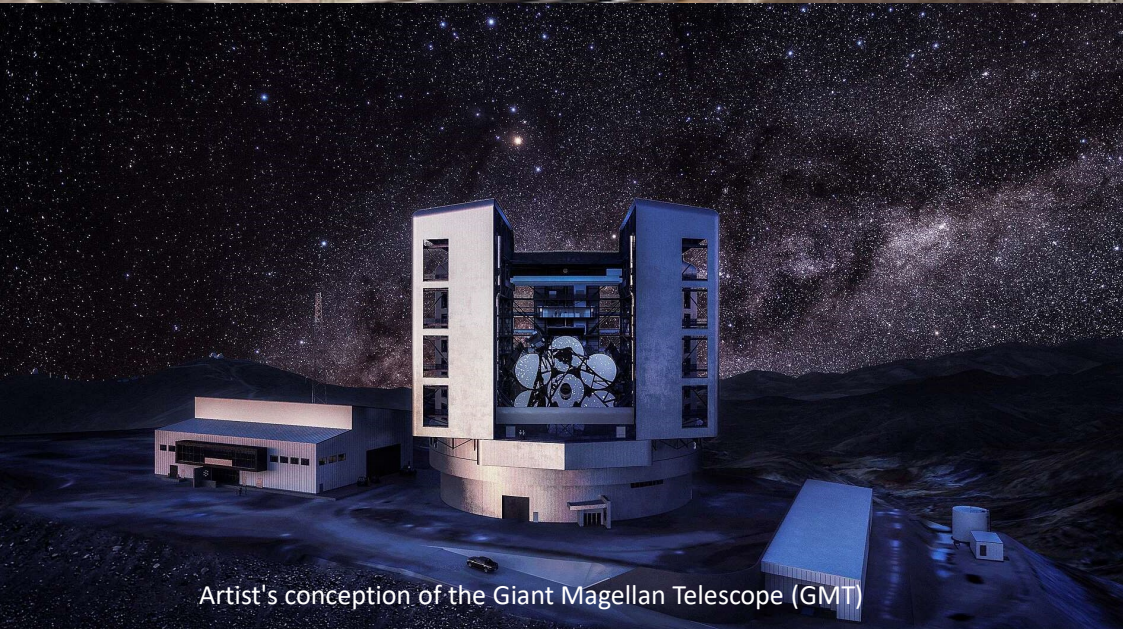
Exciting structures in a young Protoplanetary Disk that support Planet Formation - ALMA (ESO/NAOJ/NRAO)/Dong et al.



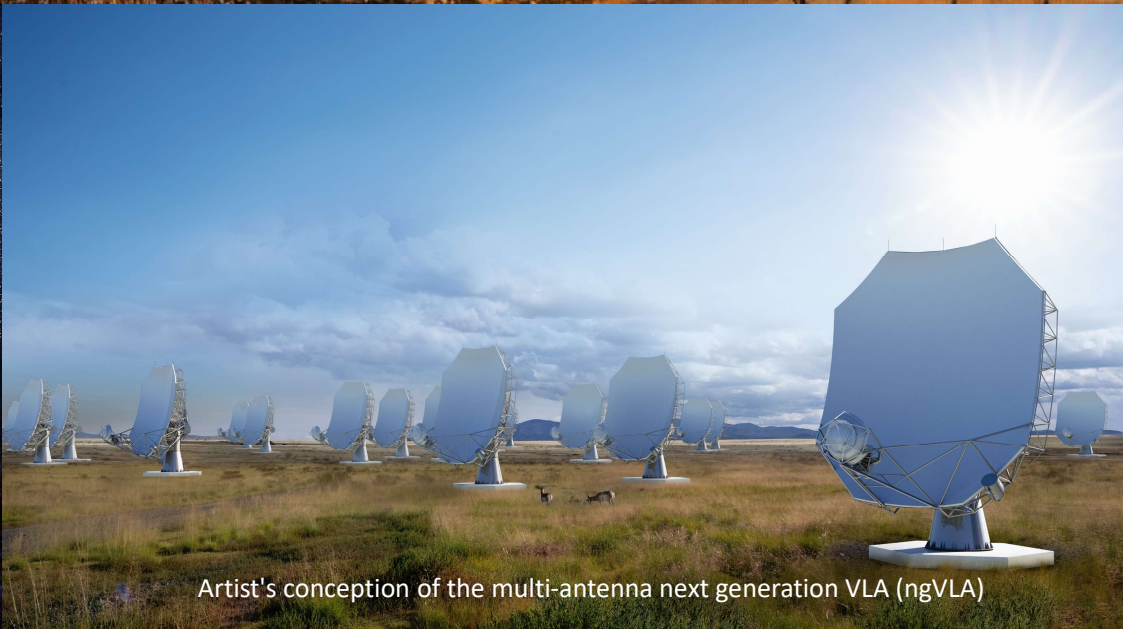
Artist's conception of the Extremely Large Telescope (ELT)



Artist's conception Square Kilometre Array Observatory (SKAO)



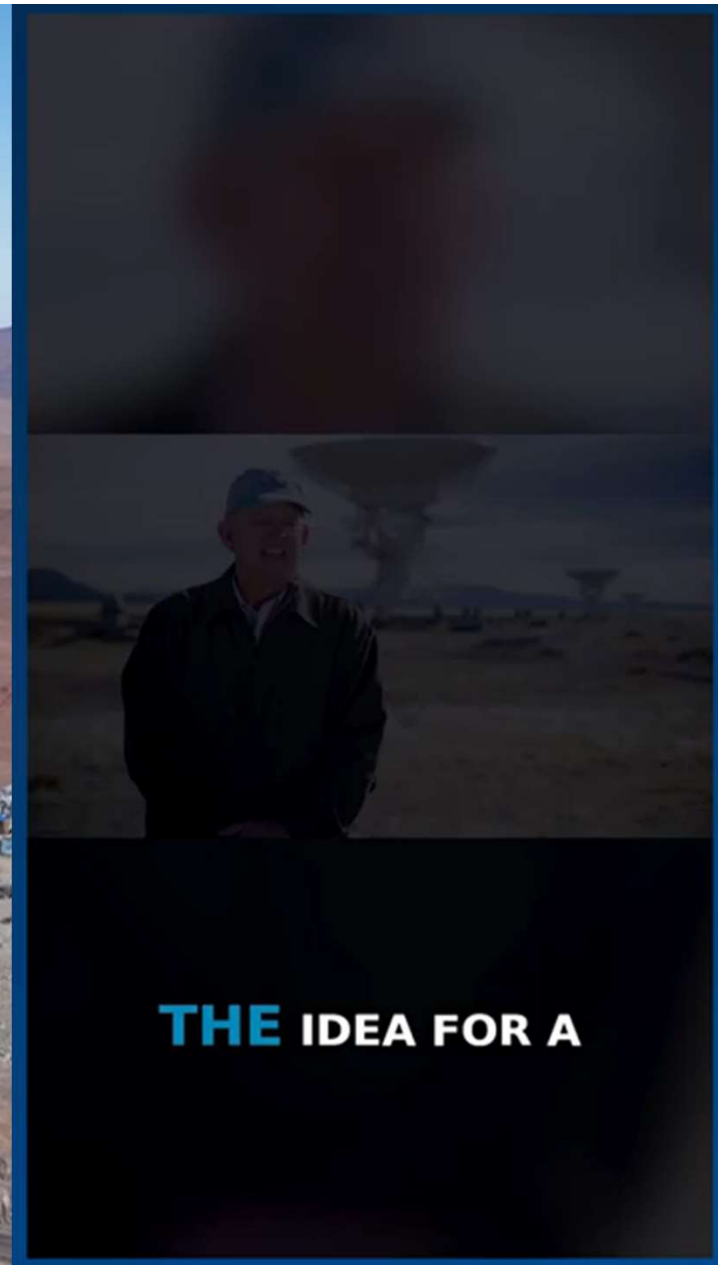
Artist's conception of the Giant Magellan Telescope (GMT)



Artist's conception of the multi-antenna next generation VLA (ngVLA)



Shielding the Extremely Large Telescope from the Atacama Desert | ELT Updates - ESO



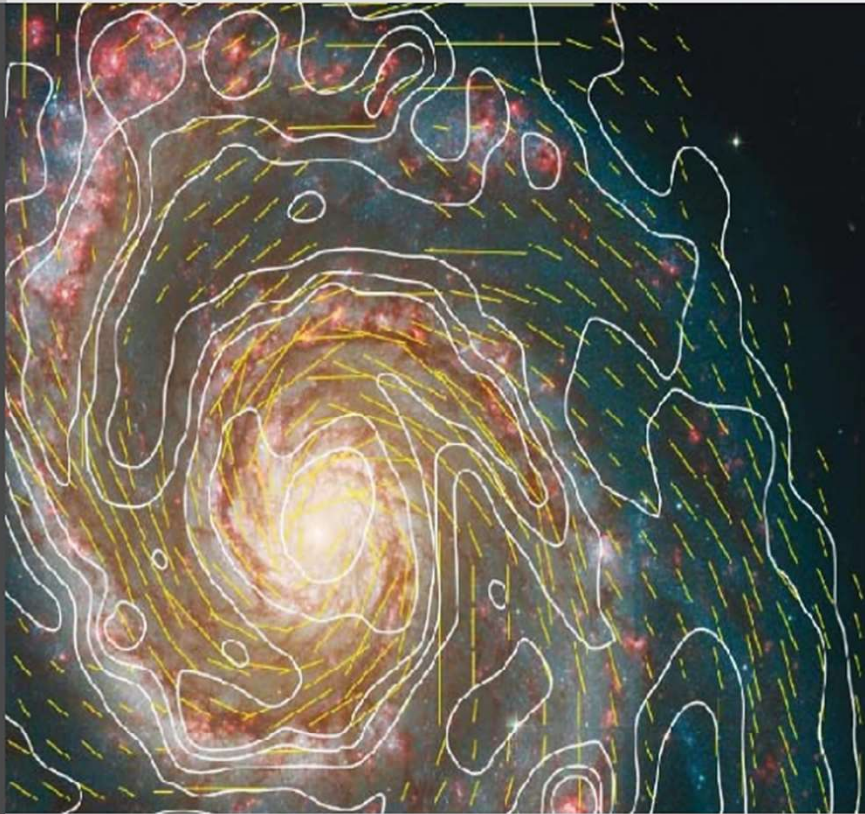
**THE IDEA FOR A**





# E-ELT Spectropolarimetry: The Science Case

A Community Proposal to ESO (July 2009)



A broad suite of astrophysical projects requiring spectropolarimetry and the E-ELT is presented. Spectropolarimetry not merely sorts photons by their wavelengths but unravels the physics of their history from the emission site all the way to the observer. Elaborating on Solar System bodies and extra-solar planets, the interstellar and intergalactic medium, young, old, and solar-like stars, supernovae, GRBs, galaxies, AGNs, weak cosmic lensing, and even the early universe, a synopsis of the unique benefits of this observing technique is developed. The aim is to stir and guide the discussion about polarimetric capabilities for the E-ELT.

## Polarimetric modeling and assessment of science cases for Giant Magellan Telescope-Polarimeter (GMT-Pol)

Ramya M Anche<sup>a</sup>, Grant Williams<sup>a</sup>, Hill Taylor<sup>c</sup>, Chris Packham<sup>b</sup>, Daewook Kim<sup>a,c</sup>, Jaren N Ashcraft<sup>a,c</sup>, Ewan S. Douglas<sup>a</sup>, and GMT-Pol team<sup>\*</sup>

<sup>a</sup>Steward Observatory, University of Arizona, 933N Cherry Avenue, Tucson, Arizona, 85721, USA

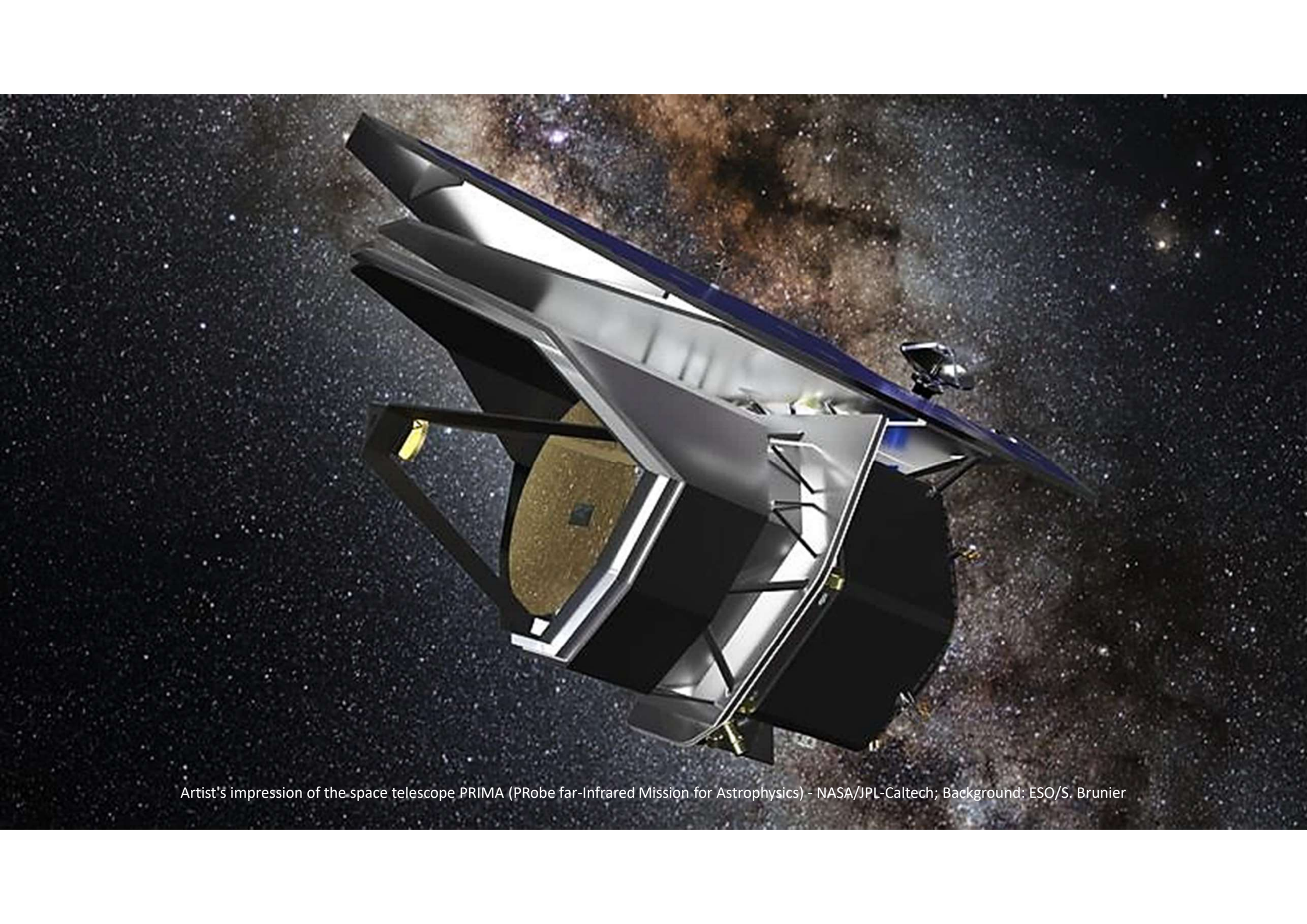
<sup>b</sup>University of Texas, San Antonio, 1 UTSA Circle, San Antonio, TX 78249

<sup>c</sup>James C. Wyant College of Optical Sciences, University of Arizona, 933N Cherry Avenue, Tucson, Arizona, 85721, USA

### ABSTRACT

Polarization observations through the next-generation large telescopes will be invaluable for exploring the magnetic fields and composition of jets in AGN, multi-messenger transients follow-up, and understanding interstellar dust and magnetic fields. The 25m Giant Magellan Telescope (GMT) is one of the next-generation large telescopes and is expected to have its first light in 2029. The telescope consists of a primary mirror and an adaptive secondary mirror comprising seven circular segments. The telescope supports instruments at both Nasmyth as well as Gregorian focus. However, none of the first or second-generation instruments on GMT has the polarimetric capability. This paper presents a detailed polarimetric modeling of the GMT for both Gregorian and folded ports for astronomical B-K filter bands and a field of view of 5 arc minutes. At 500nm, The instrumental polarization is 0.1% and 3% for the Gregorian and folded port, respectively. The linear to circular crosstalk is 0.1% and 30% for the Gregorian and folded ports, respectively. The Gregorian focus gives the GMT a significant competitive advantage over TMT and ELT for sensitive polarimetry, as these telescopes support instruments only on the Nasmyth platform. We also discuss a list of polarimetric science cases and assess science case requirements vs. the modeling results. Finally, we discuss the possible routes for polarimetry with GMT and show the preliminary optical design of the GMT polarimeter.

arXiv:2309.04560v1 [astro-ph.IM] 8 Sep 2023



Artist's impression of the space telescope PRIMA (PRObe far-Infrared Mission for Astrophysics) - NASA/JPL-Caltech; Background: ESO/S. Brunier

# Rieger, Schwabe, Suess-de Vries: The sunny beats of resonance

Frank Stefani

with thanks to

Gerrit M. Horstmann, Laurène Jouve, Martins Klevs,  
George Mamatsashvili, Tom Weier

+

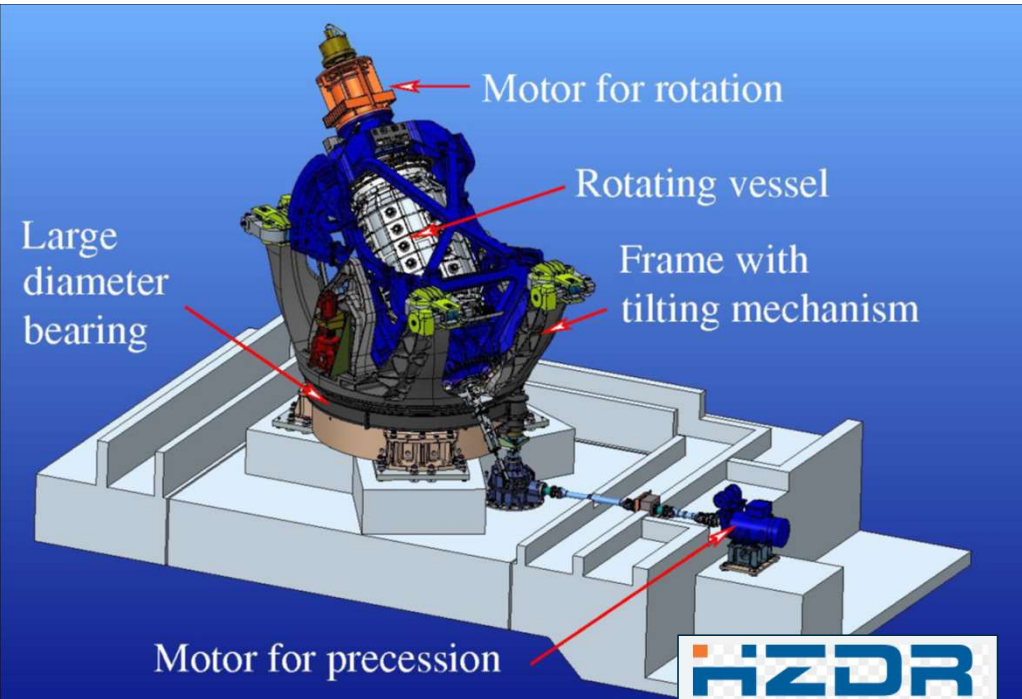
Jürg Beer, André Giesecke, Rodion Stepanov, Norbert Weber,  
and Teimuraz Zaqarashvili  
(for earlier contributions)

Virtual Nordic  
Dynamo Seminar,  
October 1, 2024

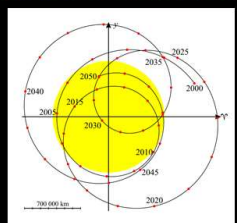
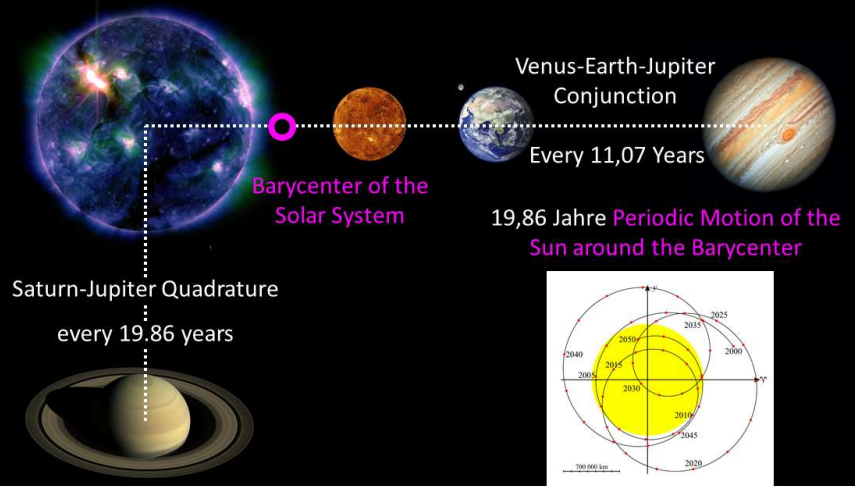
F.S. et al., Solar Physics 299 (2024), 55  
M. Klevs et al., Solar Physics 298 (2023), 90  
G. Horstmann et al., ApJ 944 (2023), 48

**HZDR**

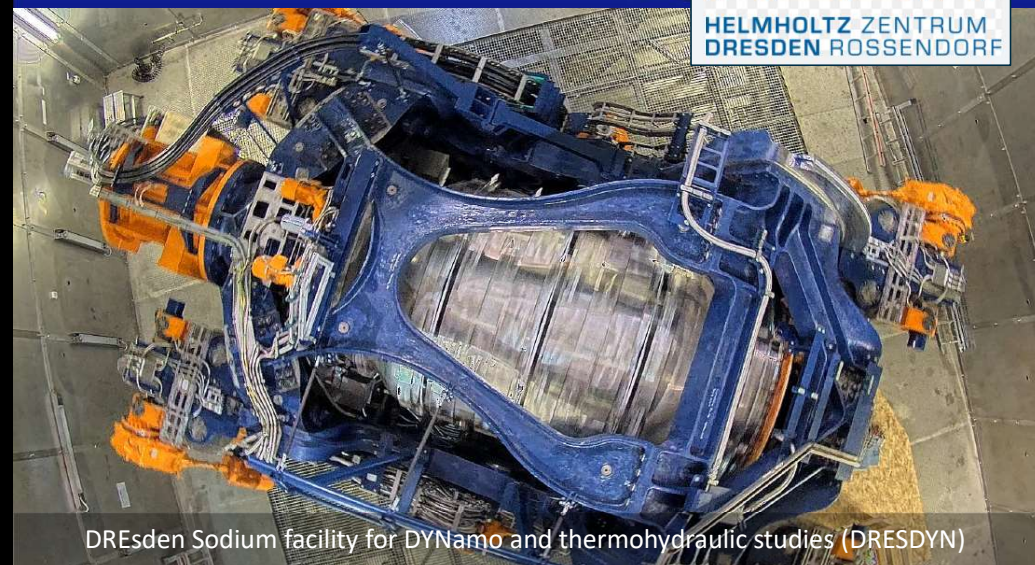
HELMHOLTZ  
ZENTRUM DRESDEN  
ROSSENDORF



**HZDR**  
HELMHOLTZ ZENTRUM  
DRESDEN ROSSENDORF



Special motion sequences in the Solar System - U. v. Kusserow, NASA





Professor  
R.E. Gershberg  
(Russia)  
Crimean Astrophysical  
Observatory, Russian  
Academy of Sciences

Professor  
N.I. Kleorin  
(Israel)  
Ben-Gurion University  
in the Negev,  
Beer-Sheva

Professor  
L.A. Pustilnik  
(Israel)  
Tel Aviv University,  
Ariel University,  
Israeli Space Agency

Professor  
V.S. Airapetian  
(USA)  
PhD Senior  
Astrophysicist  
American University, DC

Astrophysicist  
A.A. Shlyapnikov  
(Ukraine)

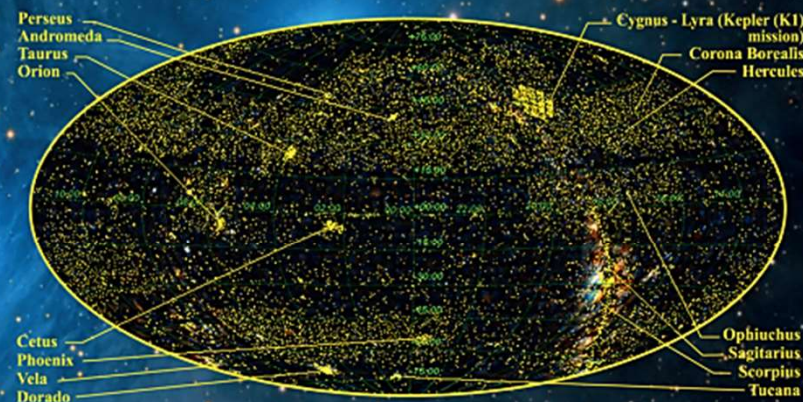
PHYSICS OF MID- AND LOW-MASS STARS WITH SOLAR-TYPE ACTIVITY AND THEIR IMPACT ON EXOPLANETARY ENVIRONMENTS

R.E. Gershberg, N.I. Kleorin,  
L.A. Pustilnik, V.S. Airapetian,  
A.A. Shlyapnikov

PHYSICS OF MID- AND LOW-MASS STARS  
WITH SOLAR-TYPE ACTIVITY  
AND THEIR IMPACT ON  
EXOPLANETARY ENVIRONMENTS

In the monograph, the authors systematize and generalize the results of studying solar-type activity that is characteristic of a significant part of mid- and low-mass stars of the Galaxy, outline the characteristics of such stars in the quiescent state, during the sporadic flares and variations of magnetic activity over the course of stellar evolution. The observational data taken over the whole range of the electromagnetic spectrum from decametric radio waves to X-rays are described in detail. The current models of stellar flares and stellar dynamo models are considered in two theoretical chapters. The last part of the book describes the impact of stellar activity of mid- and low-mass stars on exoplanetary environments. The Catalog of Stars with Solar-Type Activity is provided in the supplementary section.

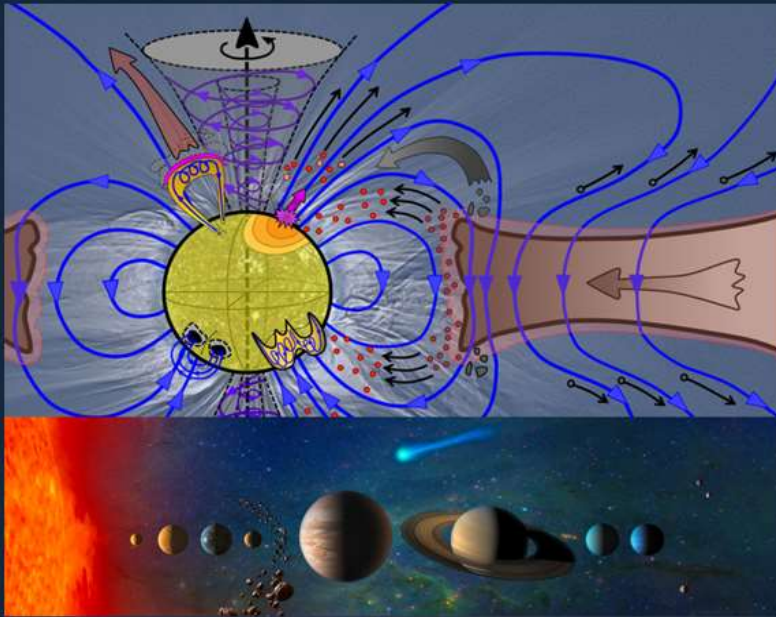
The book is intended for researchers involved in studying the physics of stars and the Sun, graduate students, and students specialized in heliophysics, astrophysics, and in the field of space physics.



Distribution of 314618 stars with solar-type activity over the celestial sphere

Ulrich von Kusserow

# On the **Formation** of the **Magnetic Solar System**

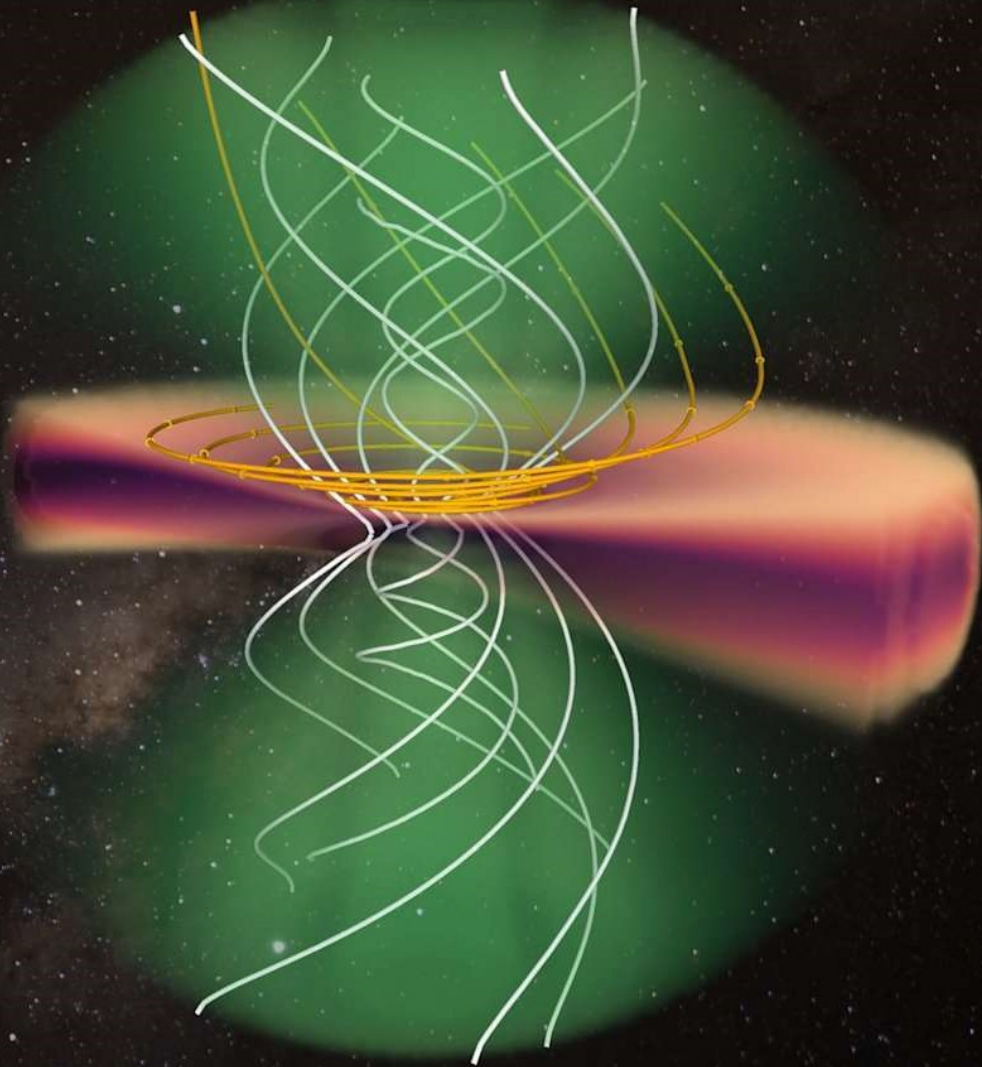


PRAXIS

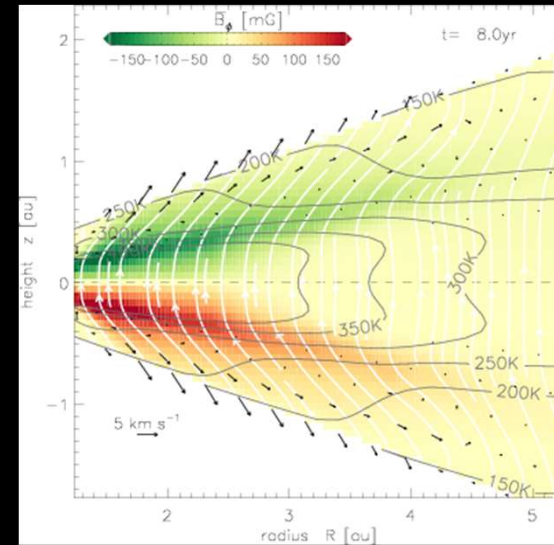
 Springer

## Table of Contents

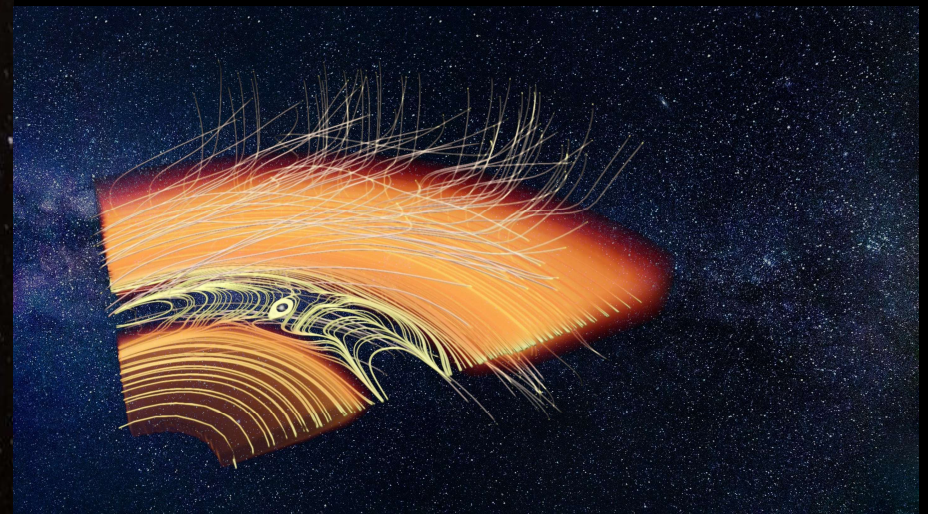
	Prologue
1.	Structure of the present Solar System and Extrasolar Sun-like Systems
2.	Magnetic Fields in the Solar System
3.	Magnetic Processes in Galaxies, Molecular and Dust clouds
4.	Star Formation in Molecular Clouds
5.	Physical and Chemical Developments in Magnetized Protostellar Disks <b>Mario Flock</b>
6.	Physics of Magnetic Protostars and Magnetic Disk Winds <b>Christian Fendt</b>
7.	Formation and Migration of Dust and Planetesimals
8.	Planet and Moon Formation in Protoplanetary Disks
9.	Models for the Formation of the Solar Planetary system
10.	Development Path of the Magnetized Young Solar System in the Hertzsprung-Russell Diagram
	Epilogue



Simulation of a gas disk in a magnetized protostellar system  
AIP/E. Sarafidou, O. Gressel; Background: AIP/A. Saviuk



MHD simulation of a protoplanetary disk with ambipolar diffusion - O. Gressel



Simulated Planet Formation in a Magnetized Protoplanetary Disk - O. Gressel

„To B Or Not To B “

Virginia Trimble, 2001



„The larger our ignorance, the  
stronger the magnetic field“

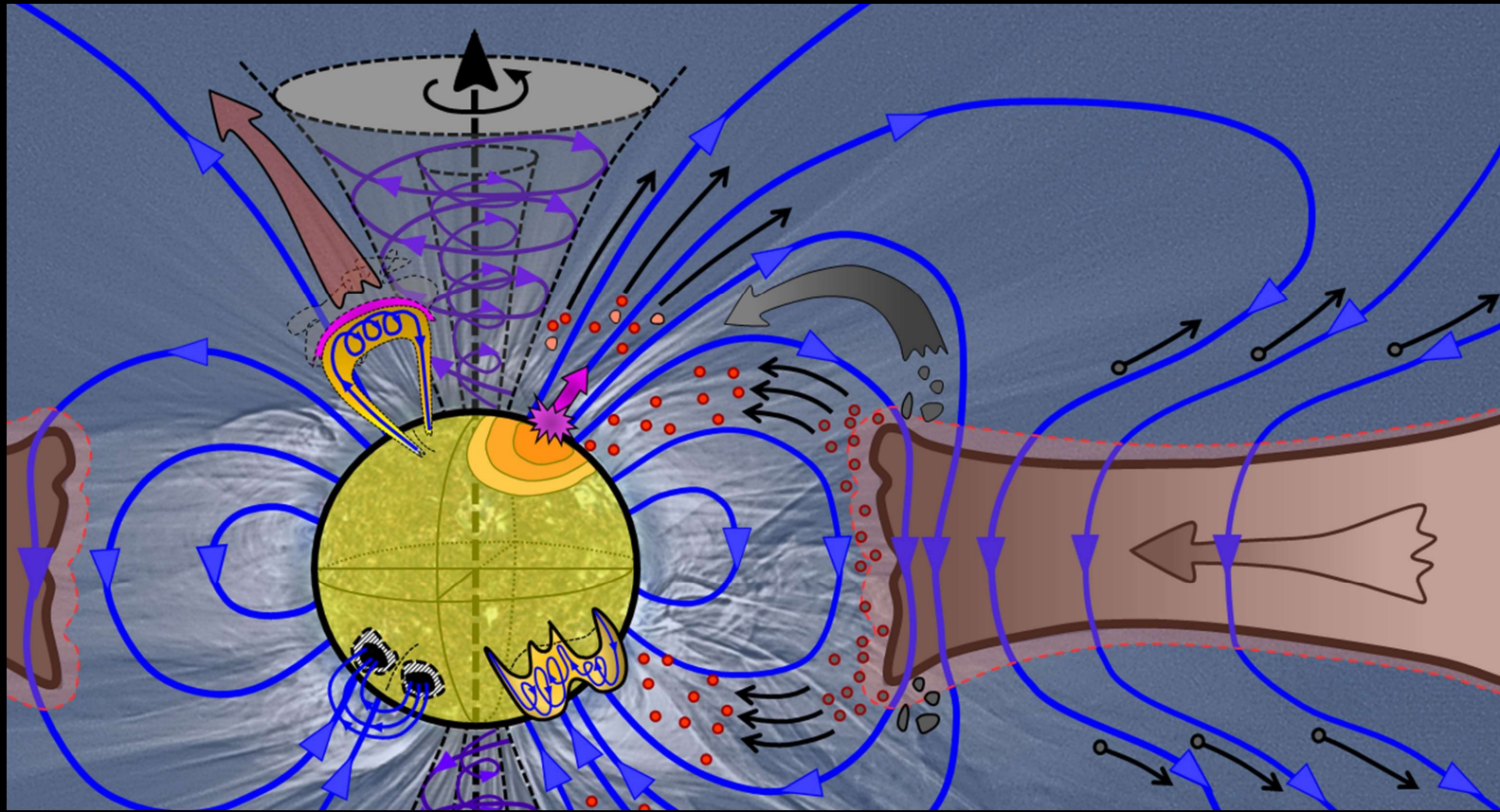
Lodewijk Woltjer, 1965



„Magnetic Fields are to Astrophysics  
as Sex is to Psychology“

Hendrik van der Hulst, 1987





$$\frac{\partial \vec{B}}{\partial t} = \vec{\nabla} \times (\vec{v} \times \vec{B}) - \vec{\nabla} \times (\eta_{OD} \cdot \vec{\nabla} \times \vec{B}) + \vec{\nabla} \times \{ \eta_{AD} \cdot (\vec{\nabla} \times \vec{B}) \times \vec{B} \} - \vec{\nabla} \times [ \vec{\nabla} \times \{ \eta_{HD} \cdot (\vec{\nabla} \times \vec{B}) \times \vec{B} \} ]$$

U. v. Kusserow, Bremen

## MHD and the Formation of the Magnetic Solar System

A didactically oriented approach